

LINGERFELT, MARY A., Ph.D. Construction and Validation of GPR55 Active and Inactive State *In Silico* Models Through the Use of Biological Assays, Mutation Data, and Structure Activity Relationships. (2016)
Directed by Dr. Patricia H. Reggio. 178 pp.

G-protein coupled receptors (GPCRs) function as both gatekeepers and molecular messengers of the cell. They relay signals that span the cell membrane mediating nearly every significant physiological process and currently represent the target of about 30% of all drugs. The signals they transmit can arise from a remarkable variety of stimuli which includes, but is not limited to, photons, neurotransmitters and hormones. GPR55, a rhodopsin-like (Class A) GPCR, has received a great deal of attention due to its emerging involvement in a multitude of physiological processes and its putative identity as a third type of cannabinoid receptor. Characterizations of GPR55 knock-out mice reveal a role for the receptor in controlling inflammatory pain, neuropathic pain, and bone resorption.¹ Myriad other studies indicate that GPR55 activation may play a part in oncogenesis and metathesis.

GPR55 can be found in numerous tissue types throughout the body and is also highly expressed throughout the cerebellum and surrounding central nervous system lending credence to the idea that this receptor may play a more crucial physiological role than originally thought.² GPR55 has an extensive physiological profile and has been shown to respond uniquely to a great number of diverse compounds. Specifically, it has been shown to recognize many cannabinoid compounds, including CB1 and CB2 endogenous ligands, phytocannabinoids and synthetic cannabinoids. Similar to the ligands of the CB1 and CB2 receptors, the endogenous ligand of GPR55,

lysophosphatidylinositol (LPI), is a lipid-derived molecule.³ LPI activates ERK1/2 and increases $[Ca^{2+}]$ and, to date, there has been no evidence that LPI interacts with the other cannabinoid receptors.

Despite innumerable prospective clinical uses hinted at by the aforementioned research no low nanomolar potency ligands of GPR55 have been identified. Nor has there been a radio-ligand developed to characterize the binding site of this receptor. Lack of such tools is a great impediment to any forward progress towards developing the GPR55 receptor as a therapeutic target for drug design.

The following research details the creation of both a GPR55 active- and a GPR55 inactive- state homology model. Towards this goal, Chapter I details the background of the discovery, pharmacological relevance and ligand scope of GPR55. Its purpose is to establish a framework for the research that follows and highlight the medical importance of this elusive receptor.

Chapter II describes the synthetic preparation of antagonists of GPR55 for use in preliminary SAR studies. The original high throughput screen that lead to the identification of novel GPR55 scaffold chemotypes from the screening of over 300,000 compounds gave rise to the piperidinyloxadiazolone compound CID23612552 and the synthetic diversification of what was then dubbed Scaffold 1.

A detailed description of the methods used in the construction of the updated R and R* state of GPR55 models is handled in Chapter III. A combination of Conformational Memories^{4,5} (using the CHARMM forcefield), Ligand Conformational Analysis (performed using Spartan (Wavefunction, Inc., Irvine, CA)) and

Macromodel/Maestro/Glide (from the Schrödinger suite) was used to build and refine both GPR55 model states.

Chapter IV then covers model validation and refinement. Using the phenylpiperazine (ML184 CID2440433) and mutations performed in the lab of Dr. Mary Abood (Temple University) it was shown that the current iteration of the GPR55 R* model was indeed a valid representation of the activated state of this receptor. This chapter also provides information that gives rise to the “Future Directions” chapter, Chapter V.

This final chapter is a look forward to the research that still remains to be done to ensure that these models will function as the accurate tools that they have the potential to be. We used the GPR55 R bundle to suggest antagonist structures that will maximize ligand/receptor interactions and hopefully give rise to nanomolar potency molecules. These ligands will need to be synthesized and tested. We also identified key residues in the active bundle (GPR55 R*) that could be mutated to enhance or verify ligand binding. Mutations that destroy receptor function, while interesting, would not have the same utility as the aforementioned kinds of mutations.

References:

1. Johns, D. G.; Behm, D. J.; Walker, D. J.; Ao, Z.; Shapland, E. M.; Daniels, D. A.; Riddick M.; Dowell, S.; Staton, P. C.; Green, P.; Shabon, U.; Bao, W.; Aiyar, N.; Yue, T. L.; Brown, A. J.; Morrison, A. D.; Douglas, S. A. The Novel Endocannabinoid Receptor GPR55 is Activated by Atypical Cannabinoids but Does Not Mediate Their Vasodilator Effects. *Br. J. Pharmacol.* **2007**, *152*, 825–831.
2. Sawzdargo, M.; Nguyen, T.; Lee, D. K.; Lynch, K. R.; Cheng, R.; Heng, H. H.; George, S. R.; O’Dowd, B. F. Identification and Cloning of Three Novel Human G

- Protein-coupled Receptor Genes GPR52, Ψ GPR53 and GPR55: GPR55 is Extensively Expressed in Human Brain. *Brain. Res. Mol. Brain. Res.* **1999**, *64*, 193–198.
3. Oka, S.; Nakajima, K.; Yamashita, A.; Kishimoto, S.; Sugiura, T. Identification of GPR55 as a Lysophosphatidylinositol Receptor. *Biochem. Bioph. Res. Co.* **2007**, *362*, 928–934.
 4. Guarnieri, F., & Weinstein, H. (1996). Conformational memories and the exploration of biologically relevant peptide conformations: an illustration for the gonadotropin-releasing hormone. *Journal of the American Chemical Society*, *118*(24), 5580-5589.
 5. Whitnell, R. M., Hurst, D. P., Reggio, P. H., & Guarnieri, F. (2008). Conformational memories with variable bond angles. *Journal of computational chemistry*, *29*(5), 741-752.

CONSTRUCTION AND VALIDATION OF GPR55 ACTIVE AND INACTIVE STATE
IN SILICO MODELS THROUGH THE USE OF BIOLOGICAL ASSAYS,
MUTATION DATA, AND STRUCTURE
ACTIVITY RELATIONSHIPS

by

Mary A. Lingerfelt

A Dissertation Submitted to
the Faculty of The Graduate School at
The University of North Carolina at Greensboro
in Partial Fulfillment
of the Requirements for the Degree
Doctor of Philosophy

Greensboro
2016

Approved by

Patricia H. Reggio
Committee Chair

© 2016 Mary A. Lingerfelt

For my father, J. G. Lingerfelt, whose support was resolute.

APPROVAL PAGE

This dissertation, written by Mary A. Lingerfelt, has been approved by the following committee of the Faculty of The Graduate School at The University of North Carolina at Greensboro.

Committee Chair Patricia H. Reggio

Committee Members Nadja Cech

Kimberly S. Petersen

Ethan W. Taylor

October 21, 2016
Date of Acceptance by Committee

October 21, 2016
Date of Final Oral Examination

ACKNOWLEDGMENTS

I would like to thank my academic advisor and committee chair Patricia H. Reggio as well as my committee members, Nadja Cech, Kimberly Petersen, and Will Taylor.

This research was supported by grants from the National Institute on Drug Abuse R01 DA023204 (MEA), R01DA035926 (MEA), P30DA013429 and K05 DA021358 (PHR) and from the National Institute of Neurological Disorders and Stroke R21 NS077347 (MEA and PHR). The content is solely the responsibility of the authors and does not necessarily represent the official views of the National Institutes of Health.

TABLE OF CONTENTS

	Page
LIST OF TABLES	viii
LIST OF FIGURES	ix
LIST OF ABBREVIATIONS.....	xii
CHAPTER	
I. THE GPR55 STORY: DISCOVERY, PATHOPHYSIOLOGICAL RELEVANCE AND LIGAND SCOPE.....	1
Introduction.....	1
GPR55 Structure	3
Pharmacology	5
Biological Relevance of GPR55	7
GPR55 Ligands.....	10
Endogenous Ligands.....	10
Cannabinoid-related Ligands of GPR55.....	12
Endocannabinoids and derivatives.....	12
Phytocannabinoids and related molecules	13
Synthetic cannabinoid ligands	15
Arylpyrazoles.....	15
Aminoalkylindoles.....	16
Coumarins	17
Magnolol derivatives	18
Non-cannabinoid Related Ligands of GPR55.....	19
References.....	23
II. DESIGN, SYNTHESIS, AND ANALYSIS OF ANTAGONISTS OF GPR55: PIPERIDINE-SUBSTITUTED 1,3,4-OXADIAZOL-2- ONES.....	32
Introduction.....	32
Design, Synthesis, and Analysis of Antagonists of Gpr55: Piperidine-Substituted 1,3,4-Oxadiazol-2-Ones	35
Abstract.....	35
Introduction.....	36
Acknowledgments.....	46

References.....	47
III. BUILDING OF THE ACTIVE AND INACTIVE STATE MODELS OF GPR55	49
Introduction.....	49
Constructing the GPR55 R and GPR55 R* TMHs.....	52
Extracellular and Intracellular Loops.....	55
Conformational Assessment of the Ligands	56
Docking of Ligands.....	58
Ligand/Receptor Minimization.....	59
References.....	60
IV. IDENTIFICATION OF CRUCIAL AMINO ACID RESIDUES INVOLVED IN AGONIST SIGNALING AT THE GPR55 RECEPTOR.....	62
Abstract.....	62
Introduction.....	63
Results.....	64
Biological Evaluation.....	64
SRE responses of mutant and wild-type GPR55 receptors.....	64
SRF responses of mutant and wild-type GPR55 receptors.....	67
Molecular Modeling.....	71
Primary interactions for agonist signaling	72
ML184 docked into the GPR55 R* bundle.....	72
Toggle switch residues.....	76
Inactive state	76
Agonist activated state	77
Disulfide bridge residues	77
Binding pocket position	79
Discussion.....	80
ML184 Docked into the GPR55R* Bundle	80
Ligand Interactions within the Binding Crevice.....	80
Conclusions.....	86
Experimental Section	86
Material and Reagents.....	86
Mutagenesis and Cell Culture.....	86
Serum Response Element (SRE) and Serum Response Factor (SRF) Assay.....	87

Modeling.....	87
Amino acid numbering system	87
Modeling of hGPR55 active-state bundle (GPR55 R*) using GPCR x-ray crystallography data	88
Conformational Memories (CM) Method for Calculating TMH Conformation.....	88
Construction of the GPR55 Active-state Bundle	90
Conformational Analysis of ML184.....	91
Docking of ML184	91
Assessment of Pair-wise Interaction Energies	92
Acknowledgments.....	93
References.....	94
V. FUTURE CONSIDERATIONS	98
Chemo-informatics Approach.....	98
Validating Chemo-informatics Virtual Search Results.....	99
Unutilized Synthesis of Analogues for Scaffold 2.....	99
References.....	103
APPENDIX A. SUPPLEMENTAL INFORMATION FOR CHAPTER II.....	104
APPENDIX B. SUPPLEMENTAL INFORMATION FOR CHAPTER IV	175

LIST OF TABLES

	Page
Table 1. GPR55 Antagonist Activity of Compounds	41
Table 2. ML184 Induced SRE Responses of Wild-type and Mutant Transfected Cells	66
Table 3. ML184 Induced SRF Responses of Wild-type and Mutant Transfected Cells	71

LIST OF FIGURES

	Page
Figure 1. Human Striatum	2
Figure 2. GPCR General Structure	3
Figure 3. GPR55 Sequence in Helix Net Form	4
Figure 4. Pathophysiological Roles of GPR55	9
Figure 5. The Structures of Lysophosphatidylinositol (LPI) and its 2-arachidonoyl-derivative (2-AGPI).....	11
Figure 6. Endocannabinoids as GPR55 Ligands	13
Figure 7. Structure of GPR55 Active Phytocannabinoids and Synthetic Derivatives Related to Δ^9 -THC.....	14
Figure 8. Arylpyrazoles SR141716A, AM251, AM281, and SR144528	16
Figure 9. Synthetic Cannabinoid Ligands WIN55,212-2, JWH015, and GW405833	17
Figure 10. 3-(2-Hydroxybenzyl)-5-isopropyl-8-methyl-2 <i>H</i> -chromen-2-one (PSB-SB-489) and 7-(1,1-dimethyloctyl)-5-hydroxy-3- (2-hydroxybenzyl)-2 <i>H</i> -chromen-2-one (PSB-SB-487)	18
Figure 11. Magnolol and Analogues.....	18
Figure 12. GPR55 Agonist Scaffolds (CID2440433, CID1172084, and CID15945391) and GPR55 Antagonist Scaffolds (CID23612552, CID1434953, and CID1261822) from HTS.....	20
Figure 13. Benzoylpiperazines Previously Reported as Glycine Transporter Inhibitors.....	20
Figure 14. Naphthylfenoterol (MNF)	21
Figure 15. Scheme 1: Synthetic Scheme for Scaffold 1	33

Figure 16. Subset of Available R-groups and Aryl-groups That Were Initially Examined.....	34
Figure 17. LPI and Lead Antagonists of GPR55	36
Figure 18. (A) Docking and Key Interactions between ML191 and GPR55	38
Figure 19. Scheme 1a: Synthesis of Acylated Piperidones	39
Figure 20. Scheme 2: Synthesis of GPR55 Antagonists.....	40
Figure 21. Analogues with Poor Activity (>15 μ M).....	43
Figure 22. Representative Images of Antagonist Screening.....	44
Figure 23. GPCR Multi-Sequence Alignment.....	51
Figure 24. δ -Opioid Receptor	51
Figure 25. CM Output for Active-State GPR55 TMH6 Clustered, Showing F6.48	52
Figure 26. Metropolis Criterion	54
Figure 27. Conformational Memory for S2.40 χ 1 from GPR55	54
Figure 28. GPR55 Agonist ML184 with Two of Six Rotatable Bonds Indicated	57
Figure 29. GRPR55 Agonist ML184 Docked (Cyan) and Global Minimum (Copper) Conformations.....	57
Figure 30. SRE Responses Induced by ML184 in GPR55 Wild Type and Mutant Transfected Cells	65
Figure 31. SRE Responses Induced by LPI in GPR55 Wild Type and Mutant Transfected Cells.....	68
Figure 32. SRF Responses Induced by ML184 in GPR55 Wild Type and Mutant Transfected Cells	69
Figure 33. SRF Responses Induced by LPI in GPR55 Wild Type and Mutant Transfected Cells.....	70

Figure 34. GPR55 Agonist ML184, Numbered to Show Torsional Angles Varied for Conformational Analysis.....	72
Figure 35. All Hydrogen and Aromatic Stacking Interactions for ML 184 at GPR55	73
Figure 36. (A) M7.39 is Engaged in a Met-aromatic Ring Interaction With the Central Benzene of ML184.....	75
Figure 37. Positions of the Toggle Switch Residues Y3.32, M3.3 and F6.48 (Contoured at Their Van der Waals Radii) in the GPR55 R and R* Models.....	76
Figure 38. Position of ML184 Relative to the Extended Toggle Switch Residues in the GPR55 Activated State	78
Figure 39. The Extracellular End of the Receptor and the Disulfide Bridge Between N-Terminal C(10) and C(260) at the EC End of TMH7.....	78
Figure 40. Positions of Q6.58 and Q7.36 Relative to the ML184 Binding Site	79
Figure 41. Scaffold 2	100
Figure 42. Scheme 3: Synthetic Scheme for Scaffold 2	101
Figure 43. Analogs Proposed for Scaffold 2 Development	101

LIST OF ABBREVIATIONS

A2-AR	A2-adenosine receptor
β arr2-GFP	β -arrestin2-green fluorescent protein
β 2-AR	β 2-adrenergic receptor
CID2745687	methyl-5-[(tert-butylcarbamothioylhydrazinyl-idene)methyl]-1-(2,4-difluorophenyl)pyrazole-4-carboxylate
CM	Conformational Memories
DMEM	Dulbecco's modified Eagle's Medium
DOR	delta opioid receptor
ERK	extracellular signal related kinase
FBS	fetal bovine serum
GPCR	G-protein-coupled receptor
HBSS	Hanks Balanced Salt Solution
LPA	lysophosphatidic acid
Rho	rhodopsin
TMH	transmembrane helix

CHAPTER I

THE GPR55 STORY: DISCOVERY, PATHOPHYSIOLOGICAL RELEVANCE AND LIGAND SCOPE

Introduction

G-protein coupled receptor 55 (GPR55), first identified and cloned in 1999, is a receptor in the Class A (rhodopsin-like) G protein-coupled receptor (GPCR) family. This receptor is expressed in myriad tissue types throughout the human body and is particularly populous in human striatum¹ (Genbank accession # NM-005683; Figure 1). In an attempt to discover ligands that could modulate GPR55 activity, screening assays were carried out on cannabinoid libraries by AstraZeneca² and GlaxoSmithKline³. It was discovered that GPR55 responded not only to endogenous or plant-derived CB₁R/ CB₂R ligands but various synthetically derived cannabinoid compounds as well. These findings sparked a debate that has raged for over a decade as to the veracity of classifying GPR55 as a novel, third type of cannabinoid receptor belonging in the same subfamily as cannabinoid receptors CBR1 and CBR2.⁴⁻⁶

The CB1 and CB2 receptors themselves are compelling targets for their potential as modifiers of drug abuse and addiction and it is thought that, if GPR55 is indeed related to these receptors it could have a similar role. Characterizations of GPR55 (-/-) (knock-out) mice^{7,8} have shown a definite role for the GPR55 receptor in inflammatory pain, neuropathic pain, and bone development with more recent studies indicating that the receptor may play an even more pervasive role in both energy metabolism and cancer

motility.^{9,10} These results suggest that the ability to manipulate the active and inactive state of GPR55 has tremendous therapeutic potential.

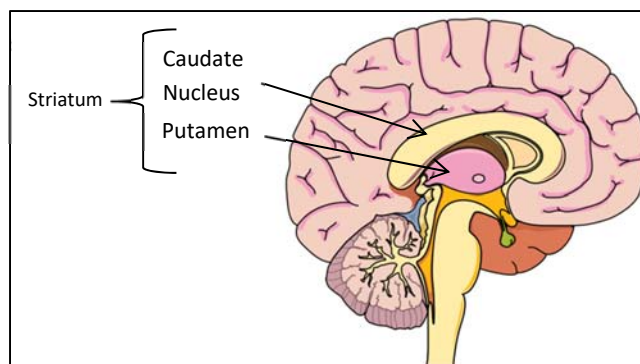


Figure 1. Human Striatum.

Discussing the pharmacology of GPR55 in a precise manner is a perplexing task at best: Certain CB1 and CB2 antagonists have been reported to act as agonists at GPR55 while other CB1/CB2 agonists have been reported to act as antagonists.¹¹ Adding to the already puzzling responses of the receptor was the identification of LPI (lysophosphatidylinositol) as the endogenous ligand for GPR55.¹² This lysophospholipid has been described as having an EC₅₀ of 200nM to 49nM¹³ by Henstridge et al. in 2009, but later data collected on LPI's effect on GPR55 has appeared to differ from lab to lab and from assay to assay.

One strategy for navigating the seemingly contradictory pharmacology of GPR55 is to step back and try to understand this receptor from the “ground” up. To do this one must first understand the basic morphology of GPCRs and GPR55 and its ligands specifically.

GPR55 Structure

GPR55 is one of many integral membrane proteins made up of seven membrane-spanning domains known transmembrane helices.^{14,15} This receptor is related to receptors of rhodopsin-like GPCRs (Class A) and shares many of their key sequence motifs (see Figure 2).

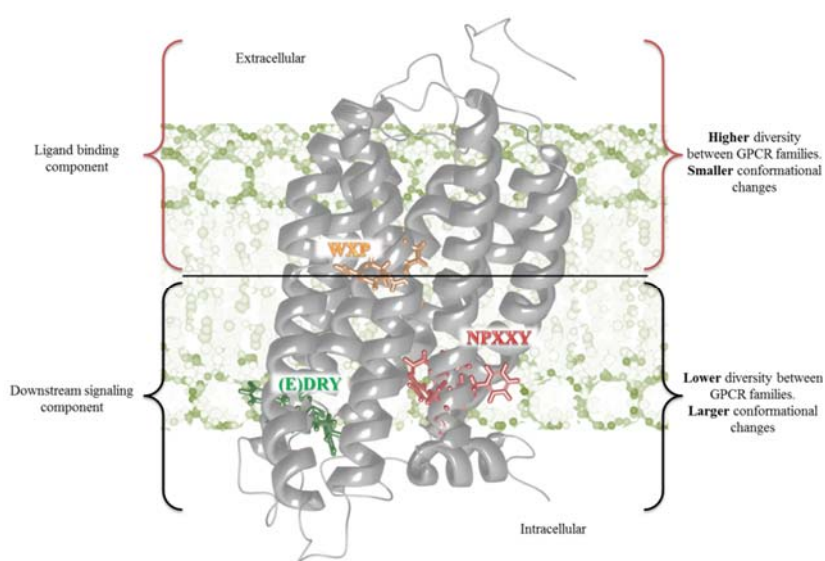


Figure 2. GPCR General Structure.

The human GPR55 (*hGPR55*) sequence is relatively unique and only shares low sequence identity with the cannabinoid receptors CB₁R and CB₂R (13.5% and 14.4%, respectively) described previously. The GPCR proteins displaying the highest percentages of homology with GPR55 are the δ -Opioid (28%), GPR35 (27%), P2Y (29%), GPR23 (30%), CCR4 (23%), LPA4 (30%) and LPA5 (30%).^{1,16} A helix net representation of the GPR55 sequence is displayed in Figure 3.¹⁷

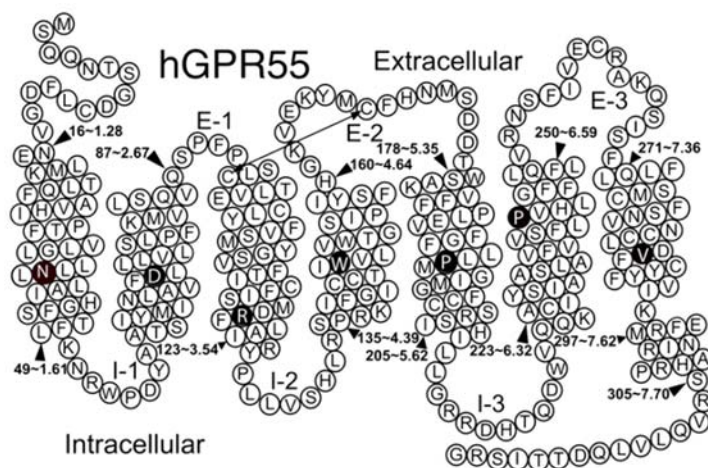


Figure 3. GPR55 Sequence in Helix Net Form.

The most highly conserved residues across Class A GPCRs are as follows: TMH1 - N1.50, TMH2 - D2.50, TMH3 - E/D3.49, R3.50, Y3.51 (DRY motif), TMH4 - W4.50, TMH5 - P5.50, TMH6 - C6.47, W6.48, X (this residue varies), P6.50 (CWXP motif), and TMH7 - N7.49, P-7.50, X, X, Y7.53 (NPXXY motif).^{*} This conservation of residues and the convenient Ballesteros-Weinstein¹⁸ numbering system make sequence patterns easily identifiable on multiple sequence alignments and allow for easy comparison among residues in the transmembrane regions of different receptors. While GPR55 possesses some of the highly conserved .50 residues (N1.50, D2.50, W4.50 and P5.50) found in many GPCRs, there are a few notable differences. GPR55 has a conservative substitution (DRF) for the TMH3 E/DRY motif, a conservative substitution (SFLP) for the TMH6 CWXP motif, and a non-conservative substitution (DVFCY) for the THM7 NPXXY motif. This sequence divergence is thought to lead to an altered level of hydration and local transmembrane flexibility and, consequently, gives rise to a distinct conformation in this region.¹⁹ Outside of the TMH region, GPR55 has an extracellular-1

(EC-1) loop that is shorter than most (three residues versus the six found in β 2-AR and Rhodopsin) and an EC-3 loop that is noticeably longer (fourteen residues long versus the five in β 2-AR and the six residues in rhodopsin, CB1 and CB2). Located on the EC2 loop there is a cysteine (C168) that is thought to form a disulfide bond with C3.25.^{11,17} This EC2 disulfide bond, while present in many Class A GPCRs (CXCR4, P2Y12, DOR, etc.) is absent in both CB1 and CB2.

To date there has been no x-ray crystallographic structure resolved for GPR55. Numerous homology models based on available GPCR crystal structures have been reported however, and will be discussed later in this chapter.^{17,19}

*[The Ballesteros–Weinstein numbering scheme is based on the presence of highly conserved residues in each of seven transmembrane (TM) helices. It consists of two numbers where the first denotes the helix, 1–7, and the second the residue position relative to the most conserved residue, defined as number 50. For example, 5.42 denotes a residue located in TMH5, eight residues before the most conserved residue, Pro5.50]

Pharmacology

CBR1 and CBR2 are themselves compelling medical targets for their potential as modifiers of drug abuse and addiction and it is thought that, if GPR55 is indeed related to these receptors, it could have a similar role. As mentioned in the introduction, the pharmacological reports of GPR55 activity are far from clear. The jury remains out for a large section of the research community as to whether GPR55 represents a new subtype of cannabinoid receptor or just a novel cannabinoid receptor modulator. Getting an answer to this question and finding an infallible way to operate the active and inactive

states of GPR55 will grant tremendous therapeutic power to medicinal chemists in the near future.

To discuss the pharmacology of GPR55 in a precise manner is a perplexing task at best: While cannabinoid receptors couple to G-proteins of the $G_{i/0}$ subfamily, as widely demonstrated in the literature,^{20,21} GPR55 has been seen to associate with a number of different G-proteins: $G_{\alpha 13}$,¹³ $G_{\alpha q/11}$,²³ $G_{\alpha q}/G_{\alpha 1}$ ²⁴ or $G_{\alpha 12/13}$ ^{13,25}; and its lack of coupling specificity seems to depend on the ligand used and the cell line in which the receptor is expressed. A range of signaling pathways can be initiated based on GPR55's interaction with individual G proteins: RhoA, MAPK cascades, actin filament formation and intracellular calcium release via the activity of phospholipase C (PLC). The resulting cascades ultimately end in the activation of extracellular signal-regulated kinase (ERK), RhoA activated kinase (ROCK) or phosphatidylinositol 3-kinase (PI3K). In addition, two transcription factors, NFAT or NFkB (that translocate to the nucleus and modulate the expression of different genes), can also be induced following GPR55 activation.^{13,25}

The evaluation of novel potential GPR55 ligands has been vigorously explored through numerous assays with differing functional endpoints: GTP γ S binding,⁷ analysis of intracellular calcium levels,^{26,28} phosphorylation of ERK1/2,^{19,29} and the activation of the small GTPase proteins Rac1, RhoA and Cdc42.^{26,28,30} Maintaining consistency between pharmacological assays has proven to be very problematic however, due to promiscuous nature of GPR55's response to ligands. It is a fundamental experimental problem when GPR55 ligands modulate not only the eponymous receptor but also CBRs, transient receptor potential vanilloid channels (TRPVs), or peroxisome proliferator-

activated receptors (PPARs).^{29,31,32} Moreover, clear monitoring of the signaling of this receptor may be dependent on intrinsic properties of GPR55 specifically. Unknowns, such as additional active conformation states,²⁸ oligomerization,^{29,31,32} allosterism,^{33,34} or biased agonism could play a pivotal role in getting the receptor to signal robustly and consistently.^{8,25,30,31} These considerations, and more, have been the topic of many recent reviews written on GPR55, demonstrating the growing interest in resolving the pharmacological conundrums of this receptor.^{11,38,39}

Biological Relevance of GPR55

GPR55 is ubiquitously expressed throughout the body; however, its primary physiological function still remains to be fully understood. The receptor has been shown to co-localize with both CB₁R and CB₂R.^{29,32} This indicates that GPR55 is extensively expressed throughout the CNS (hippocampus, putamen, caudate, thalamic nuclei) as well as being found in osteoclasts, kidneys and peripheral tissues such as the immune system (spleen, tonsil)^{7,23,39,40,41} GPR55 is also expressed in vascular endothelial cells and this has led various research groups to study the involvement of GPR55 in the regulation of vascular functions.^{6,42-44}

There is increasing evidence that GPR55 plays an integral role in the modulation of inflammatory and neuropathic pain. Activation of GPR55 enhances neuronal excitability by increasing intracellular Ca²⁺ and suppressing the K⁺ current acting on M-type channels as is seen in pro-nociception (the biological amplification of pain signals).²⁴ Moreover, Staton et al.⁸ showed that mice lacking GPR55 did not display hyperalgesia

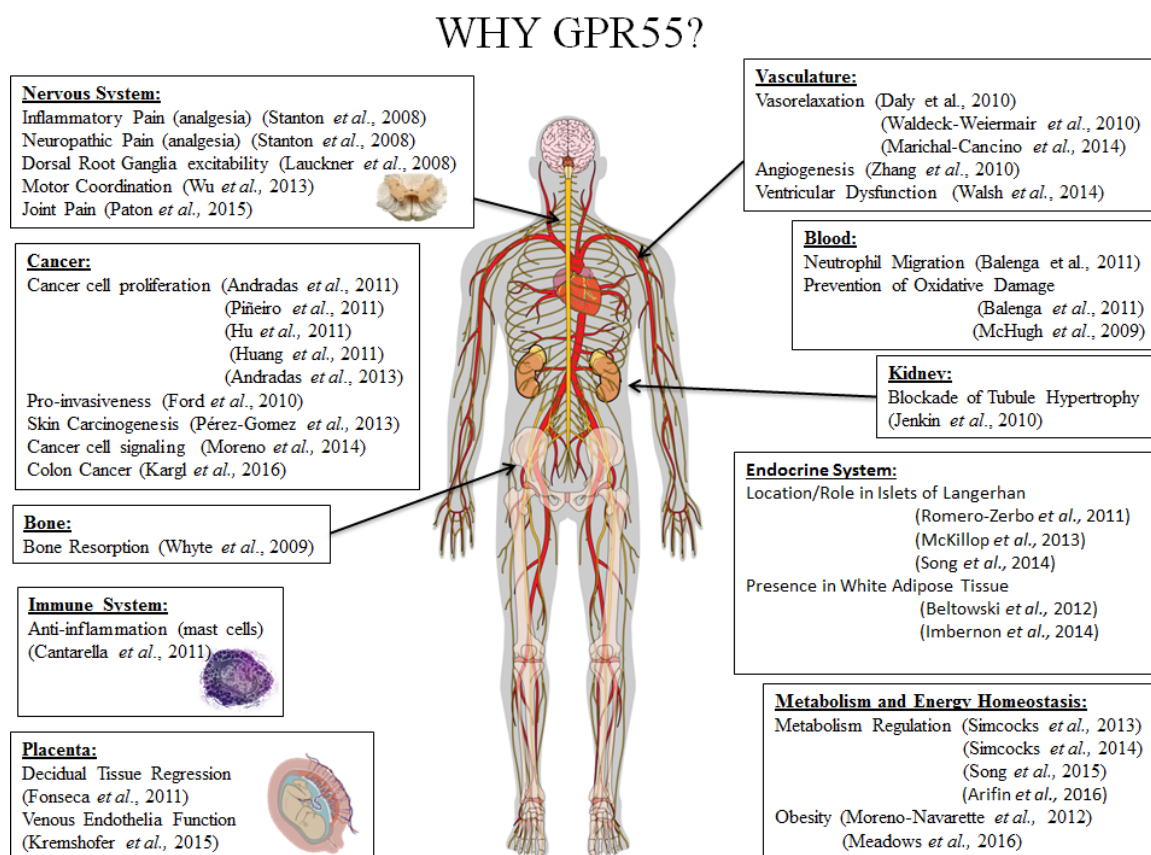
upon inflammatory or neuropathic stimuli. Results from experiments in microglial cells⁴⁵ and with neutrophils⁴⁶ further support the role of GPR55 in the inflammatory process.

A recent emerging body of evidence that points to the contribution of GPR55 to metabolic regulation and energy homeostasis.⁴⁷⁻⁴⁹ Correlations between body weight and levels of GPR55 expression in visceral adipose tissue has been reported and it is clear that GPR55, along with CB₁R, controls food intake, gut motility and insulin secretion.

GPR55 also appears to have myriad, secondary roles in other complicated disease states. There is evidence that the receptor plays a crucial part in the physio-pathology of cancer. Increased levels of LPI, the putative GPR55 endogenous ligand, have been found in plasma and ascites in patients with this pathology.^{50,51} Moreover, GPR55 expression is significantly increased in tumor tissues as compared with their healthy counterparts and its expression may be able to be used as a potential biomarker in oncology cases associated with poor prognosis.^{52,53} As mentioned previously, GPR55 signals through Rho GTPases, which control cytoskeleton organization, cell polarity and cell migration, and are closely related to tumor progression.⁵⁴⁻⁵⁶ Consequently, activation of GPR55 triggers a number of signaling cascades that stimulate cancer cell proliferation, migration, and invasion. These findings support the idea that GPR55 would make an excellent oncological therapy target in the ongoing fight against cancer.

Perhaps related to GPR55s ability to induce fibril formation and cancer cell migration is its effect on bone physiology. Whyte et al.⁵⁷ reported that manipulation of GPR55 signaling seems to regulate osteoclast polarization and bone resorption activity. Hence, GPR55 may represent a novel target for treatments of arthritis and bone loss

associated with osteoporosis. It is worth noting that GPR55 is not involved in the regulation of CNS development, gross motor movement or learned behavior. It does seem however, to play a role in motor coordination.⁵⁸ The physiological, therapeutic potential of GPR55 modulation is schematically summarized in Figure 4.



Adapted from Henstridge *et al.*⁵⁹

Figure 4. Pathophysiological Roles of GPR55.

There is an extraordinary array of evidence that implicates GPR55 in the modulation of diverse physio-pathological conditions, but issues still remain with

experimental consistency. It is clear that a drive to secure nanomolar, selective ligands of GPR55 is of utmost future importance.

GPR55 Ligands

Due to a lack of information of GPR55 three-dimensional structure and the complexity of interpreting GPR55 functionality assays, the design of potent and selective GPR55 ligands remains a major challenge for medicinal chemists. The following section is a categorization of different GPR55 modulators that have been reported so far in the literature.

Endogenous Ligands

Despite the contradictory data reported for many GPR55 ligands, the bioactive lipid lysophosphatidylinositol has demonstrated GPR55 agonism in all studies and functional assays reported so far.^{25,41} Compilation of this data led to the proposal that LPI is an endogenous non-CB₁R/ non-CB₂R ligand of GPR55. Structurally, LPI contains a glycerol core esterified with a single fatty acid in either the sn-1 or sn-2 position and an accompanying inositol substituted phosphate group.^{12,64} In a recent study performed by Oka et al.,²⁶ for identification of the molecular species of LPI in the rat brain, it was found that the predominant fatty acyl moiety was stearic acid (50.5%), followed by arachidonic acid (22.1%). 2-Arachidonoyl-containing LPI species (2-AGPI) displayed the highest potency and efficacy of the LPI species published to date (Figure 5). Due to this, 2-AGPI has been proposed as the natural LPI ligand for GPR55.^{26,65}

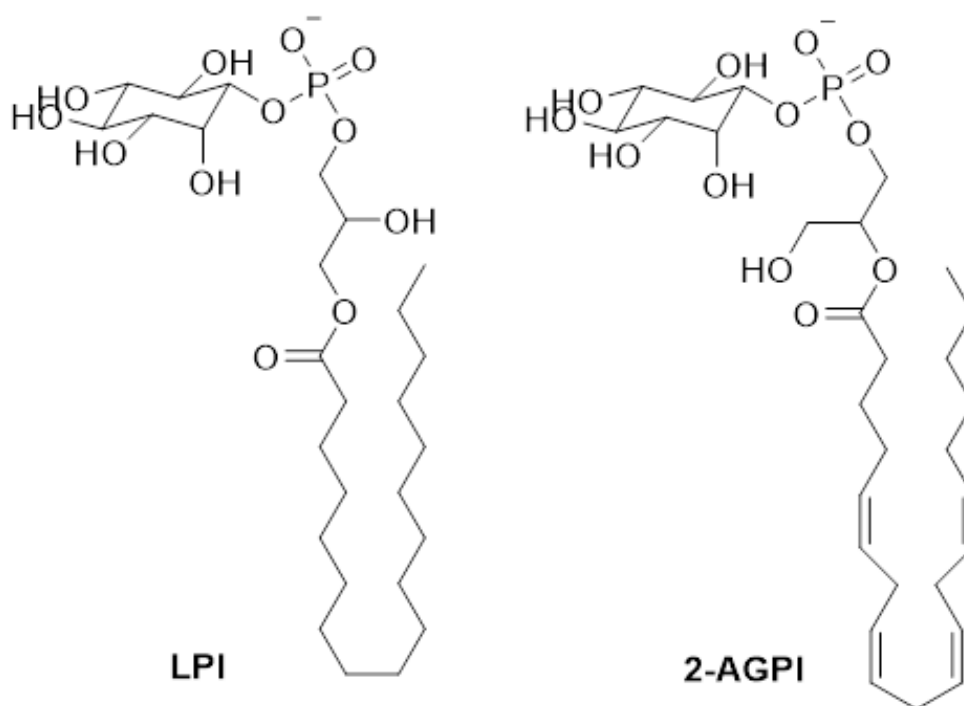


Figure 5. The Structures of Lysophosphatidylinositol (LPI) and its 2-arachidonoyl-derivative (2-AGPI).

The ability of LPI to activate GPR55 has been confirmed in various cellular systems and pharmacological outcomes. For instance, increase of LPI levels has been detected not only in diverse tumors but also in cancer cell proliferation and tumor progression processes.⁶ LPI induces phosphorylation of ERK and elicits a rapid Ca^{2+} transient (a brief increase in calcium ion) in GPR55-expressing cells.¹² Further reports have supported these findings in HEK293 cells expressing GPR55 and in large-diameter DRG neurons²⁴ and endothelial cells.²³ Henstridge et al.¹³ showed that LPI stimulates Ca^{2+} release that is dependent on $\text{G}_{\alpha 13}$ and RhoA activation and in β -arrestin PathHunter™ assays, LPI is also revealed to be a potent agonist.⁶³

Cannabinoid-related Ligands of GPR55

Endocannabinoids and derivatives. Several endogenous cannabinoid ligands have been identified as GPR55 modulators (Figure 6). Anandamide, the predominant endocannabinoid, has displayed inconsistent results in GPR55 assays. This lipid neurotransmitter stimulated [³⁵S]GTP γ S binding in the nanomolar range and caused calcium mobilization in the micromolar range, yet did not affect phosphorylation of ERK, β -arrestin signaling or receptor internalization. Two-arachidonoylglycerol, another significant endocannabinoid, showed agonist efficacy in a [³⁵S]GTP γ S binding assay but was ineffectual in β -arrestin recruitment and GPR55 internalization. These discrepancies may be due to the aforementioned incongruities between functional assays or cell systems³⁶ and, in accordance with IUPHAR (International Union of Basic and Clinical Pharmacology), do not demonstrate irrefutably that these eicosanoids are in fact GPR55 agonists.

Other endocannabinoids such as palmitoylethanolamide, noladin ether, virodhamine and oleylethanolamide resulted in [³⁵S]GTP γ S binding in transiently transfected *h*GPR55-HEK293 cells, with EC₅₀ values of 4, 10, 12 and 440 nM respectively.⁷ Results similar to these were previously reported by AstraZeneca in the same [³⁵S]GTP γ S assay.² According to those GTP γ S studies, anandamide activated GPR55 and CBRs with similar potencies while palmitoylethanolamide, virodhamine and 2-AG displayed selective action through GPR55.

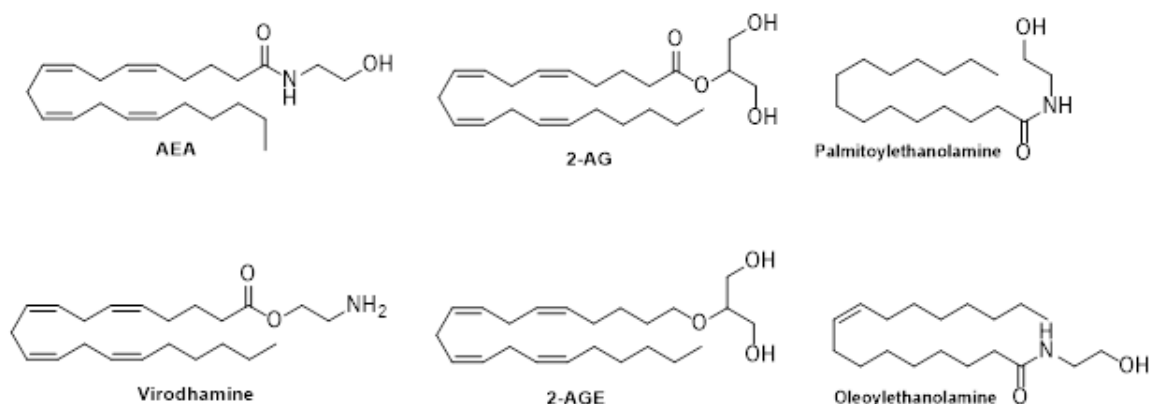


Figure 6. Endocannabinoids as GPR55 Ligands.

Phytocannabinoids and related molecules. Bioactive constituents from the plant *Cannabis sativa* and synthetic analogues (Figure 7) have also shown discrepant data regarding their GPR55 pharmacology. Delta⁹-THC exhibits activation of GPR55 in [³⁵S]GTPγS binding, RhoA assays and intracellular Ca²⁺ mobilization in transiently transfected *h*GPR55-HEK293 cells^{1,2,24} but was unable to stimulate ERK1/2 phosphorylation or β-arrestin recruitment.^{12,63} It remains to be seen whether these results are a consequence of experimental variability, differences in functional readouts or GPR55 intrinsic properties. HU210, a synthetic derivative of Δ⁹-THC, also displayed activity as GPR55 agonist in diverse assays while being inactive in others.^{7,2,63} Abnormal-cannabidiol (Abn-CBD) and the structurally related O-1602 have been reported as GPR55 selective agonists in [³⁵S]GTPγS assays with EC₅₀ values in the micromolar and nanomolar ranges respectively.^{7,6,2} Nevertheless, as has been observed with other GPR55 ligands, there have been research groups who reported a lack of activity when using different cellular systems or functional endpoints.^{26,63}

The potent CB₁R/CB₂R agonist CP55,940 has also shown conflicting data when used to stimulate GPR55, acting as an agonist in [³⁵S]GTPγS assays^{7,2} and antagonist^{23,12,5} in β-arrestin, ERK phosphorylation and Ca²⁺ mobilization tests.

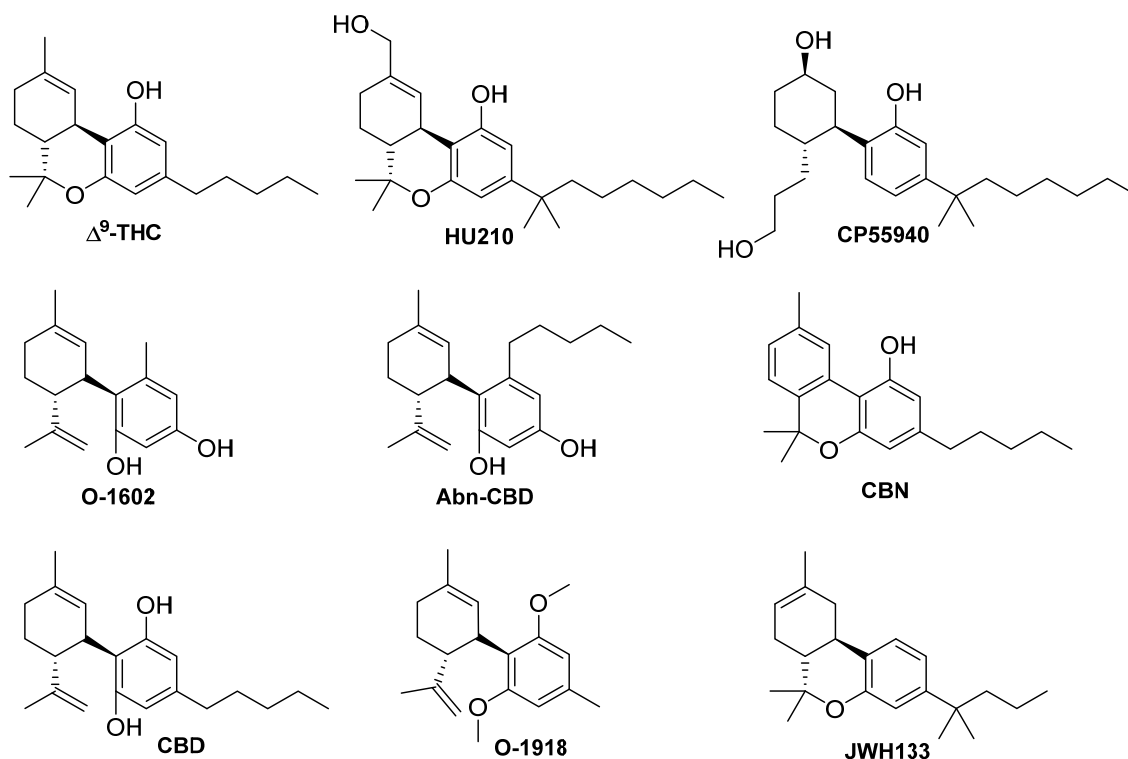


Figure 7. Structure of GPR55 Active Phytocannabinoids and Synthetic Derivatives Related to Δ^9 -THC.

Of the other phytocannabinoids, such as cannabitol and JWH133, initial studies confirmed their inactivity towards GPR55.³⁶ However, in a recent, more sensitive ERK assay, developed by Sharon Anavi-Goffer et al.,³³ it was determined that JWH133 could reduce basal pERK acting as GPR55 inverse agonist. From the same GPR55 assay, the phytocannabinoids Δ^9 -tetrahydrocannabivarin, cannabidivarin and cannabigerovarin acted as potent inhibitors of LPI and could constitute a new set of novel GPR55 ligands.

CBD, a phytocannabinoid seen recently in headlines for its omnipotent “curative” powers and whose mechanism of action is not fully understood, has also shown promising GPR55 pharmacological activity. This non-psychoactive component of marijuana acts as GPR55 antagonist preventing [³⁵S]GTPγS binding and Rho activation^{7,57,66} and was inactive in Ca²⁺ mobilization assays²⁴ and β-arrestin recruitment.⁶³ Conversely, O-1918, a synthetic derivative of CBD that does not bind to CBRs⁶⁷ acted as a GPR55 antagonist in intracellular Ca²⁺ functional analysis using endothelial cells that express GPR55.⁴²

Synthetic cannabinoid ligands.

Arylpyrazoles. The arylpyrazole scaffold has been extensively explored in the cannabinoid world, becoming very relevant in the design of CB₁R or CB₂R inverse agonists or antagonists (Figure 8). Rimonabant (SR141716A), the familiar CB₁R arylpyrazole antagonist, has been found to behave as a GPR55 agonist in some assays^{2,25,63,68} but as a GPR55 antagonist in others,^{23,24,69} exerting no effect in one additional study.¹² In comparison, SR144528, a potent CB₂R antagonist, is inactive in all the GPR55 assays reported so far. It did not induce a rise in calcium in transiently transfected *h*GPR55-HEK293 cells nor in β-arrestin binding assays.^{24,63} Also studied extensively were AM251 and AM281, CB₁R antagonists structurally related to SR141716A. AM251 behaved as a GPR55 agonist in different biochemical assays,^{3,5,7,13, 25,63,68} while AM281 did not seem to interact with the receptor⁷ or displayed very weak agonist effects.^{27, 45}

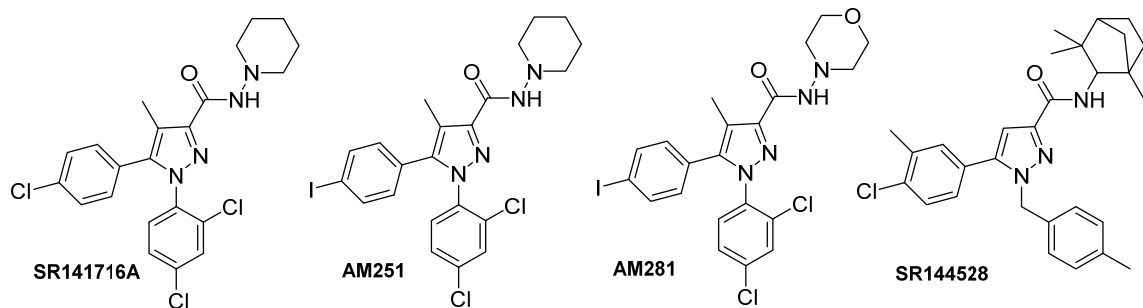


Figure 8. Arylpyrazoles SR141716A, AM251, AM281, and SR144528.

The CB₁R antagonists SR141716A, AM281 and AM251 can act as agonists while also acting as inhibitors of LPI inducing activation of ERK phosphorylation within the same cellular model. This may explain the seemingly conflicting data surrounding the GPR55 pharmacology of several CB₁R and/or CB₂R ligands. It suggests that certain arylpyrazole ligands may act in a bitopic fashion at GPR55.⁶⁹

In 2010 Daly et al.⁴³ reported that the fluorescent ligand T1117 activated GPR55 by promoting a characteristic oscillatory Ca²⁺ response in HEK293 cells stably expressing recombinant GPR55. This molecule, structurally analogous to the CB₁R ligand AM251 but linked to a fluorescent tetramethylrhodamine group, showed weak or no affinity towards CB₁R.

Aminoalkylindoles. The CB₁R/CB₂R agonist WIN55,212-2 has been used extensively to probe the endocannabinoid system (Figure 9). This significant aminoalkylindole does not display any activity at GPR55. Consistent data from various biological assays confirm that WIN55,212-2 does not bind GPR55 either as an agonist or an antagonist.^{7,2,24} JWH015, a WIN55,212-2 analogue was, however, able to activate GPR55 in [³⁵S]GTPγS assay with EC₅₀ value in the nanomolar range and was effective at

micromolar concentrations in Ca^{2+} mobilization assays.²⁴ Moreover, data from an ERK1/2 phosphorylation assay suggests that the CB₂R agonist GW405833 is a bitopic ligand of GPR55, acting as a partial agonist of GPR55 alone or as an allosteric modulator enhancing LPI signaling.³³

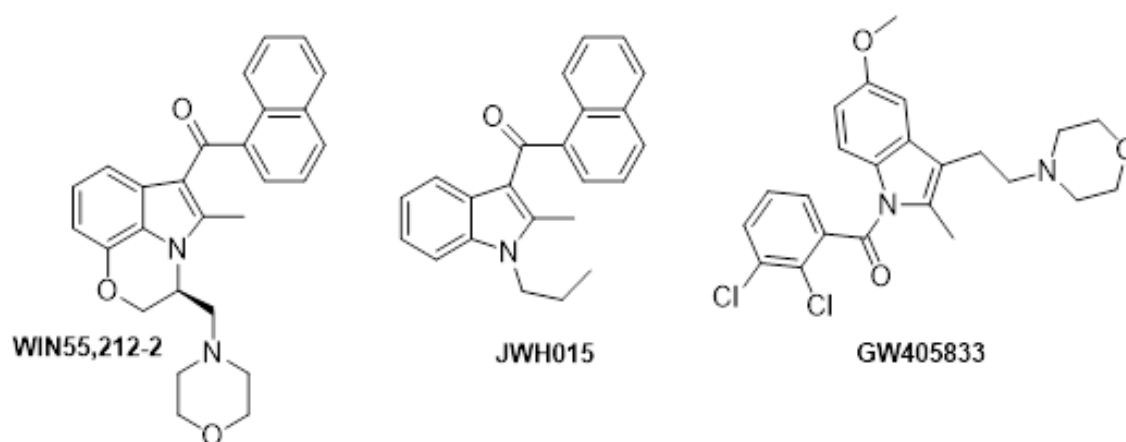


Figure 9. Synthetic Cannabinoid Ligands WIN55,212-2, JWH015, and GW405833.

Coumarins. The coumarin scaffold has shown great potential and versatility in the development of potent and highly selective CBRs ligands.⁷⁰ Reexamining this scaffold, using β -arrestin recruitment assays, uncovered 3-substituted coumarins as novel GPR55 antagonists.³⁴ Interaction with CBRs require a lipophilic substituent in position 7 (PSB-SB-487, Figure 10) while having a methyl at position 8 is favorable for GPR55 antagonism (PSB-SB-489, Figure 10). Deng et al.⁷¹ have developed computational QSAR models so that they might design coumarin derivatives with enhanced potency.

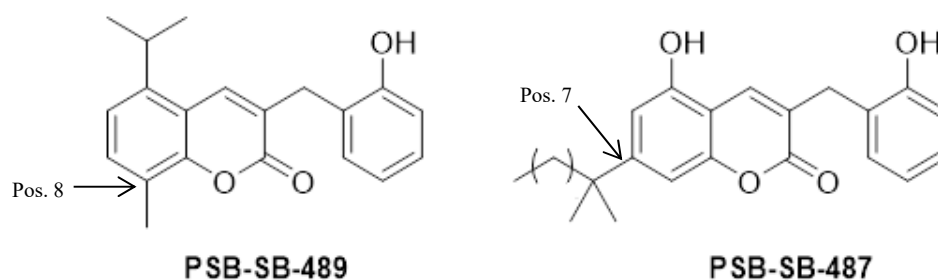


Figure 10. 3-(2-Hydroxybenzyl)-5-isopropyl-8-methyl-2*H*-chromen-2-one (PSB-SB-489) and 7-(1,1-dimethyloctyl)-5-hydroxy-3-(2-hydroxybenzyl)-2*H*-chromen-2-one (PSB-SB-487).

Magnolol derivatives. Magnolol (Figure 11) is one of the main bioactive compounds in the bark of *Magnolia officinalis*.⁷² This biphenylic compound and other related lignans are able to modulate CB₁R and CB₂R.⁷³ Magnolol acts as a partial CB₁R/CB₂R agonist whereas its major metabolite, tetrahydromagnolol, is a potent peripheral CB₂R agonist that acts as a weak antagonist of GPR55.⁷⁴ In a notable study, Müller et al.⁷⁵ developed structure-activity relationships of new magnolol analogues by varying the alkyl chains and the phenolic groups. They demonstrated that methylation of one of the hydroxyl groups (5'-hexyl-2'-methoxy-5-propylbiphenyl-2-ol) maximizes antagonistic potency when binding to GPR55. This structure represents an untapped potential lead compound in the development of new GPR55 antagonists.

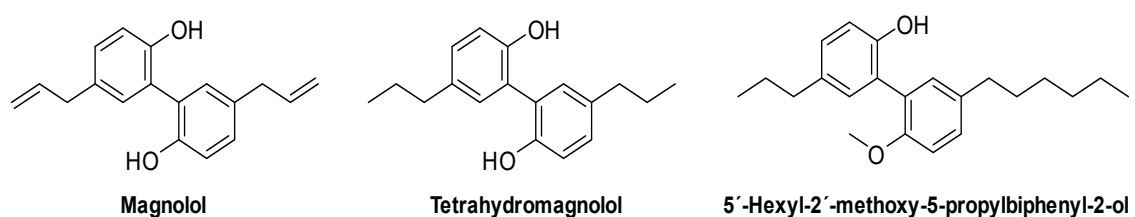


Figure 11. Magnolol and Analogues.

Non-cannabinoid Related Ligands of GPR55

The growing evidence that illuminates GPR55s involvement in innumerable biological pathways has generated great interest in this receptor as a therapeutic target.

The logical next step in maximizing this receptor's potential was the focused drive towards the identification of new selective GPR55 ligands. This drive gave rise to a collaborative project spanning three different laboratories and the Sanford-Burnham screening center of the Molecular Libraries Probe Production Centers Network (MLPCN)^{76,77} and allowed for the identification of six different GPR55 chemical scaffolds.^{76,77} This study began with high-throughput screening of a library of compounds using β -arrestin assays in U2OS cells permanently expressing HA-GPR55E and β arr2-GFP.⁵ As seen in Figure 12, Phenylpiperazine (CID2440433), triazoloquinoline (CID1172084) and morpholinesulfonylphenylamide (CID15945391), represent the potent GPR55 agonists discovered in this study⁷⁷ while piperidinyloxadiazolone (CID23612552), thienopyrimidine (CID1434953) and quinoline aryl sulfonamide CID1261822 are representative GPR55 antagonists.⁷⁶

Parallel studies,⁶⁸ undertaken by GlaxoSmithKline in 2011, validated the previously GSK developed benzoylpiperazine as a GPR55 agonists in *Saccharomyces cerevisiae* yeast and in HEK293 cells. GSK494581A, the most potent ligand, and GSK575594A, the most selective one, had been patented prior to this discovery as glycine transporter subtype 1 inhibitors (being 60-fold selective for GPR55) (Figure 13). Of note is the result that these ligands activate human but not rodent GPR55, hinting at important differences in the binding pocket of the two orthologs.

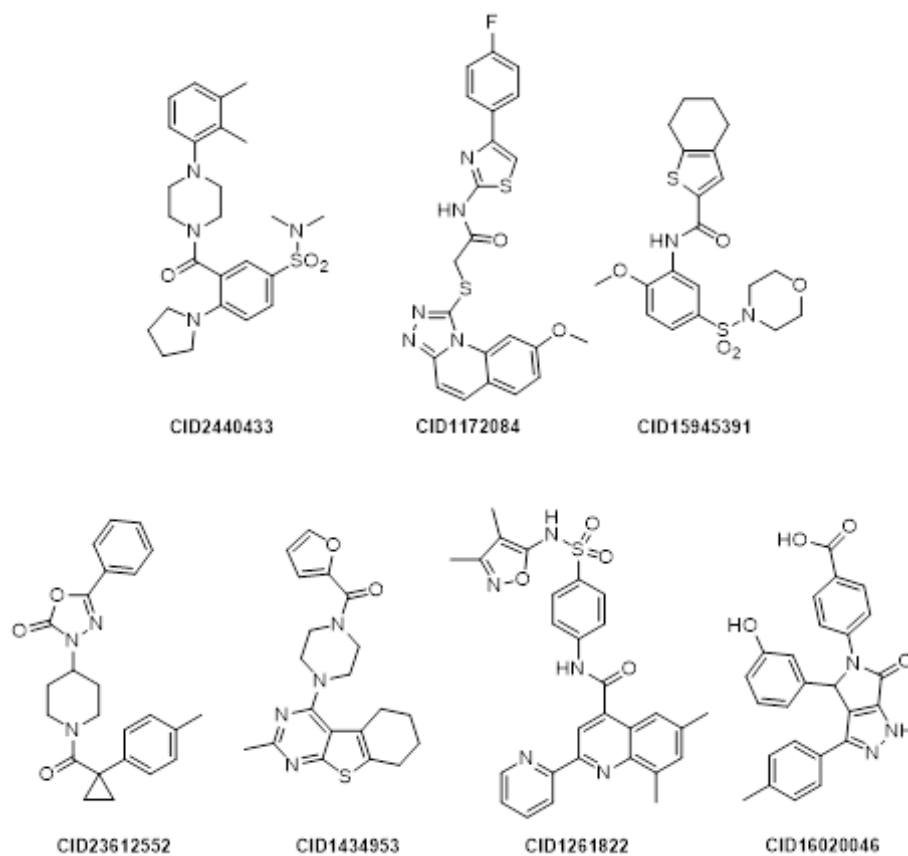


Figure 12. GPR55 Agonist Scaffolds (CID2440433, CID1172084, and CID15945391) and GPR55 Antagonist Scaffolds (CID23612552, CID1434953, and CID1261822) from HTS. CID16020046 Represents Another GPR55 Antagonist Recently Described by Kargl et al.⁷²

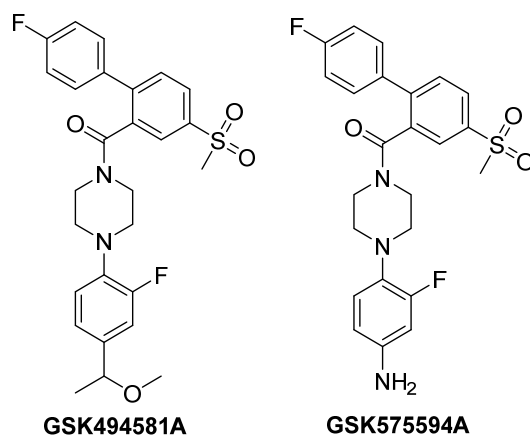


Figure 13. Benzoylpiperazines Previously Reported as Glycine Transporter Inhibitors.

In 2013, Kargl et al. identified CID16020046 (Figure 12) as a selective GPR55 antagonist.⁷⁸ This compound originated from the same MLSCN (Molecular Libraries Screening Centers Network) screen mentioned above; however, it was not selected by those researchers for further development at that time. This molecule antagonizes agonist-mediated GPR55 activation in yeast cells and inhibits GPR55-mediated intracellular Ca^{2+} release. CID16020046 reduces LPI signaling in primary human lung microvascular endothelial cells (HMVEC-L) and in human platelets suggesting yet another novel therapeutic application for GPR55.

An analogue of (*R,R'*)-fenoterol (a short-acting β 2-adrenergic agonist), with a 573-fold greater selectivity for β 2-AR than β 1-AR, has been shown to reduce GPR55 agonist efficiency.⁷⁹ The compound, (*R,R'*)-4'-methoxy-1-naphthylfenoterol (MNF, Figure 14), exerts selective inhibition of GPR55 signaling as demonstrated in various assays with readouts for ERK phosphorylation and cell motility. (*R,R'*)-MNF has been shown to reduce the pro-oncogenic activity of GPR55 thus revealing its therapeutic potential as an antitumor agent.

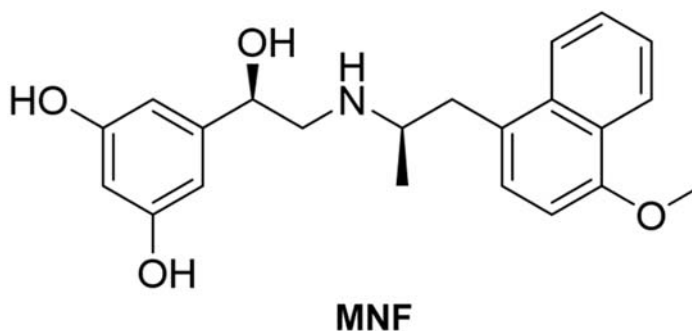


Figure 14. Naphthylfenoterol (MNF).

An analysis of the vast range of GPR55 scaffolds reported to this point may help to elucidate the structural motifs involved in modulating the activity of this receptor. It is hoped that this information will contribute to the work being done in the rational design of new compounds able to selectively and potently bind this promising target.

The construction of a comprehensive and current model of both the active and inactive state of the GPR55 receptor was therefore necessitated by the aforementioned results. Development of a binding site template, to guide the design of novel ligands with which to control the activation of this receptor, has the potential to be a vast and relatively unexploited therapeutic source. To date, no low nanomolar potency ligands have been identified or synthesized, nor has there been a radioligand developed to characterize binding at this receptor. The goal of the following research to be presented was the building, refinement and testing of two GPR55 receptor prototypes (an active state model and an inactive state model) to be used as a tool for exploring the ligand binding site. This predictive structure is essential for screening of current synthetic analogs and for the improved design of higher potency ligand profiles. Combining the extrapolative power of modern computational methods with the structure activity feedback from collaborating biochemists allows for a complete picture of the functioning model of GPR55 to be recognized.

References

1. Sawzdargo, M.; Nguyen, T.; Lee, D. K.; Lynch, K. R.; Cheng, R.; Heng, H. H.; George, S. R.; O'Dowd, B. F. Identification and Cloning of Three Novel Human G Protein-coupled Receptor Genes GPR52, Ψ GPR53 and GPR55: GPR55 is Extensively Expressed in Human Brain. *Brain. Res. Mol. Brain. Res.* **1999**, *64*, 193–198.
2. Drmota, P.; Greasley, P.; Groblewski, T. Screening Assays for Cannabinoid-Ligand Type Modulators. AstraZeneca Patent WO2004074844, 2004.
3. Brown, A. J.; Wise, A. Identification of Modulators of GPR55 Activity. GlaxoSmithKline Patent WO00186305, 2001.
4. Brown, A. J. Novel Cannabinoid Receptors. *Br. J. Pharmacol.* **2007**, *152*, 567–575.
5. Kapur, A.; Zhao, P.; Sharir, H.; Bai, Y.; Caron, M. G.; Barak, L. S.; & Abood, M. E. Atypical Responsiveness of the Orphan Receptor GPR55 to Cannabinoid Ligands. *J. Biol. Chem.* **2009**, *284*, 29817–29827.
6. Johns, D. G.; Behm, D. J.; Walker, D. J.; Ao, Z.; Shapland, E. M.; Daniels, D. A.; Riddick M.; Dowell, S.; Staton, P. C.; Green, P.; Shabon, U.; Bao, W.; Aiyar, N.; Yue, T. L.; Brown, A. J.; Morrison, A. D.; Douglas, S. A. The Novel Endocannabinoid Receptor GPR55 is Activated by Atypical Cannabinoids but Does Not Mediate Their Vasodilator Effects. *Br. J. Pharmacol.* **2007**, *152*, 825–831.
7. Ryberg, E.; Larsson, N.; Sjögren, S.; Hjorth, S.; Hermansson, N. O.; Leonova, J.; Elebring, T.; Nilsson, K.; Drmota, T.; Greasley, P. J. The Orphan Receptor GPR55 is a Novel Cannabinoid Receptor. *Br. J. Pharmacol.* **2007**, *152*, 1092–1101.
8. Staton, P. C.; Hatcher, J. P.; Walker, D. J.; Morrison, A. D.; Shapland, E. M.; Hughes, J. P.; Chong, E.; Mander, P. K.; Green, P. J.; Billinton, A.; Fulleylove, M.; Lancaster, H. C.; Smith, J. C.; Bailey, L. T.; Wise, A.; Brown, A. J.; Richardson, J. C.; Chessell, I. P. (2008). The Putative Cannabinoid Receptor GPR55 Plays a Role in Mechanical Hyperalgesia Associated with Inflammatory and Neuropathic Pain. *Pain* **2008** *139*(1), 225–236.

9. Leyva-Illades, D.; DeMorrow, S. Orphan G Protein Receptor GPR55 as an Emerging Target in Cancer Therapy and Management. *Cancer Manag. Res.* **2013**, *5*, 147–155.
10. Paul, R. K.; Wnorowski, A.; Gonzalez-Mariscal, I.; Nayak, S. K.; Pajak, K.; Moaddel, R.; Indiga, F. E.; Bernier, M.; Wainer, I. W. (R, R')-4'-methoxy-1-naphthylfenoterol Targets GPR55-mediated Ligand Internalization and Impairs Cancer Cell Motility. *Biochem. Pharmacol.* **2014**, *87*, 547–561.
11. Sharir, H.; Abood, M. E. Pharmacological Characterization of GPR55, a Putative Cannabinoid Receptor. *Pharmacol. Ther.* **2010**, *126*, 301–313.
12. Oka, S.; Nakajima, K.; Yamashita, A.; Kishimoto, S.; Sugiura, T. Identification of GPR55 as a Lysophosphatidylinositol Receptor. *Biochem. Bioph. Res. Co.* **2007**, *362*, 928–934.
13. Henstridge, C. M.; Balenga, N. A.; Ford, L. A.; Ross, R. A.; Waldhoer, M.; Irving, A. J. The GPR55 Ligand L- α -lysophosphatidylinositol Promotes RhoA-dependent Ca²⁺ Signaling and NFAT Activation. *FASEB J.* **2009**, *23*, 183–193.
14. Venkatakrisnan, A. J.; Deupi, X.; Lebon, G.; Tate, C. G.; Schertler, G. F.; Babu, M. M. Molecular Signatures of G-protein-coupled Receptors. *Nature* **2013**, *494*, 185–194.
15. Palczewski, K.; Kumasaka, T.; Hori, T.; Behnke, C. A.; Motoshima, H.; Fox, B. A.; Le Trong, I.; Teller, D. C.; Okada, T.; Stenkamp, R. E.; Yamamoto, M.; Miyano, M. (2000). Crystal Structure of Rhodopsin: A G Protein-coupled Receptor. *Science* **2000**, *289*, 739–745.
16. Elbegdorj, O.; Westkaemper, R. B.; & Zhang, Y. A Homology Modeling Study toward the Understanding of Three-dimensional Structure and Putative Pharmacological Profile of the G-protein Coupled Receptor GPR55. *J. Mol. Graph. Model.* **2013**, *39*, 50–60.
17. Kotsikorou, E.; Madrigal, K. E.; Hurst, D. P.; Sharir, H.; Lynch, D. L.; Heynen-Genel, S.; Milan, L. B.; Chung, T. D.; Seltzman, H. H.; Bai, Y.; Caron, M. G.; Barak, L.; Abood, M. E.; Reggio, P. H. Identification of the GPR55 Agonist Binding Site Using a Novel Set of High-potency GPR55 Selective Ligands. *Biochem.* **2011**, *50*, 5633–5647.
18. Ballesteros, J. A.; Weinstein, H. [19] Integrated Methods for the Construction of Three-dimensional Models and Computational Probing of Structure-function Relations in G Protein-coupled Receptors. *Methods in Neurosciences* **1995**, *25*, 366–428.

19. Kotsikorou, E.; Sharir, H.; Shore, D.; Hurst, D. P.; Lynch, D. L.; Madrigal, K. E.; Heynen-Genel, S.; Milan, L. B.; Chung, T. D. Y.; Seltzman, H. H.; Bai, Y.; Caron, M. G.; Barak, L.; Croatt, M. P.; Abood, M. E.; Reggio, P. H. Identification of the GPR55 Antagonist Binding Site Using a Novel Set of High-Potency GPR55 Selective Ligands. *Biochemistry* **2013**, *52*, 9456–9469.
20. Childers, S. R.; Deadwyler, S. A. Role of Cyclic AMP in the Actions of Cannabinoid Receptors. *Biochem. Pharmacol.* **1996**, *52*, 819–827.
21. Bonhaus, D. W.; Chang, L. K.; Kwan, J.; Martin, G. R. Dual Activation and Inhibition of Adenylyl Cyclase by Cannabinoid Receptor Agonists: Evidence for Agonist-Specific Trafficking of Intracellular Responses. *J. Pharmacol. Exp. Ther.* **1998**, *287*, 884–888.
22. Henstridge, C. M.; Balenga, N. A. B.; Ford, L. A.; Ross, R. A.; Waldhoer, M.; Irving, A. J. The GPR55 Ligand L-Alpha-Lysophosphatidylinositol Promotes RhoA-Dependent Ca²⁺ Signaling and NFAT Activation. *FASEB J.* **2009**, *23*, 183–193.
23. Waldeck-Weiermair, M.; Zoratti, C.; Osibow, K.; Balenga, N.; Goessnitzer, E.; Waldhoer, M.; Malli, R.; Graier, W. F. Integrin Clustering Enables Anandamide-Induced Ca²⁺ Signaling in Endothelial Cells via GPR55 by Protection against CB1-Receptor-Triggered Repression. *J. Cell Sci.* **2008**, *121*, 1704–1717.
24. Lauckner, J. E.; Jensen, J. B.; Chen, H.-Y.; Lu, H.-C.; Hille, B.; Mackie, K. GPR55 Is a Cannabinoid Receptor That Increases Intracellular Calcium and Inhibits M Current. *Proc. Natl. Acad. Sci. U. S. A.* **2008**, *105*, 2699–2704.
25. Henstridge, C. M.; Balenga, N. A.; Schröder, R.; Kargl, J. K.; Platzer, W.; Martini, L.; Arthur, S.; Penman, J.; Whistler, J. L.; Kostenis, E.; Waldhoer, M.; Irving, A. J. GPR55 Ligands Promote Receptor Coupling to Multiple Signalling Pathways. *Br. J. Pharmacol.* **2010**, *160*, 604–614.
26. Oka, S.; Toshida, T.; Maruyama, K.; Nakajima, K.; Yamashita, A.; Sugiura, T. 2-Arachidonoyl-Sn-Glycero-3-Phosphoinositol: A Possible Natural Ligand for GPR55. *J. Biochem.* **2009**, *145*, 13–20.
27. Henstridge, C. M. Off-Target Cannabinoid Effects Mediated by GPR55. *Pharmacology* **2012**, *89*, 179–187.
28. Park, P. S.-H. Ensemble of G Protein-Coupled Receptor Active States. *Curr. Med. Chem.* **2012**, *19*, 1146–1154.
29. Moreno, E.; Andradas, C.; Medrano, M.; Caffarel, M. M.; Pérez-Gómez, E.; Blasco-Benito, S.; Gómez-Cañas, M.; Pazos, M. R.; Irving, A. J.; Lluís, C.;

- Canela, E. I.; Fernández-Ruiz, J.; Guzmán, M.; McCormick, P. J.; Sánchez, C. Targeting CB2-GPR55 Receptor Heteromers Modulates Cancer Cell Signaling. *J. Biol. Chem.* **2014**, *289*, 21960–21972.
30. GPR18, GPR55 and GPR119: GPR55. IUPHAR/BPS Guide to Pharmacology <http://www.guidetopharmacology.org/GRAC/ObjectDisplayForward?objectId=109>. (accessed Aug 17, 2015).
31. Audet, M.; Bouvier, M. Restructuring G-Protein- Coupled Receptor Activation. *Cell* **2012**, *151*, 14–23.
32. Balenga, N. A.; Martínez-Pinilla, E.; Kargl, J.; Schröder, R.; Peinhaupt, M.; Platzer, W.; Bálint, Z.; Zamarbide, M.; Dopeso-Reyes, I.; Ricobaraza, A.; Pérez-Ortiz, J. M.; Kostenis, E.; Waldhoer, M.; Heinemann, A.; Franco, R. Heteromerization of GPR55 and Cannabinoid CB2 Receptors Modulates Signaling. *Br. J. Pharmacol.* **2014**, *171*, 5387–5406.
33. Anavi-Goffer, S.; Baillie, G.; Irving, A. J.; Gertsch, J.; Greig, I. R.; Pertwee, R. G.; Ross, R. A. Modulation of L- α -lysophosphatidylinositol/GPR55 Mitogen-Activated Protein Kinase (MAPK) Signaling by Cannabinoids. *J. Biol. Chem.* **2012**, *287*, 91–104.
34. Rempel, V.; Volz, N.; Gläser, F.; Nieger, M.; Bräse, S.; Müller, C. E. Antagonists for the Orphan G-Protein-Coupled Receptor GPR55 Based on a Coumarin Scaffold. *J. Med. Chem.* **2013**, *56*, 4798–4810.
35. Kenakin, T. P. Cellular Assays as Portals to Seven-Transmembrane Receptor-Based Drug Discovery. *Nat. Rev. Drug Discov.* **2009**, *8*, 617–626.
36. Pertwee, R. G.; Howlett, A. C.; Abood, M. E.; Alexander, S. P. H.; Marzo, V. Di; Elphick, M. R.; Greasley, P. J.; Hansen, H. S.; Kunos, G. International Union of Basic and Clinical Pharmacology. LXXIX. Cannabinoid Receptors and Their Ligands: Beyond CB1 and CB2. *Pharmacol. Rev.* **2010**, *62*, 588–631.
37. Venkatakrisnan, A. J.; Deupi, X.; Lebon, G.; Tate, C. G.; Schertler, G. F.; Babu, M. M. Molecular Signatures of G-Protein-Coupled Receptors. *Nature* **2013**, *494*, 185–194.
38. Ross, R. A. The Enigmatic Pharmacology of GPR55. *Trends Pharmacol. Sci.* **2009**, *30*, 156–163.
39. Moriconi, A.; Cerbara, I.; Maccarrone, M.; Topai, A. GPR55: Current Knowledge and Future Perspectives of a Purported “Type-3” Cannabinoid Receptor. *Curr. Med. Chem.* **2010**, *17*, 1411–1429.

40. Balenga, N. A. B.; Henstridge, C. M.; Kargl, J.; Waldhoer, M. *Pharmacology, Signaling and Physiological Relevance of the G Protein-Coupled Receptor 55.*; 1st ed.; Elsevier Inc., 2011; Vol. 62.
41. Sylantsev, S.; Jensen, T. P.; Ross, R. a; Rusakov, D. a. Cannabinoid- and Lysophosphatidylinositol-Sensitive Receptor GPR55 Boosts Neurotransmitter Release at Central Synapses. *Proc. Natl. Acad. Sci. U. S. A.* **2013**, *110*, 5193–5198.
42. Waldeck-Weiermair, M.; Zoratti, C.; Osibow, K.; Balenga, N.; Goessnitzer, E.; Waldhoer, M.; Malli, R.; Graier, W. F. Integrin Clustering Enables Anandamide-Induced Ca²⁺ Signaling in Endothelial Cells via GPR55 by Protection against CB1-Receptor-Triggered Repression. *J. Cell Sci.* **2008**, *121*, 1704–1717.
43. Bondarenko, A.; Waldeck-Weiermair, M.; Naghdi, S.; Poteser, M.; Malli, R.; Graier, W. F. GPR55-Dependent and -Independent Ion Signalling in Response to Lysophosphatidylinositol in Endothelial Cells. *Br. J. Pharmacol.* **2010**, *161*, 308–320.
43. Daly, C. J.; Ross, R. a; Whyte, J.; Henstridge, C. M.; Irving, a J.; McGrath, J. C. Fluorescent Ligand Binding Reveals Heterogeneous Distribution of Adrenoceptors and “Cannabinoid-like” Receptors in Small Arteries. *Br. J. Pharmacol.* **2010**, *159*, 787–796.
44. AlSuleimani, Y. M.; Hiley, C. R. The GPR55 Agonist Lysophosphatidylinositol Relaxes Rat Mesenteric Resistance Artery and Induces Calcium Release in Rat Mesenteric Artery Endothelial Cells. *Br. J. Pharmacol.* **2015**, *172*, 3043–3057.
45. Pietr, M.; Kozela, E.; Levy, R.; Rimmerman, N.; Lin, Y. H.; Stella, N.; Vogel, Z.; Juknat, A. Differential Changes in GPR55 during Microglial Cell Activation. *FEBS Lett.* **2009**, *583*, 2071–2076.
46. Balenga, N. A. B.; Aflaki, E.; Kargl, J.; Platzer, W.; Schröder, R.; Blättermann, S.; Kostenis, E.; Brown, A. J.; Heinemann, A.; Waldhoer, M. GPR55 Regulates Cannabinoid 2 Receptor-Mediated Responses in Human Neutrophils. *Cell Res.* **2011**, *21*, 1452–1469.
47. Liu, B.; Song, S.; Jones, P. M.; Persaud, S. J. GPR55: From Orphan to Metabolic Regulator? *Pharmacol. Ther.* **2015**, *145*, 35–42.
48. Jenkin, K. a; McAinch, A. J.; Zhang, Y.; Kelly, D. J.; Hryciw, D. H. Elevated Cannabinoid Receptor 1 and G Protein-Coupled Receptor 55 Expression in Proximal Tubule Cells and Whole Kidney Exposed to Diabetic Conditions. *Clin. Exp. Pharmacol. Physiol.* **2015**, *42*, 256–262.

49. Lanuti, M.; Talamonti, E.; Maccarrone, M.; Chiurchiù, V. Activation of GPR55 Receptors Exacerbates oxLDL-Induced Lipid Accumulation and Inflammatory Responses, While Reducing Cholesterol Efflux from Human Macrophages. *PLoS One* **2015**, *10*, e0126839.
50. Xiao, Y. J.; Schwartz, B.; Washington, M.; Kennedy, A.; Webster, K.; Belinson, J.; Xu, Y. Electrospray Ionization Mass Spectrometry Analysis of Lysophospholipids in Human Ascitic Fluids: Comparison of the Lysophospholipid Contents in Malignant vs Nonmalignant Ascitic Fluids. *Anal. Biochem.* **2001**, *290*, 302–313.
51. Sutphen, R.; Xu, Y.; Wilbanks, G. D.; Fiorica, J.; Grendys, E. C.; LaPolla, J. P.; Arango, H.; Hoffman, M. S.; Martino, M.; Wakeley, K.; Griffin, D.; Blanco, R. W.; Cantor, A. B.; Xiao, Y.; Krischer, J. P. Lysophospholipids Are Potential Biomarkers of Ovarian Cancer. *Cancer Epidemiol. Biomarkers Prev.* **2004**, *13*, 1185–1191.
52. Andradas, C.; Caffarel, M. M.; Pérez-Gómez, E.; Salazar, M.; Lorente, M.; Velasco, G.; Guzmán, M.; Sánchez, C. The Orphan G Protein-Coupled Receptor GPR55 Promotes Cancer Cell Proliferation via ERK. *Oncogene* **2011**, *30*, 245–252.
53. Pérez-Gómez, E.; Andradas, C.; Flores, J. M.; Quintanilla, M.; Paramio, J. M.; Guzmán, M.; Sánchez, C. The Orphan Receptor GPR55 Drives Skin Carcinogenesis and Is Upregulated in Human Squamous Cell Carcinomas. *Oncogene* **2013**, *32*, 2534–2542.
54. Karlsson, R.; Pedersen, E. D.; Wang, Z.; Brakebusch, C. Rho GTPase Function in Tumorigenesis. *Biochim. Biophys. Acta* **2009**, *1796*, 91–98.
55. He, D.; Wang, J.; Zhang, C.; Shan, B.; Deng, X.; Li, B.; Zhou, Y.; Chen, W.; Hong, J.; Gao, Y.; Chen, Z.; Duan, C. Down-Regulation of miR-675-5p Contributes to Tumor Progression and Development by Targeting pro-Tumorigenic GPR55 in Non-Small Cell Lung Cancer. *Mol. Cancer* **2015**, *14*, 1–14.
56. Hofmann, N. A.; Yang, J.; Trauger, S. A.; Nakayama, H.; Huang, L.; Strunk, D.; Moses, M. a; Klagsbrun, M.; Bischoff, J.; Graier, W. F. The GPR55 Agonist, L- α -Lysophosphatidylinositol, Mediates Ovarian Carcinoma Cell-Induced Angiogenesis. *Br. J. Pharmacol.* **2015**, 4107–4118.
57. Whyte, L. S.; Ryberg, E.; Sims, N. A.; Ridge, S. A.; Mackie, K.; Greasley, P. J.; Ross, R. A.; Rogers, M. J. The Putative Cannabinoid Receptor GPR55 Affects Osteoclast Function in Vitro and Bone Mass in Vivo. *Proc. Natl. Acad. Sci. U. S. A.* **2009**, *106*, 16511–16516.

58. Wu, C.-S.; Chen, H.; Sun, H.; Zhu, J.; Jew, C. P.; Wager-Miller, J.; Straiker, A.; Spencer, C.; Bradshaw, H.; Mackie, K.; Lu, H.-C. GPR55, a G-Protein Coupled Receptor for Lysophosphatidylinositol, Plays a Role in Motor Coordination. *PLoS One* **2013**, *8*, e60314.
59. Henstridge, C. M.; Balenga, N. a B.; Kargl, J.; Andradas, C.; Brown, A. J.; Irving, A.; Sanchez, C.; Waldhoer, M. Minireview: Recent Developments in the Physiology and Pathology of the Lysophosphatidylinositol-Sensitive Receptor GPR55. *Mol. Endocrinol.* **2011**, *25*, 1835–1848.
60. Dorsam, R. T.; Gutkind, J. S. G-Protein-Coupled Receptors and Cancer. *Nat. Rev. Cancer* **2007**, *7*, 79–94.
61. Lin, M.-E.; Herr, D. R.; Chun, J. Lysophosphatidic Acid (LPA) Receptors: Signaling Properties and Disease Relevance. *Prostaglandins Other Lipid Mediat.* **2010**, *91*, 130–138.
62. Pyne, N. J.; Pyne, S. Sphingosine 1-Phosphate and Cancer. *Nat. Rev. Cancer* **2010**, *10*, 489–503.
63. Yin, H.; Chu, A.; Li, W.; Wang, B.; Shelton, F.; Otero, F.; Nguyen, D. G.; Caldwell, J. S.; Chen, Y. A. Lipid G Protein-Coupled Receptor Ligand Identification Using Beta-Arrestin PathHunter Assay. *J. Biol. Chem.* **2009**, *284*, 12328–12338.
64. Nevalainen, T.; Irving, A. J. GPR55 , a Lysophosphatidylinositol Receptor with Cannabinoid Sensitivity? *Curr. Top. Med. Chem.* **2010**, *1*, 799–813.
65. Okuno, T.; Yokomizo, T. What Is the Natural Ligand of GPR55? *J. Biochem.* **2011**, *149*, 495–497.
66. Ford, L. A.; Roelofs, A. J.; Anavi-Goffer, S.; Mowat, L.; Simpson, D. G.; Irving, A. J.; Rogers, M. J.; Rajnicek, A. M.; Ross, R. a. A Role for L-Alpha-Lysophosphatidylinositol and GPR55 in the Modulation of Migration, Orientation and Polarization of Human Breast Cancer Cells. *Br. J. Pharmacol.* **2010**, *160*, 762–771.
67. Offertáler, L.; Mo, F.-M.; Bátkai, S.; Liu, J.; Begg, M.; Razdan, R. K.; Martin, B. R.; Bukoski, R. D.; Kunos, G. Selective Ligands and Cellular Effectors of a G Protein-Coupled Endothelial Cannabinoid Receptor. *Mol. Pharmacol.* **2003**, *63*, 699–705
68. Piñeiro, R.; Maffucci, T.; Falasca, M. The Putative Cannabinoid Receptor GPR55 Defines a Novel Autocrine Loop in Cancer Cell Proliferation. *Oncogene* **2011**, *30*, 142–152.

69. Valant, C.; Sexton, P. M.; Christopoulos, A. Orthosteric/Allosteric Bitopic Ligands: Going Hybrid at GPCRs. *Mol. Interv.* **2009**, *9*, 125–135.
70. Rempel, V.; Volz, N.; Hinz, S.; Karcz, T.; Meliciani, I.; Nieger, M.; Wenzel, W.; Bräse, S.; Müller, C. E. 7-Alkyl-3-Benzylcoumarins: A Versatile Scaffold for the Development of Potent and Selective Cannabinoid Receptor Agonists and Antagonists. *J. Med. Chem.* **2012**, *55*, 7967–7977.
71. Deng, F.-F.; Xie, M.-H.; Li, P.-Z.; Tian, Y.-L.; Zhang, X.-Y.; Zhai, H.-L. Study on the Antagonists for the Orphan G Protein-Coupled Receptor GPR55 by Quantitative Structure–activity Relationship. *Chemom. Intell. Lab. Syst.* **2014**, *131*, 51–60
72. Lee, Y.-J.; Lee, Y. M.; Lee, C.-K.; Jung, J. K.; Han, S. B.; Hong, J. T. Therapeutic Applications of Compounds in the Magnolia Family. *Pharmacol. Ther.* **2011**, *130*, 157–176.
73. Schuehly, W.; Paredes, J. M. V.; Kleyer, J.; Huefner, A.; Anavi-Goffer, S.; Raduner, S.; Altmann, K.-H.; Gertsch, J. Mechanisms of Osteoclastogenesis Inhibition by a Novel Class of Biphenyl-Type Cannabinoid CB(2) Receptor Inverse Agonists. *Chem. Biol.* **2011**, *18*, 1053–1064.
74. Rempel, V.; Fuchs, A.; Hinz, S.; Karcz, T.; Lehr, M.; Koetter, U.; Müller, C. E. Magnolia Extract, Magnolol, and Metabolites: Activation of Cannabinoid CB2 Receptors and Blockade of the Related GPR55. *ACS Med. Chem. Lett.* **2013**, *4*, 41–45.
75. Fuchs, A.; Rempel, V.; Müller, C. E. The Natural Product Magnolol as a Lead Structure for the Development of Potent Cannabinoid Receptor Agonists. *PLoS One* **2013**, *8*, e77739
76. Heynen-genel, S.; Dahl, R.; Shi, S.; Milan, L.; Sergienko, E.; Hedrick, M.; Dad, S.; Stonich, D.; Su, Y.; Chung, T. D. Y.; Sharir, H.; Caron, M. G.; Barak, L. S.; Aboud, M. E. Screening for Selective Ligands for GPR55-Antagonists. Probe Reports from the NIH Molecular Libraries Program; National Center for Biotechnology Information (U.S.): Bethesda, MD, 2010; <http://www.ncbi.nlm.nih.gov/books/NBK66153/>
77. Heynen-genel, S.; Dahl, R.; Shi, S.; Milan, L.; Bravo, Y.; Sergienko, E.; Hedrick, M.; Dad, S.; Stonich, D.; Su, Y.; Chung, T. D. Y.; Sharir, H.; Barak, L. S.; Aboud, M. E. Screening for Selective Ligands for GPR55-Agonists. Probe Reports from the NIH Molecular Libraries Program; National Center for Biotechnology Information (U.S.): Bethesda, MD, 2010; <Http://www.ncbi.nlm.nih.gov/books/NBK66152/>.

78. Kargl, J.; Brown, A. J.; Andersen, L.; Dorn, G.; Schicho, R.; Waldhoer, M.; Heinemann, A. A Selective Antagonist Reveals a Potential Role of G Protein-Coupled Receptor 55 in Platelet and Endothelial Cell Function. *J. Pharmacol. Exp. Ther.* **2013**, *346*, 54–66.
79. Paul, R. K.; Wnorowski, A.; Gonzalez-Mariscal, I.; Nayak, S. K.; Pajak, K.; Moaddel, R.; Indig, F. E.; Bernier, M.; Wainer, I. W. (R,R')-4'-Methoxy-1-Naphthylfenoterol Targets GPR55-Mediated Ligand Internalization and Impairs Cancer Cell Motility. *Biochem. Pharmacol.* **2014**, *87*, 547–561.
80. Kotsikorou, E.; Lynch, D. L.; Abood, M. E.; Reggio, P. H. Lipid Bilayer Molecular Dynamics Study of Lipid-Derived Agonists of the Putative Cannabinoid Receptor, GPR55. *Chem. Phys. Lipids* **2011**, *164*, 131–143

CHAPTER II

DESIGN, SYNTHESIS, AND ANALYSIS OF ANTAGONISTS OF GPR55: PIPERIDINE-SUBSTITUTED 1,3,4-OXADIAZOL-2-ONES

Introduction

The work described herein began as a collaborative project between the Reggio and Abood labs and the Sanford Burnham Screening Center of the Molecular Libraries Probe Production Centers Network (MLPCN). A series of GPR55 antagonists belonging to novel GPR55 antagonist chemotypes and having IC₅₀s in the 0.34 to 2.72 μ M range were identified (8). These compounds were then screened for agonist activity with GPR55 along with agonist/antagonist activity at both the CB1 and CB2 receptors. Several of the GPR55 antagonists identified were completely selective. Structure-activity relationship (SAR) studies of chemotype one were begun in the synthetic lab of Dr. Mitch Croatt. The results of initial ChemNavigator compound database substructure searches for Scaffolds 1-3 were used to guide the development of the research strategy to be presented in this chapter. Given GPR55's complicated pharmacological profile it is unsurprising that search results varied widely between scaffolds. Scaffold 1 had only 5 hits in the Aldrich database with a Tanimoto similarity of 70% or greater. Scaffold 2 (which will be expounded upon in Chapter IV) had 91 unique hits from the Aldrich database, of which only 39 could truly "fit" in the original GPR55 model. In contrast, Scaffold 3 had 161 unique hits from the Aldrich database, with all regions of space

sampled quite well. The readily available commercial analogs of scaffolds 2 and 3 lead to Scaffold 1 being chosen for initial ligand diversification.

The synthetic route was only three steps from simple starting materials: amide bond formation between the carboxylic acid and piperidone,³³ reductive amination of a hydrazide and the ketone,³⁴ and a carbonylative cyclization³⁵ (Scheme 1; Figure 15).

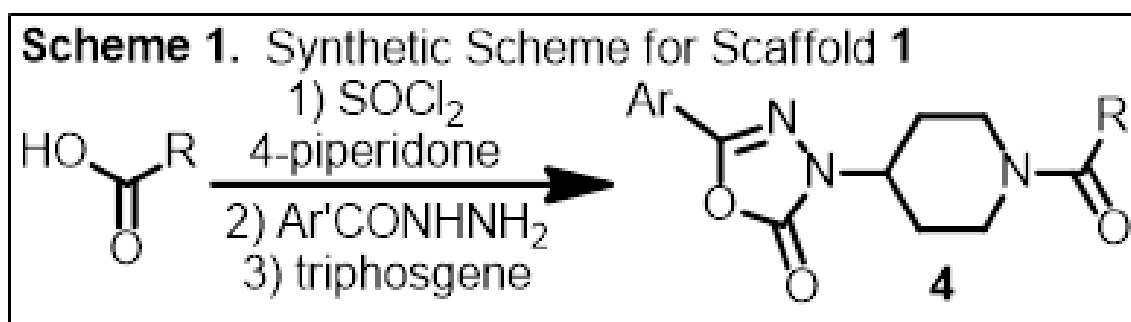


Figure 15. Scheme 1: Synthetic Scheme for Scaffold 1.

Figure 16 shows a subset of the available R-groups and Aryl-groups that were initially examined. It is also important to note that all of the commercially available analogues of parent compound **1** had the same phenyl group ($\text{Ar} = \text{Ph}$). The synthetic route proposed allowed for this position to be modified in hopes to observe a direct effect on the IC_{50} values. In the original model the carbonyl of the azoxazolone interacts with K2.60 so it is hypothesized that if we place electron-rich aryl-groups next to this heterocycle, we could strengthen the interactions between the ligand and the receptor.

Ar = Ph							
	5	6	7	8	9		
MW (amu)	389	419	424	432	399		
clogP	3.2	3.2	3.7	4.2	4.0		
clogBB	-0.2	-0.4	0.0	-0.4	-0.5		
R = cyclopropyl-anisole (as in 6)							
	Ar = 2-pyr	3-pyr	4-pyr	<i>p</i> -MeOPh	<i>p</i> -HOPh	<i>p</i> -F ₃ CPh	<i>m</i> -F ₃ CPh
	10	11	12	13	14	15	16
MW (amu)	420	420	420	450	435	487	487
clogP	2.6	2.2	2.2	3.3	2.9	4.2	4.3
clogBB	-0.7	-0.8	-0.5	-0.3	-1.2	0.1	0.1

Figure 16. Subset of Available R-groups and Aryl-groups That Were Initially Examined.

The overarching goal of the research presented in this chapter was the creation of a manageable library of synthetic antagonists with which to begin revision of the GPR55 model. It was postulated that results from the antagonist synthesis combined with mutation data from the Abood lab would aid in the revision of the initial GPR55 model that had been created in the Reggio lab. The revised model would then be used to guide synthesis of new ligands and allow for a chem-informatics search for additional chemotypes.

Design, Synthesis, and Analysis of Antagonists of Gpr55: Piperidine-Substituted 1,3,4-Oxadiazol-2-Ones

As submitted to *Organic Medicinal Chemistry Letters**

Maria Elena Meza-Aviña^{a,†}, Mary A. Lingerfelt^{a,†}, Linda M. Console-Bram^b, Thomas F. Gamage^b, Haleli Sharir^b, Kristen E. Gettys^a, Dow P. Hurst^a, Evangelia Kotsikorou^c, Derek M. Shore^a, Marc G. Caron^d, Narasinga Rao^a, Larry S. Barak^d, Mary E. Abood^{b,*}, Patricia H. Reggio^{a,*}, Mitchell P. Croatt^{a,*}

^a Department of Chemistry and Biochemistry, Natural Products and Drug Discovery Center, University of North Carolina at Greensboro, Greensboro, North Carolina 27402, United States

^b Center for Substance Abuse Research, Temple University, Philadelphia, Pennsylvania 19140, United States

^c Department of Chemistry, University of Texas-Pan American, Edinburg, Texas 78539, United States

^d Duke University Medical Center, Durham, North Carolina 27709, United States

[†] These authors contributed equally to this work

*This chapter was created by inserting the above cited paper, verbatim, with the following differences:

- 1) Figures/Tables were re-rendered/resized to match dissertation global style.
- 2) Page layout has been altered from published form to meet dissertation layout requirements (i.e. the use of 1 column vs. 2, etc.)

Abstract

A series of 1,3,4-oxadiazol-2-ones was synthesized and tested for activity as antagonists at GPR55 in cellular beta-arrestin redistribution assays. The synthesis was designed to be modular in nature so that a sufficient number of analogues could be rapidly accessed to explore initial structure-activity relationships. The design of analogues was guided by the docking of potential compounds into a model of the inactive form of GPR55. The results of the assays were used to learn more about the binding pocket of GPR55. With this oxadiazolone scaffold, it was determined that modification of the aryl group adjacent to the oxadiazolone ring was often detrimental and that the distal

cyclopropane was beneficial for activity. These results will guide further exploration of this receptor.

Introduction

GPR55, a recently orphanized, rhodopsin-like (class A) G protein-coupled receptor (GPCR), is a receptor for 1- α -lysophosphatidylinositol (LPI, Figure 17) which serves as the endogenous agonist (GenBank entry NM 005683).¹ Initial studies noted that a variety of CB1 and CB2 ligands bind to GPR55^{2,3} and more recent studies have focused on physiological roles for GPR55 in inflammatory pain,² neuropathic pain,² bone development,³ and the potential for activation of GPR55 being pro-carcinogenic.^{4,5,6,7,8} Despite the important potential biological functions of GPR55, the research is limited by the lack of both potent and selective agonists and antagonists.^{9,10}

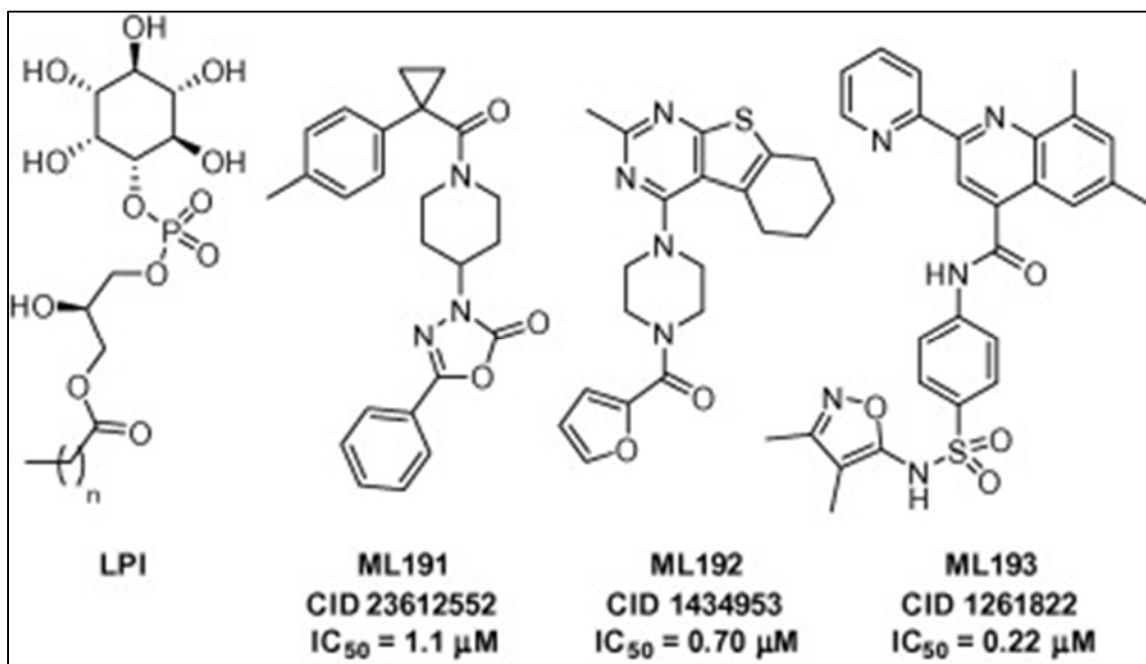


Figure 17. LPI and Lead Antagonists of GPR55.¹²

Based on a high-throughput, high-content screen of approximately 300,000 compounds from the Molecular Libraries Probe Production Centers Network initiative,¹¹ a few molecular scaffolds were identified that had relatively good selectivity and potency as antagonists at GPR55. These structures were then docked into the inactive state model of GPR55¹² to visualize the key features of the antagonists. Of the compounds that exhibited selective and moderate activity as antagonists at GPR55, three different structural families were identified as illustrated by ML191, ML192, and ML193 (Figure 17). The docking of the structures in Figure 17 into the inactive state model of GPR55 indicated a few important interactions as we previously reported.¹² Briefly, the primary interaction was hydrogen bonding between the lysine at position 2.60(80)¹³ and the oxadiazolone carbonyl in ML191, the amide carbonyl in ML192, or an oxygen of the sulfonamide in ML193. The hypothesized interactions with K2.60(80) positioned the bottom aryl rings of all three structures, as represented in Figure 18, to maintain the toggle switch interaction between M3.36(105) and F6.48(239). The remaining interactions of the ligands presented in Figure 18 and GPR55 are primarily aromatic stacking with various residues. Specifically for ML191, the toluene ring attached to the cyclopropane stacks with F169 and the phenyl group attached to the oxadiazolone stacks with F6.55(246) and F3.33(102) (Figure 18). In addition to these interactions, moderate beneficial van der Waals interactions were identified between the oxadiazolone and both M7.39(274) and Y3.32(101). Since the interactions between ML191 and GPR55 centered on the three aromatic rings of ML191, compounds were desired that modified the electronics and sterics of these areas. Hence, the ML191 synthetic studies reported herein

were undertaken to explore the SAR of this oxadiazolone class of compounds. ML191 was also chosen as the lead antagonist since there are very few structurally related compounds that could be purchased and screened compared to the available compounds for ML192 and ML193.

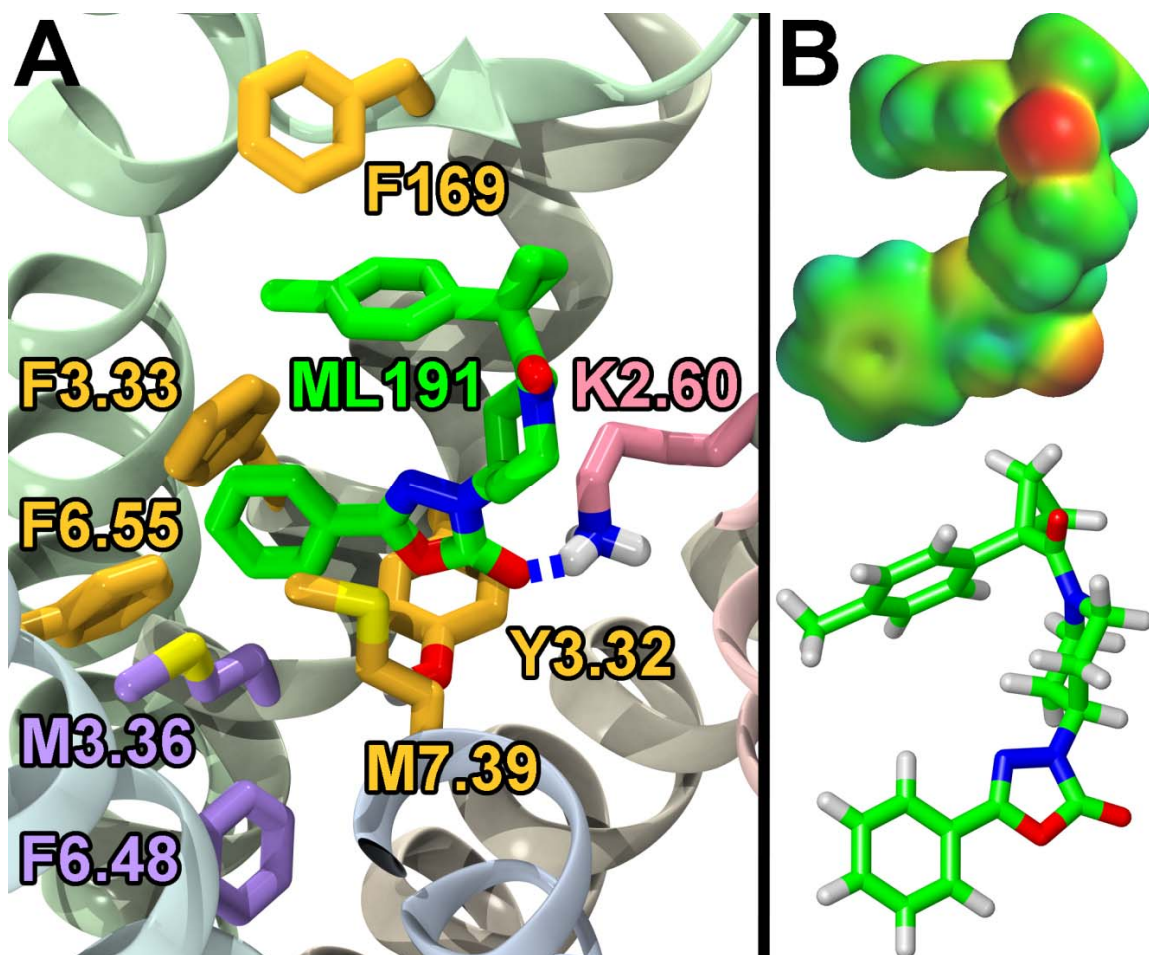


Figure 18. (A) Docking and Key Interactions between ML191 and GPR55. ML191 (Green) Has a Key H-bond Interaction with K2.60 (Pink). ML191 Also Has π -stacking or Other van der Waals Interactions with F169, F3.33, F6.55, M7.39, and Y3.32 (All Mustard). The Interactions with M7.39 and F6.55 Appear to Hinder the Rotation of M3.36 and F6.48 (Both Purple) Which Are Considered the Toggle Switch for GPR55. (B) Electrostatic Potential Map of ML191. This Figure is Adapted from Previously Published Work.¹²

Our synthetic approach to GPR55 antagonists was designed so that many different structures could be accessed to rapidly explore initial SAR, along with validating or modifying our current model (Figure 18).¹¹ The synthesis begins with the coupling of a carboxylic acid to 4-piperidone by first forming the acid chloride (Scheme 1a; Figure 19). The different acids chosen, based on the initial hit, modify the electronics and sterics of this section of the molecule. Relative to ML191, compound **2a** reduces the steric impact, **2b** increases the electron-density in the aromatic ring, and compounds **2c** and **2d** decrease the electron-density. Compounds **2e** and **2f** were selected to examine the influence of steric bulk at the position of the cyclopropane ring. The largest change in overall structure relates to the 1-naphthoic acid derivative (**2f**). Although the naphthalene ring is structurally different, this analogue can position the distal aromatic ring in a similar position as the phenyl rings of the other analogues since the bond angle for the C α will be similar to that of the cyclopropane analogues, however, this structure is much flatter.

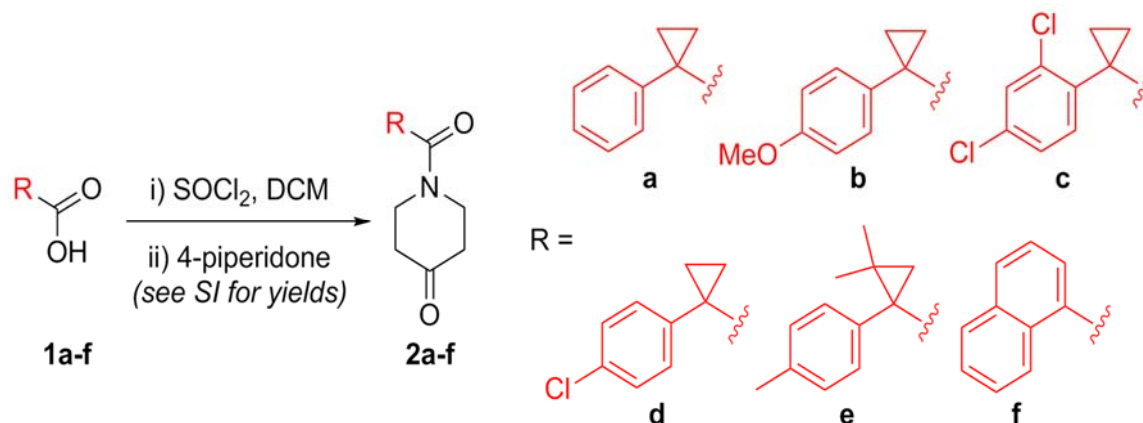


Figure 19. Scheme 1a: Synthesis of Acylated Piperidones.

With a handful of acylated piperidones prepared, the final two steps first involved a reductive coupling of aryl hydrazides (**3t–z**) with the previously synthesized piperidones (**2a–f**) to yield hydrazides **4** (Scheme 2; Figure 20).¹⁴ These compounds were then cyclocarbonylated using triphosgene to yield oxadiazolones **5**.¹⁵ The reductive coupling reactions proceeded smoothly but the products of that step were often unstable to silica gel chromatography. Therefore, the unpurified products were treated with triphosgene without further purification. This modification of the synthesis typically improved the yields of the final compounds (see Supplementary Data in Appendix A for individual yields).

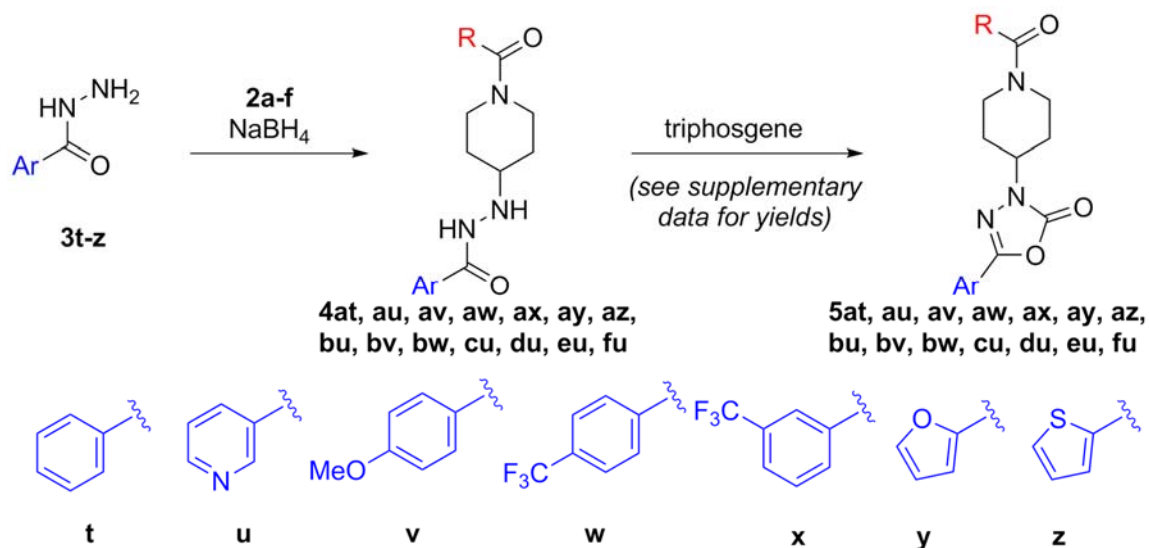


Figure 20. Scheme 2: Synthesis of GPR55 Antagonists.

Similar to the cyclopropane starting materials (**1a–f**), the hydrazides (**3t–z**) were selected to probe the electronic and steric opportunities in the binding site. Based on the current model (Figure 18), the aromatic ring adjacent to the oxadiazolone is involved in

an interaction with M3.36(105) and F6.48(239). Additionally, the oxadiazolone contributes as the key interaction between the basic carbonyl oxygen with the ammonium of K2.60(80). Thus, electron rich aromatic rings adjacent to the oxadiazolone should make the carbonyl oxygen more basic and strengthen this interaction.

A targeted exploration of the SAR of all six acids (**1a–f**) with hydrazide **3t** and all seven hydrazides (**3t–z**) with acid **1a** (Figure 19 and Table 1) was performed instead of synthesizing and exploring the biological activity of all 42 permutations of the six acids and seven hydrazides. Acid **1a** and hydrazide **3t** were chosen as the constants since these were the most simplified pieces consisting of an unsubstituted phenyl ring.

Unfortunately, there were solubility issues with some of the compounds (e.g., **5bt** and **5bv**), so additional combinations were required to elucidate the effect of the different areas of the scaffold.

Table 1

GPR55 Antagonist Activity of Compounds

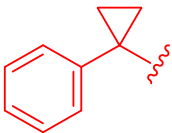
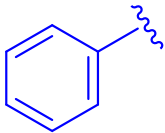
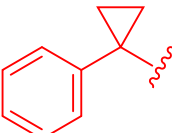
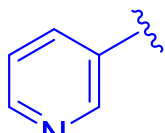
Entry, Compound	R	Ar	IC ₅₀ ^a (95% CI)
1, 5at			12 μM (3.9 - 36)
2, 5au			0.42 μM (0.075 - 2.4)

Table 1

Cont.

Entry, Compound	R	Ar	IC ₅₀ ^a (95% CI)
3, 5av			7.0 μM (0.47 - 100)
5, 5bt			insol. ^b
6, 5bv			insol. ^b
7, 5bw			1.8 μM (0.74 - 4.3)
8, 5ct			2.5 μM (1.3 - 5.0)
9, 5dt			0.64 μM (0.33 - 1.2)
10, 5et			0.77 μM (0.39 - 1.5)

Note. IC₅₀ values and 95% confidence intervals (CI) were determined by running the sample in triplicate versus a 6 μM concentration of LPI. ^bCompound was not completely soluble at the concentrations of the assay.

Compounds were initially screened via an image-based cell assay to identify antagonist activity. The rationale for using the β -arrestin recruitment assay was to provide a fair comparison of IC_{50} values since our initial report employed this assay.^{11,12} Briefly, U2OS cells overexpressing GPR55 and β arr2-GFP were exposed to LPI (6 μ M; EC_{80}) resulting in the recruitment of β -arrestin. Antagonist activity was evaluated by ligand-mediated inhibition of LPI-induced receptor activation. This strategy quickly identified the compounds that had IC_{50} values higher than 15 μ M which were excluded from further analysis (Figure 21).

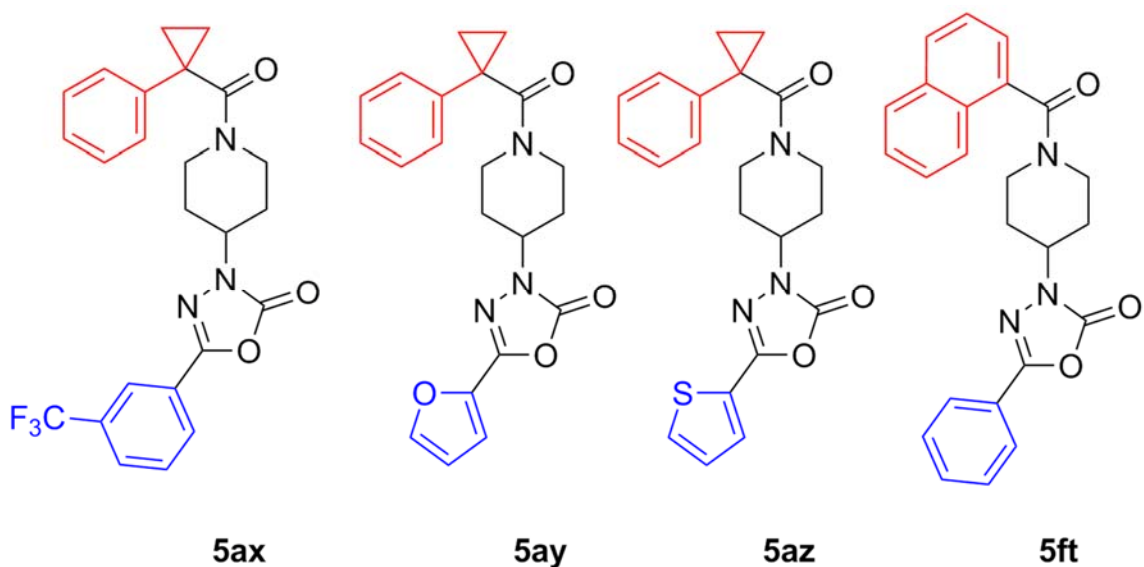


Figure 21. Analogues with Poor Activity (>15 μ M).

Concentration response curves were generated for compounds that were active at concentrations below 15 μ M employing both the image-based β -arrestin recruitment assay and the DiscoverX PathHunter® chemiluminescent β -arrestin complementation assay. In the DiscoverX PathHunter® system, CHO-K1 cells stably expressing GPR55

(fused with a β -galactosidase enzyme fragment), and β -arrestin (fused to an N-terminal deletion mutant of β -galactosidase) were used to quantitate the inhibition of LPI-induced β -arrestin activity (Figure 22, Table 1). Hence, antagonist activity was evaluated through the use of two differential means of β -arrestin quantitation, in two different cellular backgrounds (see Supplemental information, Biological Assay). IC_{50} values were similar in both methodologies.

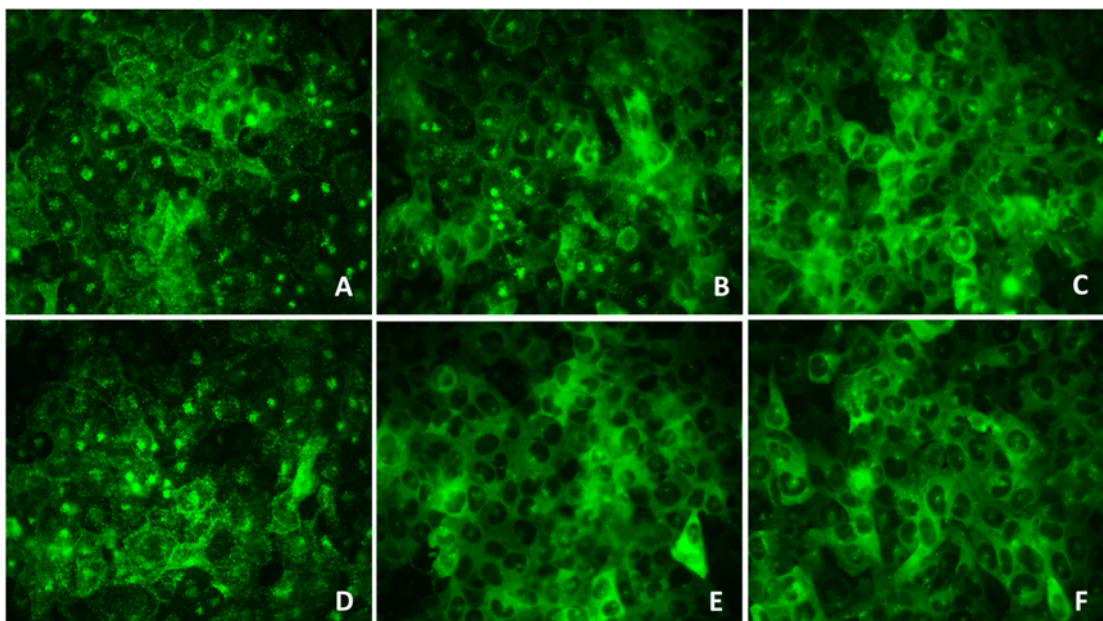


Figure 22. Representative Images of Antagonist Screening. (A) 0.1 μ M **5dt** + LPI; (B) 1.0 μ M **5dt** + LPI; (C) 10 μ M **5dt** + LPI; (D) 3 μ M LPI; (E) 10 μ M **5dt**; (F) DMSO.

Screening of the compounds allowed for a number of interesting SAR observations. First of all, pyridyl analogue **5au** demonstrated that a pyridine ring would be beneficial for both $c \log P$ as well as increasing the potency (entry 2 versus entry 1). Electron-poor aryl groups next to the oxadiazolone were detrimental (Figure 21), but electron-rich groups were also not beneficial (entry 3). As discussed earlier, it was

anticipated that the more electron-rich aryl groups next to the oxadiazolone would be beneficial electronically, but the results obtained could be validated by the electron-donating groups being larger and creating some detrimental steric interactions.

It was found that electron-rich cyclopropylaryl groups had relatively good activities (entry 7), but also typically had solubility problems (entries 5 and 6). Fortunately, analogue **5bw** was soluble, but the moderate activity illustrates that the *p*-methoxy group is detrimental since the most closely related analogue (ML191, Figure 17) was more active and the electron-withdrawing *p*-chloro analogue (**5dt**) was even more active. Dichlorophenyl analogue **5ct** had good activity, but was not as potent as compared to the monochloroaryl compound (entries 8 and 9) which could be justified based on the larger steric bulk of the second chlorine atom. Structure **5et** with the dimethylcyclopropyl group was similarly active (entry 10) as compared to the parent compound, ML191 (Figure 17) which is interesting since this compound adds more steric bulk to the cyclopropyl aryl section of the molecule, albeit in a slightly different location than analogue **5ct**. It should be noted that analogue **5et** is the only structure analyzed that is chiral. The synthesis of **5et** was racemic and the model indicates that there are no major anticipated differences in activities between the two enantiomers.

In conclusion, this letter presents initial SAR for piperidine-substituted oxadiazolone antagonists at GPR55, a recently deorphanized G protein-coupled receptor that lacks a potent and selective ligand of nanomolar potency. These data help to better define areas for improvement of this family of GPR55 antagonists since both halves of the molecule were independently modified. The activities spanned about two orders of

magnitude and will be used as a guide for future efforts which will be published in due time.

Acknowledgments

This research was supported by National Institutes of Health Grants R21NS077347, R01DA023204, T32DA007237, and P30DA013429. The authors thank Dr. Franklin J. Moy (UNCG) for assisting with analysis of NMR data and Dr. Brandie M. Ehrmann (UNCG) for acquisition of the high-resolution mass spectrometry data at the Triad Mass Spectrometry Laboratory at the University of North Carolina at Greensboro.

References

1. Henstridge, C. M.; Balenga, N. A. B.; Kargl, J.; Andradas, C.; Brown, A. J.; Irving, A.; Sanchez, C.; Waldhoer, M. Minireview: Recent Developments in the Physiology and Pathology of the Lysophosphatidylinositol-Sensitive Receptor GPR55. *Mol. Endocrinol.* **2011**, *25*, 1835–1848.
2. Staton, P. C.; Hatcher, J. P.; Walker, D. J.; Morrison, A. D.; Shapland, E. M.; Hughes, J. P.; Chong, E.; Mander, P. K.; Green, P. J.; Billinton, A.; Fulleylove, M.; Lancaster, H. C.; Smith, J. C.; Bailey, L. T.; Wise, A.; Brown, A. J.; Richardson, J. C.; Chessell, I. P. The Putative Cannabinoid Receptor GPR55 Plays a Role in Mechanical Hyperalgesia Associated with Inflammatory and Neuropathic Pain. *PAIN* **2008**, *139*, 225–236.
3. Whyte, L. S.; Ryberg, E.; Sims, N. A.; Ridge, S. A.; Mackie, K.; Greasley, P. J.; Ross, R. A.; Rogers, M. J. The Putative Cannabinoid Receptor GPR55 Affects Osteoclast Function in Vitro and Bone Mass in Vivo. *Proc. Natl. Acad. Sci. USA* **2009**, *106*, 16511–16516.
4. Ford, L. A.; Roelofs, A. J.; Anavi-Goffer, S.; Mowat, L.; Simpson, D. G.; Irving, A. J.; Rogers, M. J.; Rajnicek, A. M.; Ross, R. A. A Role for L-Alpha-Lysophosphatidylinositol and GPR55 in the Modulation of Migration, Orientation and Polarization of Human Breast Cancer Cells. *Br. J. Pharmacol.* **2010**, *160*, 762–771.
5. Andradas, C.; Caffarel, M. M.; Pérez-Gómez, E.; Salazar, M.; Lorente, M.; Velasco, G.; Guzmán, M.; Sánchez, C. The Orphan G Protein-coupled Receptor GPR55 Promotes Cancer Cell Proliferation via ERK. *Oncogene* **2011**, *30*, 245–252.
6. Pineiro, R.; Maffucci, T.; Falasca, M. The Putative Cannabinoid Receptor GPR55 Defines a Novel Autocrine Loop in Cancer Cell Proliferation. *Oncogene* **2011**, *30*, 142–152.
7. Pérez-Gómez, E.; Andradas, C.; Flores, J. M.; Quintanilla, M.; Paramio, J. M.; Guzmán, M.; Sánchez, C. The Orphan Receptor GPR55 Drives Skin Carcinogenesis and is Upregulated in Human Squamous Cell Carcinomas. *Oncogene* **2013**, *32*, 2534–2542.
8. Sharir, H.; Abood, M. E. Pharmacological Characterization of GPR55, a Putative Cannabinoid Receptor. *Pharmacol. Ther.* **2010**, *126*, 301–313.

9. Brown, A. J.; Daniels, D. A.; Kassim, M.; Brown, S.; Haslam, C. P.; Terrell, V. R.; Brown, J.; Nichols, P. L.; Staton, P. C.; Wise, A.; Dowell, S. J. Pharmacology of GPR55 in Yeast and Identification of GSK494581A as a Mixed-Activity Glycine Transporter Subtype 1 Inhibitor and GPR55 Agonist. *J. Pharmacol. Exp. Ther.* **2011**, *337*, 236–246.
10. Yin, H.; Chu, A.; Li, W.; Wang, B.; Shelton, F.; Otero, F.; Nguyen, D. G.; Caldwell, J. S.; Chen, Y. A. Lipid G Protein-Coupled Receptor Ligand Identification Using Beta-Arrestin PathHunter Assay. *J. Biol. Chem.* **2009**, *284*, 12328–12338.
11. Heynen-Genel, S.; Dahl, R.; Shi, S.; Milan, L.; Hariharan, S.; Sergienko, E.; Hendrick, M.; Dad, S.; Stonich, D.; Su, Y.; Vicchiarelli, M.; Mangravita-Novo, A.; Smith, L. H.; Chung, T. D. Y.; Sharir, H.; Caron, M. G.; Barak, L. S.; Abood, M. E. Screening for Selective Ligands for GPR55: Antagonists; National Institutes of Health: Bethesda, MD, 2010.
12. Kotsikorou, E.; Sharir, H.; Shore, D. M.; Hurst, D. P.; Lynch, D. L.; Madrigal, K. E.; Heynen-Genel, S.; Milan, L. B.; Chung, T. D. Y.; Seltzman, H. H.; Bai, Y.; Caron, M. G.; Barak, L. S.; Croatt, M. P.; Abood, M. E.; Reggio, P. H. Identification of the GPR55 Antagonist Binding Site Using a Novel Set of High-Potency GPR55 Selective Ligands. *Biochem.* **2013**, *52*, 9456–9469.
13. Kapur, A.; Zhao, P.; Sharir, H.; Bai, Y.; Caron, M. G.; Barak, L. S.; Abood, M. E. Atypical Responsiveness of the Orphan Receptor GPR55 to Cannabinoid Ligands. *J. Biol. Chem.* **2009**, *284*, 29817–29827.
14. Verheijen, J. C.; Richard, D. J.; Curran, K.; Kaplan, J.; Lefever, M.; Nowak, P.; Malwitz, D. J.; Brooijmans, N.; Toral-Barza, L.; Zhang, W.-G.; Lucas, J.; Hollander, I.; Ayril-Kaloustian, S.; Mansour, T. S.; Yu, K.; Zask, A. Discovery of 4-Morpholino-6-aryl-1H-pyrazolo[3,4-d]pyrimidines as Highly Potent and Selective ATP-Competitive Inhibitors of the Mammalian Target of Rapamycin (mTOR): Optimization of the 6-Aryl Substituent. *J. Med. Chem.* **2009**, *52*, 8010–8024.
15. Jiang, L. -L.; Tan, Y.; Zhu, X. -L.; Wang, Z. -F.; Zuo, Y.; Chen, Q.; Xi, Z.; Yang, G. -F. *J. Ag. Food Chem.* **2010**, *58*, 2643–2651.

CHAPTER III

BUILDING OF THE ACTIVE AND INACTIVE STATE MODELS OF GPR55

Introduction

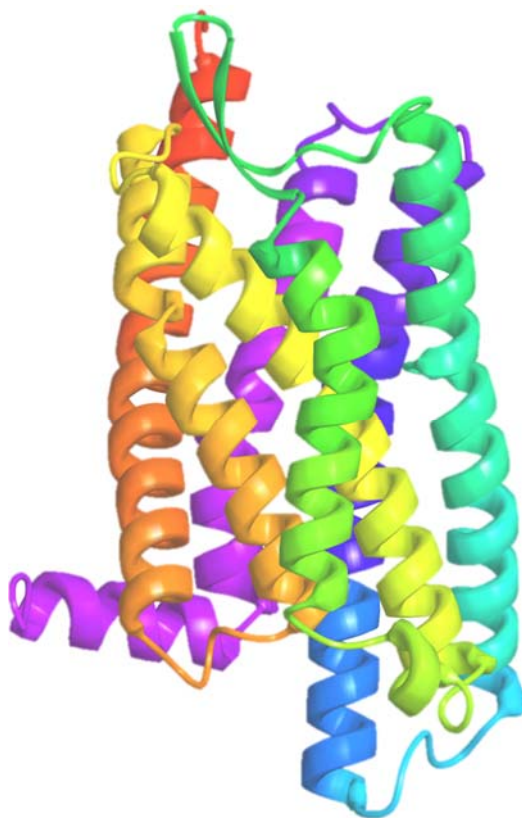
The previous GPR55 homology model (Evangelia et al.)¹, was created using the crystal structure of the β 2-adrenergic receptor (Protein Data Bank entry 2RH1)² as a template. That model was later altered to reflect several structural elements that were observed in the recently crystallized structure of the CXCR4 receptor in its inactive state.³ The impetus for the current revision of the receptor originates from the pursuit of two goals: (a) A desire to explain new mutation results, suggesting that K2.60 and E3.29 are crucial residues for binding in GPR55 and (b) The need to have an up-to-date model that reflects the high degree of sequence homology GPR55 shares with a logically chosen crystal structure template and that incorporates the structural information gleaned from both the agonist and antagonist ligands that have been synthesized thus far.

In the work discussed here, the Ballesteros-Weinstein numbering system for Class A GPCRs will be used.⁴ In this numbering system, the position of each residue is labeled by two numbers. The first (1 through 7) corresponds to the transmembrane helix (TMH) in which the residue is located. The number following the helix indicates the residue's position relative to the most highly conserved residue (among Class A GPCRs) in that helix. The conserved residue in each helix being given the number .50 and residues before or after it are numbered accordingly.

Sequence alignments (Figure 23) have been compiled which compare GPR55 with CB1, CB2, the h- δ -opioid receptor and other Class A GPCRs. These alignments allow for a more facile comparison of amino acid sequence similarities and deviations between receptors. The same highly conserved residues that have been used in the past to align the sequences of CB1⁵⁻⁹ and CB2^{10,11} to that of bovine rhodopsin were used as alignment guides for GPR55. These residues are the most highly conserved residues across Class A GPCRs: TMH1 - N1.50, TMH2 - D2.50, TMH3 - E/D3.49, R3.50, Y3.51 (DRY motif), TMH4 - W4.50, TMH5 - P5.50, TMH6 - C6.47, W6.48, X (this residue varies), P6.50 (CWXP motif), and TMH7 - N7.49, P-7.50, X, X, Y7.53. Sequence patterns are easily identifiable on multiple sequence alignments and allow for easy comparison among residues in the transmembrane regions of different receptors. While GPR55 possesses some of the highly conserved .50 residues (N1.50, D2.50, W4.50 and P5.50) found in many GPCRs, there are a few notable differences. GPR55 has a conservative substitution (DRF) for the TMH3 E/DRY motif, a conservative substitution (SFLP) for the TMH6 CWXP motif, and a non-conservative substitution (DVFCY) for the THM7 NPXXY motif. Outside of the TMH region, GPR55 has an extracellular-1 (EC-1) loop that is shorter than most (three residues versus the six found in β 2-AR and Rhodopsin) and an EC-3 loop that is noticeably longer (fourteen residues long versus the five in β 2-AR and the six residues in rhodopsin, CB1 and CB2). Based upon sequence alignments from the Reggio lab, the template chosen for the new GPR55 models was the **δ -Opioid Receptor**.¹² See Figure 24.

	3	3	3	3	3	3	3	3	3	3	3	3	3	3	3	3	3	3	3	3	3	3	3	3	TMH #
	3	3	3	3	3	3	3	3	4	4	4	4	4	4	4	4	4	4	4	4	4	5	5	5	←
Receptor type	2	3	4	5	6	7	8	9	0	1	2	3	4	5	6	7	8	9	0	1	Res. IDs				
Rho	A	T	L	G	G	E	I	A	L	W	S	L	V	V	L	A	I	E	R	Y					
D3	D	V	M	M	C	T	A	S	I	L	N	L	C	A	I	S	I	D	R	Y					
D2L3	D	V	M	M	C	T	A	S	I	L	N	L	C	A	I	S	I	D	R	Y					
D2S	D	V	M	M	C	T	A	S	I	L	N	L	C	A	I	S	I	D	R	Y					
D2L	D	V	M	M	C	T	A	S	I	L	N	L	C	A	I	S	I	D	R	Y					
D1	D	I	M	C	S	T	A	S	I	L	N	L	C	V	I	S	V	D	R	Y					
S1P1	M	F	V	A	L	S	A	S	V	F	S	L	L	A	I	A	I	E	R	Y					
CB1	V	T	A	S	F	T	A	S	V	G	S	L	F	L	T	A	I	D	R	Y					
CB2	V	T	M	T	F	T	A	S	V	G	S	L	L	L	T	A	I	D	R	Y					
Orexin	Q	A	V	S	V	S	V	A	V	L	T	L	S	F	I	A	L	D	R	W					
Beta-2	D	V	L	C	V	T	A	S	I	E	T	L	C	V	I	A	V	D	R	Y					
A2A	V	L	V	L	T	Q	S	S	I	F	S	L	L	A	I	A	I	D	R	Y					
Beta-1	D	V	L	C	V	T	A	S	I	E	T	L	C	V	I	A	L	D	R	Y					
MOR	D	Y	Y	N	M	F	T	S	I	F	T	L	C	T	M	S	V	D	R	Y					
DOR	D	Y	Y	N	M	F	T	S	I	F	T	L	T	M	M	S	V	D	R	Y					
KOR	D	Y	Y	N	M	F	T	S	I	F	T	L	T	M	M	S	V	D	R	Y					

Figure 23. GPCR Multi-Sequence Alignment.

Figure 24. δ -Opioid Receptor.

Constructing the GPR55 R and GPR55 R* TMHs

Updating the receptor models mandated an assessment of sequence-dictated conformational divergences of the GPR55 transmembrane helices (TMH) from the chosen 1.8 angstrom δ -opioid receptor crystallographic template. The Monte Carlo/simulated annealing technique CM¹³ was used to study the conformations of four GPR55 TMHs (TMHs 1, 5, 6, 7) with important sequence divergences from the DOR template. This technique allows for thorough exploration of conformations of TMHs containing helix deforming residues such as Proline, Glycine, Serine or Threonine.

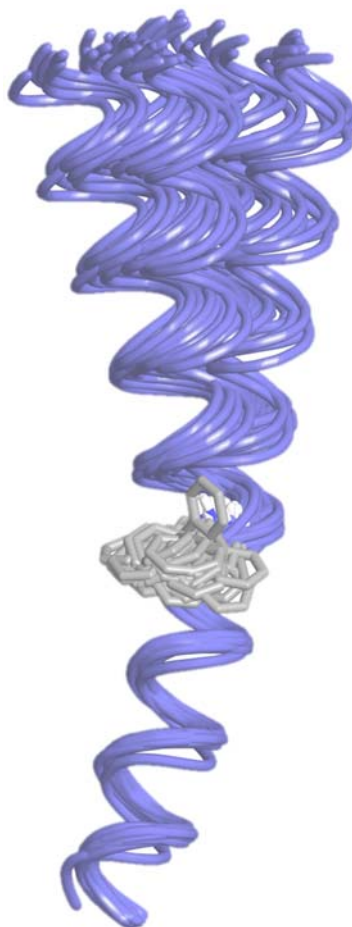


Figure 25. CM Output for Active-State GPR55 TMH6 Clustered, Showing F6.48.

Conformational Memories explores the low free energy conformations possible for a helix of interest using Monte Carlo simulated annealing. The CM method, developed by Guarnieri and Wilson¹³ and expanded by Guarnieri and Weinstein,¹⁴ was used originally to thoroughly explore the dihedral conformational space of a molecule, independent of the dihedral conformation of the initial molecular structure. The method has been expanded to allow the variation of bond angles in addition to dihedral angles.¹⁵ CM combines Monte Carlo exploration of the dihedral angle space with simulated annealing (MC/SA) to determine the range of values in which each dihedral angle is capable of existing within a broad temperature range. In the CM calculations used to construct the GPR55 TMHs under consideration, the backbone dihedrals of each helix were set to the standard ϕ (-63°) and ψ (-41.6°) for transmembrane helices. The established protocol is then to allow all torsion angles to vary $\pm 10^\circ$, and to allow a larger variation of $\pm 50^\circ$ in regions containing flexible series of residues.¹⁶

The CM calculation is performed in two phases: an exploratory phase and a biased annealing phase. In the exploratory phase, a random walk is used to first identify the region of conformational space most probable for each torsion angle and bond angle. The initial temperature for each run was 3000 K with 50,000 Monte Carlo steps applied to each torsion or bond angle variation with step-wise cooling, over 18 steps, to a final temperature of 310 K. Each step consists of varying two dihedral angles and one bond angle chosen at random from the entire set of variable angles. The torsion angles and bond angles are randomly picked at each temperature and each move is accepted or rejected using the **Metropolis Criterion** (Figure 26).¹⁷

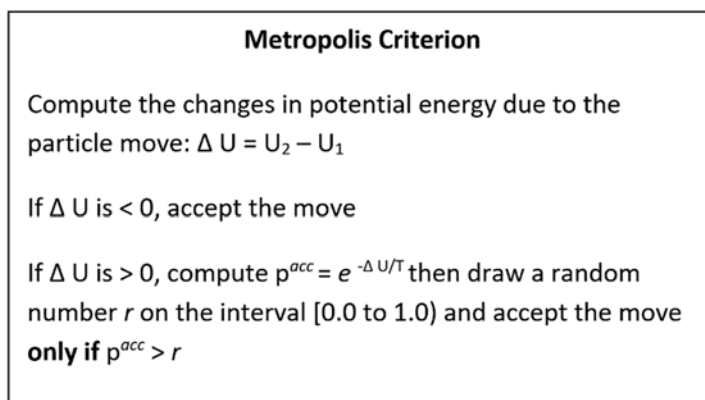


Figure 26. Metropolis Criterion.

Accepted conformations in the Exploratory Phase are used to create “memories” of torsion angles and bond angles that were accepted (Figure 27). This information provides a map of the accessible conformational space of each TMH as a function of temperature. In the biased annealing phase, the only torsion angle and bond angle moves attempted are those that would keep the angle in the “populated conformational space” mapped at 310 K in the exploratory phase. The biased annealing phase for the calculations reported here began at 749.4 K with cooling to 310 K in 7 steps.

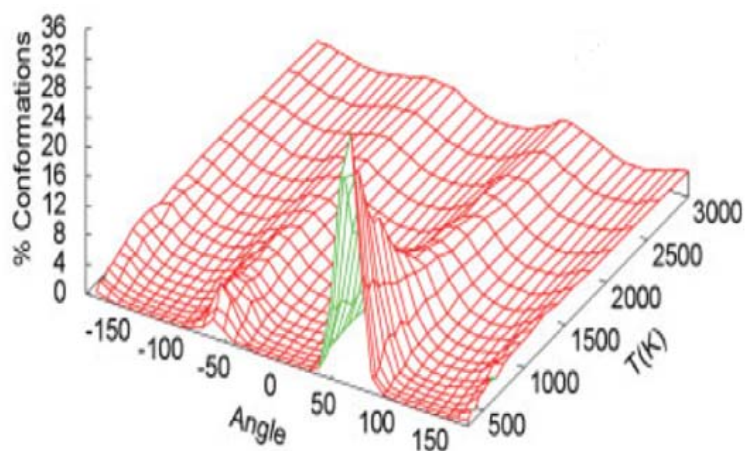


Figure 27. Conformational Memory for S2.40 χ_1 from GPR55.

One hundred eight structures were output at 310 K. The output from each TMH study was then superimposed on the corresponding template helix in the δ -Opioid receptor template from the intracellular (IC) end of the receptor up to the .50 residue. This particular superposition was to allow for examination of how CM represented the variation that could occur at the extracellular (EC) end of each TMH. The only exception to this superposition was TMH6 which had to be superimposed from the IC portion of the helix downward so as to represent the GPR55 R* “kicked out” region, occurring upon receptor activation, of the bottom of the helix. A helix was selected for inclusion in the revised GPR55 model that fit in the bundle with no van der Waals overlaps with residues on other TMHs.

Extracellular and Intracellular Loops

Extracellular and intracellular loops connecting all 7 TMHs were then added using MODELLER v8.2.26. MODELLER is a computer program used in producing homology models of protein tertiary structures.¹⁸ It employs a technique originating in nuclear magnetic resonance known as *satisfaction of spatial restraints*, by which a set of geometrical criteria are used to create a probability density function for the location of each atom in the protein.

Energy minimizations were performed using Macromodel and the OPLS2005 all-atom force field (version 9.8, Schrödinger, LLC, New York, NY). A distance-dependent dielectric, 8.0 Å extended non-bonded cutoff, 20.0 Å electrostatic cutoff, and 4.0 Å hydrogen bond cutoff were used. The minimization was performed in two stages. In the first stage, a harmonic constraint was placed on all the TMH backbone torsions (ϕ , ψ , and ω), with this constraint gradually reduced to zero in 500-step increments (using a total of

5000 steps to reach zero). In addition, a 500 kcal/mol harmonic constraint was placed on the backbone torsions of the loops. The minimization consisted of a conjugate gradient minimization using a distance-dependent dielectric, performed in 1000-step increments until the bundle reached the 0.05 kJ/mol gradient. In the second stage of the calculation, the TMH portion of the bundle was frozen, but the loops were allowed to relax. The generalized Born/surface area continuum solvation model for water as implemented in MacroModel was used. This stage of the calculation consisted of a Polak-Ribier conjugate gradient minimization in 1000-step increments until the bundle reached the 0.05 kJ/mol gradient.

Conformational Assessment of the Ligands

A complete systematic conformational analysis of ligands (both agonists and antagonists) to be docked in the GPR55 models was performed, in parallel to the CM and prior to the docking of each ligand in its respective receptor, using *ab initio* Hartree-Fock calculations at the 6-31G* level as encoded in the Spartan molecular modeling program (Wavefunction, Inc., Irvine, CA). Specifically, HF 6-31G* 6-fold conformer searches were performed for all rotatable bonds within a molecule (Figure 28). In each conformer search, local energy minima were identified by rotation of a subject torsion angle through 360° in 60° increments (6-fold search), followed by HF 6-31G* energy minimization of each rotamer generated. To calculate the difference in energy between the global minimum energy conformer of each compound and its final docked conformation, rotatable bonds in the global minimum energy conformer were driven to their corresponding value in the final docked conformation, and the single-point energy of the

resultant structure was calculated at the HF 6–31G* level. As an example of the output, the global minimum energy conformer of ML184 and the actual docked conformer are shown below superimposed on all heavy atoms (Figure 29).

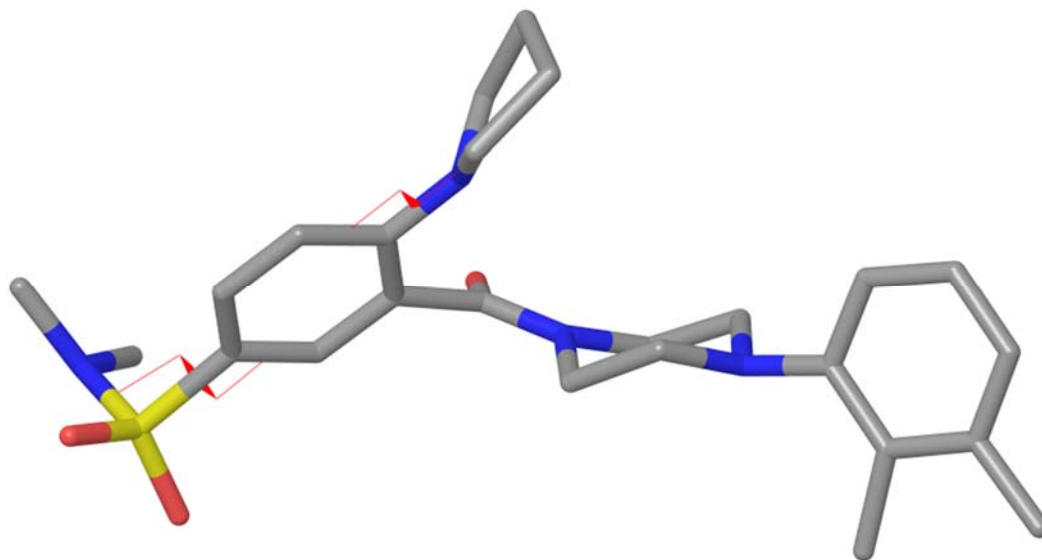


Figure 28. GPR55 Agonist ML184 with Two of Six Rotatable Bonds Indicated.

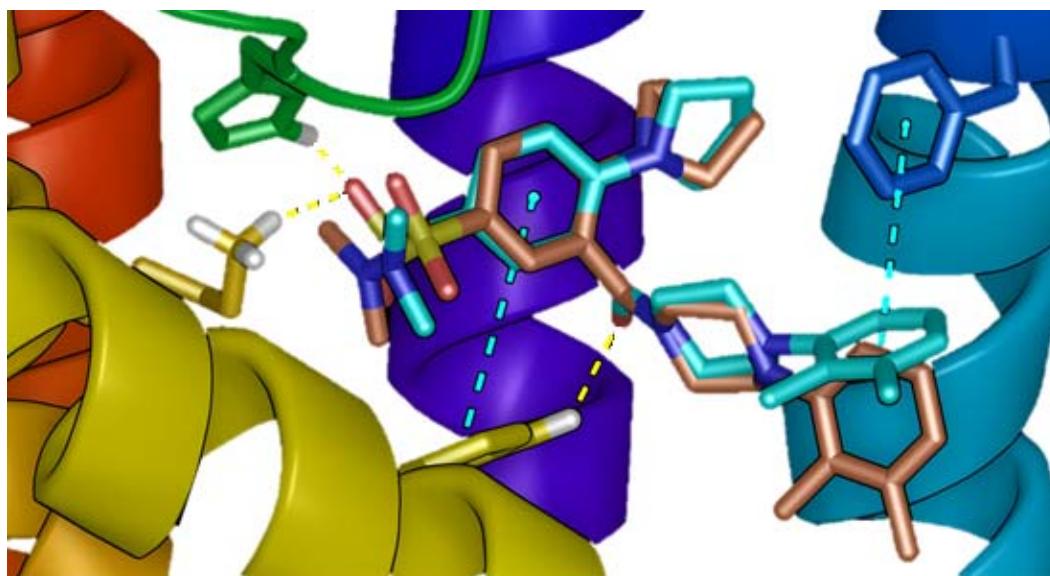


Figure 29. GRPR55 Agonist ML184 Docked (Cyan) and Global Minimum (Copper) Conformations.

Docking of Ligands

The lowest energy conformation of all ligands was used, unless otherwise noted, for all receptor docking studies. The Schrödinger module, Induced Fit, (Schrödinger Inc. Portland, OR) was used to explore possible binding conformations and receptor site interactions in the GPR55 R and R* models. The binding site of the receptor was defined by the area enclosed in a box with dimensions 26Å x 26Å x 26Å (the default value).

Because the endogenous ligand, LPI, is negatively charged, it is likely that a positively charged amino is a primary interaction site for GPR55 ligands. The only positively charged amino acid in the binding pocket of the original model was K2.60 (80). Recent K2.60A and E3.29A mutation studies suggest that both of these charged residues are crucial for ligand activation at GPR55 (M. Lingerfelt et al., manuscript submitted to *Biochemistry*). For this reason, both K2.60 (80) and E3.29A (98) were set as the center of the box and a hydrogen bond with K2.60 (80) was defined as a constraint. The two constraints (enclosing box and hydrogen bond) were used for both steps that Induced Fit Docking (IFD) performs.

The initial receptor minimization that IFD implements in preparation for docking ligands was omitted because the receptor model had already been energy minimized. For the first Glide calculation, receptor and ligand Van der Waals radii were set to the default value of 0.50 and the number of maximum poses to be produced was also set to 40. During the Prime stage of the calculation, amino acids within 5.0Å of the ligand were refined to better accommodate the ligand. Since the GPR55 receptor is a transmembrane protein, an implicit membrane was used during the Prime refinement step. During the

second step, the actual docking of the ligand performed by the module GLIDE, the top 30 poses produced by the first calculation were re-docked in the receptor. Docked poses that were within 40.0 kcal/mol of the absolute relative lowest one were kept.

Ligand/Receptor Minimization

To optimize the ligand/receptor interaction in the receptor/ligand complexes, each was minimized using Macromodel 9.1 (Schrödinger Inc.; Portland, OR). As described above in the section for bundle construction, 500 steps of Polak-Ribier conjugate gradient minimization using force field defined dielectric were performed. A harmonic constraint was placed on all the TMH backbone torsions (ϕ , ψ , and ω) to preserve the general shape of the helices during minimization. The sidechains of the TMH region, the loops and termini were allowed to relax. The Generalized Born/Surface Area (GB/SA) continuum solvation model for water as is implemented in Macromodel 9.1 was used for minimizing the loop regions. An 8.0Å nonbonded cutoff (updated every 10 steps), a 20.0Å electrostatic cutoff, and a 4.0Å hydrogen bond cutoff were used in each stage of the calculation. The transmembrane region and the docked ligand were then frozen while the loops were minimized. An example of the resultant ligand/receptor interaction energies for GPR55 agonist ML184 and the GPR55 R* bundle can be seen in Supplemental Table 1 in Chapter IV.

References

1. Kotsikorou, E.; Madrigal, K. E.; Hurst, D. P.; Sharir, H.; Lynch, D. L.; Heynen-Genel, S.; Milan, L. B.; Chung, T. D.; Seltzman, H. H.; Bai, Y.; Caron, M. G.; Barak, L.; Abood, M. E.; Reggio, P. H. Identification of the GPR55 Agonist Binding Site Using a Novel Set of High-potency GPR55 Selective Ligands. *Biochem.* **2011**, *50*, 5633–5647.
2. Cherezov, V.; Rosenbaum, D. M.; Hanson, M. A.; Rasmussen, S. G.; Thian, F. S.; Kobilka, T. S.; Choi, H. J.; Kuhn, P.; Weis, W. I.; Kobilka, B. K.; Stevens, R. C. High-resolution Crystal Structure of an Engineered Human Beta2-adrenergic G Protein-coupled Receptor. *Science* **2007**, *318*, 1258–1265.
3. Zhang, C.; Srinivasan, Y.; Arlow, D. H.; Fung, J. J.; Palmer, D.; Zheng, Y.; Green, H. F.; Pandey, A.; Dror, R. O.; Shaw, D. E.; Weis, W. I.; Coughlin, S. R.; Kobilka, B. K. High-resolution Crystal Structure of Human Protease-activated Receptor 1 Bound to the Antagonist Vorapaxar. *Nature* **2012**, *492*, 387–392.
4. Ballesteros, J. A.; Weinstein, H. Integrated Methods for the Construction of Three Dimensional Models and Computational Probing of Structure Function Relations in G Protein-coupled Receptors. In Sealfon, S. C., Conn, P. M., editors, *Methods in Neurosciences* **1995**, pp. 366–428.
5. Barnett-Norris, J., Hurst, D. P., Lynch, D. L., Guarnieri, F., Makriyannis, A., & Reggio, P. H. (2002). Conformational Memories and the Endocannabinoid Binding Site at the Cannabinoid CB1 Receptor. *J. Med. Chem.* **2002**, *45*, 3649–3659.
6. Bramblett, R. D., Panu, A. M., Ballesteros, J. A., & Reggio, P. H. (1995). Construction of a 3D Model of the Cannabinoid CB1 Receptor: Determination of Helix Ends and Helix Orientation. *Life Sciences* **1995**, *56*, 1971–1982.
7. Hurst, D. P.; Lynch, D. L.; Barnett-Norris, J.; Hyatt, S. M.; Seltzman, H. H.; Zhong, M.; Song, Z. H.; Nie, J.; Lewis, D.; Reggio, P. H. (2002). N-(piperidin-1-yl)-5-(4-chlorophenyl)-1-(2,4-dichlorophenyl)-4-methyl-1H-pyrazole-3-carboxamide (SR141716A) Interaction with LYS 3.28(192) is Crucial for its Inverse Agonism at the Cannabinoid CB1 Receptor. *Molecular Pharmacology* **2002**, *62*, 1274–1287.
8. McAllister, S. D.; Hurst, D. P.; Barnett-Norris, J.; Lynch, D.; Reggio, P. H.; Abood, M. E. Structural Mimicry in Class A G Protein-coupled Receptor Rotamer Toggle Switches: The Importance of the F3.36(201)/W6.48(357) Interaction in Cannabinoid CB1 Receptor Activation. *J. Biol. Chem.* **2004**, *279*, 48024–48037.

9. McAllister, S. D.; Rizvi, G.; Anavi-Goffer, S.; Hurst, D. P.; Barnett-Norris, J.; Lynch, D. L.; Reggio, P. H.; Abood, M. E. (2003). An Aromatic Microdomain at the Cannabinoid CB1 Receptor Constitutes an Agonist/Inverse Agonist Binding Region. *J. Med. Chem.* **2003**, *46*, 5139–5152.
10. Song, Z. H., Slowey, C. A., Hurst, D. P., & Reggio, P. H. (1999). The Difference between the CB1 and CB2 Cannabinoid Receptors at Position 5.46 is Crucial for the Selectivity of WIN55212-2 for CB2. *Mol. Pharmacol.* **1999**, *56*, 834–840.
11. Nebane, N. M.; Hurst, D. P.; Carrasquer, C. A.; Qiao, Z.; Reggio, P. H.; & Song, Z. H. Residues Accessible in the Binding-site Crevice of Transmembrane Helix 6 of the CB2 Cannabinoid Receptor. *Biochemistry* **2008**, *47*, 13811–13821.
12. Granier, S.; Manglik, A.; Kruse, A. C.; Kobilka, T. S.; Thian, F. S.; Weis, W. I.; Kobilka, B. K. Structure of the δ -opioid Receptor Bound to Naltrindole. *Nature* **2012**, *485*, 400–404.
13. Guarnieri, F.; Wilson, S. R. Conformational memories and a simulated annealing program that learns: Application to LTB₄. *J. Comput. Chem.* **1995**, *16*, 648–653.
14. Guarnieri, F.; Weinstein, H. Conformational Memories and the Exploration of Biologically Relevant Peptide Conformations: An Illustration for the Gonadotropin-releasing Hormone. *J. Am. Chem. Soc.* **1996**, *118*, 5580–5589.
15. Whitnell, R. M.; Hurst, D. P.; Reggio, P. H.; Guarnieri, F. Conformational Memories with Variable Bond Angles. *J. Comput. Chem.* **2008**, *29*, 741–752.
16. Barnett-Norris, J.; Guarnieri, F.; Hurst, D. P.; Reggio, P. H. Exploration of Biologically Relevant Conformations of Anandamide, 2-arachidonylglycerol, and their analogues using conformational memories. *J. Med. Chem.* **1998**, *41*, 4861–4872.
17. Roberts, G. O. A Note on Acceptance Rate Criteria for CLTs for Metropolis-Hastings Algorithms. *J. Appl. Probab.* **1999**, 1210–1217.
18. Fiser, A.; Šali, A. Modeller: Generation and Refinement of Homology-based Protein Structure Models. *Method. Enzymol.* **2003**, *374*, 461–491.

CHAPTER IV

**IDENTIFICATION OF CRUCIAL AMINO ACID RESIDUES INVOLVED IN
AGONIST SIGNALING AT THE GPR55 RECEPTOR**

As Submitted to Biochemistry

Mary A. Lingerfelt[†], Pingwei Zhao[‡], Haleli P. Sharir[‡], Dow P. Hurst[†], Patricia H. Reggio[†] and Mary E. Abood[‡]

[†]Department of Chemistry and Biochemistry, UNC-Greensboro, Greensboro, North Carolina 27402 United States

[‡]Center for Substance Abuse Research, Lewis Katz School of Medicine at Temple University, Philadelphia, Pennsylvania 19140, United States

This chapter was created by inserting the above cited paper, verbatim, with the following differences:

- 1) Figures/Tables were re-rendered/resized to match dissertation global style.
- 2) Page layout has been altered from published form to meet dissertation layout requirements (i.e. the use of 1 column vs. 2, etc.)

Abstract

GPR55 is a newly de-orphanized Class A GPCR that has been implicated in inflammatory pain, neuropathic pain, metabolic disorder, bone development, and cancer. Few potent GPR55 ligands have been identified to date. This is largely due to an absence of information about salient features of GPR55, such as residues important for signaling and residues implicated in the GPR55 signaling cascade. The goal of the work reported here was to identify residues that are key for the signaling of the GPR55 endogenous ligand, 1- α -lysophosphatidylinositol (LPI), as well as the signaling of the GPR55 agonist, ML184, (CID 2440433, 3-[4-(2,3-dimethylphenyl)piperazine-1-carbonyl]-N,N-dimethyl-

4-pyrrolidin-1-ylbenzenesulfonamide). SRE and SRF luciferase assays were used as read-outs for studying LPI and ML184 signaling at the GPR55 mutants. A GPR55 R* model based on the recent DOR crystal structure was used to interpret the resultant mutation data. Two residues were found to be crucial for agonist signaling at GPR55, K2.60 and E3.29, suggesting that these residues form the primary interaction site for ML184 and LPI at GPR55. Y3.32F, H(170)F and F6.55A/L mutation results suggested that these residues are part of the orthosteric binding site for ML184, while Y3.32L, M3.36A and F6.48A mutation results suggest the importance of a Y3.32/M3.36/F6.48 cluster in the GPR55 signaling cascade. C(10)A and C(260)A mutations suggest that these residues form a second disulfide bridge in the extracellular domain of GPR55, occluding ligand extracellular entry in the TMH1-TMH7 region of GPR55. Taken together, these results provide the first set of discrete information on residues important for LPI and ML184 signaling and for GPR55 activation. This information should aid in the rational design of next generation GPR55 ligands and hopefully the creation of the first high affinity GPR55 radioligand, a tool that is sorely needed in the field.

Introduction

GPR55 [GenBank accession number NM005683] is a Class A G-protein coupled receptor (GPCR) that recognizes a sub-set of cannabinoid CB1 and CB2 ligands, suggesting that GPR55 may be a cannabinoid receptor.¹ Subsequently, 1- α -lysophosphatidylinositol¹⁻² was reported to be the endogenous ligand of GPR55. GPR55 has been found to be implicated in inflammatory pain, neuropathic pain, metabolic disorder, bone development, and cancer,³ indicating the real potential of GPR55 ligands

as therapeutics. In search of more potent GPR55 ligands and in collaboration with the Sanford-Burnham Institute, we performed high throughput screens for GPR55 agonists and antagonists using the NIH library of 300,000 compounds and identified several novel GPR55 chemotypes for each.⁴ One of these compounds from the agonist screen is ML184, (CID 2440433, 3-[4-(2,3-dimethylphenyl) piperazine-1-carbonyl]-N,N-dimethyl-4-pyrrolidin-1-ylbenzenesulfonamide)⁵ (EC_{50} =263nM). However, despite these ligand development efforts, the best GPR55 ligands (like ML184) remain active at sub-micromolar concentrations, concentrations not low enough for the development of a GPR55 radioligand.

To address this situation, we reasoned that knowledge of GPR55 structure, particularly binding pocket residues important for ligand signaling and those involved in the receptor activation would greatly aid rational GPR55 drug design approaches. To this end, we report here a GPR55 mutation study guided and analysed using a GPR55 R* model based on the recent delta opioid receptor (DOR) crystal structure. This study identifies multiple residues important for ML184 signaling and for GPR55 activation.

Results

Biological Evaluation

SRE responses of mutant and wild-type GPR55 receptors. HEK293 cells transiently transfected with both pGL4.33 [luc2P/SRE/Hygro] and each of the mutants, as well as, WT were made to assess agonist-induced receptor activation of SRE. The SRE assay assesses the contribution of MAPK/ERK signaling pathway for GPR55 activity.

We found that the WT GPR55 has an EC₅₀ value of 56 nM for the agonist ML184 (Figure 30 and Table 2).

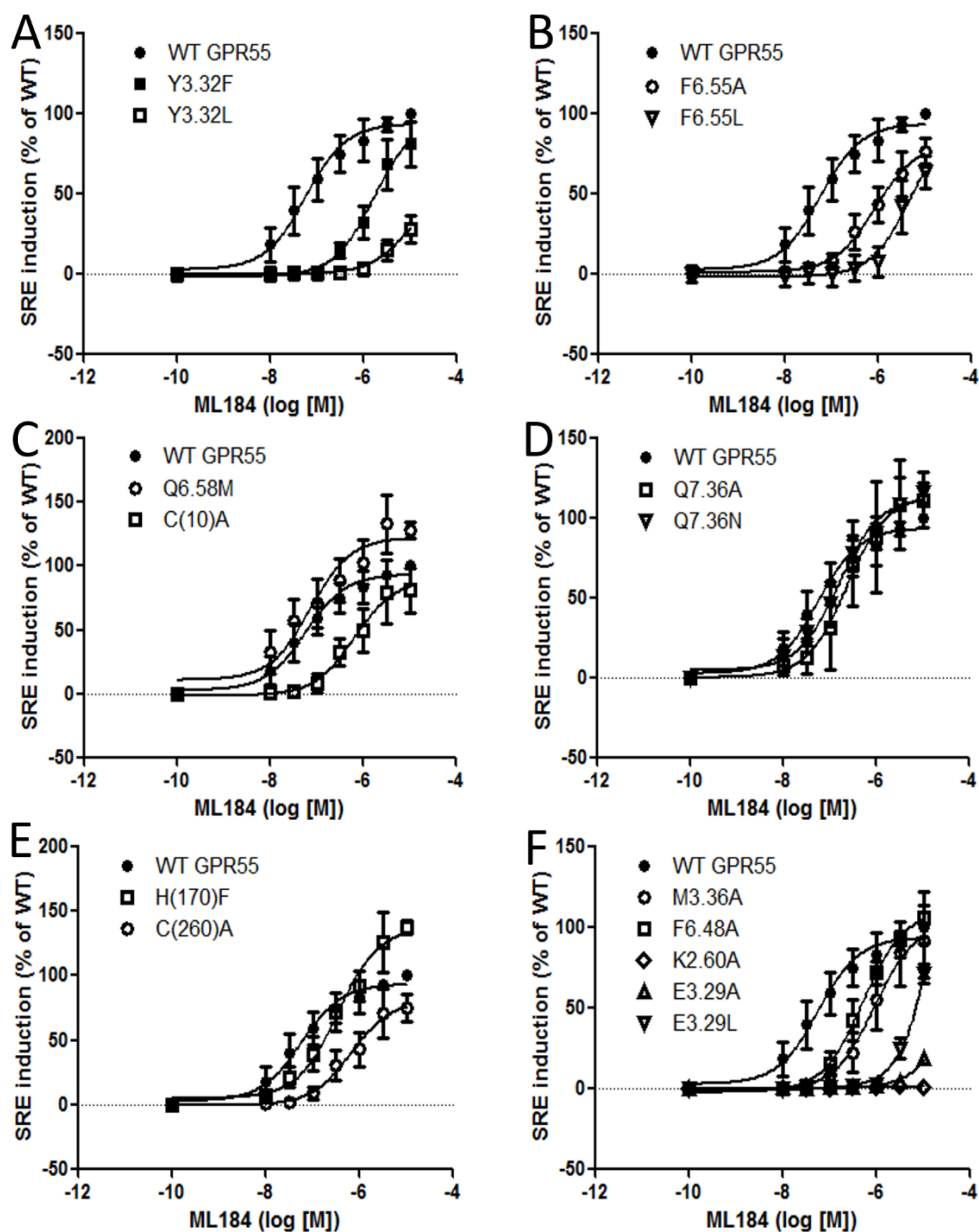


Figure 30. SRE Responses Induced by ML184 in GPR55 Wild Type and Mutant Transfected Cells. (A) WT GPR55, Y3.32F and Y3.32L. (B) WT GPR55, F6.55A and F6.55L. (C) WT GPR55, Q6.58M and C(10)A. (D) WT GPR55, Q7.36A and Q7.36N. (E) WT GPR55, H(170)F and C(260)A. (F) WT GPR55, M3.36A, F6.48A, K2.60A, E3.29A and E3.29L.

Table 2

ML184 Induced SRE Responses of Wild-type and Mutant Transfected Cells

ML184	EC ₅₀ (nM)	CI (nM)	Fold/WT
WT	56	24 to 133	-
Y3.32F	1659	670 to 4110	30
Y3.32L	9514	718 to 126100	170
F6.55A	840	345 to 2045	15
F6.55L	5131	1034 to 25460	92
Q6.58M	72	22 to 237	1
C(10)A	635	197 to 2044	11
H(170)F	341	158 to 734	6
C(260)A	657	222 to 1941	12
Q7.36A	230	57 to 920	4
Q7.36N	154	69 to 342	3
M3.36A	900	290 to 2790	16
F6.48A	514	266 to 993	9
K2.60A	NO response	-	-
E3.29A	>30000	very wide	-
E3.29L	>30000	Very wide	-

Note. From $n \geq 3$ experiments

We determined that the EC₅₀ value did not change regardless of the level of receptor expression (See Figure S1 in Supporting Information). Mutants Y3.32F and Y3.32L showed right shifted SRE response curves with EC₅₀'s higher than WT (Figure 30 A). The mutants F6.55A and F6.55L induced a similar SRE response to ML184 with right shifted curves. The Q6.58M curve was almost identical to that of WT indicating this mutant is not important to GPR55 receptor function. The mutant C(10)A showed an increased EC₅₀ value (636 nM). Very similarly, the mutant C(260)A induced an

increased EC_{50} value (657 nM), suggesting the existence of a disulfide bridge (see below). Q7.36A and Q7.36N showed similar responses to WT indicating this amino acid is not critical for agonist induced GPR55 receptor activation. The response curve of H(170)F only showed a slight difference from that of WT. Mutant M3.36A, F6.48A, E3.29A and E3.29L all showed increased EC_{50} values. E3.29A and E3.29L showed very little responses. Among all the mutants, K2.60A did not show any response in the SRE assay indicating that K2.60A rendered the GPR55 receptor non- functional.

In addition to the agonist ML184, the endogenous ligand (LPI) was used in the SRE assay for all the mutants (Figure 31). K2.60A did not show any LPI induced responses compared with WT. E3.29A and E3.29L showed a slight response at high concentration of LPI. F6.55A, F6.55L, Q6.58M, Q7.36A and Q7.36N all showed similar curves as to WT. Y3.32F, Y3.32L, C(10)A, H(170)F, C(260)A, M3.36A and F6.48A showed right shifted curve compared with WT. The LPI induced SRE response did not reach plateau for all the constructs including WT GPR55, thus no EC_{50} value was calculated.

SRF responses of mutant and wild-type GPR55 receptors. In addition to the SRE assay, the SRF assay was used to investigate another signaling pathway of GPR55. The SRF response is an indicator of G12-RhoA pathway activation which GPR55 has been reported to induce.⁶ The study of two distinct signaling pathways of GPR55 broadens the understanding of effects of these mutants on GPR55 function. Thus, the SRF assay was used to test GPR55 mutants in addition to the SRE assay (Figure 32 and Figure 33).

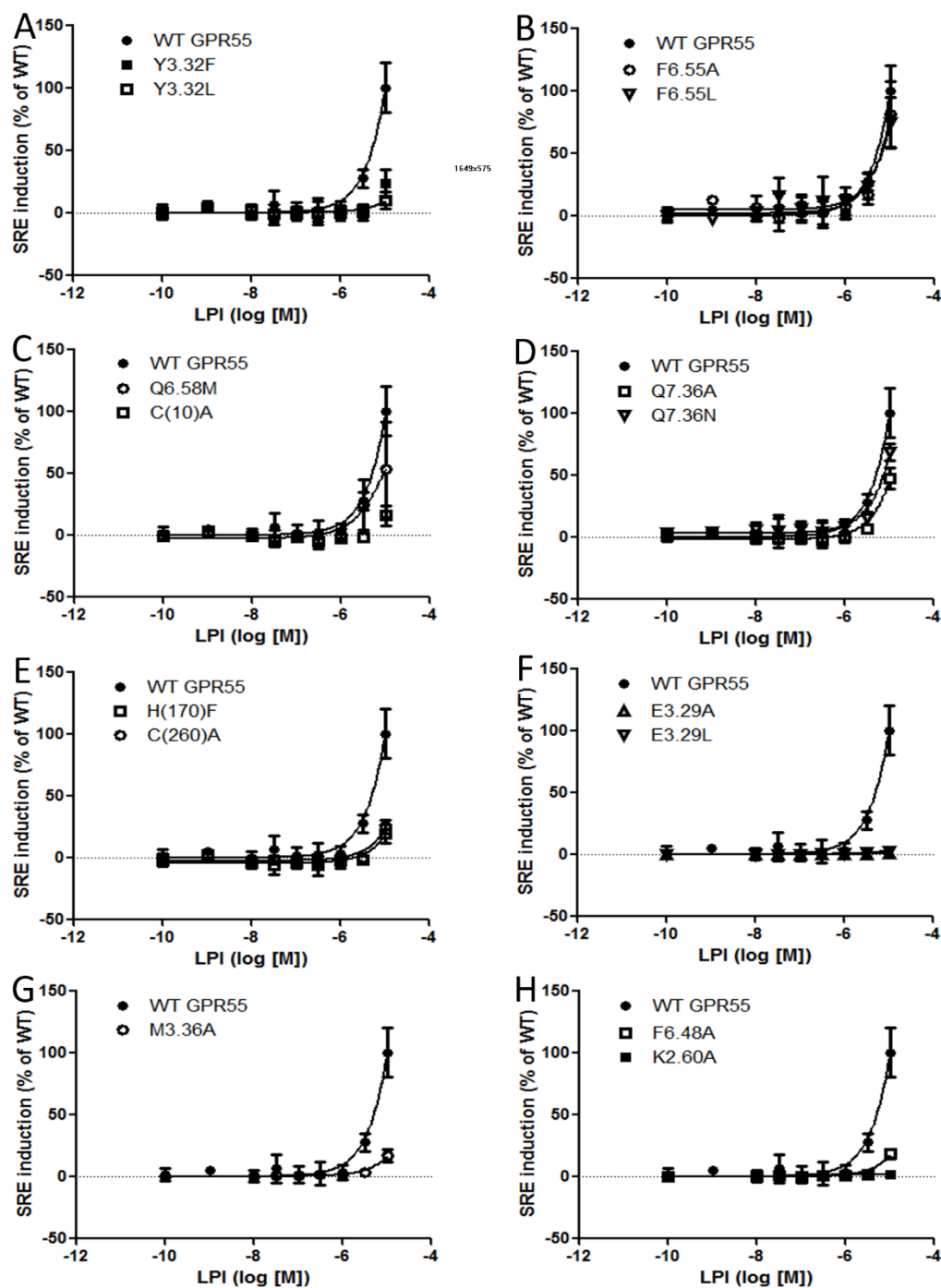


Figure 31. SRE Responses Induced by LPI in GPR55 Wild Type and Mutant Transfected Cells. (A) WT GPR55, Y3.32F and Y3.32L. (B) WT GPR55, F6.55A and F6.55L. (C) WT GPR55, Q6.58M and C(10)A. (D) WT GPR55, Q7.36A and Q7.36N. (E) WT GPR55, H(170)F and C(260)A. (F) WT GPR55, E3.29A and E3.29L. (G) WT GPR55 and M3.36A. (H) WT GPR55, F6.48A and K2.60A.

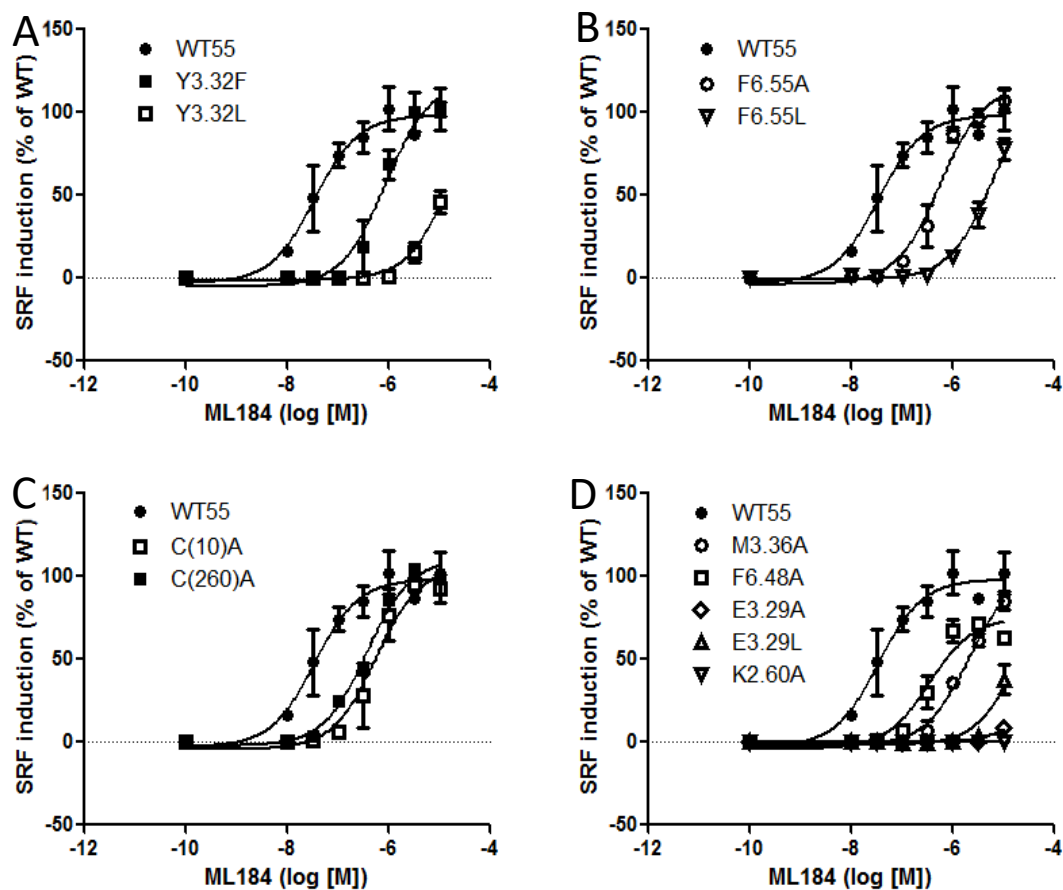


Figure 32. SRF Responses Induced by ML184 in GPR55 Wild Type and Mutant Transfected Cells. (A) WT GPR55, Y3.32F and Y3.32L. (B) WT GPR55, F6.55A and F6.55L. (C) WT GPR55, C(10)A and C(260)A. (D) WT GPR55, M3.36A, F6.48A, K2.60A, E3.29A and E3.29L.

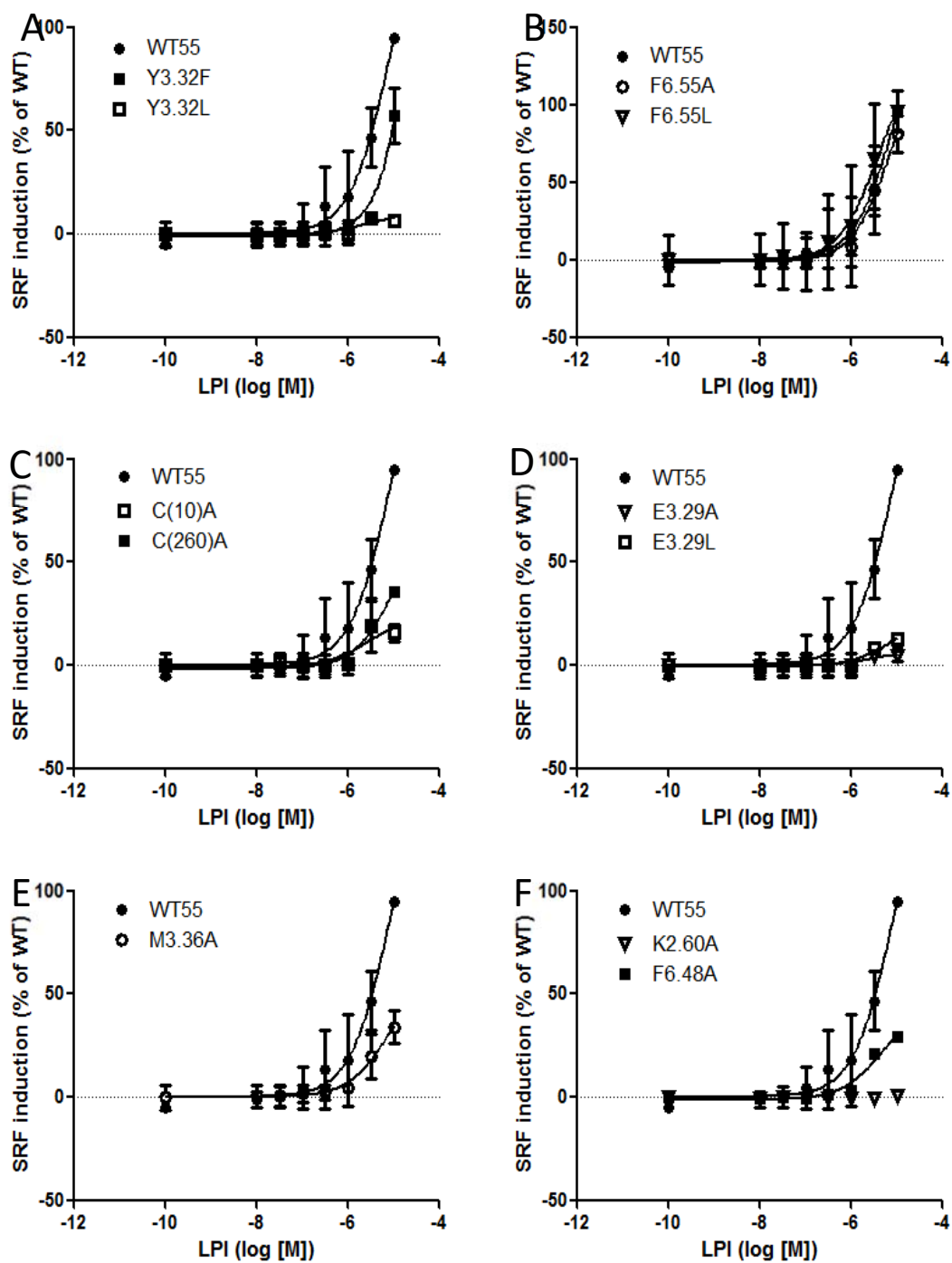


Figure 33. SRF Responses Induced by LPI in GPR55 Wild Type and Mutant Transfected Cells. (A) WT GPR55, Y3.32F and Y3.32L. (B) WT GPR55, F6.55A and F6.55L. (C) WT GPR55, C(10)A and C(260)A. (D) WT GPR55, E3.29A and E3.29L. (E) WT GPR55 and M3.36A. (F) WT GPR55, F6.48A, K2.60A.

Y3.32F and Y3.32L showed right shifted curves compared with WT. Y3.32L had a higher EC₅₀ value (864 μM; Figure 32). Similar to the SRE assay, the F6.55A and F6.55L had higher EC₅₀ values than WT (Figure 32, Table 3). Both C(10)A and C(260)A showed less response than WT. M3.36A, F6.48A, E3.29A and E3.29L all behaved in the SRF assay similar to in the SRE assay with reduced responses. K2.60A was not able to induce any response in the SRF assay similar to its inactivity in the SRE assay.

Table 3

ML184 Induced SRF Responses of Wild-type and Mutant Transfected Cells

ML184	EC ₅₀ (nM)	CI (nM)	Fold/WT
WT	33	15 to 75	-
Y3.32F	851	449 to 1615	26
Y3.32L	864000	very wide	26182
F6.55A	550	338 to 893	17
F6.55L	10500	4663 to 23630	318
C(10)A	554	254 to 1206	17
C(260)A	363	201 to 656	11
M3.36A	2044	1415 to 2952	62
F6.48A	335	177 to 633	10
K2.60A	NO response	-	-
E3.29A	> 30000	very wide	-
E3.29L	> 30000	very wide	-

Note. $n \geq 3$ experiments.

Molecular Modeling

No x-ray crystal structure for GPR55 has been reported. For this reason, a GPR55 activated state (R*) model based upon the crystal structure of the delta-opioid receptor

(DOR) was used to interpret the mutation results reported here.⁷ Glide docking studies in this model focused on ML184. These studies were used to identify a docking site for ML184 in the GPR55 R* model that involves residues on TMHs2-3-5-6 and the EC-2 loop.

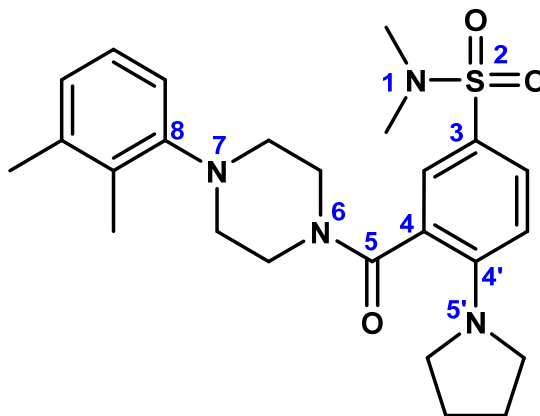
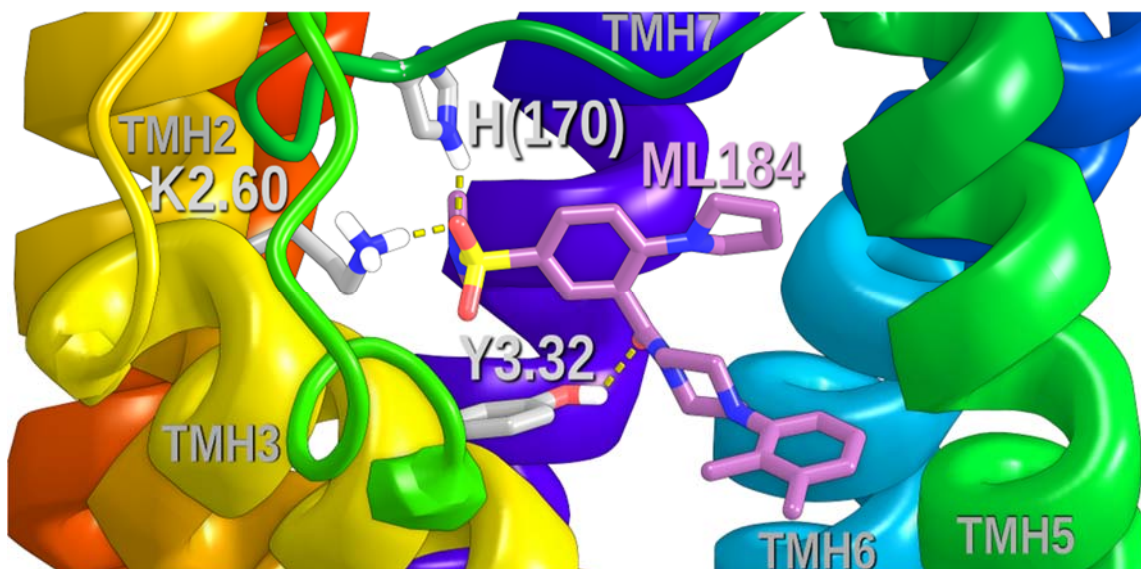


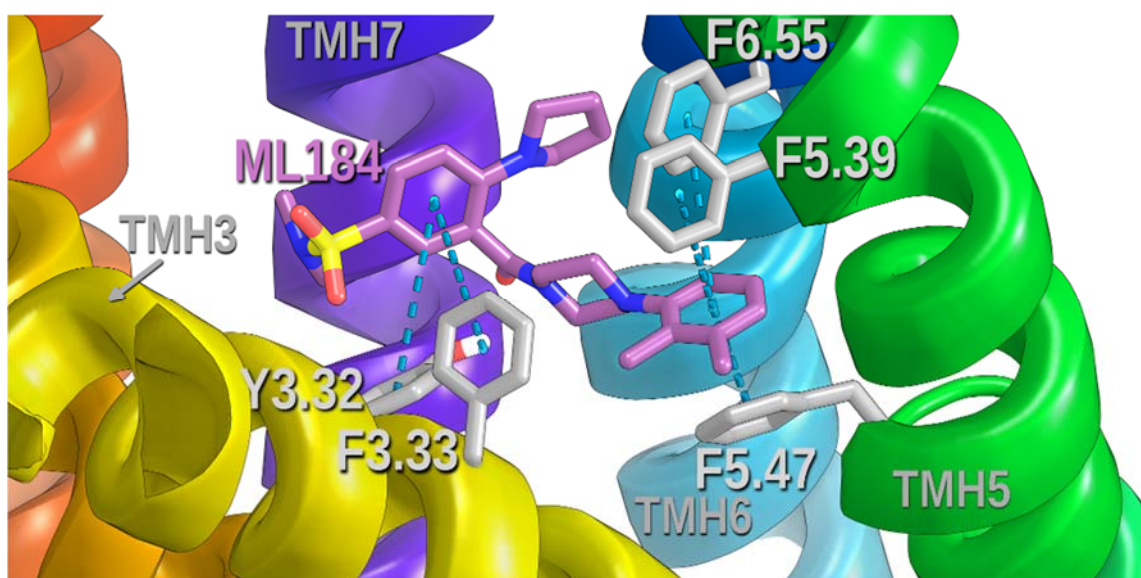
Figure 34. GPR55 Agonist ML184, Numbered to Show Torsional Angles Varied for Conformational Analysis.

Primary interactions for agonist signaling.

ML184 docked into the GPR55 R bundle.* Figure 35 describes the ML184 binding site identified by Glide. Figure 35 A shows all hydrogen bonding interactions for ML184 at GPR55. Here, the ML184 sulfonamide oxygen hydrogen bonds directly with K2.60 (H bond (N-O) distance, 2.8 Å; (N-H—O) angle, 174°). H(170) in the EC-2 loop also forms a hydrogen bond with an ML184 sulfonamide oxygen (H bond (N-O) distance, 2.8 Å ; (N-H—O) angle, 150°). Y3.32 forms a hydrogen bond with the ML184 carboxamide oxygen (H bond (N-O) distance, 2.8 Å; (N-H—O) angle, 163°).



(A)

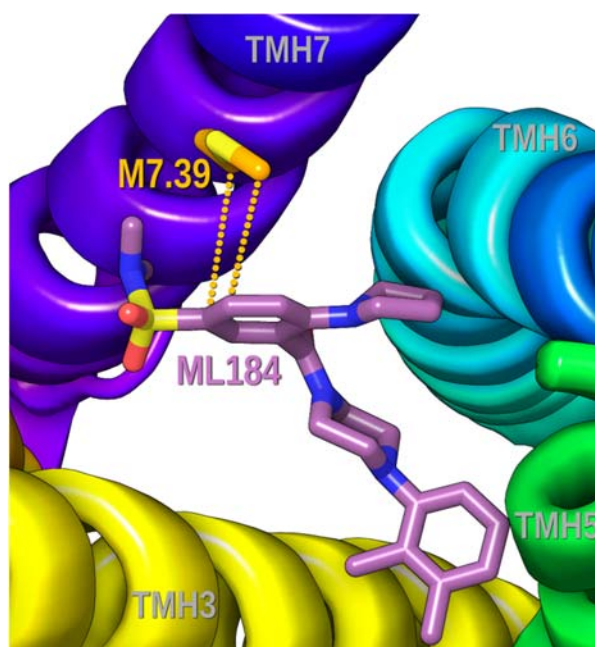


(B)

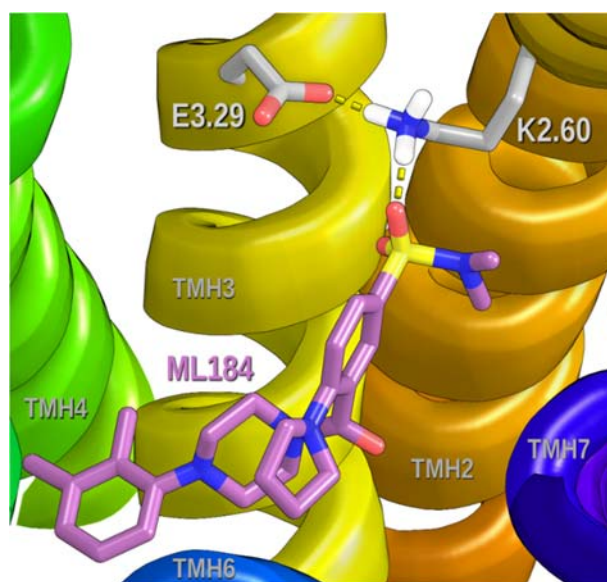
Figure 35. All Hydrogen and Aromatic Stacking Interactions for ML 184 at GPR55. (A) This Figure Shows All Hydrogen Bonding Interactions for ML184 at GPR55. The View is Looking from TMHs 4 and 5 towards TMH7. Hydrogen Bonding is Shown with Dotted Yellow Lines. (B) This Figure Shows All Aromatic Stacking Interactions for ML184 at GPR55. The View is Looking from TMH 4 towards TMH6. Aromatic Stacking Interactions are Shown with Light Blue Dotted Lines between Ring Centroids.

In addition to hydrogen bonding, ML184 also has aromatic stacking interactions in its binding site. Figure 35 B shows all of these aromatic stacking interactions. Y3.32 and F3.33 form aromatic stacks with the ML184 benzene ring proximal to the ML184 sulfonamide moiety (Y3.32 ring centroid to centroid distance 5.6 Å; angle 70°); (F3.33 ring centroid to centroid distance 6.5 Å; angle 47°). F6.55 forms an aromatic stacking interaction with the distal, dimethyl-phenyl ring of ML184 (ring centroid to centroid distance 5.4 Å; angle 88°), while F5.39 and F5.47 also form aromatic stacks with the central ML184 aromatic ring (F5.39 ring centroid to centroid distance 5.3 Å; angle 70°; F5.47 ring centroid to centroid distance 4.5 Å; angle 41°).

M7.39 is engaged in a Met-aromatic ring interaction with the central benzene of ML184 (Distances to central benzene ring centroid from M7.39 sidechain atoms CG 5.1 Å, SD 5.3 Å, CE 4.4 Å) (see Figure 36 A).⁸ In this orientation, the sulfur points up, with adjacent carbons pointing down towards phenyl ring carbons on ML184. ML184 also has an indirect interaction with E3.29, as this residue holds K2.60 (with which ML184 has a direct hydrogen bond) in a salt bridge that directs K2.60 towards the ML184 binding site (see Figure 36 B). The ML184 conformer docked here is 1.91 kcal/mol above the ML184 global minimum.



(A)



(B)

Figure 36. (A) M7.39 is Engaged in a Met-aromatic Ring Interaction With the Central Benzene of ML184.⁸ In This Orientation, the Sulfur Points Up, with Adjacent Carbons Pointing Down Towards Phenyl Ring Carbons on ML184. (B) Although There is no Direct Interaction Between ML184 and E3.29 in the Current Model, Modeling Suggests That E3.29 Forms a Salt Bridge with K2.60. This Salt Bridge Positions K2.60 for Interaction with ML184. The View Here is From TMH6 Looking Towards TMH2/3.

Toggle switch residues. GPR55 shares with the P2Y12⁹ and hPAR-1¹⁰ receptors, a Y/F3.32-M3.36-F6.48 cluster of residues that likely acts as the toggle switch for activation of GPR55. Figure 37 illustrates these toggle switch residues contoured at their Van der Waals radii in the inactive (R) and the activated (R*) state.

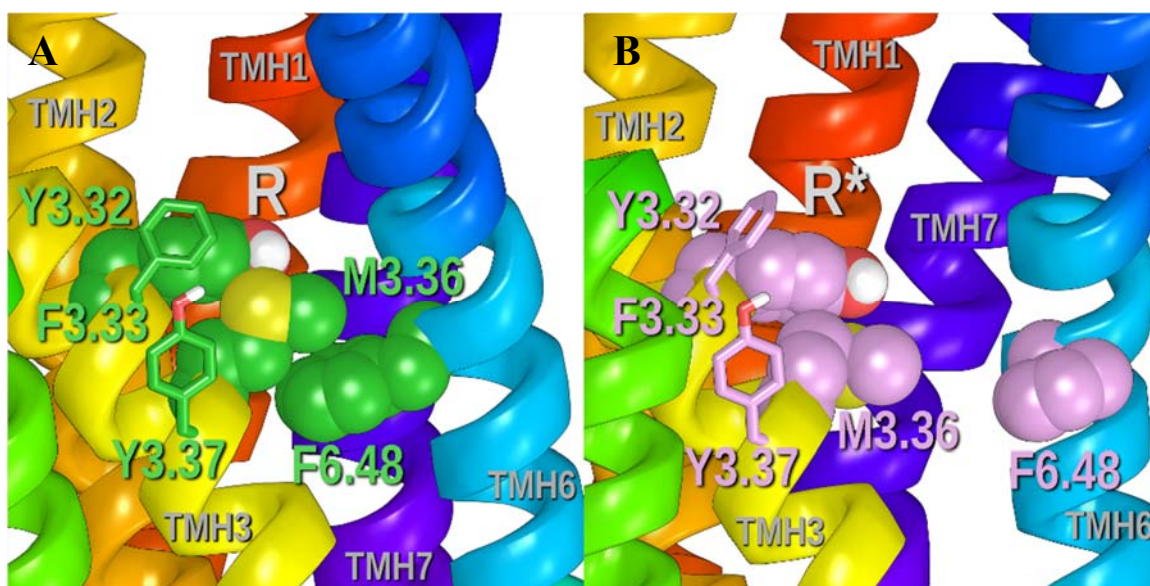


Figure 37. Positions of the Toggle Switch Residues Y3.32, M3.36, and F6.48 (Contoured at Their van der Waals Radii) in the GPR55 R and R* Models. Additional Aromatic Residues in the Region of the Toggle Switch Help Stabilize the Cluster of Residues. These are F3.33 and Y3.37.

Inactive state. In the inactive state (Figure 37 A), Y3.32 ($\chi_1 = 178^\circ$) sits extracellular to M3.36 ($\chi_1 = -170^\circ$), maintaining Van der Waals interactions with M3.36. M3.36 ($\chi_1 = -170^\circ$) is stacked over F6.48 ($\chi_1 = -90^\circ$). M3.36 also has a methionine/aromatic ring interaction with F6.48 (Distances to F6.48 benzene ring centroid from M3.36 sidechain atoms CG 3.6 Å, SD 4.6 Å, CE 3.8 Å).⁸ Additional aromatic residues in the

region of the toggle switch help stabilize the cluster of residues. These are F3.33

($\chi_1 = -74^\circ$) and Y3.37 ($\chi_1 = -57^\circ$).

Agonist activated state. ML184 binding causes Y3.32 to change conformations ($\chi_1 = 178^\circ$ to $\chi_1 = -157^\circ$), because Y3.32 is a direct ligand binding site residue. Figure 37 B illustrates that the movement of Y3.32 frees M3.36 to undergo a conformational change ($\chi_1 = -170^\circ$ trans to $\chi_1 = -75^\circ$ g⁺), which then allows F6.48 to undergo its ($\chi_1 = -90^\circ$ g⁺ to $\chi_1 = -177^\circ$ trans) conformational change. The F6.48 conformational change causes flexing in the SFXP hinge region of GPR55, straightening TMH6 and breaking the ionic lock (R3.50/Q6.30) producing an opening at the intracellular end of GPR55 for G protein coupling. F3.33 ($\chi_1 = -81^\circ$) and Y3.37 ($\chi_1 = -55^\circ$) remain members of the extended cluster. Figure 38 illustrates the position of ML184 to the extended toggle switch residues in the GPR55 activated state.

Disulfide bridge residues. As described in the Methods section, the high degree of sequence homology between GPR55 and the CXCR4 receptor,¹¹ particularly in the EC regions, dictated several modifications to our initial set of GPR55 models.¹² These were (1) the introduction of EC helical extensions on TMH5-7 of GPR55; (2) the introduction of a β sheet motif into the EC-2 loop in GPR55; and (3) the introduction of a disulfide bridge between Cys(10) in the N-terminus and Cys(260) in the EC-3 loop near the top of TMH7.¹³ In the current paper, we tested the importance of a Cys(10)-Cys(260) disulfide bridge via single point mutations. Figure 39 illustrates the extracellular end of the receptor and the disulfide bridge between N-terminal C(10) and C(260) at the EC end of TMH7.

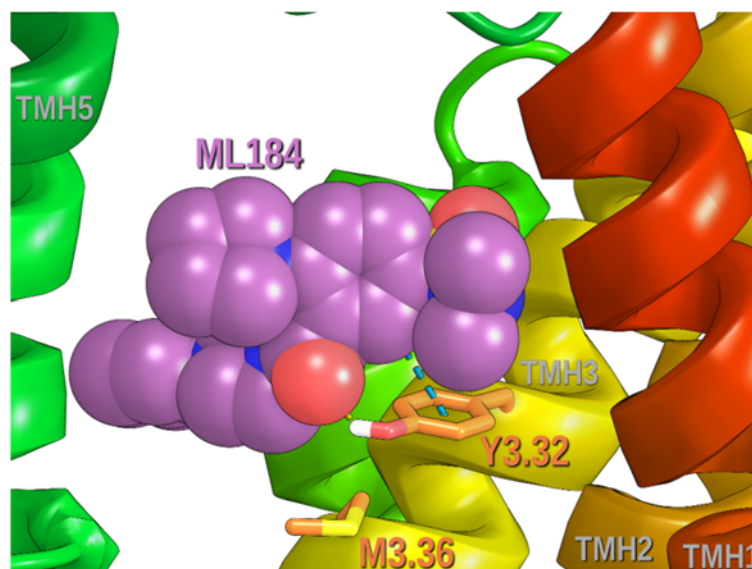


Figure 38. Position of ML184 Relative to the Extended Toggle Switch Residues in the GPR55 Activated State. ML184 (Contoured at its Van der Waals Radii) is Positioned above Y3.32 and Interacts Directly with it. The Movement of Y3.32 for This ML184 Interaction, Permits M3.36 (χ_1 trans to g^+) and, in Turn, F6.48 (χ_1 g^+ to trans) to Change to Their R* Conformations.

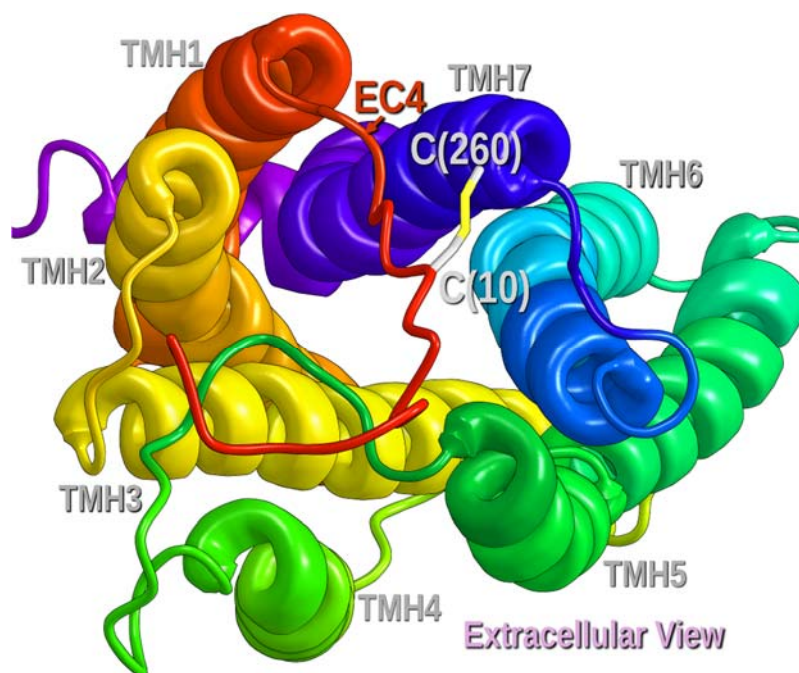


Figure 39. The Extracellular End of the Receptor and the Disulfide Bridge Between N-Terminal C(10) and C(260) at the EC End of TMH7.

Binding pocket position. Figure 40 illustrates the positions of Q6.58 and Q7.36 relative to the ML184 binding site. These residues are positioned relatively high on the EC end of TMHs 6 and 7 and above the ML184 binding pocket in our current GPR55 R* model. In our first GPR55 model, Q6.58 was near the nitrogen in the pendant five membered ring of ML184 and able to form a hydrogen bonding interaction with this nitrogen.¹⁴ As discussed in the next section, mutation results suggested that Q6.58 and Q7.36 do not interact with ML184. This necessitated a re-orientation of ML184 in the binding pocket in the current model.

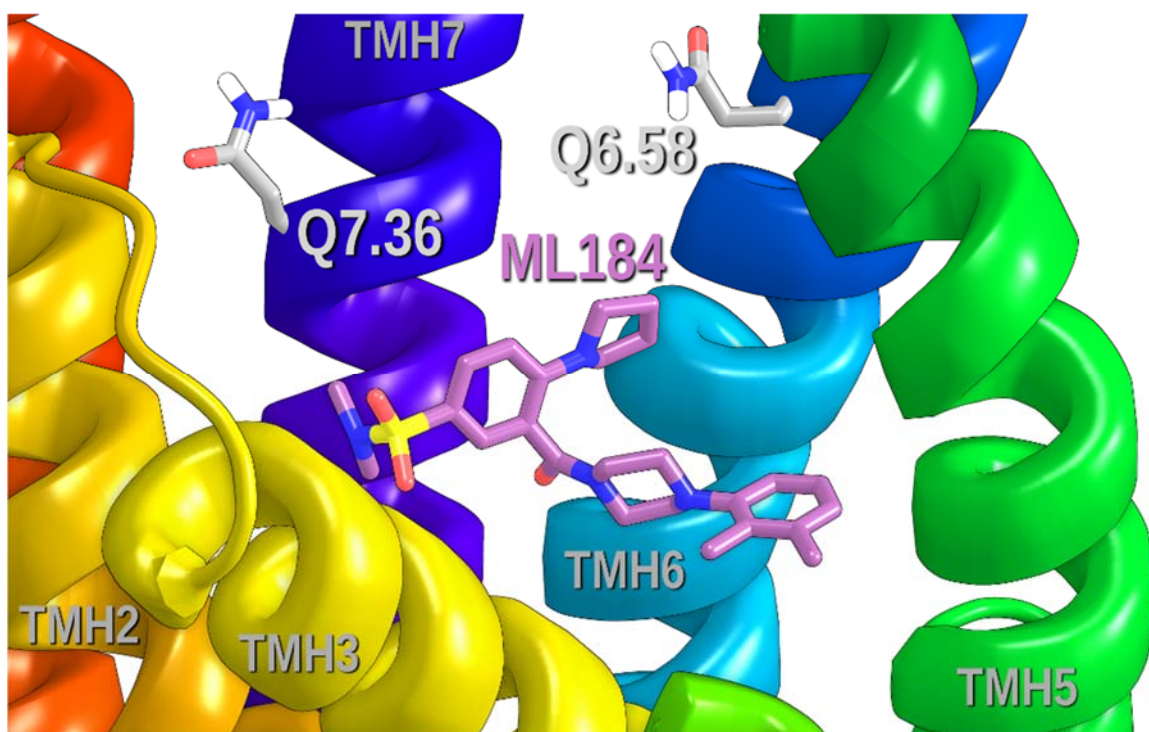


Figure 40. Positions of Q6.58 and Q7.36 Relative to the ML184 Binding Site. Both Residues are Clearly Above the ML184 Binding Site.

Discussion

ML184 Docked into the GPR55R* Bundle

When one begins the characterization of the ligand binding pocket in a newly de-orphanized receptor, like GPR55, mutation studies are crucial to understanding the binding pocket. Our original GPR55 models (R and R*) were based on a beta-2-adrenergic receptor template.¹²⁻¹³ In this model, we docked ML184 so that the ligand piperazine and di-methyl phenyl ring segment was vertical in the binding pocket, while the rest of the ligand occupied a horizontal space near the extracellular loops. Mutation results reported here clearly necessitate that a reorientation of ML184 occur in the binding pocket. In the refined model reported here, we also took advantage of crystal structures that were unavailable at the time of the original model creation and found that the delta-opioid receptor (DOR) crystal structure⁷ was a more appropriate template for the next generation model. The DOR, for example has a PRO at position 4.59, as does GPR55. The beta-2-adrenergic receptor, on the other hand, has a PRO shifted by one residue to 4.60. In addition, the DOR has the same toggle switch partner as GPR55, M3.36.

Ligand Interactions within the Binding Crevice

As predicted by previous studies conducted on the GPR55 receptor in the Reggio lab, the current model has a crucial hydrogen bonding interaction between ML184 and K2.60 on TMH 2 (see Figure 35A or 35B) that results in the strongest ligand Interaction Energy (-9.4 kcal/mol) of any residue in the GPR55 R* bundle (see Table S-1 in Appendix B). A strong hydrogen bond between the electronegative sulfonamide and the

positive lysine is consistent with the experimental results that show a complete loss of signaling upon the K2.60 mutation to an alanine (see Tables 2 and 3).

Mutation of E3.29 to either an alanine or a leucine resulted in a profound reduction of receptor signaling as well. Though there is no direct interaction between ML184 and E3.29 in the current model, modelling suggests that E3.29 forms a salt bridge with K2.60 (see Figure 36 B). This salt bridge positions K2.60 for interaction with ML184. The loss of this residue's directing capability for K2.60 via the E3.29/A/L mutations effectively make K2.60 less available in the binding pocket, leading to a considerable loss of function.

At the ML184 binding site, the EC-2 loop residue, H(170), serves as a hydrogen bond donor to the ML184 sulfonamide oxygen (see Figure 35 A). The Interaction Energy for ML184 with H(170) is -3.5 kcal/mol (see Table S-1 in Appendix B). Simultaneously, the sulfonamide oxygen also receives a hydrogen bond from K2.60. Because hydrogen bonding is stronger when the donating residue is charged, the H170 hydrogen bond with ML184 is weaker (-3.5 kcal/mol) than that with K2.60 (-9.1 kcal/mol) (see Table S-1 in Appendix B). The pKa of histidine is 6.0. At physiological pH, about 10% of histidine residues are protonated. We assume here that H(170) is uncharged. An H(170)F mutation removes the hydrogen bonding ability of residue 170, but not its ability to form aromatic interactions. Mutation of H(170) to a phenylalanine resulted in a 6-fold reduction in SRE responses (see Table 2). The magnitude of the effect upon mutation is consistent with the loss of a hydrogen bond. In addition, the fact that H(170) mutation affected ML184's signaling suggests indirectly that there is also a C(168)/C3.25 disulfide bond in GPR55.

This bond requires that the EC-2 loop extend over to TMH3 to link with C3.25 and therefore is responsible for the H(170) location in the GPR55 R* model. In addition, inspection of GPCR crystal structures that contain the analogous disulfide bridges reveal that the second residue after the disulfide bridge typically points down into the binding crevice. H(170) is the second residue after the C(168)/C3.25 disulfide bridge.

Y3.32 serves two functions in GPR55. It is a binding site residue (see Figure 35 A and B) and also part of the extended toggle switch for GPR55 activation (see Figure 37). A stepwise loss of function is seen when Y3.32 is first mutated to a phenylalanine (30-fold loss, see Table 2) and then a leucine (170-fold loss, see Table 2). At the ML184 binding site, Y3.32 donates a hydrogen bond to the ML184 carboxamide oxygen (Figure 35 A) and forms an aromatic stacking interaction with the ML184 central benzene ring (Figure 35 B) proximal to the ML184 sulfonamide moiety. The first mutation, Y3.32F, removes the residue's potential to donate a hydrogen bond. The magnitude of the effect (30-fold loss) is consistent with Y3.32 serving as the lone hydrogen bond donor to ML184 in this region. The second mutation, Y3.32L, removes both hydrogen bonding and aromatic stacking interactions from the ML184 binding site at this position. The 170-fold reduction in EC_{50} (see Table 2) is consistent with the loss of two important interactions for ML184. Y3.32F mutation results are also consistent with Y3.32's participation in the extended toggle switch region in GPR55, as loss of aromaticity at 3.32 in the Y3.32L mutant should have a profound effect on signaling (170-fold reduction in EC_{50} ; see Table 2).

The current model of GPR55 places F6.55 facing inward towards the binding crevice. This residue forms an aromatic stacking interaction with the distal, dimethyl-phenyl ring of ML184 (Figure 35 B; Interaction Energy = -5.1 kcal/mol; see Table S-1 in Appendix B). The F6.55A mutation resulted in a 15-fold loss in EC₅₀ for ML184, consistent with the loss of this aromatic stacking interaction. The F6.55L resulted in an even larger loss in EC₅₀ (92-fold). This mutation not only removes an aromatic stacking interaction, but also causes crowding in the ML-84 binding pocket. This crowding causes ML184 to shift position and the net result would be reduced binding site interactions. The 92-fold loss in EC₅₀ is consistent with such an alteration.

The x-ray crystal structure of the beta-1-adrenergic receptor complexed with Gs protein shows that TMH6 has straightened by flexing its proline kink at P6.50.¹⁵ This conformational change also impacts binding pocket residues. W6.48 has been shown to change its conformational state within the binding pocket upon receptor activation (χ_1 g⁺ → trans). In the inactive state, W6.48 is typically held in its χ_1 =g⁺ conformation by another binding pocket residue. Together, this pair of residues is known as the “toggle switch.”¹⁶ In the GPR55 activated state model reported here, Y3.32, M3.36 and F6.48 form an extended toggle switch (see Figure 37), with additional interactions from F3.33 and Y3.37. The mutation effects of Y3.32 are discussed above in the context of their effects on the ML184 binding pocket interactions and upon signaling. For both the SRE and SRF readouts used here, mutation of M3.36 to alanine had a significant impact on signaling (16-fold, 62-fold). Mutation of the toggle switch residues M3.36 and F6.48 resulted in increased EC₅₀ values, but these mutants were able to ultimately reach SRE

induction comparable to wild-type. As ML184 is a GPR55 agonist, it is expected that its position in the bundle would not cause it to interfere with the receptor's ability to activate. This is verified by the experimental data and is what is observed in the current ligand receptor complex.

Class A GPCRs typically have a disulfide bridge between a residue in the EC-2 loop and Cys3.25 near the top of TMH3. The sequence of GPR55 suggests that it likely has this disulfide bridge as well. Mutation studies of these Cys residues typically result in loss of function as the EC-2 – C3.25 disulfide bridge is important for binding pocket structure.¹⁷ The CXCR4^{11,18} and CCR5¹⁹ crystal structures reveal the existence of a second disulfide bridge that links the N terminus of the receptor to the EC end of TMH7, forming what has been called the fourth EC loop.¹⁹ This loop has been proposed to shape the entrance of the ligand-binding pocket and to add rigidity to the overall surface of the receptor.¹⁹ The sequences of ~30% of Class A GPCRs contain such Cys residues, including the lysophospholipid (LPA), bradykinin (B1-2), endothelin (ETA-B), melanocortin (MC1-5), serotonin (5-HT), purinergic (P2Y), and orphan receptors, such as GPR55. The structure of one of the latest resolved rhodopsin-like receptors, P2Y12, revealed the presence of such an EC-4 loop;⁹ however, the conservation of these residues does not necessarily imply the formation of a EC-4 loop (see crystal structures of dopamine D3²⁰ and serotonin, 5HT1B²¹ receptors). Because the GPR55 sequence suggests the presence of an EC-4 loop, this second disulfide bridge was incorporated into our GPR55 model and was tested via C(10)A and C(260)A mutations here. Results reported here show that each mutation impacts ML184 activation of GPR55, although

these mutations are not devastating (11-fold for C(10)A; 12-fold for C(260)A). We have taken these results as evidence that this disulfide bridge is present in GPR55 and have retained this bridge in our model (see Figure 39). It should be noted that the EC-4 loop may have larger effects on GPR55 agonists other than ML184, as it has been proposed that this fourth loop shapes the entrance of the ligand-binding pocket.¹⁹

Q6.58 and Q7.36 are located at the extreme EC ends of TMH6 and TMH7 (see Figure 40). In our first GPR55 model, Q6.58 was near the nitrogen in the pendant five membered ring of ML184 and able to form a hydrogen bonding interaction with this nitrogen.¹² A Q6.58M mutation should have resulted in the loss of this hydrogen bond and a significant reduction in ML184 EC₅₀. However, at the Q6.58M/A mutations, ML184 retained WT signaling. This result is a key result from a modelling perspective because it clearly suggested that a different binding mode for ML184 should be sought.

Also in our previous GPR55 R model, Q7.36 interacted simultaneously with K2.60 and with antagonist, ML192.¹³ The re-orientation of ML184 dictated by the Q6.58M/A mutations dictated that Q7.36 should have no ligand interactions. Consistent with this result, experimental data reported here shows that at both the Q7.36A and Q7.36N mutant, ML184 retains WT signaling.

Quite recently, additional synthetic ligands, as well as another endogenous agonist for GPR55 have been described.²² The synthetic ligands employed our previous model as a guide for ligand design. The mutation results reported here will be important for the design of more potent and efficacious agonists for GPR55.

Conclusions

Results reported here identify key GPR55 residues that are important for agonist signaling, as well as residues implicated in the agonist activated signaling cascade. Two residues crucial for ML184 signaling at GPR55 are K2.60 and E3.29. Three additional residues, Y3.32, H(170) and F6.55, are important for ML184 signaling. Further, results suggest that a cluster of residues, F3.32/M3.36/F6.48 serves as the toggle switch for activation of GPR55. GPR55 also likely possesses, a second disulfide bridge that links the N terminus of the receptor to the EC end of TMH7. This loop has been called the fourth EC loop.¹⁹ All of these results provide, for the first time, structural information that should aid in the rational design of next generation GPR55 ligands. It is hoped that this will lead to a high affinity GPR55 radioligand, a tool that is sorely needed in the field.

Experimental Section

Material and Reagents

Soy LPI (purchased from Sigma-Aldrich), and ML184 (MolPort) were dissolved in dimethyl sulfoxide to a concentration of 10 mM. The SRE reporter, pGL4.33[luc2P/SRE/Hygro] and the SRF-RE reporter, pGL4.34[luc2P/SRF-RE/Hygro] were from Promega.

Mutagenesis and Cell Culture

The M3.36A, F6.48A, K2.60A, E3.29A, E3.29L, Y3.32F, Y3.32L, F6.55A, F6.55L, Q6.58M, C(10)A, H(170)F, C(260)A, Q7.36A and Q7.36N mutants of the human GPR55 in the vector pcDNA3 were constructed using the QuikChange site-

directed mutagenesis kit (Stratagene). DNA sequencing subsequently confirmed the presence of the desired mutation only.

Serum Response Element (SRE) and Serum Response Factor (SRF) Assay

HEK293 cells were transiently transfected with GPR55 and pGL4.33 [luc2P/SRE/Hygro] or pGL4.34 [luc2P/SRF-RE/Hygro] vector reporter plasmids using Lipofectamine 2000 as described by the manufacturer (Invitrogen). Transfected HEK293 cells were seeded (60,000 cells per well) in 96-well plates. Five hours later, medium was changed to 1% FBS/DMEM. Cells were incubated overnight. The next day cells were treated with ligands for 5 h in serum-free DMEM medium at 37°C. After treatment, cells were lysed by 1X lysis buffer for 10 min at room temperature. Plates were read to record bioluminescent light immediately after the injection of 40µl Luciferin ($\geq 250\mu\text{M}$) per well. Luminescence was measured in an Envision 2104 multilabel Reader (PerkinElmer). Luminescence values are given as relative light units. Concentration-effect curves for agonist-mediated receptor activation were analyzed by nonlinear regression techniques using GraphPad Prism 5.0 software (GraphPad) and data were fitted to sigmoidal dose-response curves to obtain EC50 values.

Modeling

Amino acid numbering system. The amino acid numbering system used here is the Ballesteros-Weinstein numbering system²³ in which the most highly conserved residue across Class A GPCRs in each TMH is assigned a number .50. This number is preceded by the TMH number and can be followed by the absolute sequence number in parentheses. For example, the most highly conserved residue in TMH4 is W4.50. For

GPR55, this residue is W4.50(146). The residue preceding this residue is I4.49(145) and the residue following it is V4.51(147). Loop residues in this system are identified by their absolute sequence numbers only.

Modeling of hGPR55 active-state bundle (GPR55 R*) using GPCR x-ray crystallography data. The model of the activated form of GPR55 (GPR55 R*) described in the current work was created using the 1.8 Å crystal structure of the human delta opioid receptor (hDOR, PDB id: 4N6H) as a template.⁷ Transmembrane regions of GPR55 vs. hDOR in which the placement of prolines differed (GPR55 transmembrane helices (TMHs) 1, 5, 6 and 7) were explored using the Conformational Memories (CM) method described below.²⁴

Conformational Memories (CM) Method for Calculating TMH Conformation

The CM method uses multiple Monte Carlo/simulated annealing random walks employing the CHARMM force field. Backbone ϕ and ψ torsions in regions of interest (i to i-4 of a proline) were allowed to vary $\pm 50^\circ$, while all other backbone torsion angles were allowed to vary $\pm 10^\circ$. Side chain torsions were allowed to vary $\pm 180^\circ$. All bond angles were allowed to vary $\pm 8^\circ$ except for C-S-C angles that were allowed to vary $\pm 15^\circ$. A minimum set of 108 conformers was generated for each GPR55 helix, independently, in a distance dependent dielectric at 310 K.

TMH1 in GPR55 has a Pro at position 1.41 not found in DOR. An ideal helix ($\phi = -62.9^\circ$, and $\psi = -41.6^\circ$) with the GPR55 sequence was built, and the region containing the proline and 4 residues prior to the Pro (i to i-4, A1.37 - P1.41) was varied using CM.

TMH5 in GPR55 has two prolines, the highly conserved P5.50 and an additional one at position 5.41. TMH5 of the DOR crystal structure was mutated to the GPR55 sequence and the backbone dihedrals from P5.41 to K5.37 were varied to explore the possible conformations caused by this second, proline.

TMH6 in GPR55 has a conservative SFXP substitution in place of the highly conserved Class A CWXP motif. Biophysical studies have indicated that there is a salt bridge, or ionic lock (between R3.50 near the intracellular (IC) end of TMH3 and D/E6.30 at the IC end of TMH6), common to all Class A GPCRs that is broken upon activation. The breaking of this ionic lock allows TMH6 to straighten, moving its intracellular (IC) end away from the TMH bundle.²⁵ For this reason, it was crucial to explore the conformational space of GPR55 TMH6 which has a glutamine (Q) at position 6.30 in place of a typical aspartic (D) or glutamic (E) acid. The GPR55 TMH6 sequence was built, using the ideal helix values ($\phi = -62.9^\circ$, and $\psi = -41.6^\circ$) and the *i* to *i*-4 region around the Pro (P6.50-V6.46) was varied using CM.

TMH7 in GPR55 lacks the highly conserved Class A GPCR NPXXY motif having instead a DVXXY sequence. Traditionally the NPXXY motif influences the conformation of TMH7 and places Y7.53 in the correct position to interact with F7.60 on Helix 8 (Hx8, a short intracellular extension of TMH7 that lies usually parallel to the cell membrane). For receptors that possess an NPXXY motif, we have typically designated the backbone region of P7.50- X7.46 region as variable. For GPR55 TMH7, an ideal helix ($\phi = -62.9^\circ$, and $\psi = -41.6^\circ$) was built and the *i* to *i*-4 region in which there is normally a Pro (V7.50 - C7.46) was varied using CM.

Construction of the GPR55 Active-state Bundle

Transmembrane helices 2, 3 and 4 of the DOR were mutated to the corresponding GPR55 residues, while helices chosen from the CM output that would fit in the bundle were substituted in the bundle. This included a straightened TMH6 conformer for which the TMH3-TMH6 ionic lock was broken, reflecting the R* state. Incorporated into this new bundle were updates from previous homology models of GPR55¹³⁻¹⁴ created in this lab: The high degree of sequence homology between GPR55 and the CXCR4 receptor,¹¹ particularly in the EC regions, dictated several modifications to the model. These were (1) the introduction of EC helical extensions on TMH5-7 of GPR55; (2) the introduction of a β sheet motif into the EC-2 loop in GPR55; and, (3) the introduction of a disulfide bridge between Cys(10) in the N-terminus and Cys(260) in the EC-3 loop near the top of TMH7.

The resulting homology model was then optimized using the following protocol¹³: The energy of the GPR55 R* bundle was minimized using the OPLS 2005 force field in Macro-model 9.9 (Schrödinger Inc., Portland, OR). An 8.0-Å extended non-bonded cutoff (updated every 10 steps), a 20.0-Å electrostatic cutoff, and a 4.0-Å hydrogen bond cutoff were used in each stage of the calculation. The minimization was performed in three stages. Each stage consisted of a Polak- Ribier conjugate gradient minimization in 1000-step increments until the bundle reached a 0.05 kJ/mol gradient. In the first stage of the calculation, the TMH region of the receptor was held stationary and the loops were allowed to relax using the generalized born/surface area continuum solvation model for water (Macro-model). In the second stage, the loops were frozen and the side chains of

the TMHs were allowed to adjust. A distance dependent dielectric was used for this minimization. In the third stage, the N and C termini were minimized using the protocol described, for the loops, above. In this stage, only the termini were minimized.

Conformational Analysis of ML184

A complete conformational analysis of the GPR55 agonist ML184 (CID2440433) was performed using *ab initio* Hartree-Fock (HF) calculations at the 6–31G* level as encoded in Jaguar (version 9.0, Schrodinger, LLC, New York, NY). Hartree-Fock 6–31G* six-fold conformer searches were performed for the rotatable bonds, N1-S2, S2-C3, C4'-N5', C4-C5, C5-N6, N7-C8 (see numbering system in Fig 29), of ML184 as follows: In each conformer search, local energy minima were identified by rotation of a subject torsion angle through 360° in 60° increments (6-fold search), followed by HF 6–31G* energy minimization of each rotamer generated. To calculate the energy difference between the global minimum energy conformer of ML184 and its final docked conformation, rotatable bonds in the global minimum energy conformer were driven to their corresponding value in the final docked conformation and the single point energy of the resultant structure was calculated at the HF 6–31G* level. This difference was calculated to be 1.91 kcal/mol.

Docking of ML184

A low free-energy conformer of ML184 was used as input for receptor docking. ML184 was initially docked manually in the binding site of the GPR55 R* model, after which the automatic docking program, Glide (Schrodinger Inc.), was used to explore other possible binding conformations and receptor site interactions. Extra precision (XP)

and flexible docking with ring sampling were selected for the docking setup. Lysine 2.60(80), a previously identified ligand interaction site,¹² was defined as a hydrogen bond donor and was used as a constraint for the automatic docking of the ligand. The energy of the ligand/GPR55 R* complex was minimized using the OPLS 2005 force field in Macro-model 9.9 (Schrödinger Inc., Portland, OR). An 8.0-Å extended non-bonded cutoff (updated every 10 steps), a 20.0-Å electrostatic cutoff, and a 4.0-Å hydrogen bond cutoff were used in each stage of the calculation as described previously. The dock with the best Glide score (-9.1) was selected as the final ML184/GPR55 R* model.

Assessment of Pair-wise Interaction Energies

After defining the atoms of ML184 as one group (Group 1) and the atoms corresponding to a residue that lines the binding site in the final ligand/GPR55 R* complex as another group (Group 2), Macromodel (version 8.6, Schrödinger, LLC, New York, NY) was used to output the pair-wise interaction energy (coulombic and Van der Waals) for a given pair of atoms. The pairs corresponding to Group 1 (ligand) and Group 2 (residue of interest) were then summed to yield the interaction energy between the ligand and that residue. The ML184/GPR55 R* complex was found to have interaction energies totaling to -55.9 kcal/mol. Taking the conformational energy cost for ML184 (1.91 kcal/mol) into account, the final total energy for the ML184/GPR55 R* complex was found to be -54.0 kcal/mol. A breakdown of interaction energies is provided in Table S-1.

Acknowledgments

This research was supported by grants from the National Institute on Drug Abuse R01 DA023204 (MEA), R01DA035926 (MEA), P30DA013429 and K05 DA021358 (PHR) and from the National Institute of Neurological Disorders and Stroke R21 NS077347 (MEA and PHR). The content is solely the responsibility of the authors and does not necessarily represent the official views of the National Institutes of Health. We would like to thank Lawrence Barak of the NIDA sponsored Duke P30 Center of Excellence for technical support.

References

1. Kapur, A.; Zhao, P.; Sharir, H.; Bai, Y.; Caron, M. G.; Barak, L. S.; Abood, M. E. Atypical Responsiveness of the Orphan Receptor GPR55 to Cannabinoid Ligands. *J. Biol. Chem.* **2009**, *284* (43), 29817–29827.
2. (a) Henstridge, C. M.; Balenga, N. A.; Ford, L. A.; Ross, R. A.; Waldhoer, M.; Irving, A. J. The GPR55 Ligand L-alpha-lysophosphatidylinositol Promotes RhoA-dependent Ca²⁺ Signaling and NFAT Activation. *Faseb. J.* **2009**, *23* (1), 183-93; (b) Oka, S.; Toshida, T.; Maruyama, K.; Nakajima, K.; Yamashita, A.; Sugiura, T. 2-Arachidonoyl-sn-glycero-3-phosphoinositol: A Possible Natural Ligand for GPR55. *J. Biochem.* **2009**, *145* (1), 13-20; (c) Oka, S.; Nakajima, K.; Yamashita, A.; Kishimoto, S.; Sugiura, T., Identification of GPR55 as a Lysophosphatidylinositol Receptor. *Biochem. Biophys. Res. Commun.* **2007**, *362* (4), 928–934.
3. (a) Sawzdargo, M.; Nguyen, T.; Lee, D. K.; Lynch, K. R.; Cheng, R.; Heng, H. H.; George, S. R.; O'Dowd, B. F. Identification and Cloning of Three Novel Human G Protein-coupled Receptor Genes GPR52, PsiGPR53 and GPR55: GPR55 is Extensively Expressed in Human Brain. *Brain Res Mol Brain Res* **1999**, *64*, 193-8; (b) Staton, P. C.; Hatcher, J. P.; Walker, D. J.; Morrison, A. D.; Shapland, E. M.; Hughes, J. P.; Chong, E.; Mander, P. K.; Green, P. J.; Billinton, A.; Fulleylove, M.; Lancaster, H. C.; Smith, J. C.; Bailey, L. T.; Wise, A.; Brown, A. J.; Richardson, J. C.; Chessell, I. P. The Putative Cannabinoid Receptor GPR55 Plays a Role in Mechanical Hyperalgesia Associated with Inflammatory and Neuropathic Pain. *Pain* **2008**, *139*, 225-36; (c) Whyte, L. S.; Ryberg, E.; Sims, N. A.; Ridge, S. A.; Mackie, K.; Greasley, P. J.; Ross, R. A.; Rogers, M. J. The Putative Cannabinoid Receptor GPR55 Affects Osteoclast Function In Vitro and Bone Mass In Vivo. *Proc. Natl. Acad. Sci. USA* **2009**, *106*, 16511-6; (d) Ford, L. A.; Roelofs, A. J.; Anavi-Goffer, S.; Mowat, L.; Simpson, D. G.; Irving, A. J.; Rogers, M. J.; Rajnicek, A. M.; Ross, R. A. A Role for L-alpha-lysophosphatidylinositol and GPR55 in the Modulation of Migration, Orientation and Polarization of Human Breast Cancer Cells. *Br. J. Pharmacol.* **2010**, *160*, 762-71; (e) Andradas, C.; Caffarel, M. M.; Perez-Gomez, E.; Salazar, M.; Lorente, M.; Velasco, G.; Guzman, M.; Sanchez, C. The Orphan G Protein-coupled Receptor GPR55 Promotes Cancer Cell Proliferation Via ERK. *Oncogene* **2010**, *30*, 245-252; (f) Pineiro, R.; Maffucci, T.; Falasca, M. The Putative Cannabinoid Receptor GPR55 Defines a Novel Autocrine Loop in Cancer Cell Proliferation. *Oncogene* **2010**, *30*, 142–152.
4. (a) Heynen-Genel, S.; Dahl, R.; Shi, S.; Milan, L.; Hariharan, S.; Sergienko, E.; Hedrick, M.; Dad, S.; Stonich, D.; Su, Y.; Vicchiarelli, M.; Mangravita-Novo, A.; Smith, L. H.; Chung, T. D. Y.; Sharir, H.; Caron, M. G.; Barak, L. S.; Abood, M. E.

- Screening for Selective Ligands for GPR55 - Antagonists. In *Probe Reports NIH Molecular Libraries Program*, 2010; (b) Heynen-Genel, S.; Dahl, R.; Shi, S.; Milan, L.; Hariharan, S.; Bravo, Y.; Sergienko, E.; Hedrick, M.; Dad, S.; Stonich, D.; Su, Y.; Vicchiarelli, M.; Mangravita-Novo, A.; Smith, L. H.; Chung, T. D. Y.; Sharir, H.; Barak, L. S.; Abood, M. E. Screening for Selective Ligands for GPR55 - Agonists. In *Probe Reports NIH Molecular Libraries Program*, 2010.
- Heynen-Genel, S.; Dahl, R.; Shi, S.; Milan, L.; Hariharan, S.; Bravo, Y.; Sergienko, E.; Hedrick, M.; Dad, S.; Stonich, D.; Su, Y.; Vicchiarelli, M.; Mangravita-Novo, A.; Smith, L. H.; Chung, T. D. Y.; Sharir, H.; Barak, L. S.; Abood, M. E. Screening for Selective Ligands for GPR55. In *Probe Reports NIH Molecular Libraries Program*, 2010.
 - Lauckner, J. E.; Jensen, J. B.; Chen, H. Y.; Lu, H. C.; Hille, B.; Mackie, K. GPR55 is a Cannabinoid Receptor That Increases Intracellular Calcium and Inhibits M Current. *Proc. Natl. Acad. Sci. USA* **2008**, *105*, 2699–2704.
 - Granier, S.; Manglik, A.; Kruse, A. C.; Kobilka, T. S.; Thian, F. S.; Weis, W. I.; Kobilka, B. K. Structure of the delta-opioid receptor bound to naltrindole. *Nature* **2012**, *485*, 400–404.
 - Valley, C. C.; Cembran, A.; Perlmutter, J. D.; Lewis, A. K.; Labello, N. P.; Gao, J.; Sachs, J. N. The Methionine-aromatic Motif Plays a Unique Role in Stabilizing Protein Structure. *J. Biol. Chem.* **2012**, *287*, 34979–34991.
 - Zhang, K.; Zhang, J.; Gao, Z. G.; Zhang, D.; Zhu, L.; Han, G. W.; Moss, S. M.; Paoletta, S.; Kiselev, E.; Lu, W.; Fenalti, G.; Zhang, W.; Muller, C. E.; Yang, H.; Jiang, H.; Cherezov, V.; Katritch, V.; Jacobson, K. A.; Stevens, R. C.; Wu, B.; Zhao, Q. Structure of the Human P2Y₁₂ Receptor in Complex with an Antithrombotic Drug. *Nature* **2014**, *509*, 115–118.
 - Zhang, C.; Srinivasan, Y.; Arlow, D. H.; Fung, J. J.; Palmer, D.; Zheng, Y.; Green, H. F.; Pandey, A.; Dror, R. O.; Shaw, D. E.; Weis, W. I.; Coughlin, S. R.; Kobilka, B. K. High-resolution Crystal Structure of Human Protease-activated Receptor 1. *Nature* **2012**, *492*, 387–392.
 - Wu, B.; Chien, E. Y.; Mol, C. D.; Fenalti, G.; Liu, W.; Katritch, V.; Abagyan, R.; Brooun, A.; Wells, P.; Bi, F. C.; Hamel, D. J.; Kuhn, P.; Handel, T. M.; Cherezov, V.; Stevens, R. C. Structures of the CXCR4 Chemokine GPCR with Small-Molecule and Cyclic Peptide Antagonists. *Science* **2010**, *330*, 1066–1071.
 - Kotsikorou, E.; Madrigal, K. E.; Hurst, D. P.; Sharir, H.; Lynch, D. L.; Heynen-Genel, S.; Milan, L. B.; Chung, T. D.; Seltzman, H. H.; Bai, Y.; Caron, M. G.; Barak, L.; Abood, M. E.; Reggio, P. H. Identification of the GPR55 Agonist Binding

- Site Using a Novel Set of High-Potency GPR55 Selective Ligands. *Biochemistry* **2011**, *50*, 5633–5647.
13. Kotsikorou, E.; Sharir, H.; Shore, D. M.; Hurst, D. P.; Lynch, D. L.; Madrigal, K. E.; Heynen-Genel, S.; Milan, L. B.; Chung, T. D.; Seltzman, H. H.; Bai, Y.; Caron, M. G.; Barak, L. S.; Croatt, M. P.; Abood, M. E.; Reggio, P. H. Identification of the GPR55 Antagonist Binding Site Using a Novel Set of High-potency GPR55 Selective Ligands. *Biochemistry* **2013**, *52*, 9456–9469.
 14. Kotsikorou, E.; Madrigal, K. E.; Hurst, D. P.; Sharir, H.; Lynch, D. L.; Heynen-Genel, S.; Milan, L. B.; Chung, T. D.; Seltzman, H. H.; Bai, Y.; Caron, M. G.; Barak, L.; Abood, M. E.; Reggio, P. H. Identification of the GPR55 agonist binding site using a novel set of high-potency GPR55 selective ligands. *Biochemistry* **2011**, *50*, 5633–5647.
 15. Rasmussen, S. G.; DeVree, B. T.; Zou, Y.; Kruse, A. C.; Chung, K. Y.; Kobilka, T. S.; Thian, F. S.; Chae, P. S.; Pardon, E.; Calinski, D.; Mathiesen, J. M.; Shah, S. T.; Lyons, J. A.; Caffrey, M.; Gellman, S. H.; Steyaert, J.; Skiniotis, G.; Weis, W. I.; Sunahara, R. K.; Kobilka, B. K. Crystal Structure of the Beta2 Adrenergic Receptor-Gs Protein Complex. *Nature* **2011**, *477*, 549–555.
 16. McAllister, S. D.; Hurst, D. P.; Barnett-Norris, J.; Lynch, D.; Reggio, P. H.; Abood, M. E. Structural Mimicry in Class A G Protein-coupled Receptor Rotamer Toggle Switches: The Importance of the F3.36(201)/W6.48(357) Interaction in Cannabinoid CB1 Receptor Activation. *J. Biol. Chem.* **2004**, *279* (46), 48024–48037.
 17. (a) Perlman, J. H.; Wang, W.; Nussenzveig, D. R.; Gershengorn, M. C., A disulfide bond between conserved extracellular cysteines in the thyrotropin-releasing hormone receptor is critical for binding. *J. Biol. Chem.* **1995**, *270*, 24682–5; (b) Hwa, J.; Reeves, P. J.; Klein-Seetharaman, J.; Davidson, F.; Khorana, H. G., Structure and function in rhodopsin: further elucidation of the role of the intradiscal cysteines, Cys-110, -185, and -187, in rhodopsin folding and function. *Proc. Natl. Acad. Sci. USA* **1999**, *96*, 1932–1935.
 18. Qin, L.; Kufareva, I.; Holden, L. G.; Wang, C.; Zheng, Y.; Zhao, C.; Fenalti, G.; Wu, H.; Han, G. W.; Cherezov, V.; Abagyan, R.; Stevens, R. C.; Handel, T. M., Structural biology. Crystal Structure of the Chemokine Receptor CXCR4 in Complex with a Viral Chemokine. *Science* **2015**, *347*, 1117–1122.
 19. Szpakowska, M.; Perez Bercoff, D.; Chevigne, A. Closing the Ring: A Fourth Extracellular Loop in Chemokine Receptors. *Sci. Signal.* **2014**, *7*, pe21.
 20. Chien, E. Y.; Liu, W.; Zhao, Q.; Katritch, V.; Han, G. W.; Hanson, M. A.; Shi, L.; Newman, A. H.; Javitch, J. A.; Cherezov, V.; Stevens, R. C. Structure of the Human

- Dopamine D3 Receptor in Complex with a D2/D3 Selective Antagonist. *Science* **2010**, *330*, 1091–1095.
21. Wang, C.; Jiang, Y.; Ma, J.; Wu, H.; Wacker, D.; Katritch, V.; Han, G. W.; Liu, W.; Huang, X. P.; Vardy, E.; McCorvy, J. D.; Gao, X.; Zhou, X. E.; Melcher, K.; Zhang, C.; Bai, F.; Yang, H.; Yang, L.; Jiang, H.; Roth, B. L.; Cherezov, V.; Stevens, R. C.; Xu, H. E. Structural Basis for Molecular Recognition at Serotonin Receptors. *Science* **2013**, *340*, 610–614.
 22. (a) Morales, P.; Whyte, L.; Chicharro, R.; Gomez-Canas, M.; Pazos, R.; Goya, P.; Irving, A. J.; Fernandez-Ruiz, J.; Ross, R.; Jagerovic, N. Identification of Novel GPR55 Modulators Using Cell-Impedance-Based Label-Free Technology. *J. Med. Chem.* **2016**; (b) Yrjola, S.; Parkkari, T.; Navia-Paldanius, D.; Laitinen, T.; Kaczor, A. A.; Kokkola, T.; Adusei-Mensah, F.; Savinainen, J. R.; Laitinen, J. T.; Poso, A.; Alexander, A.; Penman, J.; Stott, L.; Anskat, M.; Irving, A. J.; Nevalainen, T. J. Potent and Selective N-(4-sulfamoylphenyl)thiourea-based GPR55 Agonists. *Eur. J. Med. Chem.* **2016**, *107*, 119-32; (c) Guy, A. T.; Nagatsuka, Y.; Ooashi, N.; Inoue, M.; Nakata, A.; Greimel, P.; Inoue, A.; Nabetani, T.; Murayama, A.; Ohta, K.; Ito, Y.; Aoki, J.; Hirabayashi, Y.; Kamiguchi, H. Neuronal Development. Glycerophospholipid Regulation of Modality-specific Sensory Axon Guidance in the Spinal Cord. *Science* **2015**, *349*, 974–977.
 23. Ballesteros, J.; Weinstein, H. Integrated Methods for the Construction of Three-dimensional Models and Computational Modeling of Structure-function Relations in G-protein-coupled Receptors. *Methods in Neurosciences* **1995**, *25*, 366–428.
 24. (a) Guarnieri, F.; Weinstein, H., Conformational Memories and the Exploration of Biologically Relevant Peptide Conformations: An Illustration for the Gonadotropin-Releasing Hormone. *J. Amer. Chem. Soc.* **1996**, *118*, 5580-5589; (b) Whitnell, R. M.; Hurst, D. P.; Reggio, P. H.; Guarnieri, F., Conformational memories with variable bond angles. *J. Comput. Chem.* **2008**, *29*, 741–752.
 25. Jensen, A. D.; Guarnieri, F.; Rasmussen, S. G.; Asmar, F.; Ballesteros, J. A.; Gether, U. Agonist-induced Conformational Changes at the Cytoplasmic Side of Transmembrane Segment 6 in the Beta 2 Adrenergic Receptor Mapped by Site-selective Fluorescent Labeling. *J. Biol. Chem.* **2001**, *276*, 9279–9290.

CHAPTER V

FUTURE CONSIDERATIONS

Now that there are models of the GPR55 active and inactive states it is imperative that the models continue to be refined. It is also necessary that they be used as the tools that they were designed to be to suggest new directions for ligand development.

Chemo-informatics Approach

A shift in focus to other scaffolds will likely be needed owing to the fact that the analogs synthesized thus far have not reached low nanomolar efficacies. One approach to scaffold diversification is receptor-based core hopping. New scaffolds for both GPR55 agonists and antagonists can be explored using the Schrodinger suite module CoreHopper. This task option in the Schrodinger small-molecule discovery suite allows for rapid screening of novel cores to help overcome undesirable properties of a ligand by creating new lead compounds with improved core properties while preserving key R-group interactions. Core hopping can also potentially be used for generation of novel derivatives to a known ligand (such as LPI). Chemotypes produced by the CoreHopper program can be used to explore the 102 million-compound library of commercially available compounds in the IReasearch library in ChemNavigator. Once a subset of structures has been identified, these structures can then be converted to three-dimensional form, energy minimized and then subjected to high throughput docking in the updated models using the Induced Fit Docking module discussed in Chapter III.

Validating Chemo-informatics Virtual Search Results

It would be necessary for select compounds from the virtual search to be purchased and evaluated in Dr. Abood's lab. Antagonist compounds (initially at 10 μM) could be screened for their ability to inhibit the β -arrestin trafficking caused by the GPR55 agonist, LPI, using high content imaging by established methodology (described in Chapter II). Compounds found to inhibit LPI's β -arrestin trafficking can then be 1) counter-screened for their ability to inhibit receptor internalization and 2) their ability to antagonize LPI induced ERK1/2 signaling in a 96-well plate format using a LI-COR Odyssey imager for quantification of responses. Agonist compounds (initially at 10 μM) will be screened for their ability to stimulate β -arrestin trafficking, using high content imaging as described in Chapter II. Compounds found to produce β -arrestin trafficking will be counter-screened for their ability to produce receptor internalization as described above.

This would be the point in this endeavor where heretofore unassessed analogs could be designed using each new scaffold identified. If a large number of compounds is generated and found to be active, factors such as cost and future synthetic practicality will be used to filter the final range of compounds to be assessed.

Unutilized Synthesis of Analogues for Scaffold 2

The structure of Scaffold 2 (from the original Burnham Screen mentioned in Chapters I–IV previously) can be divided into two primary areas, the furyl amide and a tricyclic heteroaromatic group, either of which could be modified (Figure 41). The proposed synthetic plans are shown in Scheme 3 (Figure 42). The amide section of *18* can

be connected using the corresponding acid chloride,¹ and there are a multitude of variants possible at this position. The fused, heteroaromatic section can be put together from readily available ketones, ethyl cyanoacetate, and elemental sulfur (S₈) using the Gewald synthesis.² The resulting 2-aminothiophene can be reacted with a nitrile under acidic conditions and then dehydrated using phosphoryl chloride to provide electrophilic coupling partners 20.³ These two sections can then be brought together to provide the desired analogues (21).⁴ This synthesis can be modified as needed to give rise to the different compounds, but the basic route can be followed for most of the structures proposed in Figure 43.

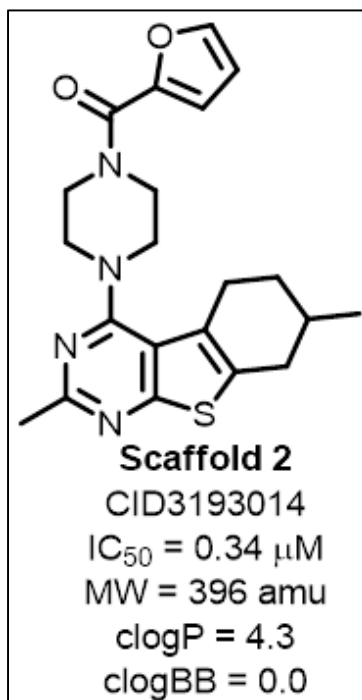


Figure 41. Scaffold 2.

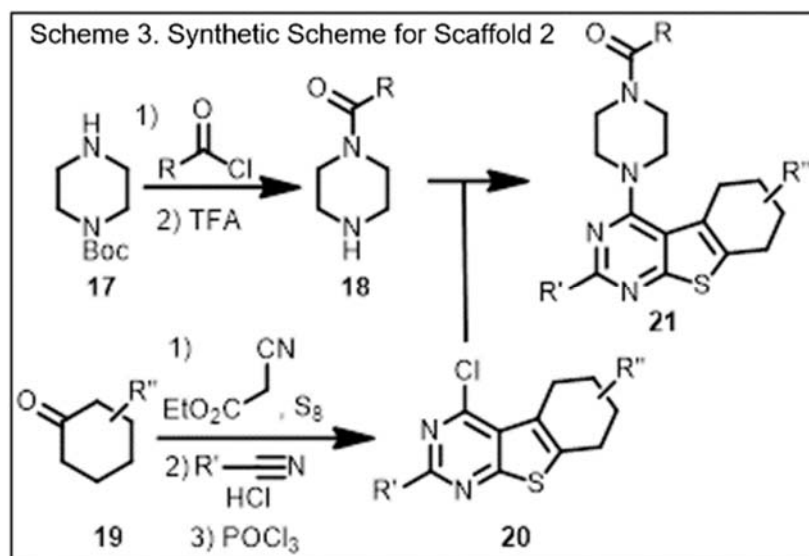


Figure 42. Scheme 3: Synthetic Scheme for Scaffold 2.

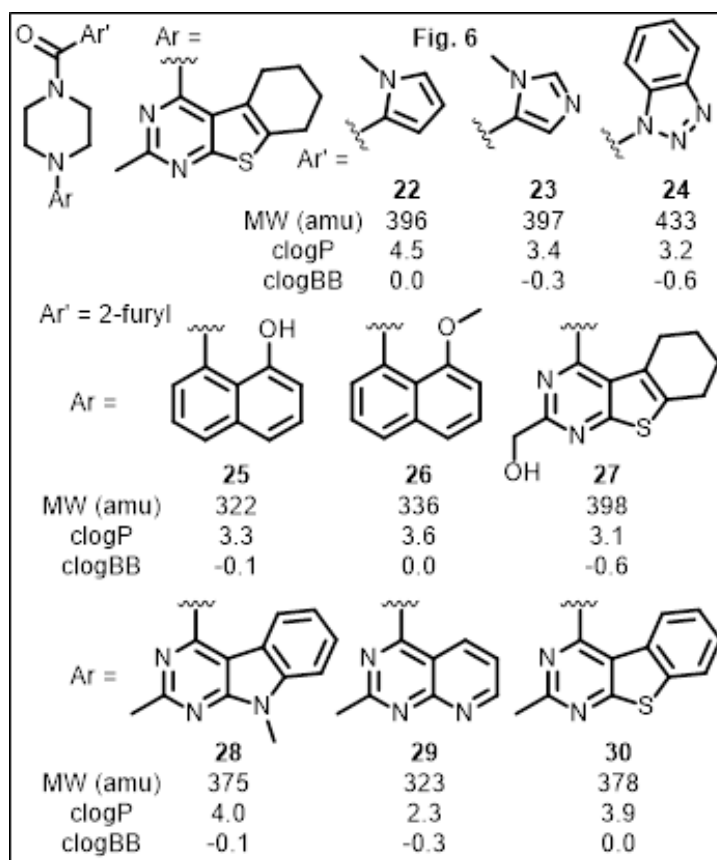


Figure 43. Analogs Proposed for Scaffold 2 Development.

The analogs that should be targeted for synthesis initially are ones that would modify the furan group due to the fact that there are very few commercially available structures that extend out in this area of the binding pocket. This area of the binding pocket is of known importance due to mutation data highlighting ligand interactions with K2.60 and Y3.32. Compounds 25 and 26 were designed to have an intramolecular hydrogen-bond to rigidify the structure in the binding pocket and to allow other moieties on the ligand to explore available space. Alcohol 27 explores the potential for additional hydrogen bonds (hydrogen bond donation to S7.32 and hydrogen bond acceptance with Q6.58).

It is now known from the mutation data detailed in Chapter IV that Q6.58 does not interact with GPR55 agonists in the binding pocket as it sits high in the EC side of the receptor. It remains to be seen if that mutation would have an effect on antagonists of GPR55. Analogs in Figure 43 were proposed based on the fit they had with the original receptor model and so will need to be re-evaluated to confirm their validity in the current, model.

References

1. Wu, Y.; Kuntz, J. D.; Carpenter, A. J.; Fang, J.; Sauls, H. R.; Gomez, D. J.; Ammala, C.; Xu, Y.; Hart, S.; Tadepalli, S. 2,5-Disubstituted pyridines as potent GPR119 agonists. *Bioorganic & Medicinal Chemistry Letters* **2010**, *20*, 2577–2581.
2. Huang, Y.; mling, A. The Gewald multicomponent reaction. *Molecular Diversity* **2011**, *15*, 3–33.
3. Golub, A. G.; Bdzhola, V. G.; Briukhovetska, N. V.; Balanda, A. O.; Kukharenko, O. P.; Kotey, I. M.; Ostrynska, O. V.; Yarmoluk, S. M. Synthesis and biological evaluation of substituted (thieno[2,3-d]pyrimidin-4-ylthio)carboxylic acids as inhibitors of human protein kinase CK2. *European Journal of Medicinal Chemistry* **2011**, *46*, 870–876.
4. Manhas, M. S.; Amin, S. G.; Dayal, B. Heterocyclic compounds. V. 2,4-Disubstituted thienopyrimidones. *Journal of Heterocyclic Chemistry* **1976**, *13*, 633–638.

APPENDIX A**SUPPLEMENTAL INFORMATION FOR CHAPTER II****Supporting Information for:**

Design, Synthesis, and Analysis of Antagonists of GPR55: Piperidine-Substituted
1,3,4-Oxadiazol-2-Ones

Maria Elena Meza-Aviña^{a,†}, Mary A. Lingerfelt^{a,†}, Linda M. Console-Bram^b, Thomas F. Gamage^b, Haleli Sharir^b, Kristen E. Gettys^a, Dow P. Hurst^a, Evangelia Kotsikorou^c, Derek M. Shore^a, Marc G. Caron^d, Narasinga Rao^a, Larry S. Barak^d, Mary E. Abood^{b,*}, Patricia H. Reggio^{a,*}, Mitchell P. Croatt^{a,*}

^aDepartment of Chemistry and Biochemistry, Natural Products and Drug Discovery Center, University of North Carolina at Greensboro, Greensboro, North Carolina 27402, United States

^bCenter for Substance Abuse Research, Temple University, Philadelphia, Pennsylvania 19140, United States

^cDepartment of Chemistry, University of Texas – Pan American, Edinburg, Texas 78539, United States

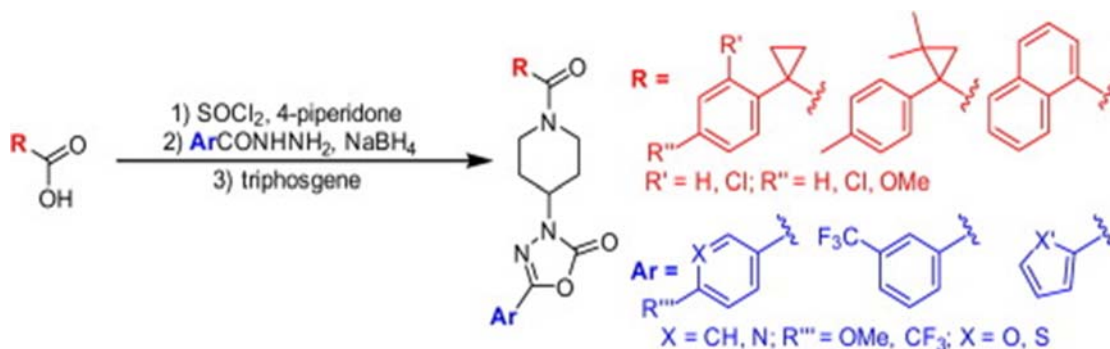
^dDuke University Medical Center, Durham, North Carolina 27709, United States

[†]These authors contributed equally to this work

Table of Contents

Graphical Abstract	106
General Information.....	106
Synthesis of Hydrazides 3a-f.....	107
Characterization of Hydrazides 3w and 3x.....	107
General Method for Synthesis of Piperidones 2a-f.....	108
Characterization of Piperidones 2a-f	109
General Method for Synthesis of Oxadiazolones 5	113
Characterization of Oxadiazolones 5	114
Spectra Data	125
Biological Assay	167
Modeling Methods.....	168
Results.....	172
Literature Cited.....	174

Graphical Abstract

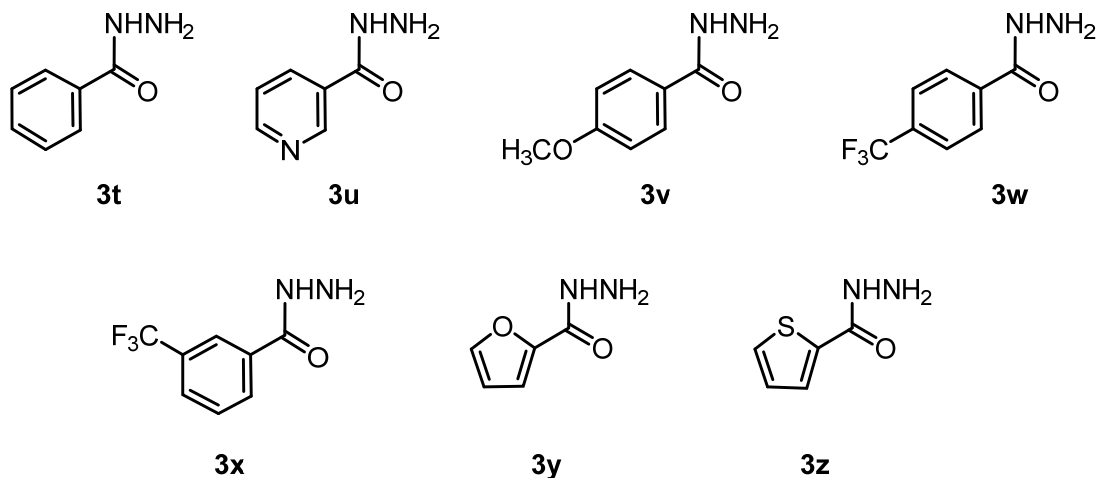


General Information

Solvents and reagents were obtained from commercial sources and used without further purification; anhydrous solvents were dried following standard procedure, reaction progress was monitored by TLC (Silica gel 60 F₂₅₄) glass plates visualized with UV light and permanganate stain. The anhydrous reactions were performed in oven dried glassware under nitrogen atmosphere. Chromatographic purification was performed using silica gel (60 Å, 32-63µm). NMR spectra were recorded in CDCl_3 using a Bruker AVANCE DRX 300 spectrometer (300 MHz for ^1H), JEOL ECA spectrometer (500 MHz for ^1H and 125 MHz for ^{13}C). Chemical shifts reported in ppm using tetramethylsilane as reference for the ^1H NMR and the residual solvent peak for ^{13}C (77 ppm). The abbreviations used to describe peak splitting patterns are: s = singlet, d = doublet, t = triplet, sept = septet, dd = doublet of doublets, m = multiplet. Coupling constants, J , are reported in hertz (Hz). IR was obtained with Perkin Elmer FTIR Spectrometer One and Spectrometer 65 with ATR sampling accessories. Frequencies are

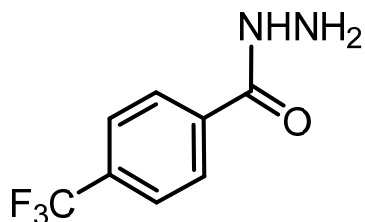
in cm^{-1} . High Resolution Mass Spectra were acquired on a ThermoFisher Scientific LTQ Orbitrap XL MS system.

Synthesis of Hydrazides 3a-f



The hydrazides **3v-x** were synthesized following the reported procedure in the literatureⁱ and hydrazides **3t**, **3u**, **3y**, and **3z** were purchased from Acros. Compound **3v** matched the data previously reports and **3w** and **3x**, are fully characterized below.

Characterization of Hydrazides 3w and 3x



4-Trifluoromethyl-benzoic acid hydrazide (**3w**):

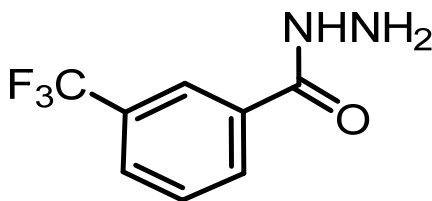
White solid (2.54 g, 12.4 mmol, 75%).

¹H NMR (CDCl₃, 400 MHz): δ = 10.01 (s, 1H), 8.01 (d, *J* = 8.2 Hz, 2H), 7.81 (d, *J* = 8.2 Hz, 2H), 4.59 (s, 2H).

¹³C NMR (CDCl₃, 100 MHz): δ = 164.6, 137.1, 131.2 (q, *J* = 31.5 Hz, 1C), 127.9 (2C), 125.3 (q, *J* = 3.8 Hz, 2C), 123.9 (q, *J* = 270.0 Hz, 1C).

IR: 3335, 1621, 1577, 1536, 1504, 1318, 1136, 1112, 1065, 928, 865, 771, 690, 607 cm⁻¹.

HRMS (ESI): C₈H₈F₃N₂O⁺ [M+H]⁺ calculated: 205.05832; found: 205.05817.



3-Trifluoromethyl-benzoic acid hydrazide (3x):

White solid (85 mg, 0.42 mmol, 60%).

¹H NMR (CDCl₃, 400 MHz): δ = 10.1 (s, 1H), 8.16 (s, 1H), 8.12 (d, *J* = 7.8 Hz, 1H), 7.85 (d, *J* = 7.8 Hz, 1H), 7.69 (t, *J* = 7.8 Hz, 1H), 4.95 (s, 2H).

¹³C NMR (CDCl₃, 100 MHz): δ = 164.5, 134.3, 131.1, 127.8, 129.3 (q, *J* = 31.5 Hz, 1C), 127.8 (q, *J* = 3.8 Hz, 1C), 124.1 (q, *J* = 270.8 Hz, 1C), 123.7 (q, *J* = 3.8 Hz, 1C).

IR: 3305, 1639, 1615, 1518, 1482, 1437, 1321, 1308, 1283, 1161, 1119, 1090, 1070, 818, 691, 642, 594 cm⁻¹.

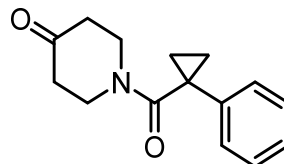
HRMS (ESI): C₈H₈F₃N₂O⁺ [M+H]⁺ calculated: 205.05832; found: 205.05809.

General Method for Synthesis of Piperidones 2a-f

Thionyl chloride (4 eq) was added dropwise to an oven-dried round bottomed flask containing commercially available acid **1a-f** (0.212 mmol – 29.0 mmol) and

dichloromethane (0.3 M). The reaction was stirred at 50 °C for one hour. The resulting solution was concentrated under vacuum and re-dissolved in dichloromethane (20 mL, 0.11 M) and added dropwise to a round bottom flask at 0 °C containing 4-piperidone (1.26 eq), triethylamine (7.5 eq), and THF (0.06 M). After 15 minutes the solution was refluxed at 50 °C for 24 hours. The reaction was carefully quenched with saturated aqueous ammonium chloride and extracted with chloroform (3 x 20 mL). The resultant organic layers were combined and dried over Na₂SO₄, decanted and concentrated under vacuum. Product purification was achieved by silica gel flash chromatography (40% ethyl acetate/60% hexane).

Characterization of Piperidones 2a-f



1-(1-Phenyl-cyclopropanecarbonyl)-piperidin-4-one (2a):

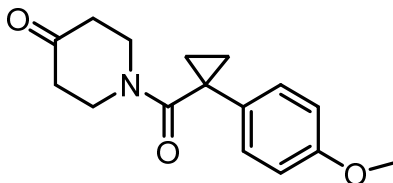
White solid (798 mg, 3.3 mmol, 36%).

¹H NMR (CDCl₃, 400 MHz): δ = 7.35 - 7.26 (m, 2H), 7.25 - 7.21 (m, 3 H), 3.95- 3.67 (br, 4H), 2.50 - 2.25 (br, 2H), 2.05 - 1.91 (br, 2H), 1.46 (dd, *J* = 6.9, 4.6 Hz, 2H), 1.24 (dd, *J* = 6.9, 4.6 Hz, 2H).

¹³C NMR (CDCl₃, 100 MHz): δ = 207.4, 171.5, 140.3, 129.2 (2C), 127.0, 125.7 (2C), 44.5, 41.9, 40.8 (2C), 29.8, 14.8 (2C).

IR: 3008, 2873, 2359, 2341, 1714, 1633, 1427, 1316, 1270, 1232, 1188, 1079, 981, 760, 738, 698, 600, 572 cm^{-1} .

HRMS (ESI): $\text{C}_{15}\text{H}_{18}\text{NO}_3$ [$\text{M}-\text{H}+\text{H}_2\text{O}$] calculated: 260.12867; found: 260.1285.



1-[1-(4-Methoxy-phenyl)-cyclopropanecarbonyl]-piperidin-4-one (2b):

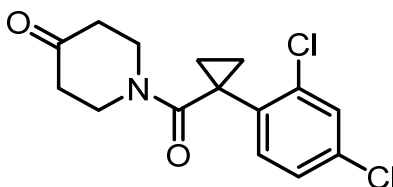
Pale yellow crystalline solid (2.51 g, 13.0 mmol, 52%).

^1H NMR (CDCl_3 , 500 MHz): δ = 7.16 (dt, J = 5.2, 2.9 Hz, 2H), 6.84 (dt, J = 5.7, 2.3 Hz, 2H), 3.80 - 3.89 (m, 2H), 3.70 - 3.80 (br m, 2H), 3.78 (s, 3H) 2.39 (br m, 2H), 1.97 (br m, 2H), 1.39 (dd, J = 6.9, 4.6 Hz, 2H), 1.16 (dd, J = 6.9, 4.6 Hz, 2H).

^{13}C NMR (CDCl_3 , 125 MHz): δ = 207.5, 171.8, 158.6, 132.2, 127.2 (2C), 114.5 (2C), 55.5, 41.8 (2C), 40.7 (2C), 29.1, 14.3 (2C).

IR: 2957, 1716, 1633, 1509, 1468, 1435, 1425, 1312, 1277, 1239, 1180, 1031, 979, 831, 811, 652, 560 cm^{-1} .

HRMS (ESI): $\text{C}_{16}\text{H}_{20}\text{NO}_3$ [$\text{M}+\text{H}$] $^+$ calculated: 274.14377; found: 274.14304.



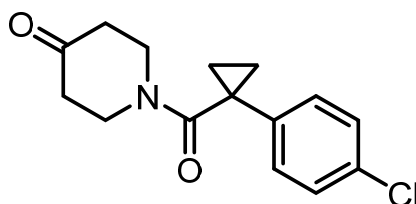
1-[1-(2,4-Dichloro-phenyl)-cyclopropanecarbonyl]-piperidin-4-one (2c):

White solid (540 mg, 1.73 mmol, 68%).

¹H NMR (CDCl₃, 500 MHz): δ = 7.40 (s, 1H), 7.20 - 7.27 (m, 2H), 3.68 (br m, 4H), 2.15 (br m, 4H), 1.67 (dd, *J* = 6.9, 4.6 Hz, 2H), 1.14 (dd, *J* = 6.9, 4.6 Hz, 2H).

¹³C NMR (CDCl₃, 125 MHz): δ = 207.1, 171.0, 137.8, 137.5, 133.8, 130.3, 130.0, 127.7, 43.8 (2C), 40.8 (2C), 28.9, 14.6 (2C).

HRMS (ESI): C₁₅H₁₅Cl₂NO₂ [M+H]⁺ calculated: 312.05581; found: 312.05524.

**1-[1-(4-Chloro-phenyl)-cyclopropanecarbonyl]-piperidin-4-one (2d):**

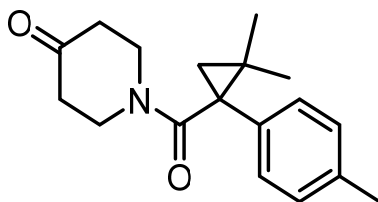
Pale yellow solid (5.06 g, 25.4 mmol, 21%).

¹H NMR (CDCl₃, 500 MHz): δ = 7.29 (d, *J* = 8.6 Hz, 2H), 7.18 (d, *J* = 8.6 Hz, 2H), 3.90-3.65 (br m, 4H), 2.41 (br m, 2H), 2.08 (br m, 2H), 1.47 (dd, *J* = 6.9, 4.6 Hz, 2H), 1.21 (dd, *J* = 6.9, 4.6 Hz, 2H).

¹³C NMR (CDCl₃, 125 MHz): δ = 207.0, 171.1, 138.9, 132.8, 129.4 (2C), 127.2 (2C), 44.5, 41.9, 40.8 (2C), 29.4, 15.0 (2C).

IR: 3009, 1726, 1685, 1491, 1388, 1371, 1338, 1247, 1178, 1096, 1045, 1014, 951, 931, 828, 762, 753, 716, 678, 544 cm⁻¹.

HRMS (ESI): C₁₅H₁₇ClNO₂ [M+H]⁺ calculated: 278.09423; found: 278.09387.



1-(2,2-Dimethyl-1-*p*-tolyl-cyclopropanecarbonyl)-piperidin-4-one (2e):

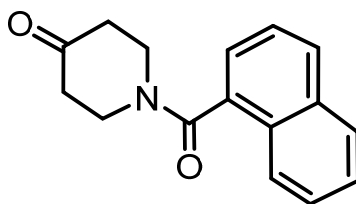
White solid (160 mg, 0.560 mmol, 38%).

¹H NMR (CDCl₃, 500 MHz): δ = 7.32 (d, *J* = 9.2 Hz, 2H), 7.10 (d, *J* = 9.2 Hz, 2H), 4.12-3.98 (br m, 2H), 3.82-3.77 (br m, 1H), 3.55-3.49 (br m, 1H), 2.35-2.27 (br, 5H), 2.15-2.09 (br m, 1H), 1.88-1.79 (br m, 1H), 1.31 (d, *J* = 5.2 Hz, 2H), 1.29 (s, 3H), 1.10 (d, *J* = 5.2 Hz, 2H), 0.86 (s, 3H).

¹³C NMR (CDCl₃, 125 MHz): δ = 207.6, 170.9, 136.8, 134.7, 129.4 (2C), 129.1 (2C), 44.7, 41.6, 41.2, 40.8, 38.5, 25.0 (2C), 24.5, 22.7, 21.2.

IR: 2981, 2929, 2357, 2341, 1714, 1634, 1449, 1418, 1307, 1263, 1231, 1219, 1135, 1081, 807, 760, 739, 657, 573 cm⁻¹.

HRMS (ESI): C₁₈H₂₃NO₂ [M+Na]⁺ calculated: 308.1621; found:308.1639.



1-(1-Naphthalen-2-yl-cyclopropanecarbonyl)-piperidin-4-one (2f):

Clear oil oil (5.00 g, 29.0 mmol, 20%).

¹H NMR (CDCl₃, 500 MHz): δ = 7.94 - 7.89 (m, 2H), 7.88 – 7.85 (m, 1H), 7.57 - 7.77 (m, 4H), 4.21 (t, J = 6.3 Hz, 2H), 3.51 (t, J = 6.0 Hz, 2H), 2.69 (t, J = 6.3 Hz, 2H), 2.32 (q, J = 6.3 Hz, 2H).

¹³C NMR (CDCl₃, 100 MHz): δ = 206.5, 169.6, 133.4, 133.3, 129.4, 129.3, 128.5, 127.2, 126.5, 125.1, 124.3, 123.6, 45.7, 41.5, 40.9, 40.8.

IR: 3053, 2964, 2360, 1713, 1631, 1507, 1470, 1435, 1366, 1314, 1279, 1244, 1199, 1150, 973, 800, 780, 627 cm⁻¹.

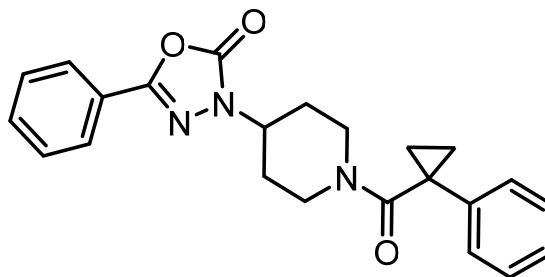
HRMS (ESI): C₁₆H₁₆NO₂⁺ [M+H]⁺ calculated: 254.11756; found: 254.11882.

General Method for Synthesis of Oxadiazolones 5

Ketones **2a-f** (0.083 mmol – 5.40 mmol) was combined with the corresponding hydrazine (**3t-z**; 1.09 eq) and methanol (0.05 M) in an oven-dried round bottomed flask and stirred at 30 °C for 1 hour. The temperature was raised to 50 °C for an additional 2 hours. The reaction was cooled to 0 °C and sodium borohydride (1.05 eq) was added. The reaction was allowed to warm to room temperature, stirred for 2 hours, quenched with brine, and extracted with dichloromethane (3 x 20 mL). The resultant organic layer was dried over Na₂SO₄, decanted, and concentrated under vacuum. The crude hydrazide (**4**) was then solubilized in THF (0.011 M) at 0 °C and triethylamine (2.6 eq) and triphosgene (0.67 eq) were sequentially added. The reaction was stirred at room temperature for 24 hours, quenched with brine, and extracted with ethyl acetate (3 x 20 mL). The resultant organic layer was dried over Na₂SO₄, decanted and concentrated under vacuum. Product purification was achieved by silica gel flash chromatography (gradient elution starting

with 25:75 ethyl acetate:hexane and ending with a 50:50 ethyl acetate:hexane) to yield azoxazolones **5**.

Characterization of Oxadiazolones **5**



5-Phenyl-3-[1-(1-phenyl-cyclopropanecarbonyl)-piperidin-4-yl]-3H-[1,3,4]oxadiazol-2-one (5a):

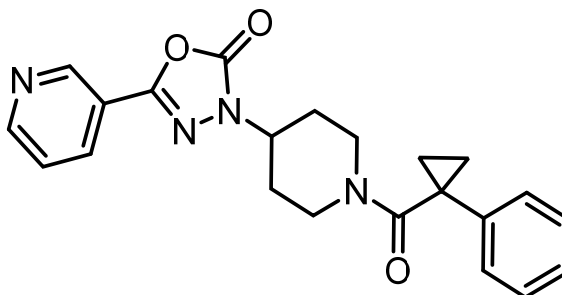
White solid (100 mg, 0.257 mmol, 74%).

¹H NMR (CDCl₃, 500 MHz): δ = 7.83-7.80 (m, 2H), 7.54 - 7.42 (m, 3H), 7.36 - 7.31 (m, 2H), 7.25-7.18 (m, 3H), 4.76-4.75 (br m, 1H), 4.28-4.10 (br m, 2H), 2.97-2.75 (br m, 2H), 2.01-1.90 (br m, 2H), 1.75-1.66 (br m, 1H), 1.65-1.52 (br, 1H), 1.50-1.41 (br m, 2H), 1.25-1.18 (br m, 2H).

¹³C NMR (CDCl₃, 100 MHz): δ = 171.1, 153.5, 153.0, 140.6, 131.8, 129.1 (2C), 129.0 (2C), 126.6, 125.8 (2C), 125.5 (2C), 123.9, 53.2, 44.6, 41.3, 29.8 (2C), 29.6, 15.3 (2C).

IR: 2934, 2359, 2341, 1772, 1635, 1449, 1431, 1353, 1154, 993, 739, 690, 580 cm⁻¹.

HRMS (ESI): C₄₆H₄₇N₆O₆ [2M+H]⁺ calculated: 779.35516; found: 779.3574.



3-[1-(1-phenyl-cyclopropanecarbonyl)-piperidin-4-yl]-5-pyridin-3-yl-3H-[1,3,4]oxadiazol-2-one (5au):

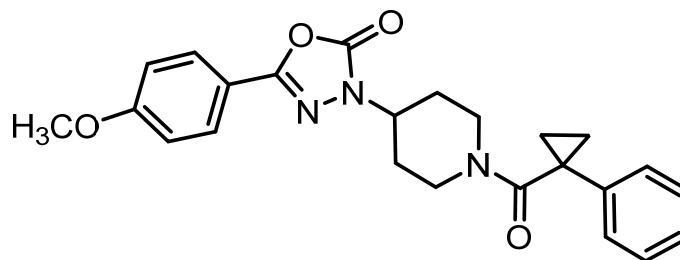
Light yellow-orange solid (105 mg, 0.269 mmol, 13%).

¹H NMR (CDCl₃, 500 MHz): δ = 9.06 (br s, 1H), 8.74 (br s, 1H), 8.06 (dt, J = 2.0, 8.0 Hz, 1H), 7.42 (dd, J = 5.1, 8.0 Hz, 1H), 7.33 - 7.31 (m, 2H), 7.23-7.18 (m, 3H), 4.77-4.72 (br m, 1H), 4.28-4.10 (br m, 2H), 2.95-2.72 (br m, 2H), 2.01-1.88 (br m, 2H), 1.75-1.66 (br, 1H), 1.65-1.60 (br, 1H), 1.49-1.40 (br m, 2H), 1.25-1.18 (br m, 2H).

¹³C NMR (CDCl₃, 100 MHz): δ = 171.1, 152.6, 152.4, 151.5, 147.1, 140.6, 133.0, 129.0 (2C), 126.7, 125.5 (2C), 123.9, 120.5, 53.5, 44.6, 41.3, 29.8 (2C), 29.6, 15.3 (2C).

IR: 3179, 2955, 2863, 1784, 1625, 1610, 1456, 1432, 1412, 1328, 1160, 988, 740, 702, 690, 580 cm⁻¹.

HRMS (ESI): C₄₆H₄₇N₆O₆ [2M+H]⁺ calculated: 779.35516; found: 779.3574.



5-(4-Methoxy-phenyl)-3-[1-(1-phenyl-cyclopropanecarbonyl)-piperidin-4-yl]-3H-[1,3,4]oxadiazol-2-one (5av):

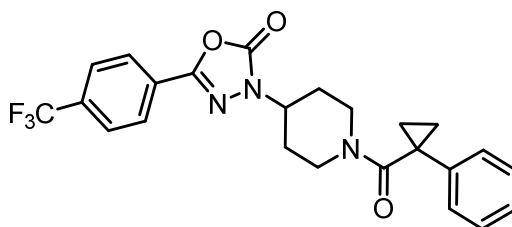
White solid (223 mg, 0.53 mmol 43%).

¹H NMR (CDCl₃, 400 MHz): δ = 7.76 (d, J = 9.0, 2H), 7.37-7.29 (m, 2H), 7.25 -7.17 (m, 3H), 6.96 (d, J = 9.0 Hz, 2H), 4.74 (br s, 1H), 4.32-4.17 (br s, 1H), 4.12 (sept, J = 5.0 Hz, 1H), 3.87 (s, 3H), 2.98-2.70 (br m, 2H), 2.05-1.84 (br m, 2H), 1.80-1.65 (br m, 1H), 1.64-1.50 (br, 1H), 1.51-1.35 (br, 2H), 1.30-1.14 (br, 2H).

¹³C NMR (CDCl₃, 100 MHz): δ = 171.2, 162.4, 153.6, 153.2, 140.7, 129.0 (2C), 127.6 (2C), 126.6, 125.5 (2H), 116.4, 114.6 (2C), 55.7, 53.1, 44.6, 41.3, 29.9 (2C), 29.6, 15.3 (2C).

IR: 2936, 1765, 1632, 1612, 1508, 1440, 1352, 1249, 1176, 1161, 1029, 1017, 836, 744, 693, 609, 574 cm⁻¹.

HRMS (ESI): C₂₄H₂₆N₃O₄ [M+H]⁺ calculated: 420.19178, found: 420.18976.



3-[1-(1-phenyl-cyclopropanecarbonyl)-piperidin-4-yl]-5-(4-trifluoromethyl-phenyl)-3H-[1,3,4] oxadiazol-2-one (5aw):

White solid (85.1 mg, mmol 87%).

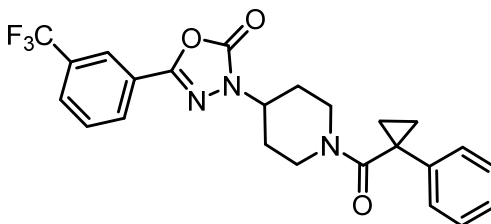
¹H NMR (CDCl₃, 400 MHz): δ = 7.94 (d, J = 8.1 Hz, 2H), 7.75 (d, J = 8.1 Hz, 2H), 7.37-7.32 (m, 2H), 7.25 -7.17 (m, 3H), 4.77 (br, 1H), 4.30-4.13 (br m, 2H), 2.97-2.73 (br m,

2H), 2.05-1.83 (br m, 2H), 1.80-1.65 (br m, 1H), 1.64-1.50 (br, 1H), 1.50-1.35 (br, 2H), 1.32-1.18 (br, 2H).

^{13}C NMR (CDCl_3 , 100 MHz): δ = 171.2, 152.7, 152.3, 140.6, 133.3 (q, J = 32.4 Hz, 1C), 129.0 (2C), 127.2, 126.7, 126.2 (q, J = 3.8 Hz, 2C), 126.1 (2C), 125.5 (2C), 123.7 (q, J = 271.0 Hz, 1C), 53.5, 44.6, 41.3, 29.9 (2C), 29.6, 15.2 (2C).

IR: 2846, 2863, 2354, 2341, 1776, 1633, 1437, 1321, 1170, 1150, 1119, 1107, 1063, 1011, 992, 856, 847, 736, 699, 570, 515 cm^{-1} .

HRMS (ESI): $\text{C}_{24}\text{H}_{22}\text{F}_3\text{N}_3\text{NaO}_3$ $[\text{M}+\text{Na}]^+$ calculated: 480.15054 found: 480.1529



3-[1-(1-phenyl-cyclopropanecarbonyl)-piperidin-4-yl]-5-(3-trifluoromethyl-phenyl)-3H-[1,3,4] oxadiazol-2-one (5ax):

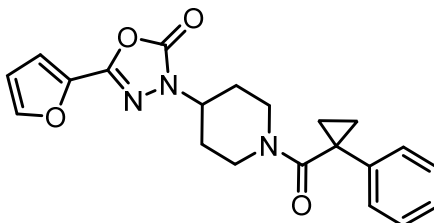
White solid (117 mg, 0.253 mmol, 62%).

^1H NMR (CDCl_3 , 500 MHz): δ = 8.09 (s, 1H), 8.00 (d, J = 7.8 Hz, 1H), 7.75 (d, J = 7.8 Hz, 1H), 7.63 (t, J = 7.8 Hz, 1H), 7.34 (t, J = 7.8 Hz, 2H), 7.25 -7.20 (m, 3H), 4.77 (br, 1H), 4.30-4.13 (br m, 2H), 3.00 - 2.80 (br m, 2H), 2.05-1.83 (br m, 2H), 1.80-1.65 (br m, 1H), 1.64-1.50 (br, 1H), 1.50-1.35 (br, 2H), 1.32-1.18 (br, 2H).

^{13}C NMR (CDCl_3 , 100 MHz): δ = 171.8, 152.7, 152.3, 140.6, 132.0 (q, J = 33.4 Hz, 1C), 129.9, 129.0 (2C), 128.8, 128.2 (q, J = 3.8 Hz, 1C), 126.7, 125.6 (2C), 124.8, 123.6 (q, J = 271.0 Hz, 1C), 122.7 (q, J = 3.8 Hz, 1C), 53.5, 44.6, 41.3, 29.9 (2C), 29.6, 15.2 (2C).

IR: 2934, 2360, 2340, 1778, 1736, 1638, 1431, 1307, 1276, 1169, 1155, 1128, 1073, 1032, 994, 743, 693, 575 cm^{-1} .

HRMS (ESI): $\text{C}_{24}\text{H}_{23}\text{F}_3\text{N}_3\text{O}_3^+$ $[\text{M}+\text{H}]^+$ calculated: 458.16860, found: 458.16885.



5-Furan-2-yl-3-[1-(1-phenyl-cyclopropanecarbonyl)-piperidin-4-yl]-3H-

[1,3,4]oxadiazol-2-one (5ay):

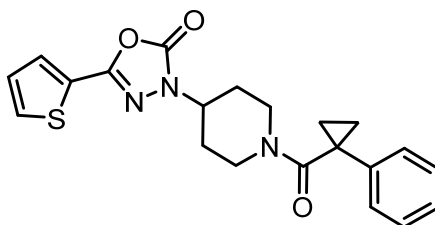
White solid (79 mg, 0.208 mmol, 51%).

$^1\text{H NMR}$ (CDCl_3 , 500 MHz): δ = 7.59 (d, J = 1.8 Hz, 1H), 7.34-7.31 (m, 2H), 7.23-7.17 (m, 3H), 6.97 (d, J = 3.7 Hz, 1H), 6.56 (dd, J = 3.7, 1.8 Hz, 1H), 4.72 (br, 1H), 4.29-4.10 (br m, 2H), 2.95-2.70 (br m, 2H), 2.05-1.90 (br m, 2H), 1.80-1.57 (br m, 2H), 1.45 (br, 2H), 1.21 (br, 2H).

$^{13}\text{C NMR}$ (CDCl_3 , 125 MHz): δ = 171.1, 152.1, 149.9, 145.8, 140.6, 139.0, 129.0 (2C), 126.6, 125.3 (2C), 113.9, 112.2, 53.5, 44.6, 42.2, 29.8 (2C), 29.5, 15.3 (2C).

IR: 2928, 2861, 2359, 2341, 1778, 1634, 1434, 1326, 1151, 1038, 995, 949, 904, 741, 699, 572 cm^{-1} .

HRMS (ESI): $\text{C}_{42}\text{H}_{43}\text{N}_6\text{O}_8$ $[2\text{M}+\text{H}]^+$ calculated: 759.31369 found: 759.3155.



3-[1-(1-Phenyl-cyclopropanecarbonyl)-piperidin-4-yl]-5-thiophene-2-yl-3H-[1,3,4]oxadiazol-2-one (5az):

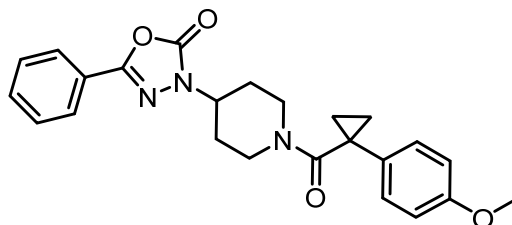
White solid (80 mg, 0.202 mmol, 49%).

¹H NMR (CDCl₃, 500 MHz): δ = 7.56 (dd, *J* = 1.3, 3.8 Hz, 1H), 7.50 (dd, *J* = 1.3, 5.0 Hz, 1H), 7.35-7.31 (m, 2H), 7.24-7.18 (m, 3H), 7.12 (dd, *J* = 3.8, 5.0 Hz, 1H), 4.80-4.65 (br, 1H), 4.25-4.15 (br, 1H), 4.15-4.05 (m, 1H), 2.95-2.70 (br m, 2H), 2.00-1.85 (br, 2H), 1.75-1.62 (br, 1H), 1.62-1.50 (br, 1H), 1.45 (br, 2H), 1.22 (br, 2H).

¹³C NMR (CDCl₃, 100 MHz): δ 171.0, 152.2, 150.0, 140.3, 129.7, 129.2, 128.8 (2C), 128.0, 126.5, 125.3, 125.2 (2C), 53.1, 44.4, 41.1, 29.6 (2C), 29.4, 15.1 (2C).

IR: 3085, 2928, 2860, 2358, 2341, 1768, 1633, 1613, 1430, 1324, 1272, 1153, 1045, 1012, 987, 857, 738, 699, 578 cm⁻¹.

HRMS (ESI): C₂₁H₂₂N₃O₃S[M+H]⁺ calculated: 396.13764; found: 396.1381.



3-{1-[1-(4-Methoxy-phenyl)-cyclopropanecarbonyl]-piperidin-4-yl}-5-phenyl-3H-[1,3,4]oxadiazol-2-one (5bt):

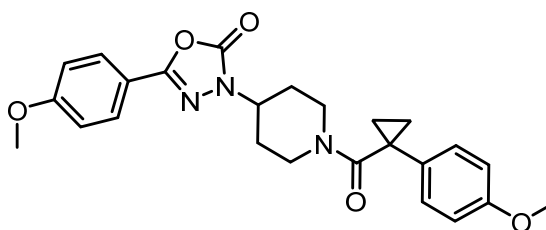
White solid (190 mg, 0.453 mmol 62%).

¹H NMR (CDCl₃, 500 MHz): δ = 7.81 (br d, J = 6.7 Hz, 2H), 7.51-7.45 (m, 3H), 7.15 (br d, J = 9.0 Hz, 2H), 6.86 (br d, J = 9.0 Hz, 2H), 4.80-4.65 (br, 1H), 4.35-4.20 (br m, 1H), 4.14 (tt, J = 4.6, 10.9 Hz, 1H), 3.78 (s, 3H), 3.00-2.70 (br m, 2H), 2.08-1.51 (br m, 4H), 1.47-1.35 (br m, 2H), 1.20-1.12 (br m, 2H).

¹³C NMR (CDCl₃, 100 MHz): δ 171.4, 158.3, 153.5, 153.1, 132.6, 131.8, 129.1, 126.8, 125.8 (4C), 123.9, 114.4, 114.3, 55.5, 53.3, 53.1, 44.5, 41.3, 29.9, 29.1, 14.7 (2C).

IR: 2906, 2869, 1763, 1629, 1513, 1449, 1430, 1322, 1245, 1181, 1154, 1038, 1021, 997, 856, 823, 731, 684, 657, 592, 572 cm⁻¹.

HRMS (ESI): C₂₄H₂₆N₃O₄ [M+H]⁺ calculated: 420.19178; found: 420.1928.



5-(4-Methoxy-phenyl)-3-{1-[1-(4-methoxy-phenyl)-cyclopropanecarbonyl]-piperidin-4-yl}-3H-[1,3,4]oxadiazol-2-one (5bv):

White solid (91.4 mg, 0.209 mmol 81%).

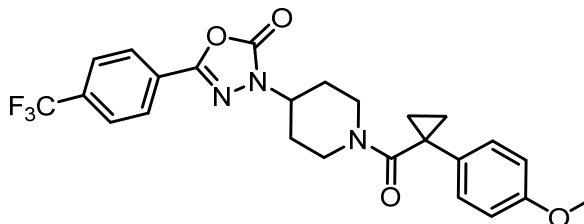
¹H NMR (CDCl₃, 500 MHz): δ = 7.75 (br d, J = 9.2 Hz, 2H), 7.14 (br d, J = 9.2 Hz, 2H), 6.96 (br d, J = 9.2 Hz, 2H), 6.87 (br d, J = 9.2 Hz, 2H), 4.80-4.65 (br, 1H), 4.35-4.18 (br, 1H), 4.12 (tt, J = 10.9, 4.6 Hz, 1H), 3.87 (s, 3H), 3.79 (s, 3H), 3.00-2.70 (br m, 2H), 2.02-

1.80 (br, 2H), 1.80-1.64 (br, 1H), 1.64-1.50 (br, 1H), 1.48-1.36 (br m, 2H), 1.20-1.12 (br m, 2H).

^{13}C NMR (CDCl_3 , 125 MHz): δ = 171.4, 162.4, 158.3, 153.6, 153.2, 132.6, 127.6 (2C), 126.9 (2C), 116.4, 114.6 (2C), 114.3 (2C), 55.7, 55.5, 53.1, 44.6, 41.3, 29.9 (2C), 29.1, 14.7 (2C).

IR: 2948, 2357, 2341, 1762, 1632, 1509, 1436, 1246, 1176, 1156, 1025, 996, 832, 740, 733, 607, 571, 525 cm^{-1} .

HRMS (ESI): $\text{C}_{25}\text{H}_{28}\text{N}_3\text{O}_5$ $[\text{M}+\text{H}]^+$ calculated: 450.20235; found: 450.2014.



3-{1-[1-(4-Methoxy-phenyl)-cyclopropanecarbonyl]-piperidin-4-yl}-5-(4-trifluoromethyl-phenyl)-3H-[1,3,4]oxadiazol-2-one (5bw):

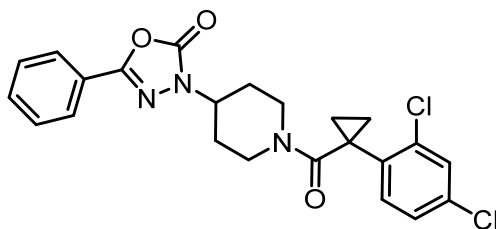
White solid (104 mg, 0.213 mmol, 88%).

^1H NMR (CDCl_3 , 500 MHz): δ = 7.94 (d, J = 8.1 Hz, 2H), 7.74 (d, J = 8.1 Hz, 2H), 7.15 (br d, J = 8.6 Hz, 2H), 6.87 (br d, J = 8.6 Hz, 2H), 4.80-4.66 (br, 1H), 4.35-4.20 (br, 1H), 4.16 (tt, J = 10.9, 4.0 Hz, 1H), 3.78 (s, 3H), 3.00-2.70 (br m, 2H), 2.05-1.85 (br, 2H), 1.80-1.64 (br, 1H), 1.64-1.48 (br, 1H), 1.42-1.34 (br m, 2H), 1.21-1.10 (br m, 2H).

^{13}C NMR (CDCl_3 , 125 MHz): δ = 171.5, 158.4, 152.7, 152.3, 133.3 (q, J = 32.5 Hz, 1C), 132.6, 127.2, 127.0 (2C), 126.2 (q, J = 3.8 Hz, 2C), 126.1 (2C), 123.7 (q, J = 272.5 Hz, 1C), 114.4 (2C), 55.5, 53.5, 44.5, 41.3, 29.9 (2C), 29.1, 14.60 (2C).

IR: 2954, 2924, 2359, 2341, 1784, 1622, 1513, 1441, 1415, 1321, 1250, 1157, 1127, 1064, 1029, 994, 854, 819, 748, 735, 590, 560 cm^{-1} .

HRMS (ESI): $\text{C}_{25}\text{H}_{25}\text{F}_3\text{N}_3\text{O}_4$ $[\text{M}+\text{H}]^+$ calculated: 488.17917; found: 488.1795.



3-{1-[1-(2,4-Dichloro-phenyl)-cyclopropanecarbonyl]-piperidin-4-yl}-5-phenyl-3H-[1,3,4]oxadiazol-2-one (5ct):

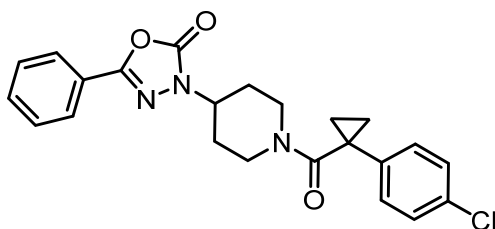
White solid (35.9 mg, 0.078 mmol 48%).

$^1\text{H NMR}$ (CDCl_3 , 300 MHz): δ = 7.82 (dd, J = 7.8, 1.5 Hz, 2H), 7.53-7.45 (m, 4H), 7.26-7.23 (m, 2H), 4.49-4.18 (br m, 2H), 4.11 (tt, J = 10.9, 4.6 Hz, 1H), 2.81 (td, J = 11.5, 2.3 Hz, 2H), 1.87-1.76 (br m, 2H), 1.74 – 1.59 (m, 4H), 1.18 - 1.12 (br m, 2H).

$^{13}\text{C NMR}$ (CDCl_3 , 125 MHz): δ = 170.7, 153.5, 153.1, 138.0, 137.5, 133.5, 131.8, 130.4, 130.1, 129.2 (2C), 127.5, 125.8 (2C), 123.9, 53.0, 43.7 (2C), 29.8 (2C), 28.9, 14.4 (2C).

IR: 2924, 2852, 2358, 2341, 1815, 1770, 1717, 1615, 1449, 1350, 1275, 1066, 957, 920, 772, 729, 688, 572 cm^{-1} .

HRMS (ESI): $\text{C}_{23}\text{H}_{22}\text{Cl}_2\text{N}_3\text{O}_3$ $[\text{M}+\text{H}]^+$ calculated: 458.10382; found: 458.10321.



3-{1-[1-(4-Chloro-phenyl)-cyclopropanecarbonyl]-piperidin-4-yl}-5-phenyl-3H-[1,3,4]oxadiazol-2-one (5dt):

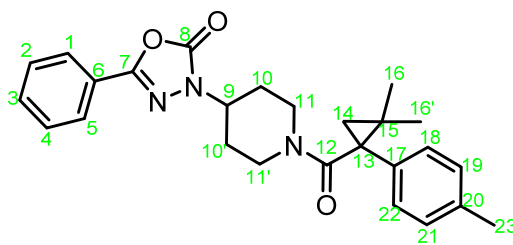
White solid (0.404 mg, 0.95 mmol, 19%).

¹H NMR (CDCl₃, 500 MHz): δ = 7.84-7.80 (m 2H), 7.54-7.45 (m, 3H), 7.31 (br d, J = 8.6 Hz, 2H), 7.14 (br d, J = 8.6 Hz, 2H), 4.85-4.70 (br, 1H), 4.20-4.11 (br, 1H), 4.15 (tt, J = 10.9, 4.6 Hz, 1H), 3.00-2.70 (br m, 2H), 2.04-1.85 (br, 2H), 1.85-1.67 (br, 1H), 1.67-1.54 (br, 1H), 1.54-1.40 (br m 2H), 1.25-1.15 (br m, 2H).

¹³C NMR (CDCl₃, 100 MHz): δ = 170.6, 153.5, 153.0, 139.3, 132.4, 132.0, 129.1 (3C), 127.0, 125.8 (4C), 123.9, 53.1, 44.6, 41.4, 29.9 (2C), 29.2, 15.4 (2C).

IR: 2939, 2864, 2359, 2341, 1765, 1636, 1613, 1492, 1430, 1401, 1356, 1324, 1154, 1097, 1036, 1021, 1011, 992, 813, 738, 691, 583 cm⁻¹.

HRMS (ESI): C₂₃H₂₃ClN₃O₃ [M+H]⁺ calculated: 424.14225; found: 424.1425.



3-[1-(2,2-Dimethyl-1-p-tolyl-cyclopropanecarbonyl)-piperidin-4-yl]-5-phenyl-3H-[1,3,4]oxadiazol-2-one (5et):

White solid (72 mg, 0.172 mmol, 49%).

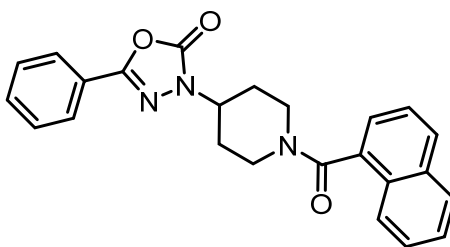
¹H NMR (CDCl₃, 500 MHz): δ = 7.83 (d, J = 7.0 Hz, 1H), 7.76 (d, J = 7.0 Hz, 1H), 7.53-7.43 (br m, 3H), 7.34 (d, J = 8.1 Hz, 2H), 7.16-7.11 (br m, 2H), 4.68-4.43 (br m, 2H), 4.17-

4.08 (br m, 1H), 3.21-2.90 (br m, 1H), 2.70-2.63 (br m, 1H), 2.32 (s, 3H), 1.95-1.70 (br m, 4H), 1.32-1.22 (br, 4H), 1.12-1.06 (m, 1H), 0.87 (s, 3H).

¹³C NMR (CDCl₃, 125 MHz, multiple peaks observed due to rotational isomers): δ 170.7 & 170.6 (1C, C12), 153.5 & 153.2 (1C, C8), 153.0 (1C, C7), 136.5 & 136.4 (1C, C17), 135.1 (1C, C20), 131.7 & 131.6 (1C, C3), 129.4 (2C, C19, C21), 129.2 (2C, C2, C4), 129.1 (2C, C1, C5), 125.7 & 125.6 (2C, C18, C22), 123.9 (1C, C6), 53.3 & 53.1 (1C, C9), 44.7 & 44.4 (1C, C11), 40.9 & 40.8 (1C, C11'), 38.6 (1C, C13), 30.3 & 30.2 & 30.1 & 29.5 (2C, C10, C10'), 25.2 (2C, C16, C14), 24.5 & 24.1 (1C, C15), 22.8 & 22.7 (1C, C16'), 21.2 (1C, C23).

IR: 2931, 2867, 1776, 1618, 1447, 1431, 1354, 1325, 1038, 1019, 992, 736, 686, 569, 518 cm⁻¹.

HRMS (ESI): C₂₇H₃₁N₃O₅ [M+FA-H]⁻ calculated: 476.21910; found: 476.2206.



3-[1-(1-Naphthalen-1-carbonyl)-piperidin-4-yl]-5-phenyl-3H-[1,3,4]oxadiazol-2-one
(5ft):

White solid (0.677 mg, 1.70 mmol, 60%).

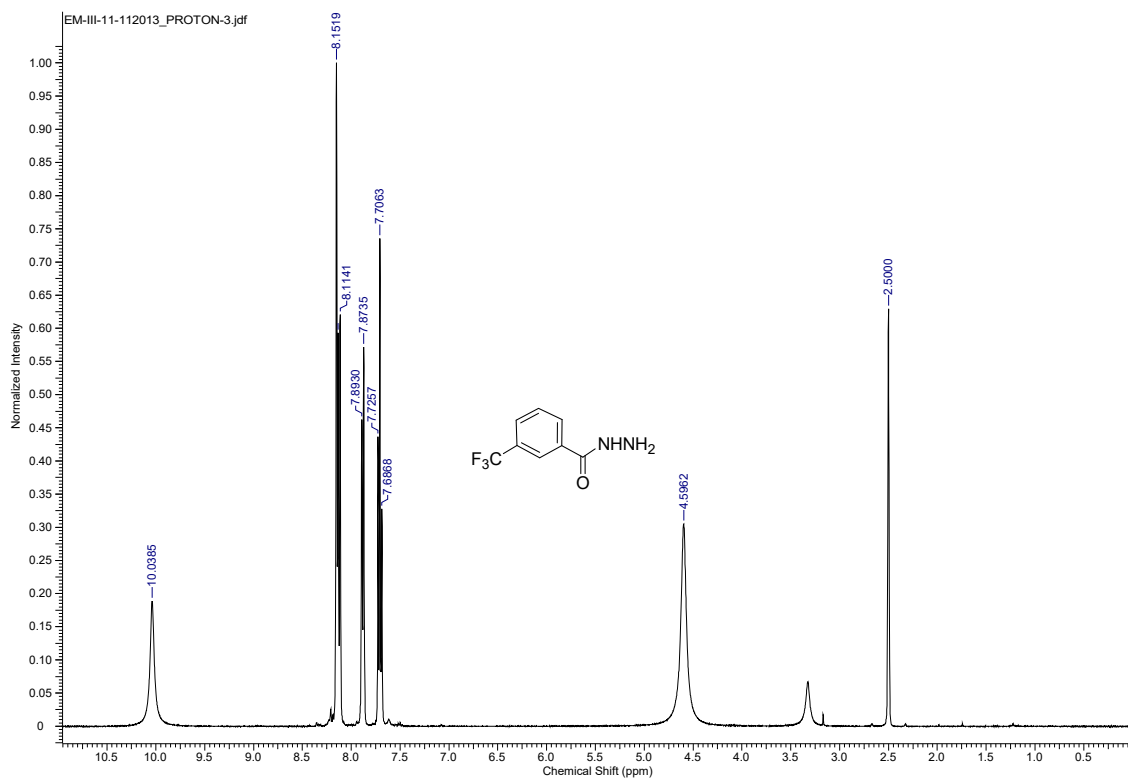
^1H NMR (CDCl_3 , 500 MHz): $\delta = 8.09 - 7.78$ (m, 5H), $7.64 - 7.40$ (m, 7H), 5.06 (d, $J = 13.0$ Hz, 1H), $4.33 - 4.23$ (m, 1H), $3.62 - 3.53$ (m, 1H), $3.17 - 3.02$ (m, 2H), $2.29 - 2.11$ (m, 2H), $2.01 - 1.74$ (m, 2H).

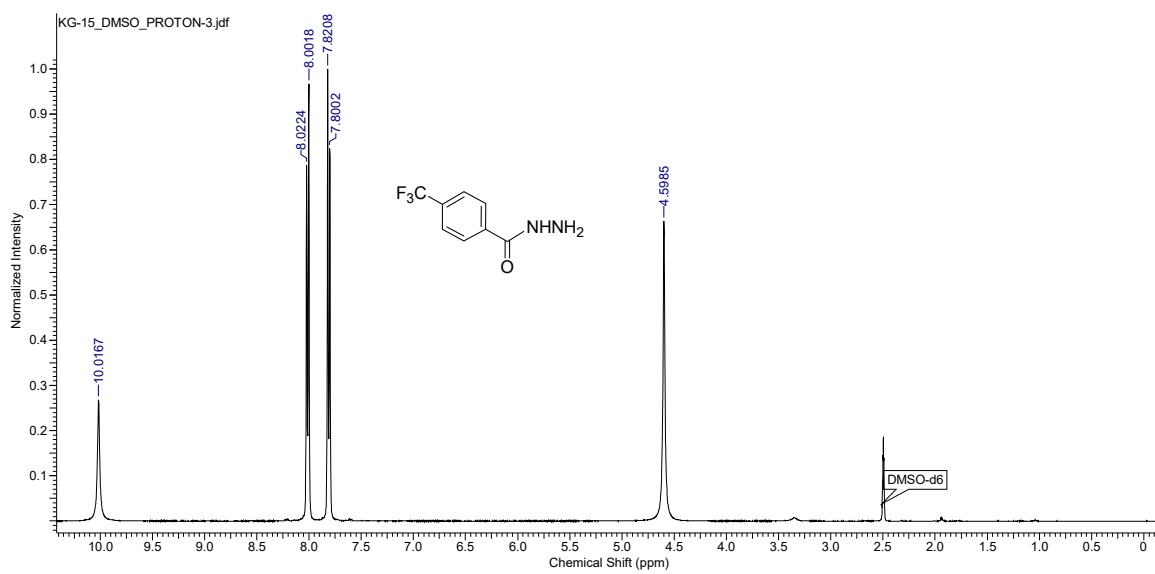
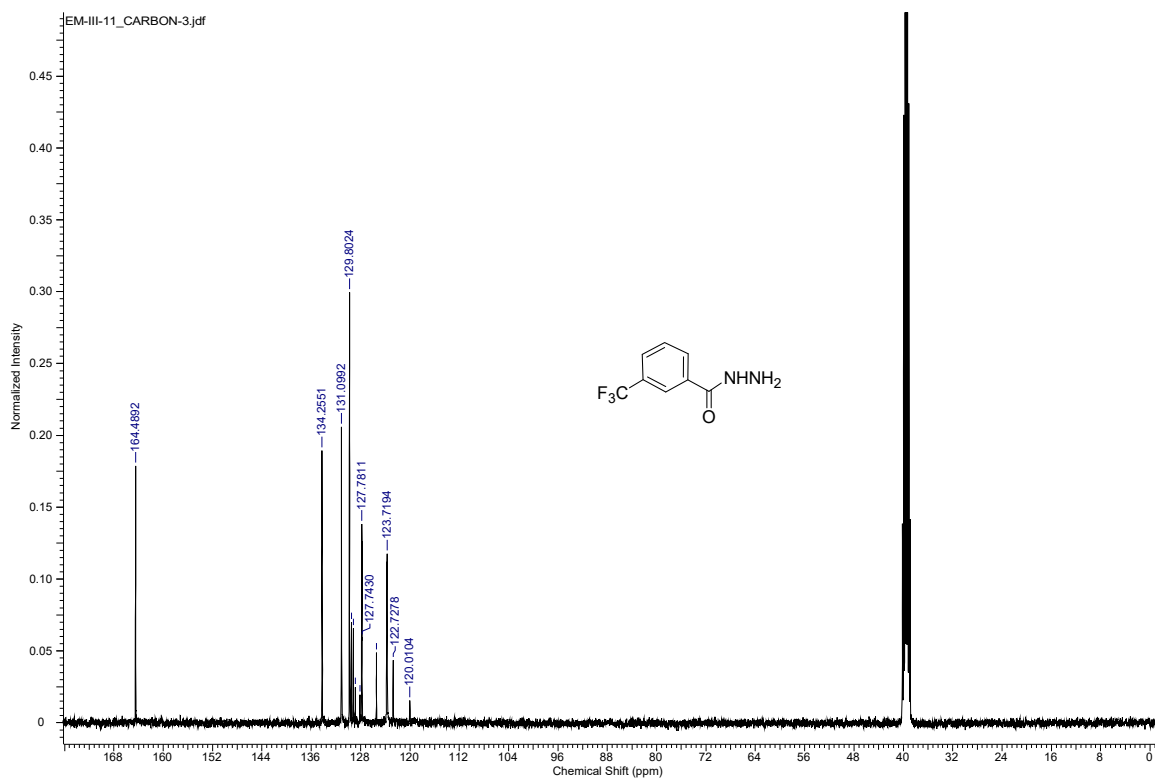
^{13}C NMR (CDCl_3 , 100 MHz, multiple peaks observed due to rotational isomers): $\delta = 169.5$, 153.5 , 152.9 , 134.0 , 133.5 , 131.7 , 129.7 , 129.5 , 129.3 , 129.0 (2C), 128.6 , 127.2 , 126.6 , 125.7 (2C), 125.2 , 124.8 , 123.7 , 53.1 , 46.0 , 40.5 , 31.0 , 30.1 .

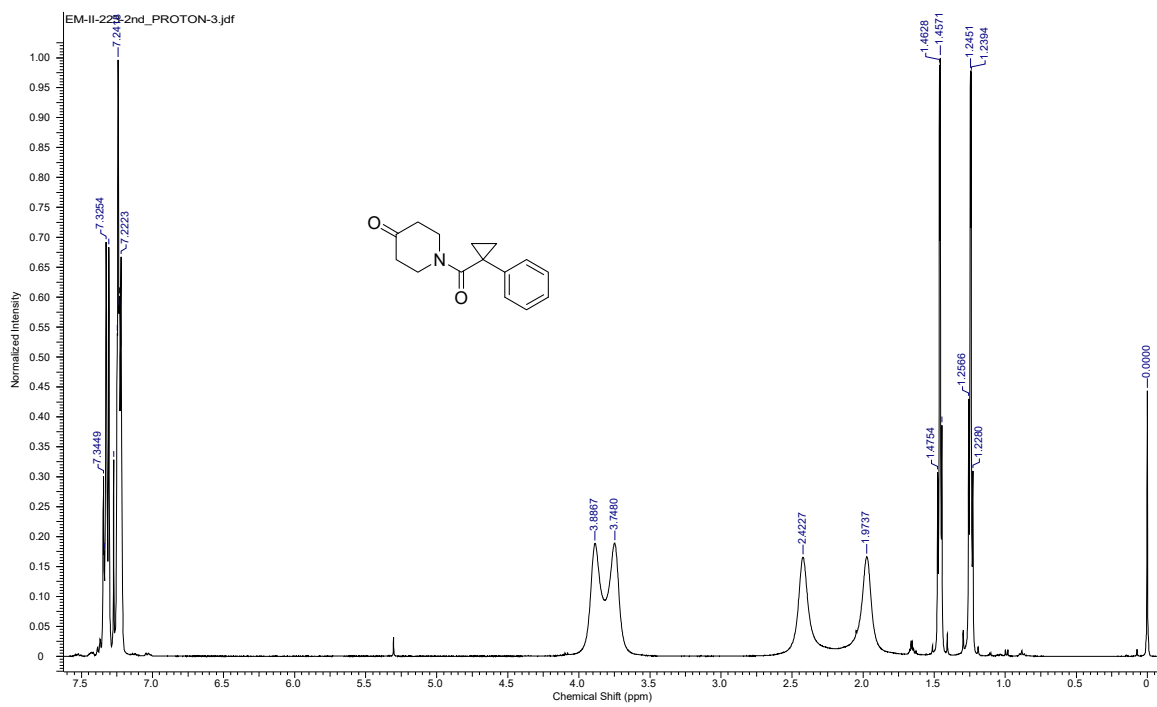
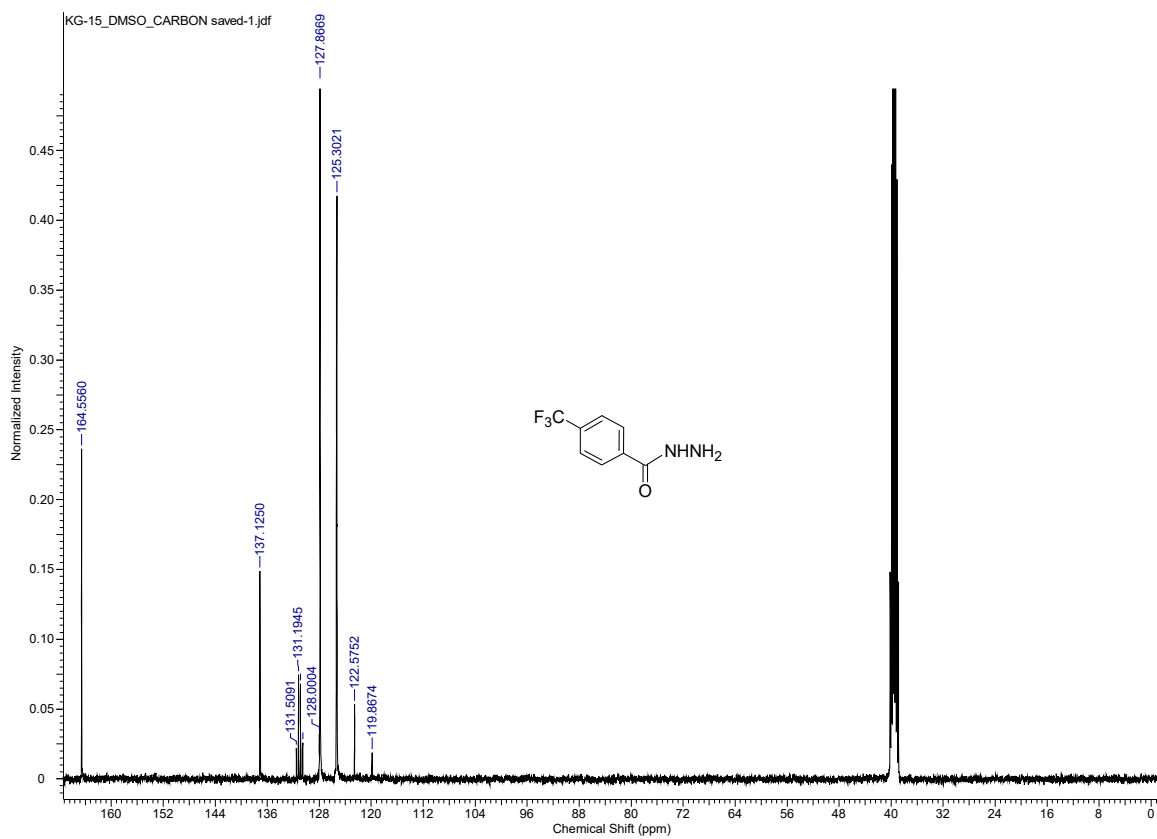
IR: 2933 , 2359 , 2341 , 1768 , 1629 , 1448 , 1436 , 1352 , 1323 , 981 , 796 , 777 , 732 , 687 , 675 , 632 , 584 cm^{-1} .

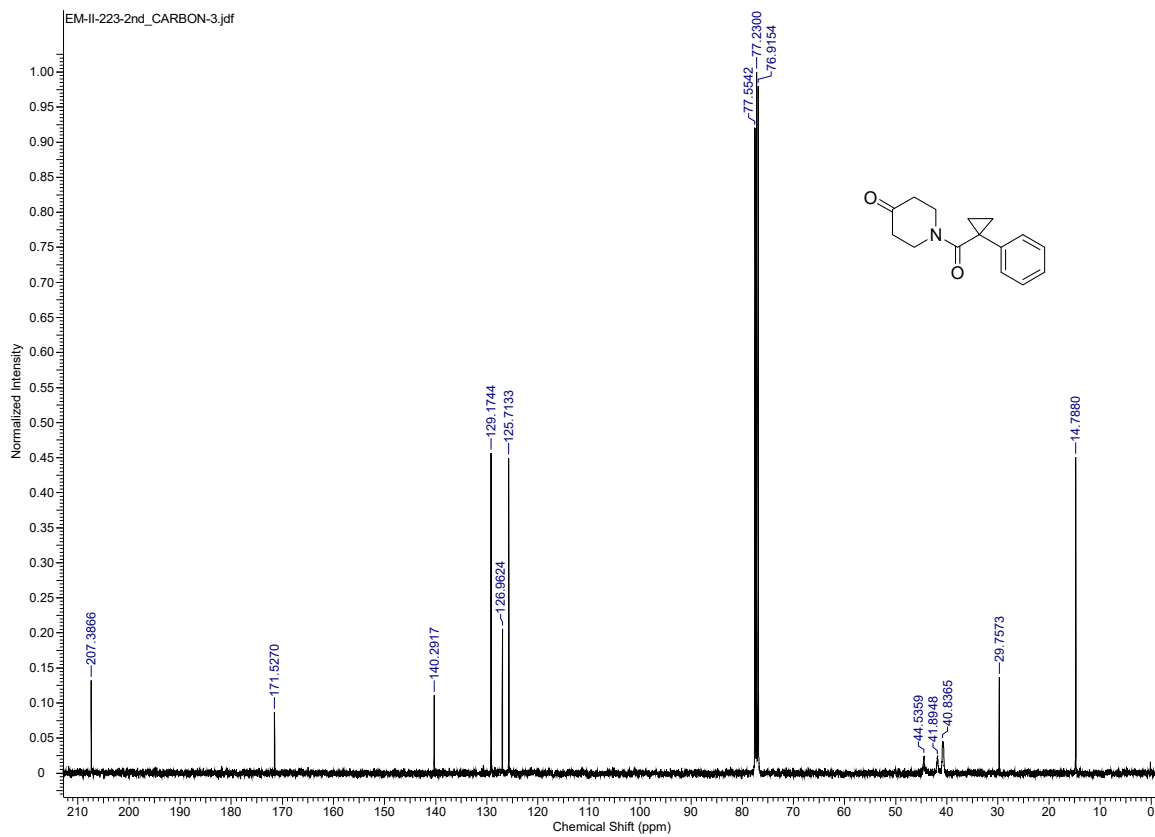
HRMS (ESI): $\text{C}_{24}\text{H}_{21}\text{N}_3\text{NaO}_3$ $[\text{M}+\text{Na}]^+$ calculated: 422.14751 ; found: 422.1471 .

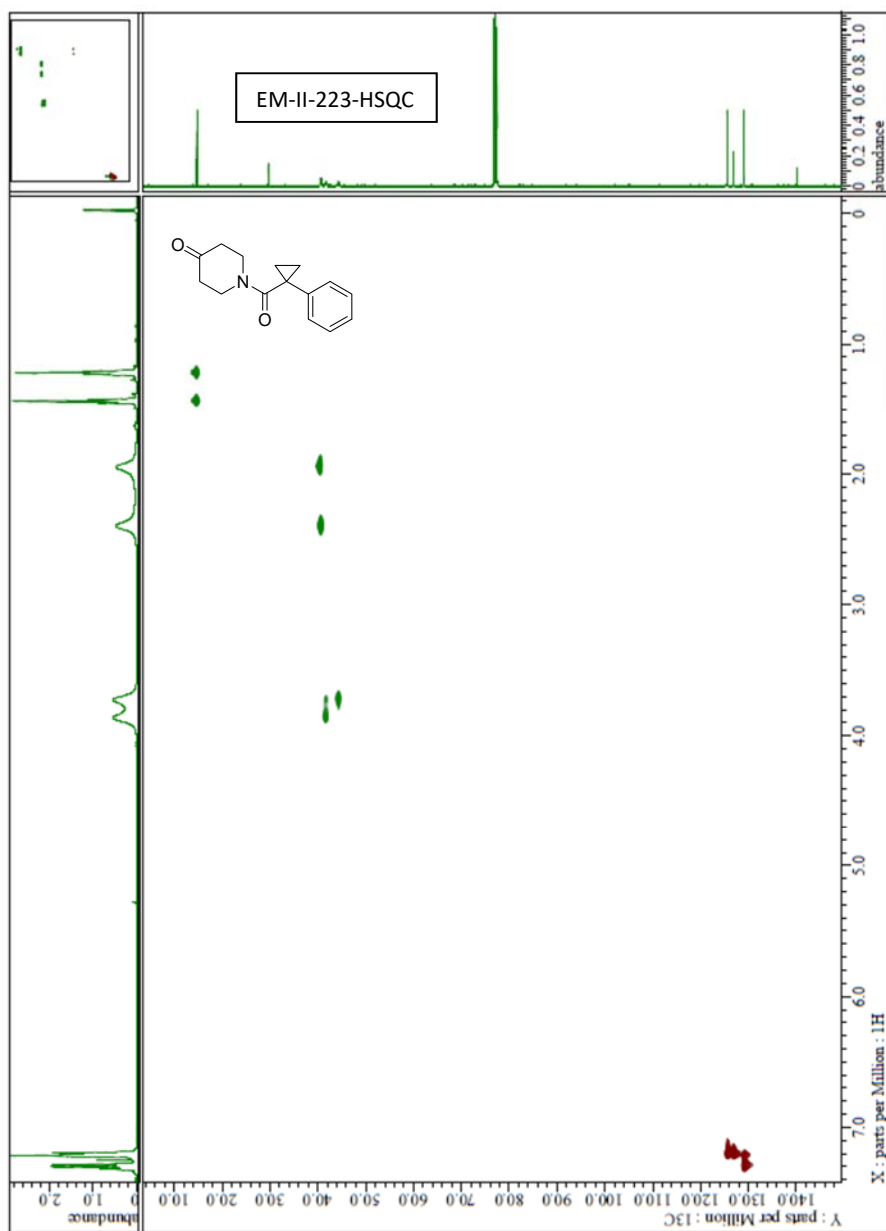
Spectra Data

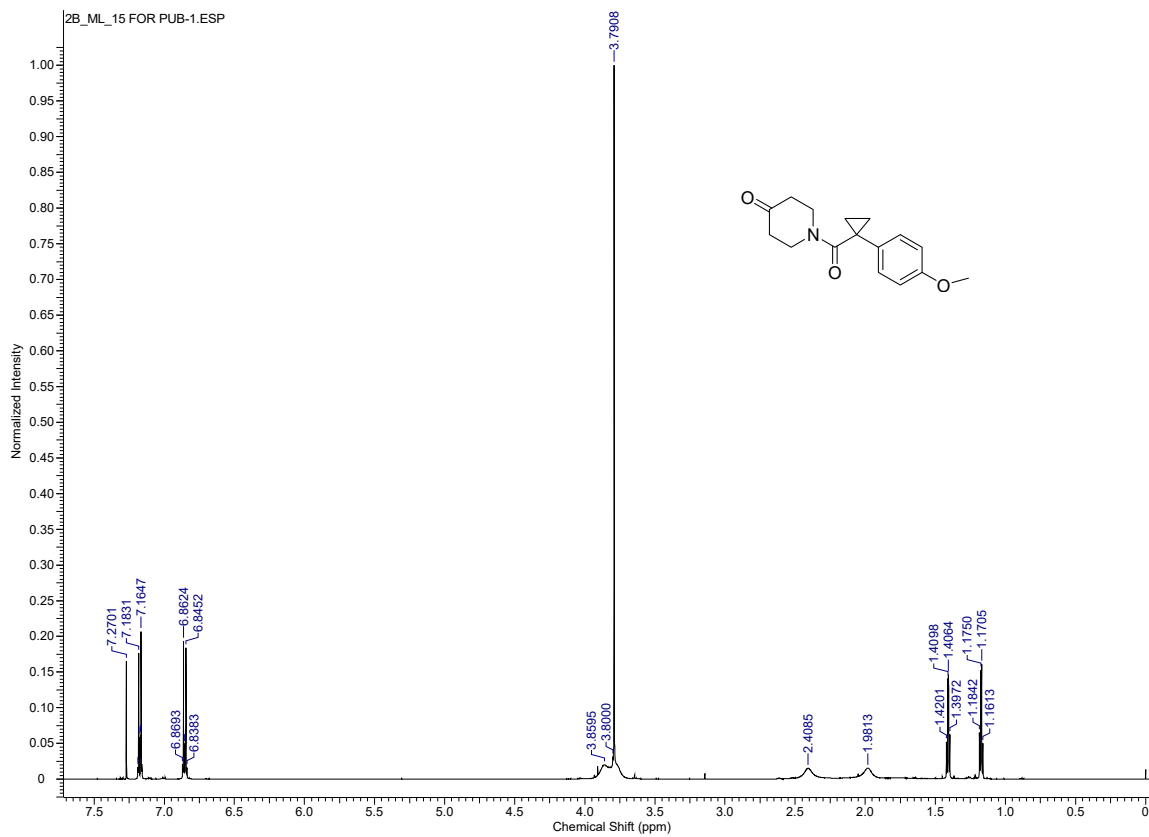


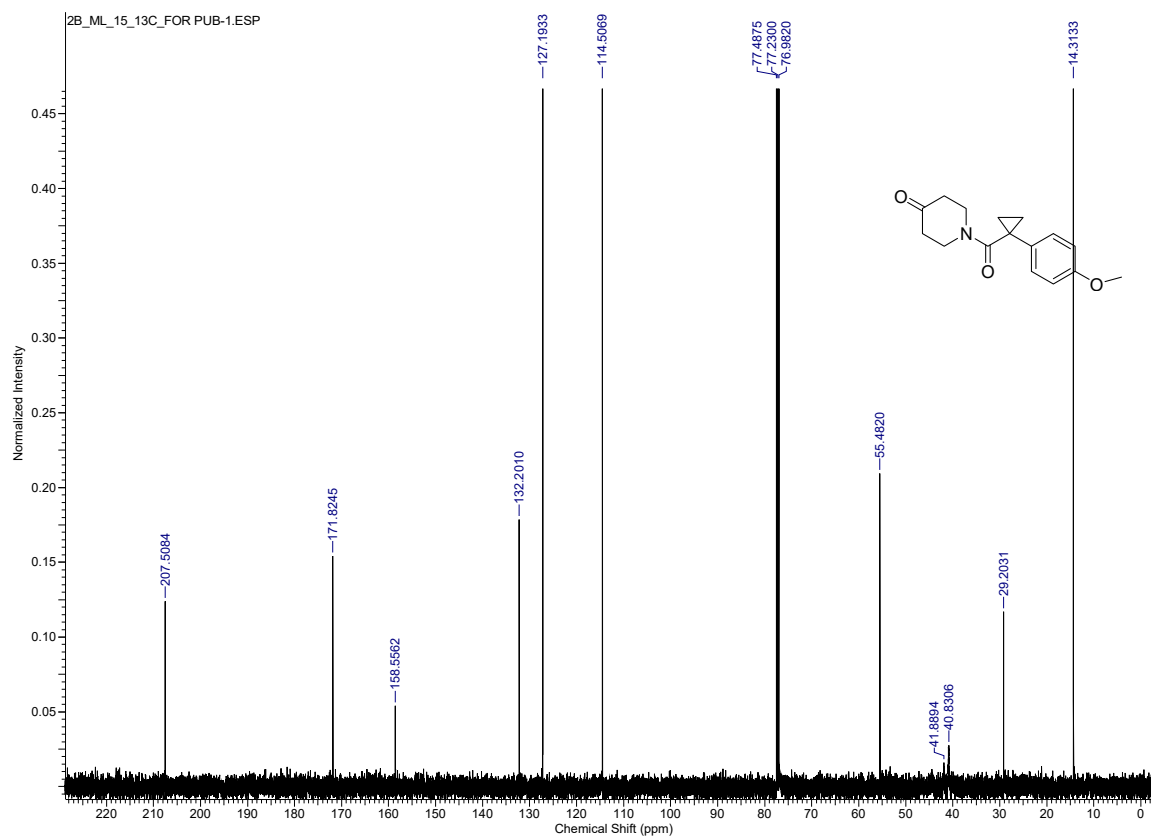


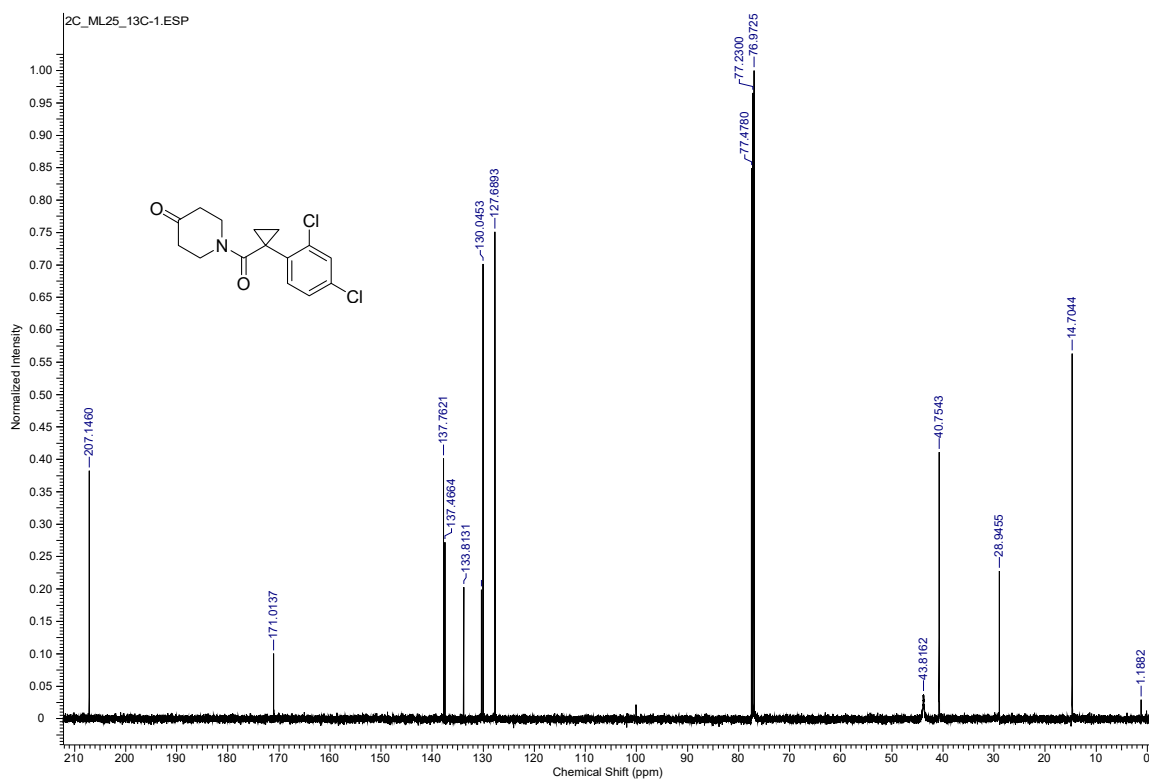
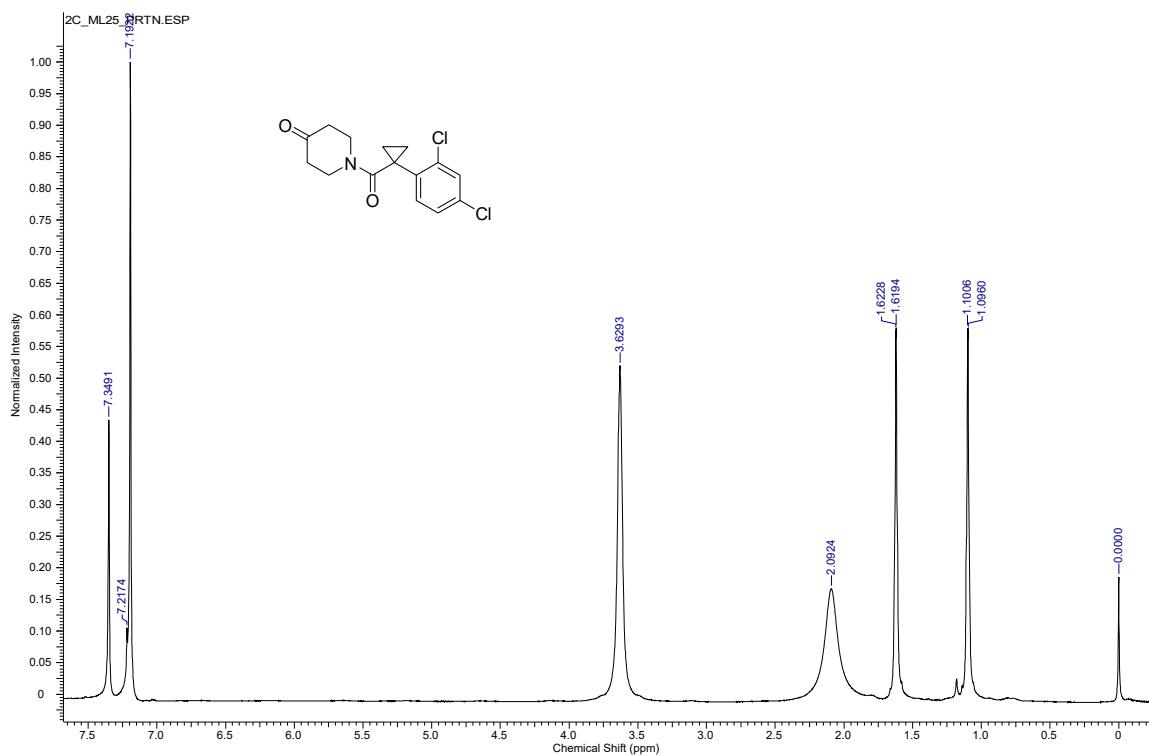


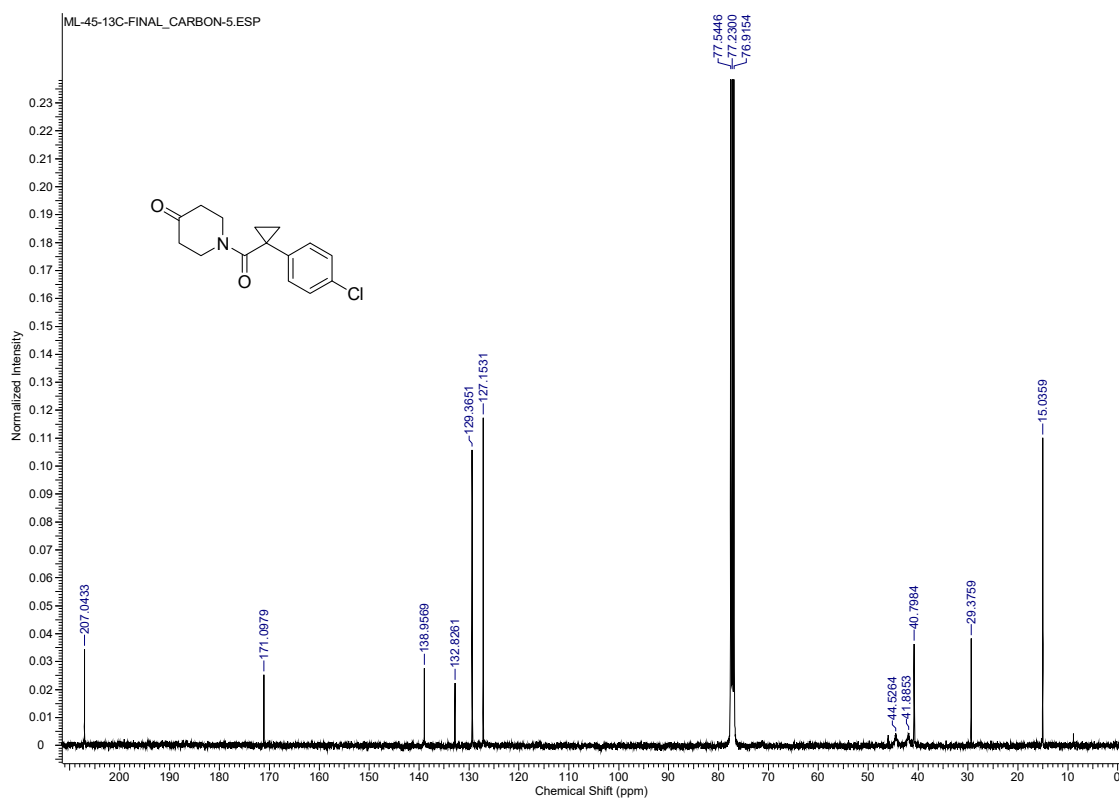
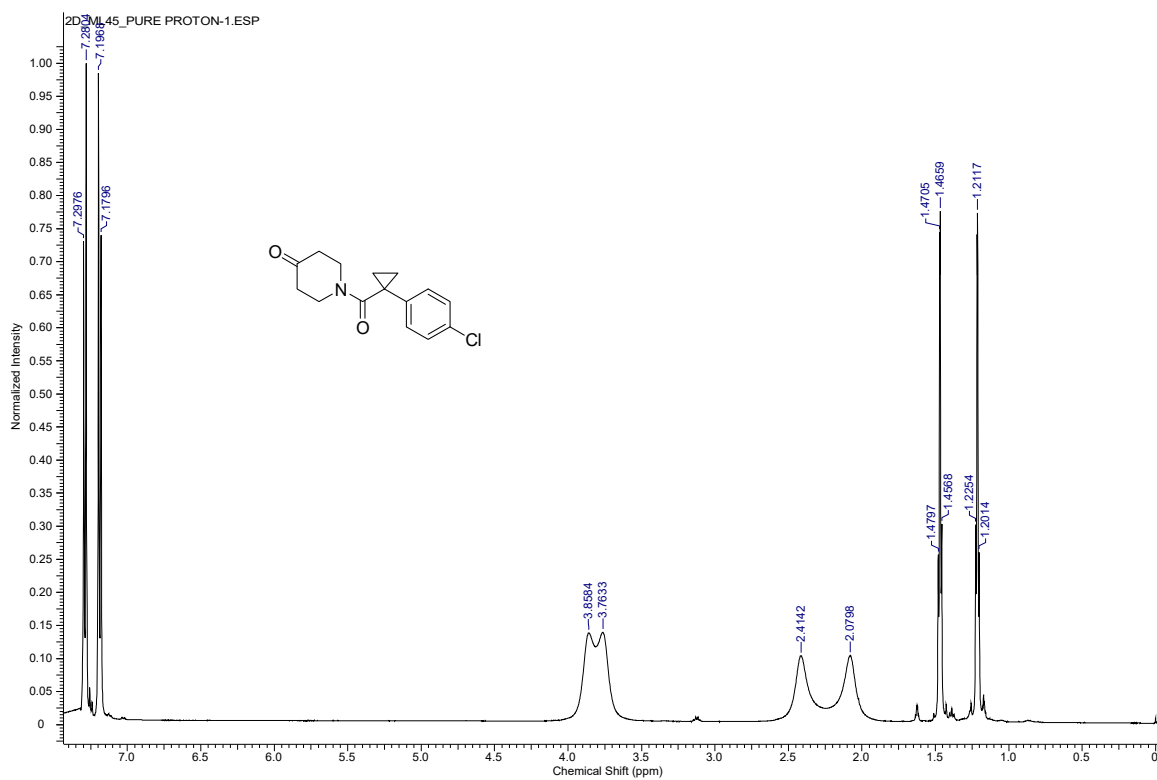


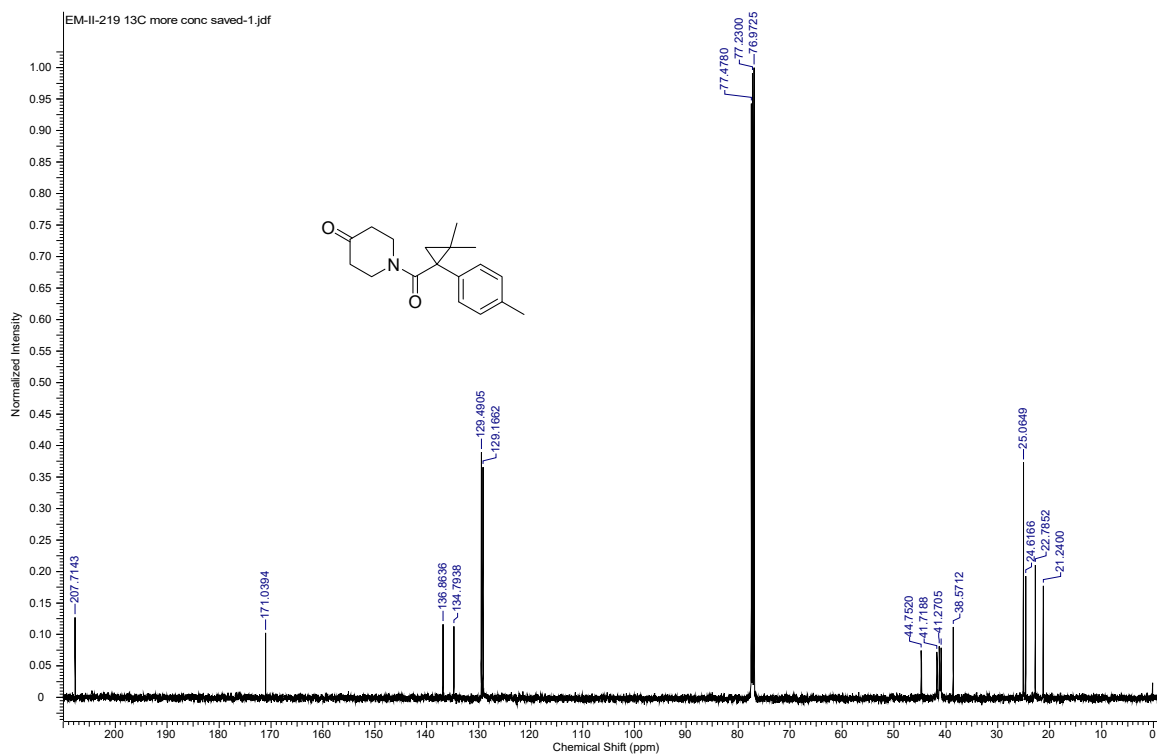
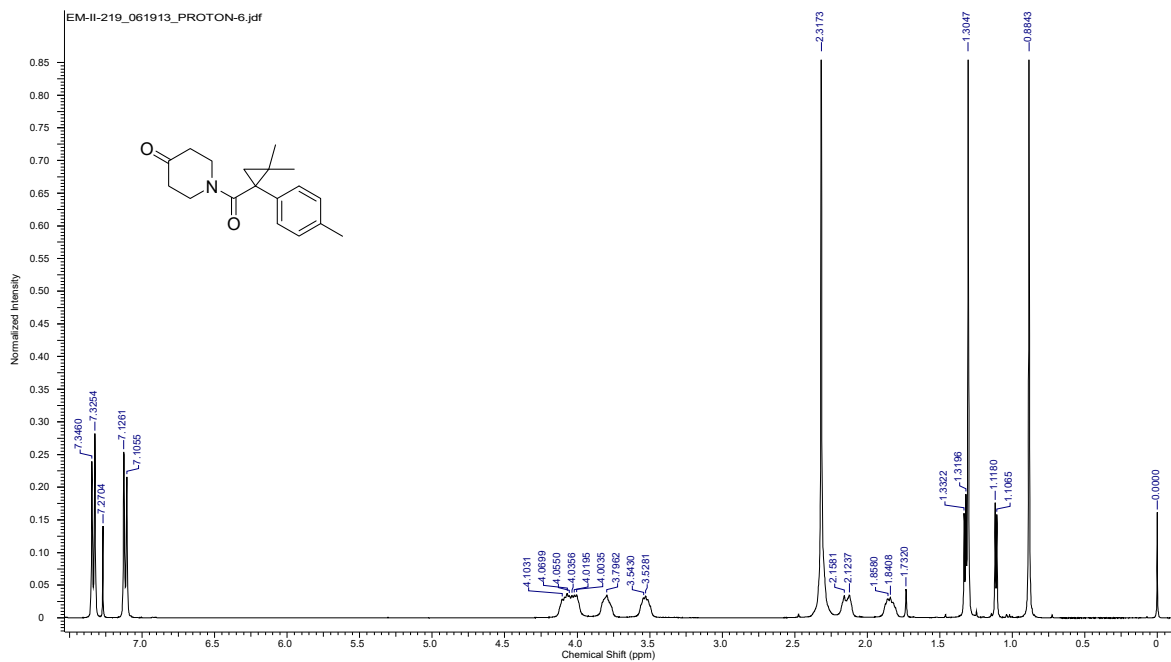


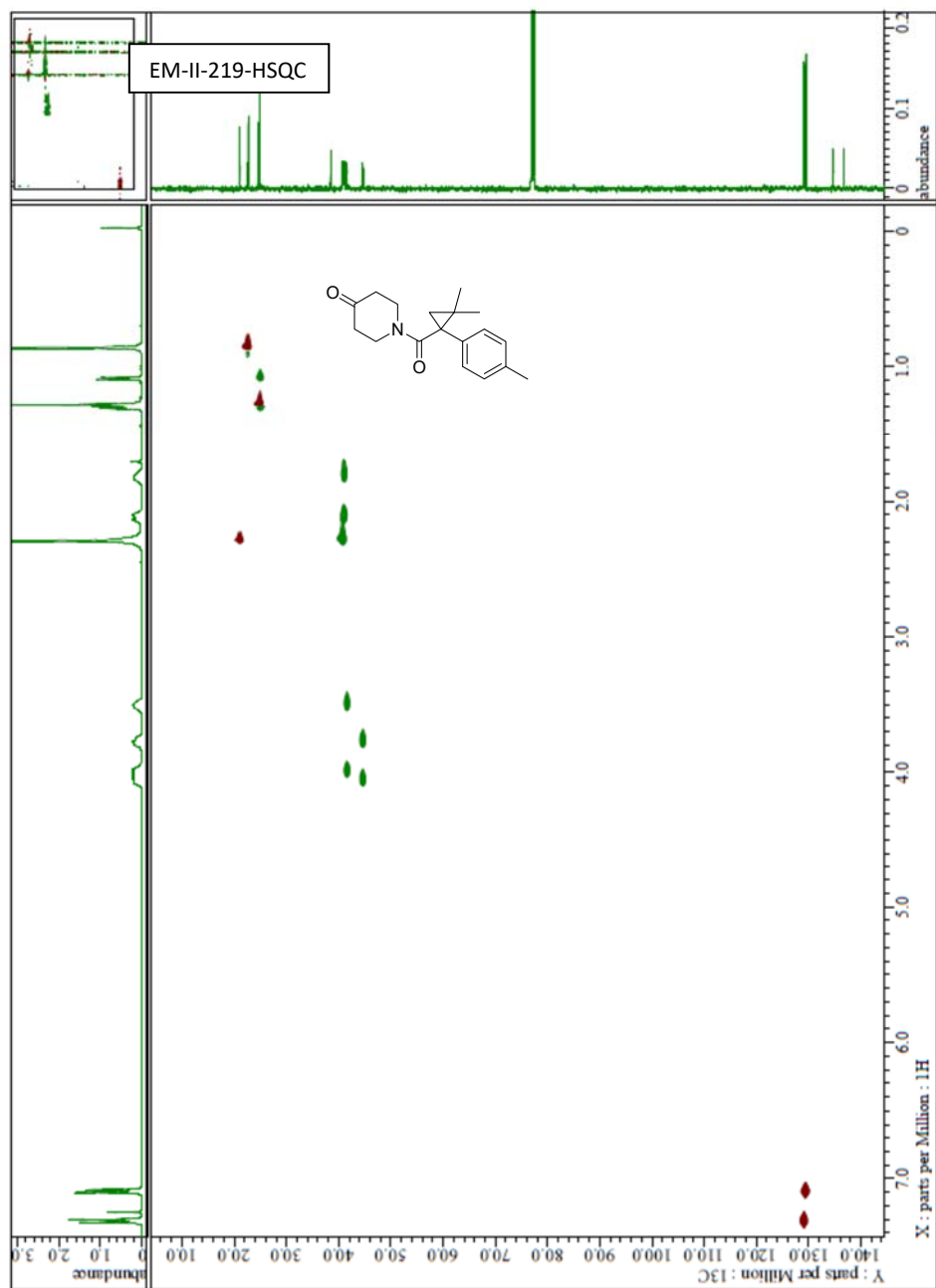


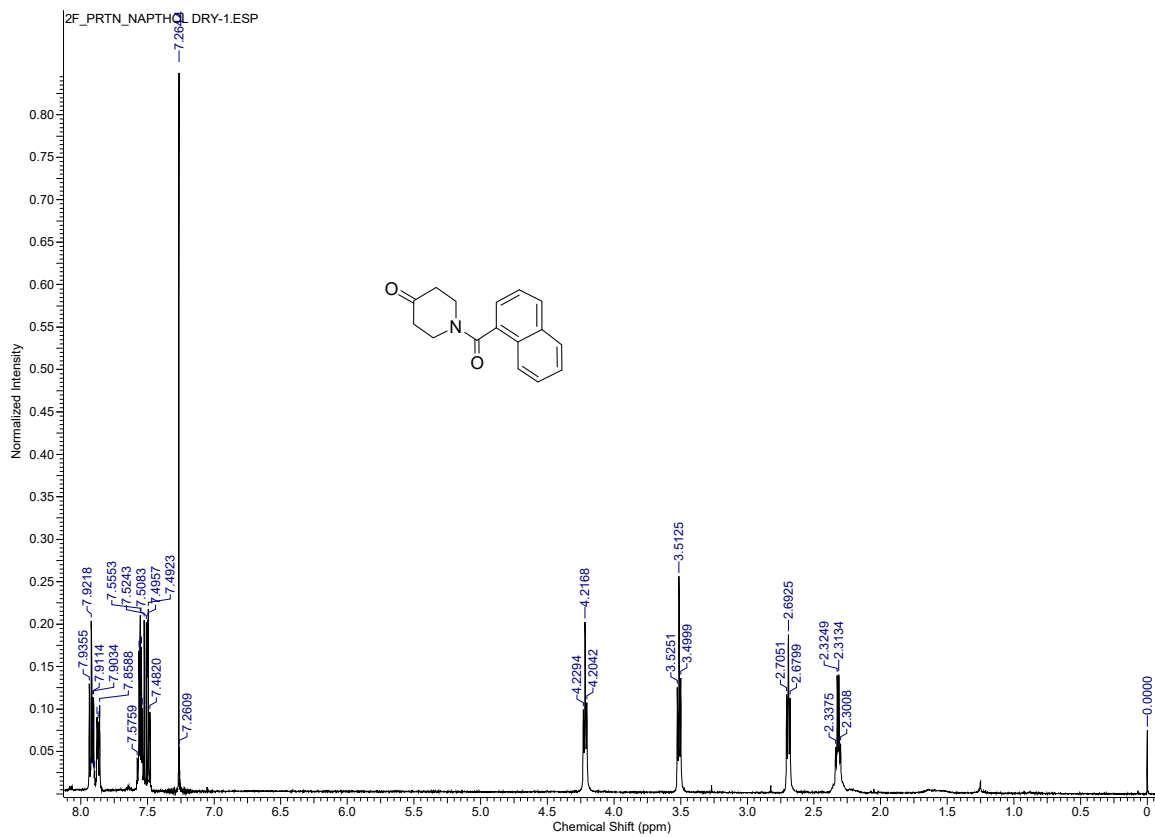


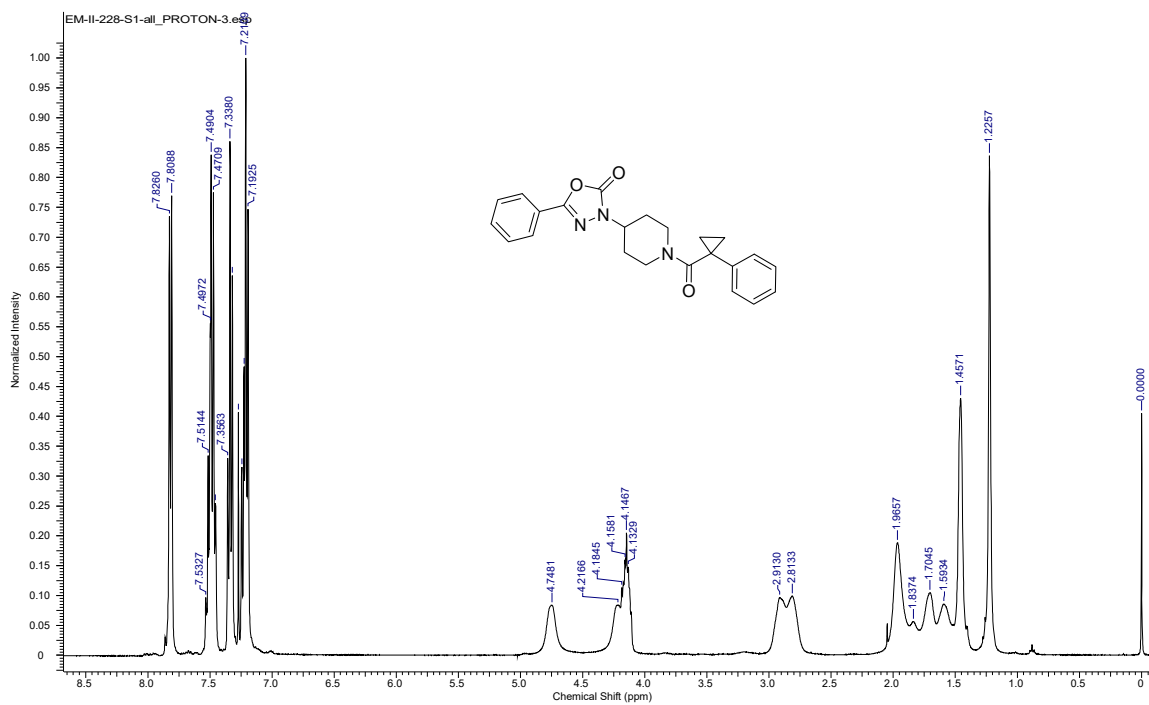
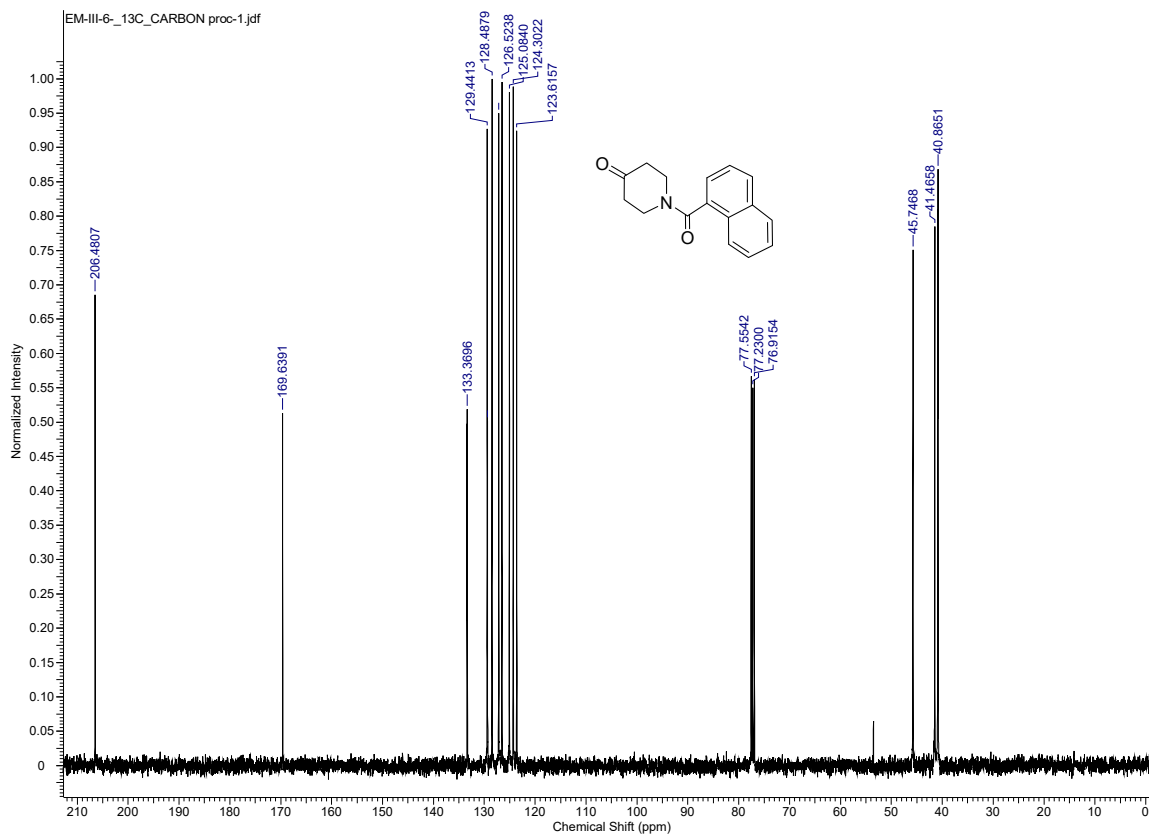


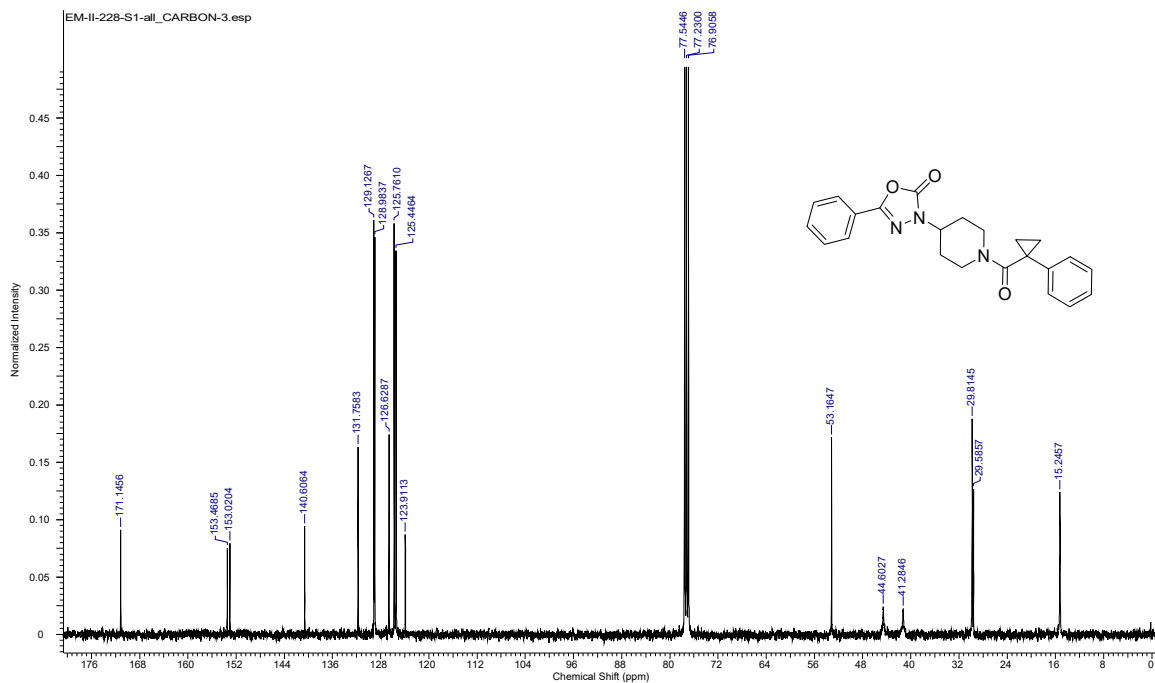


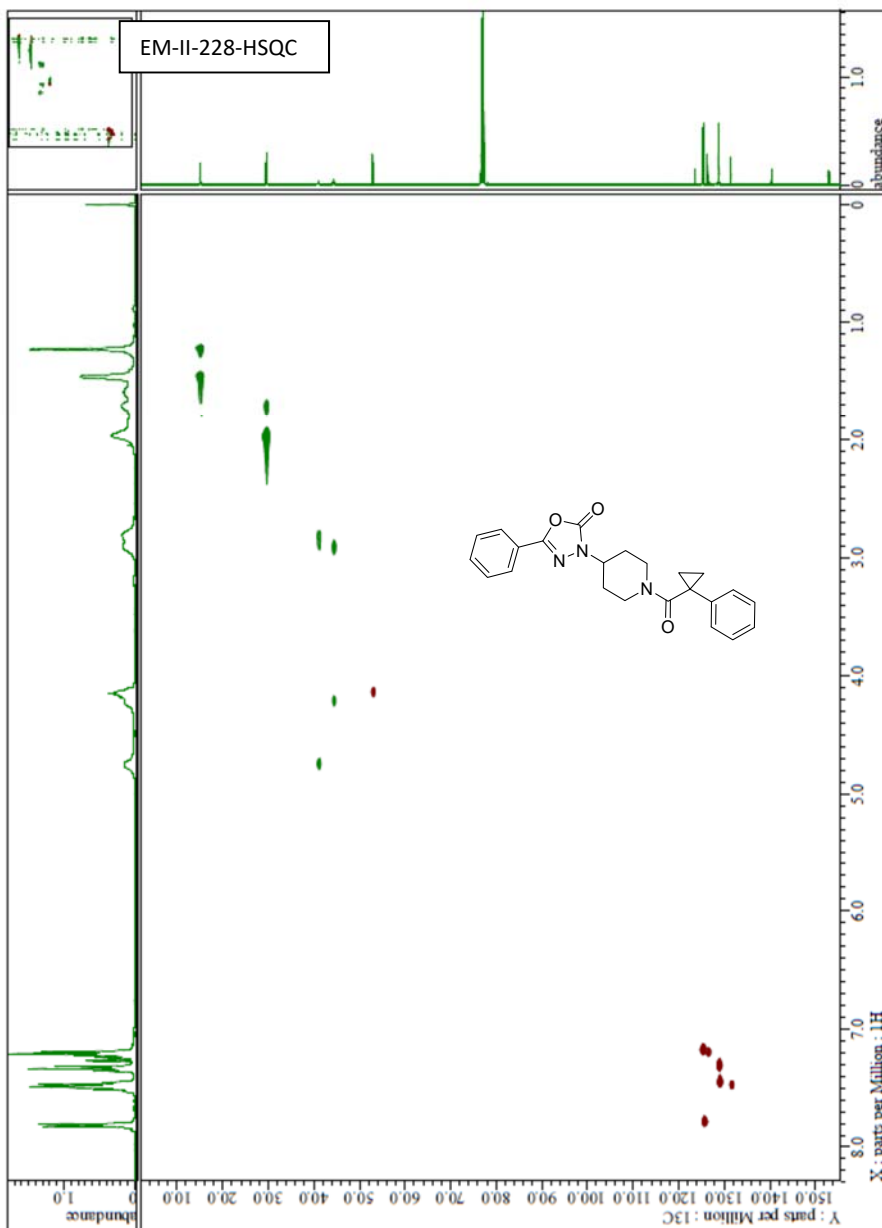


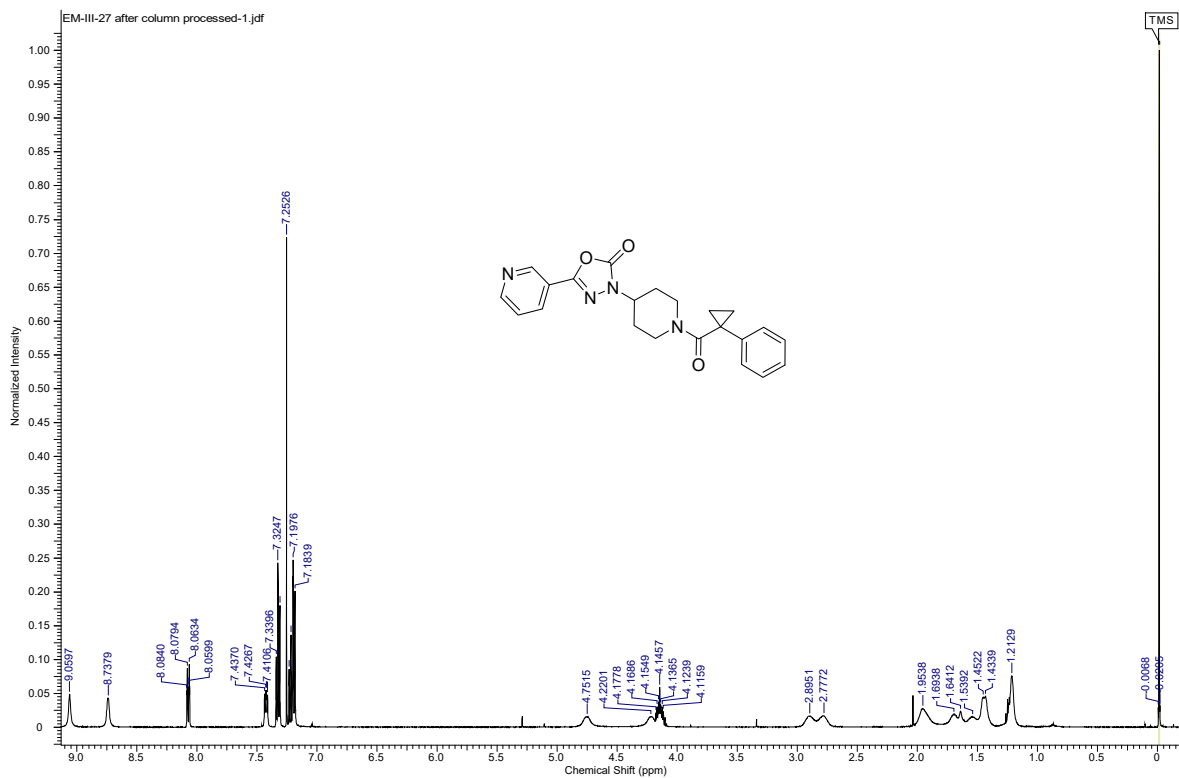


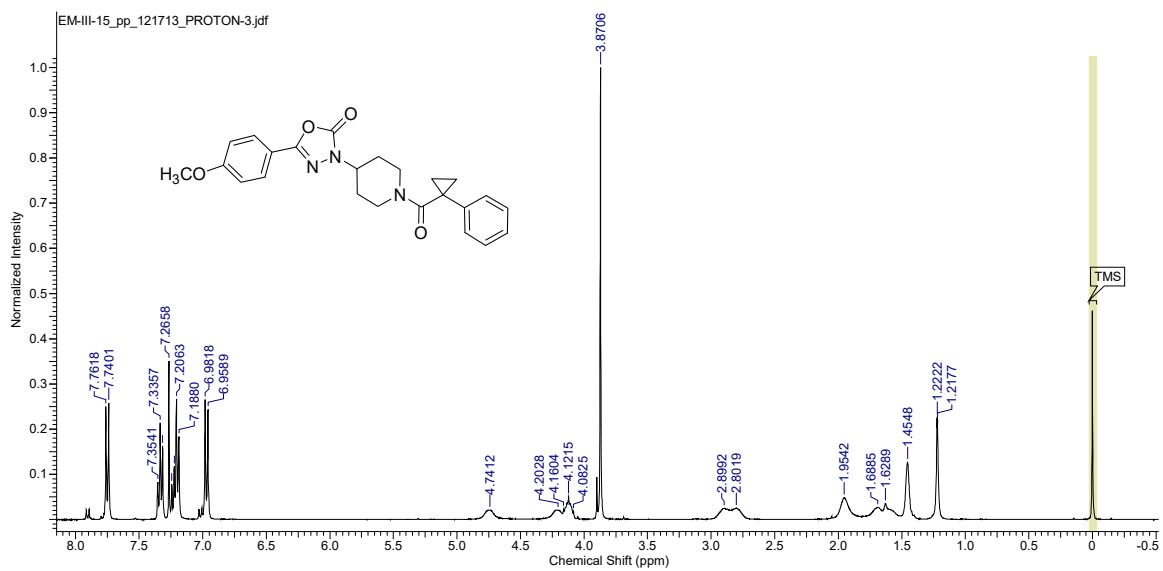
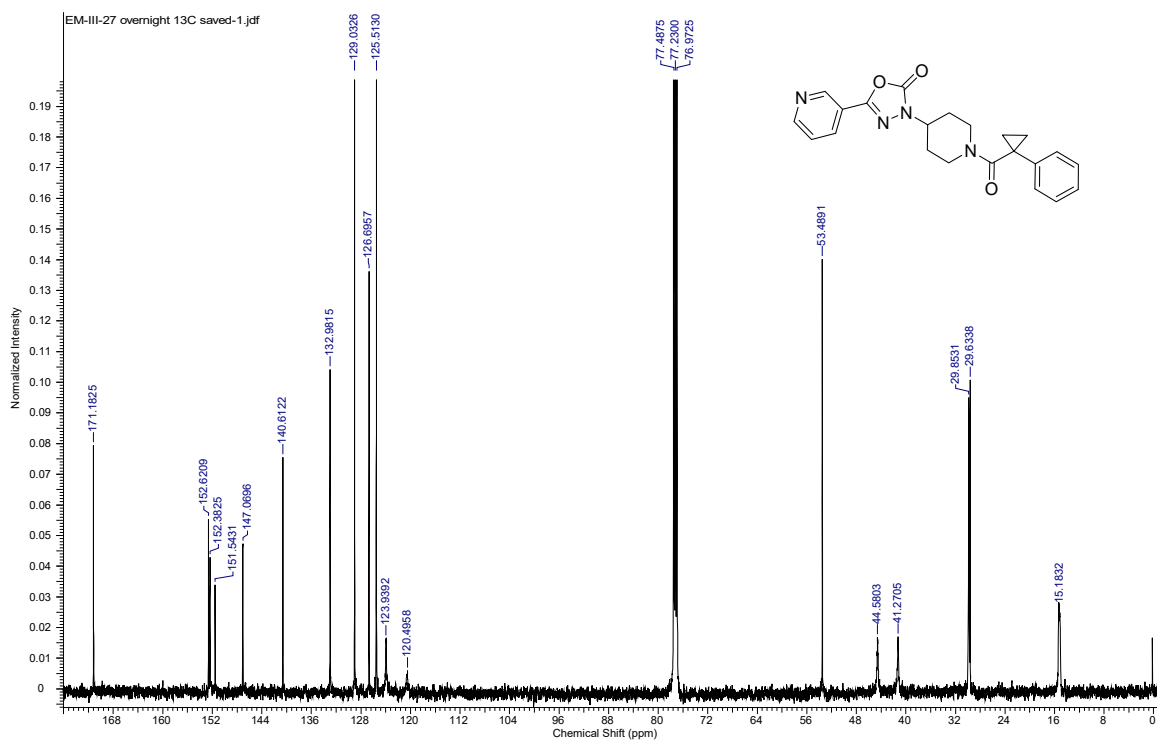


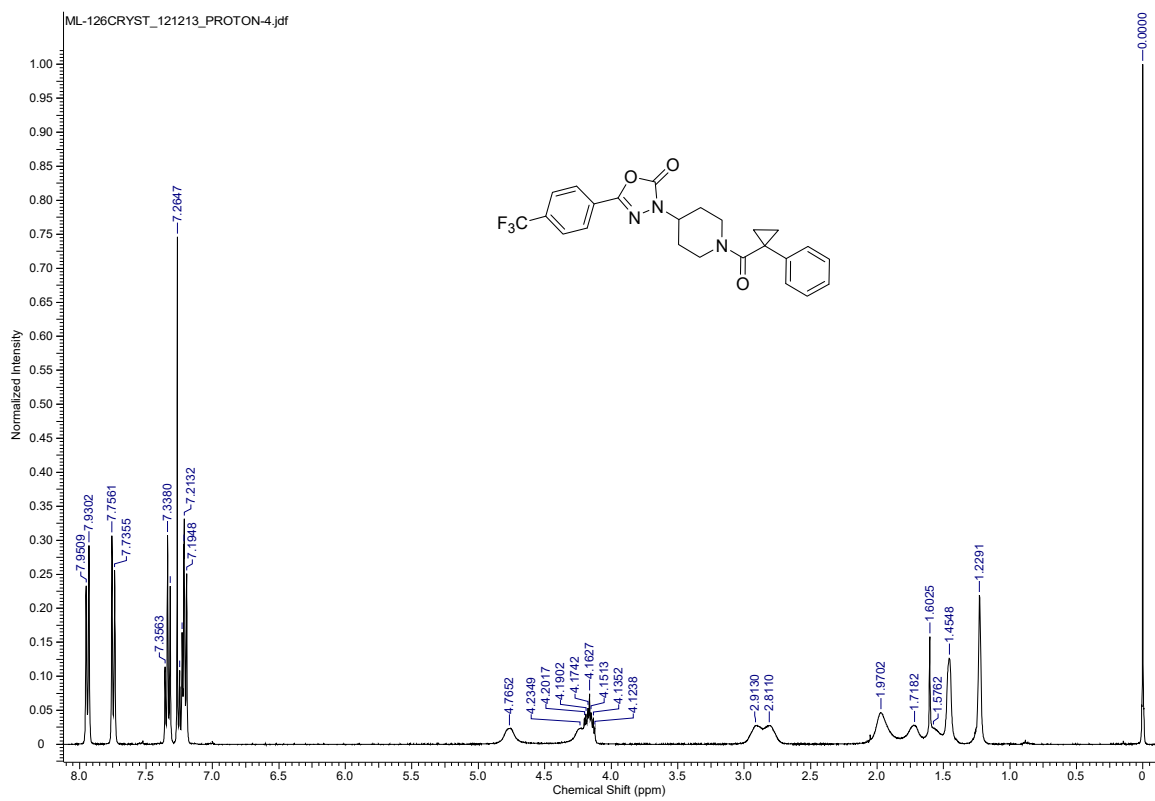
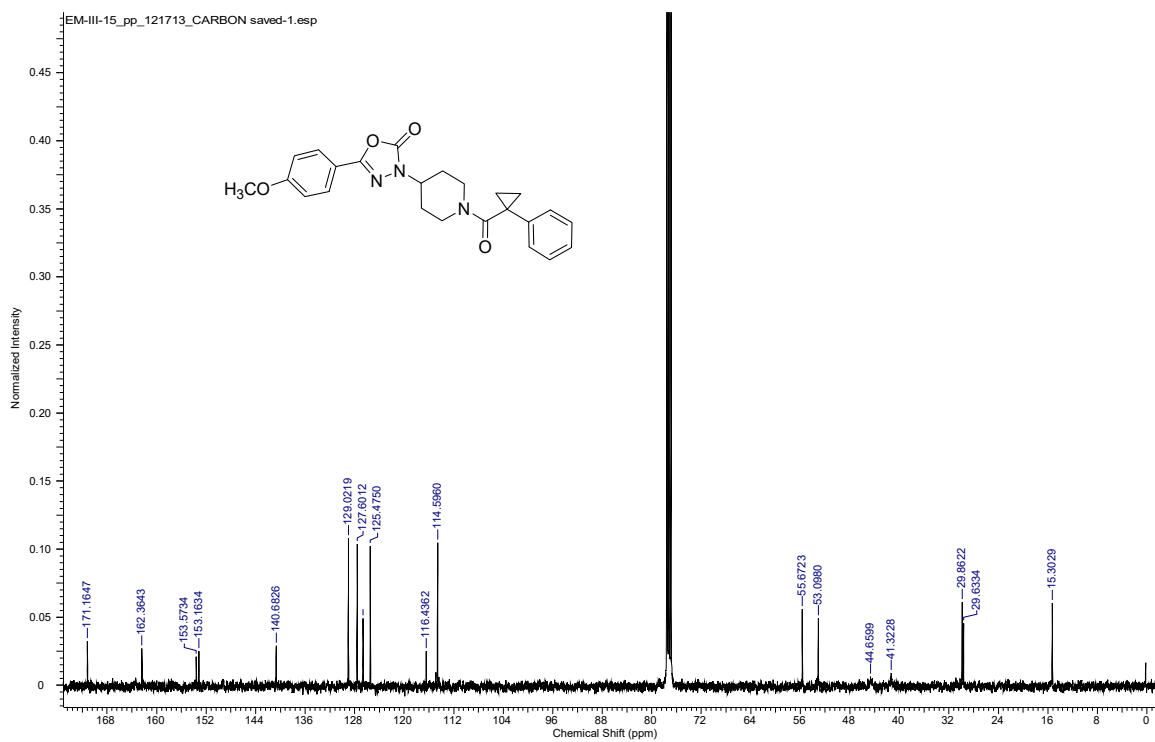


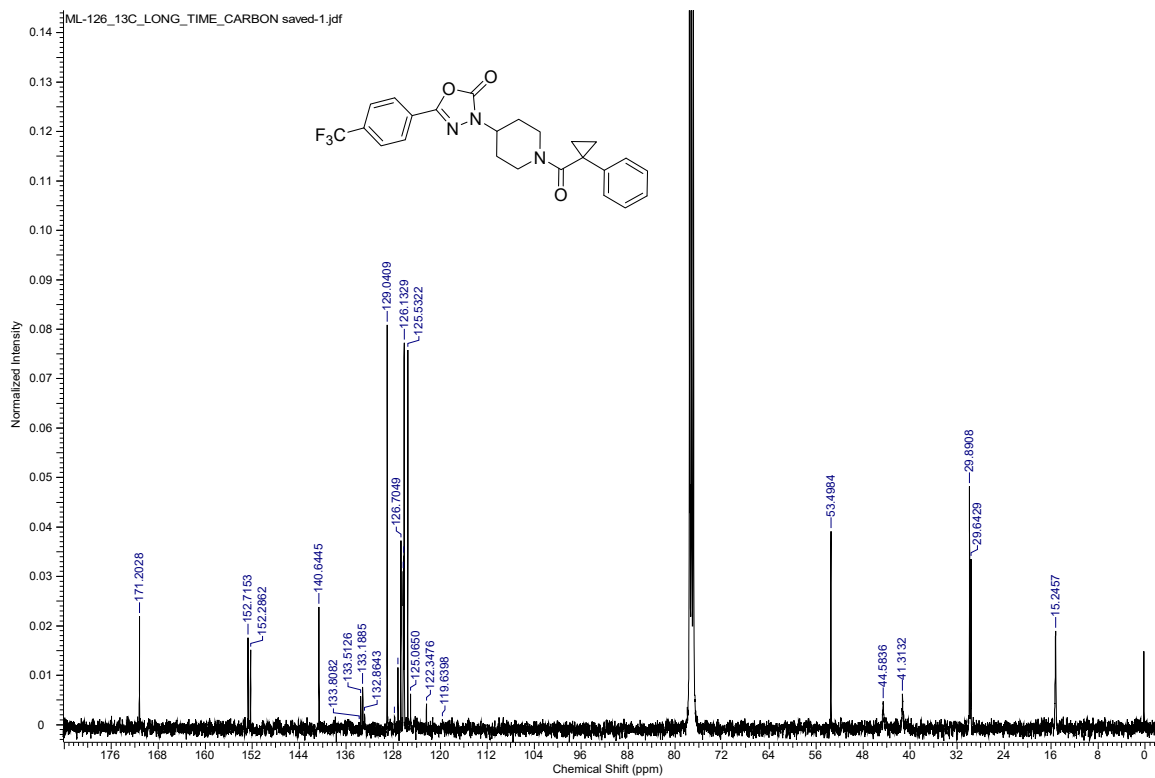


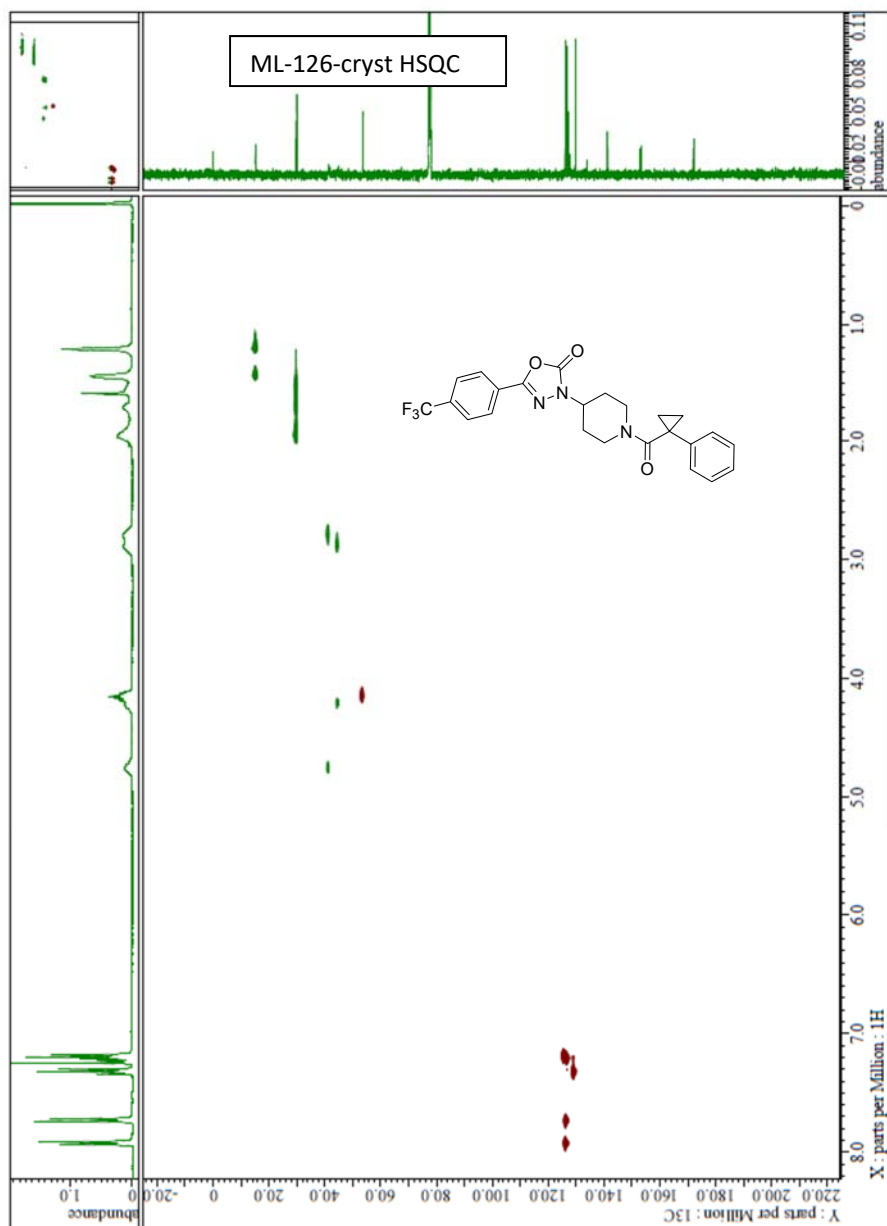


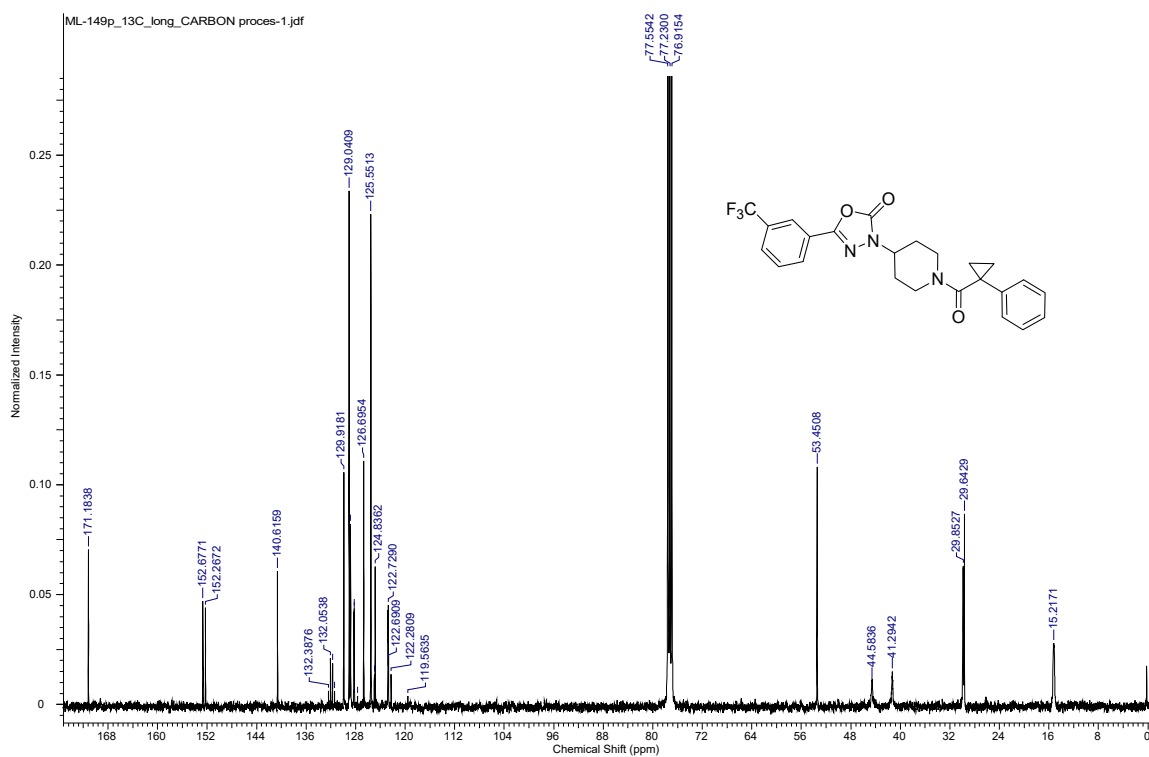
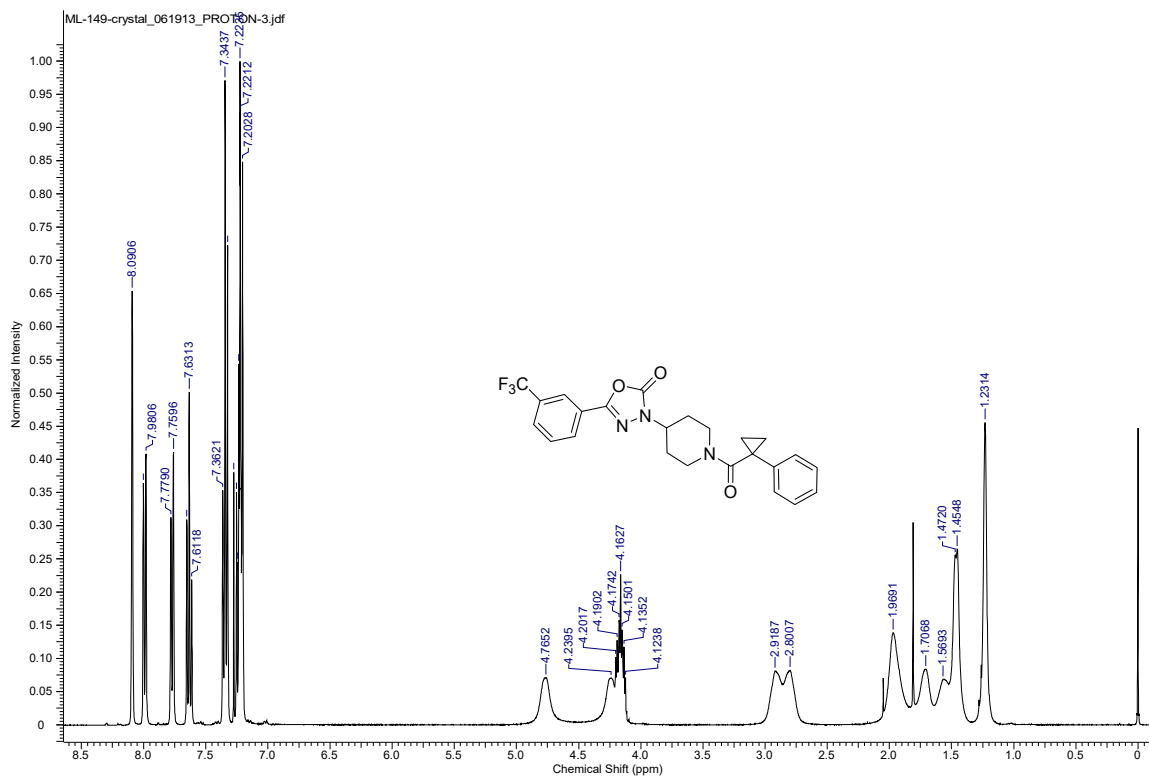


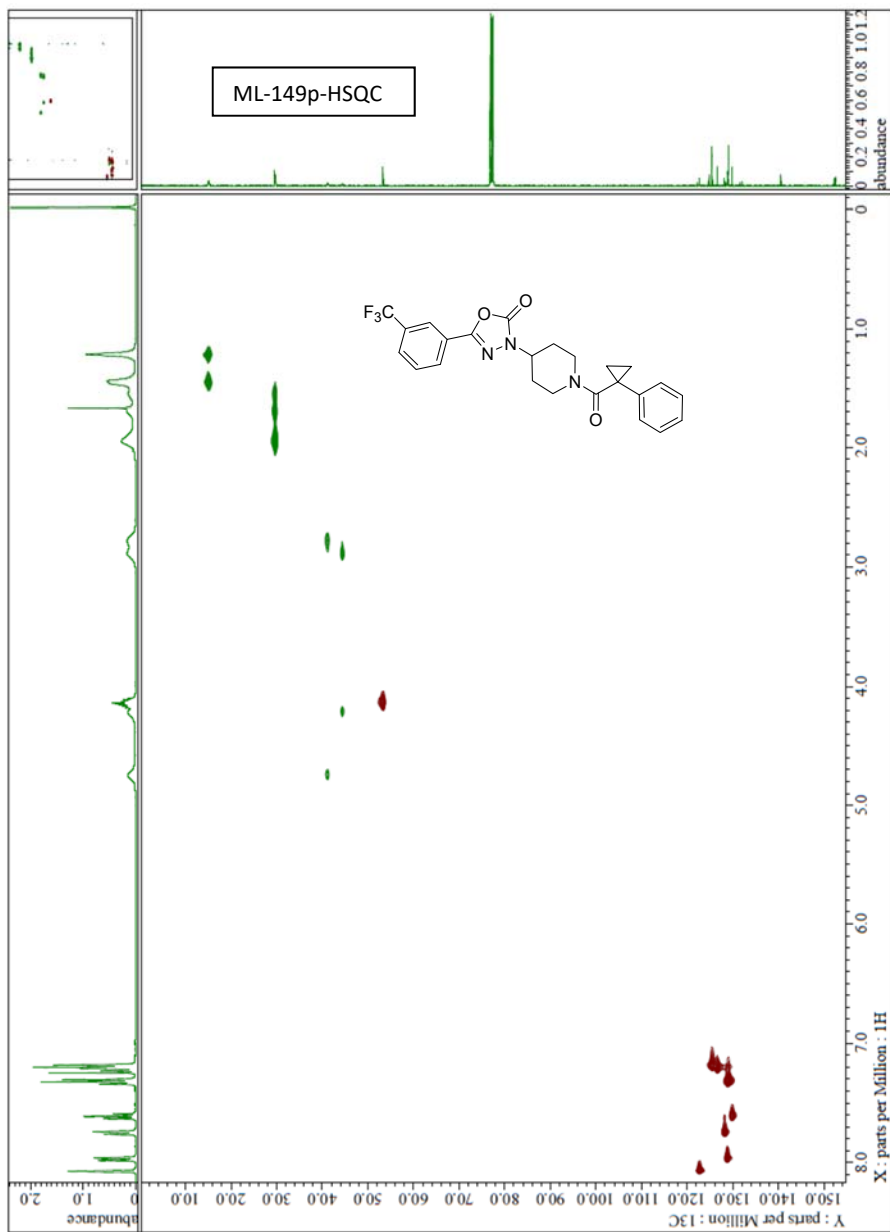


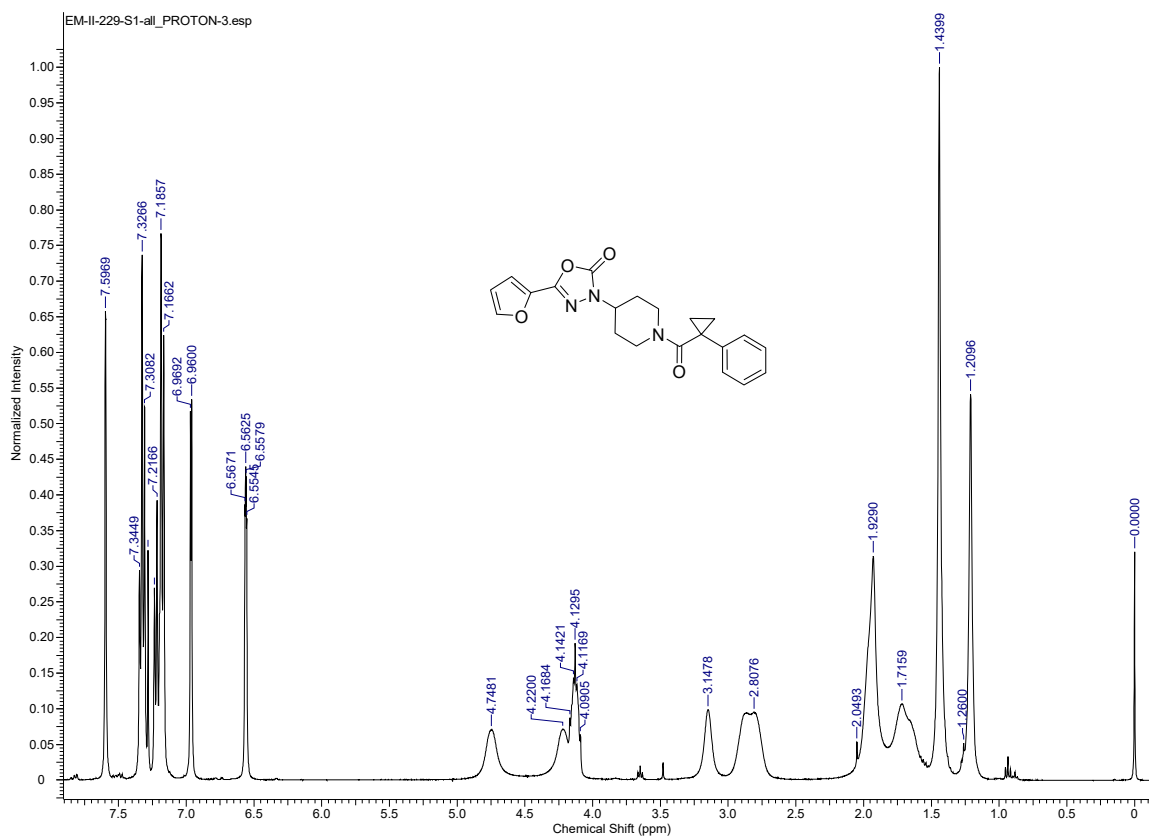


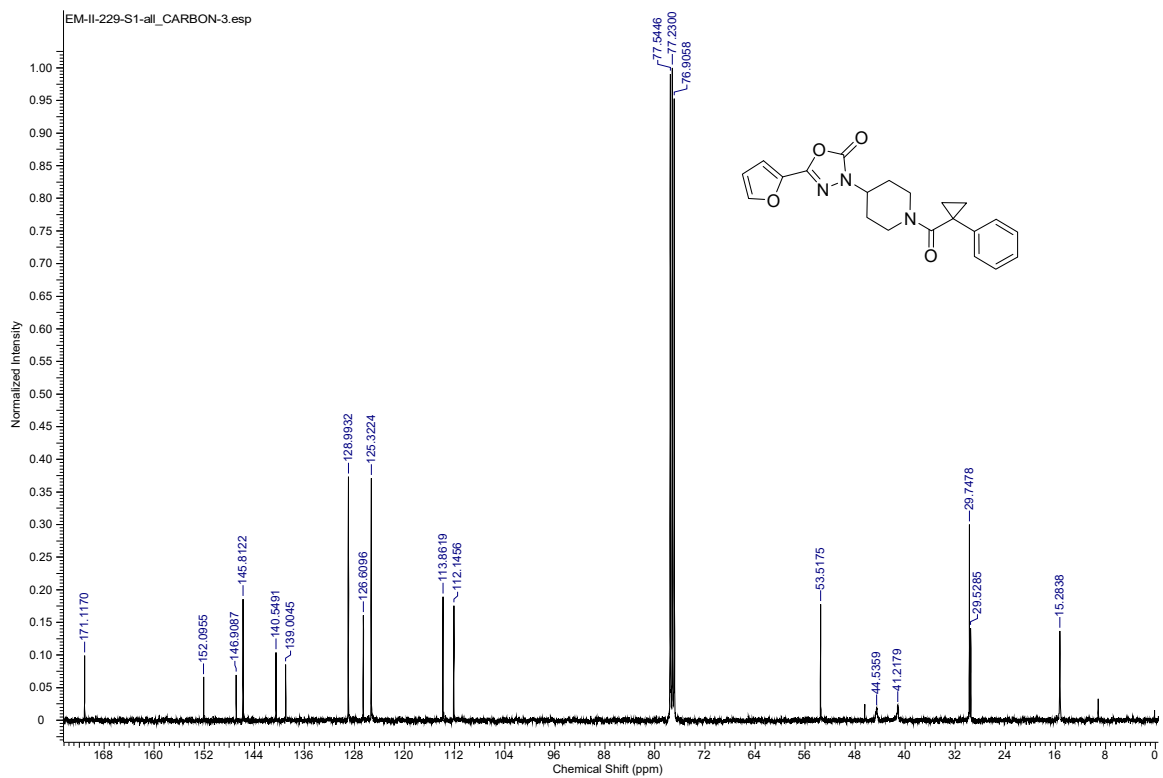


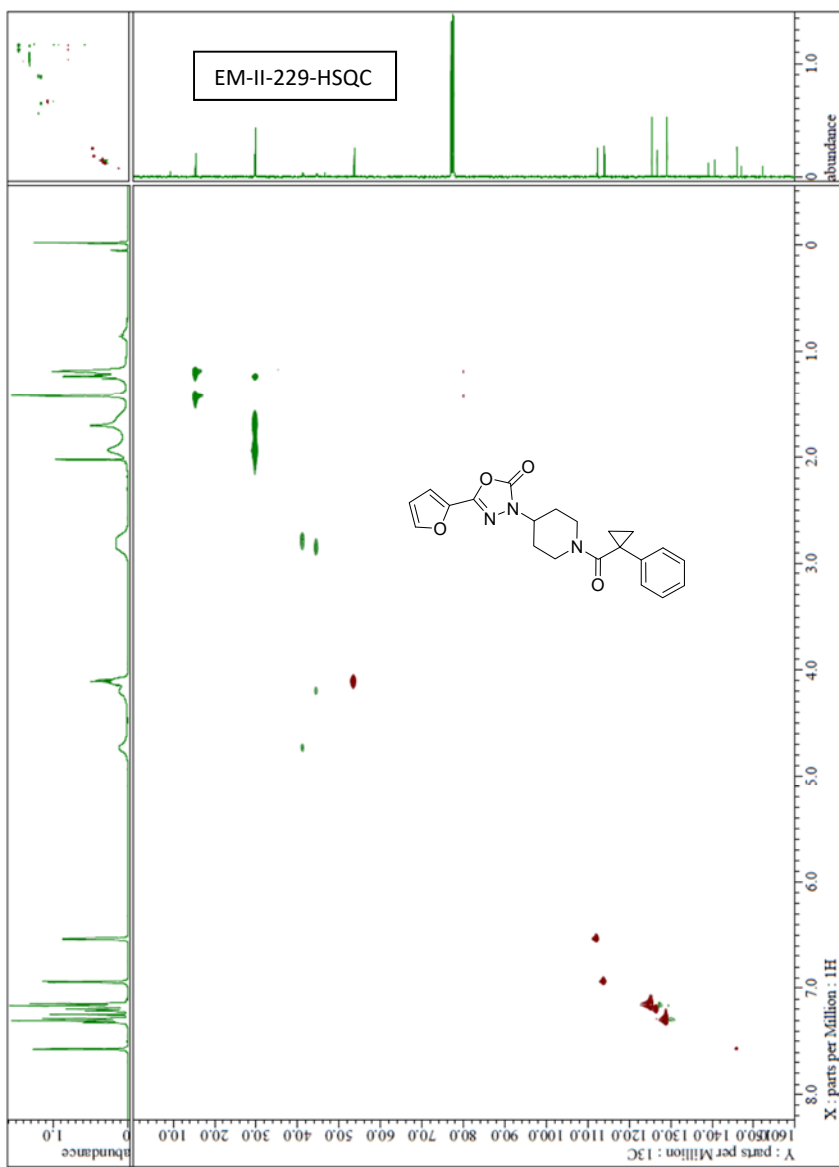


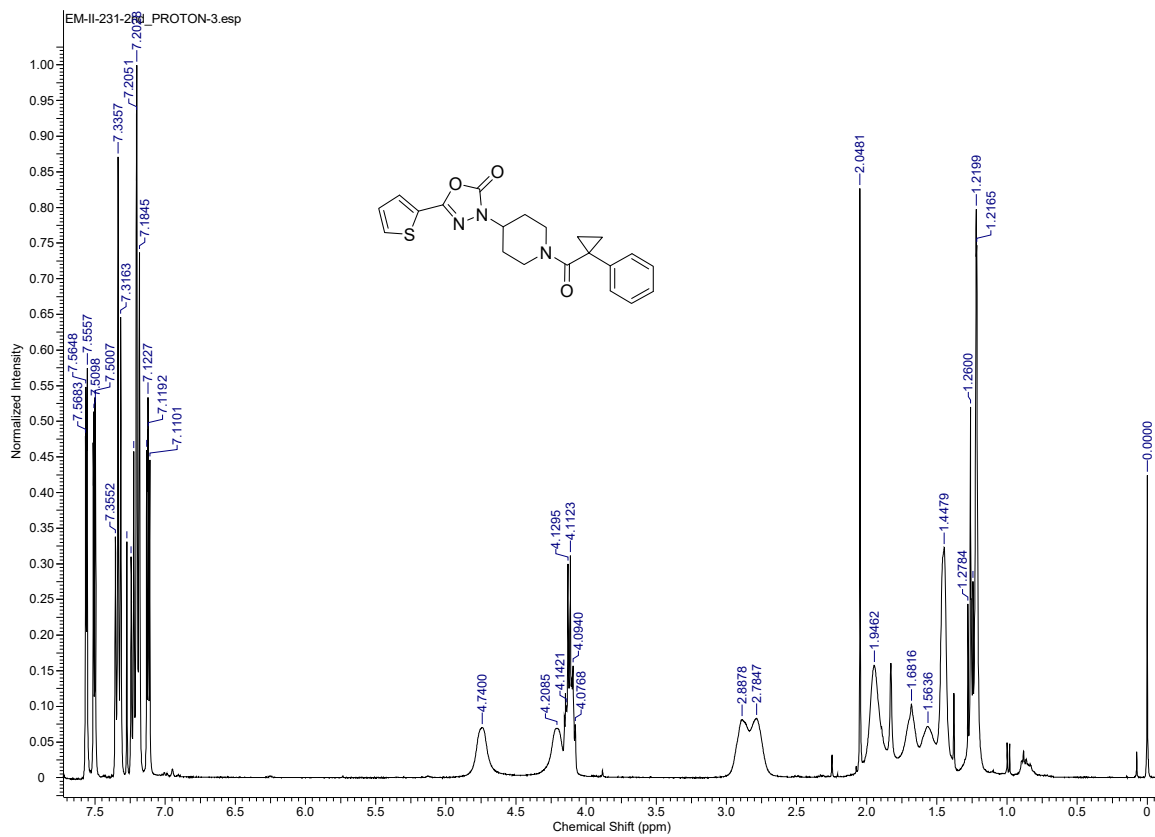


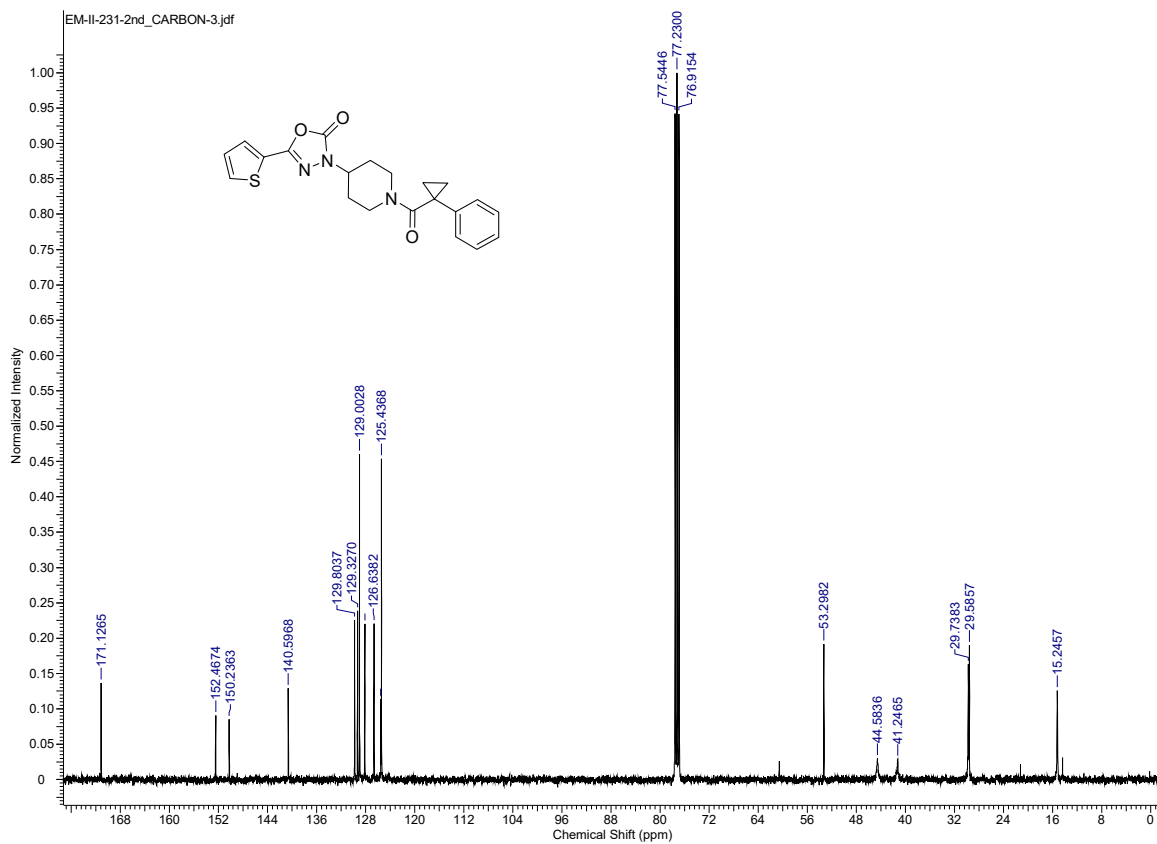


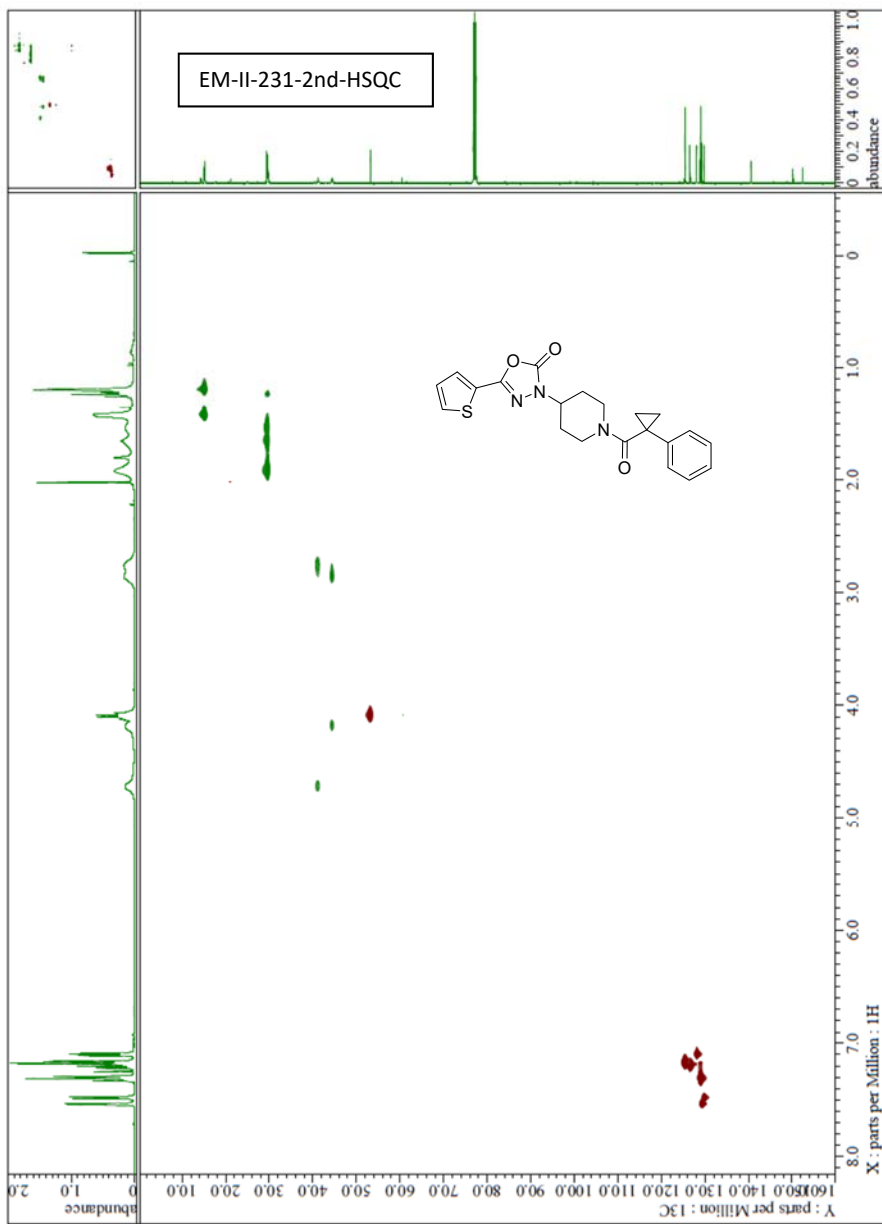


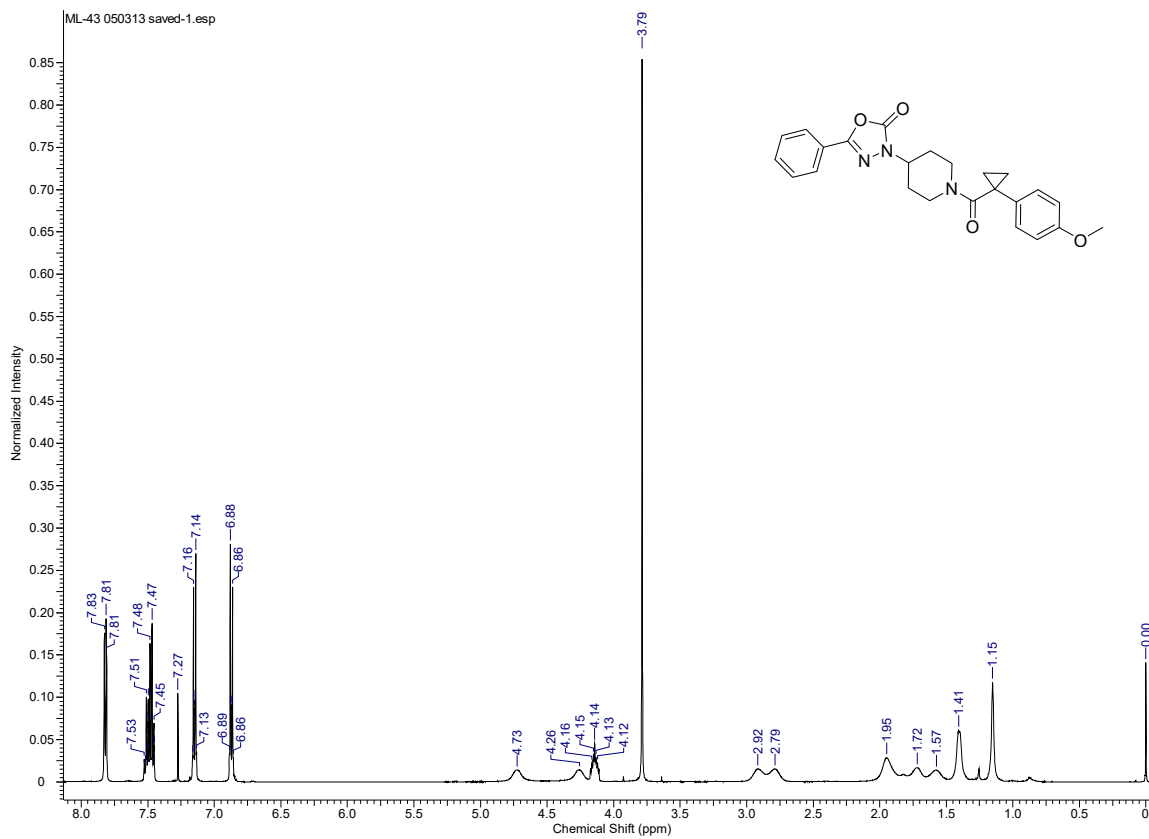


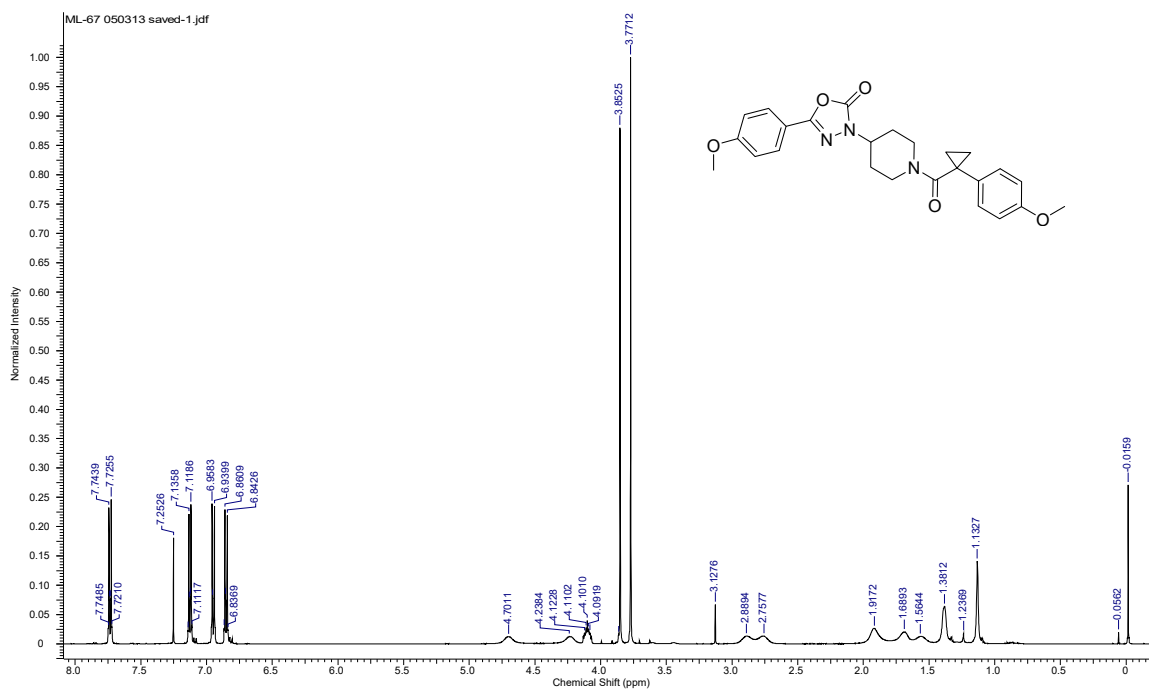
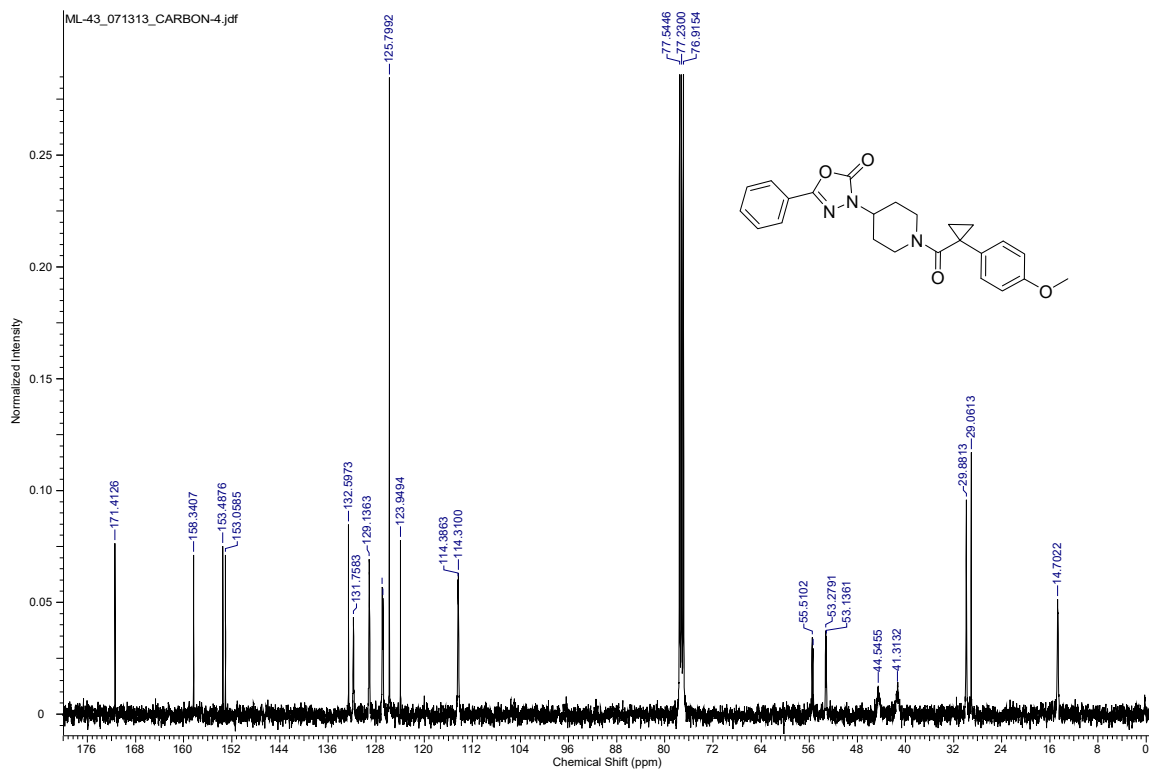


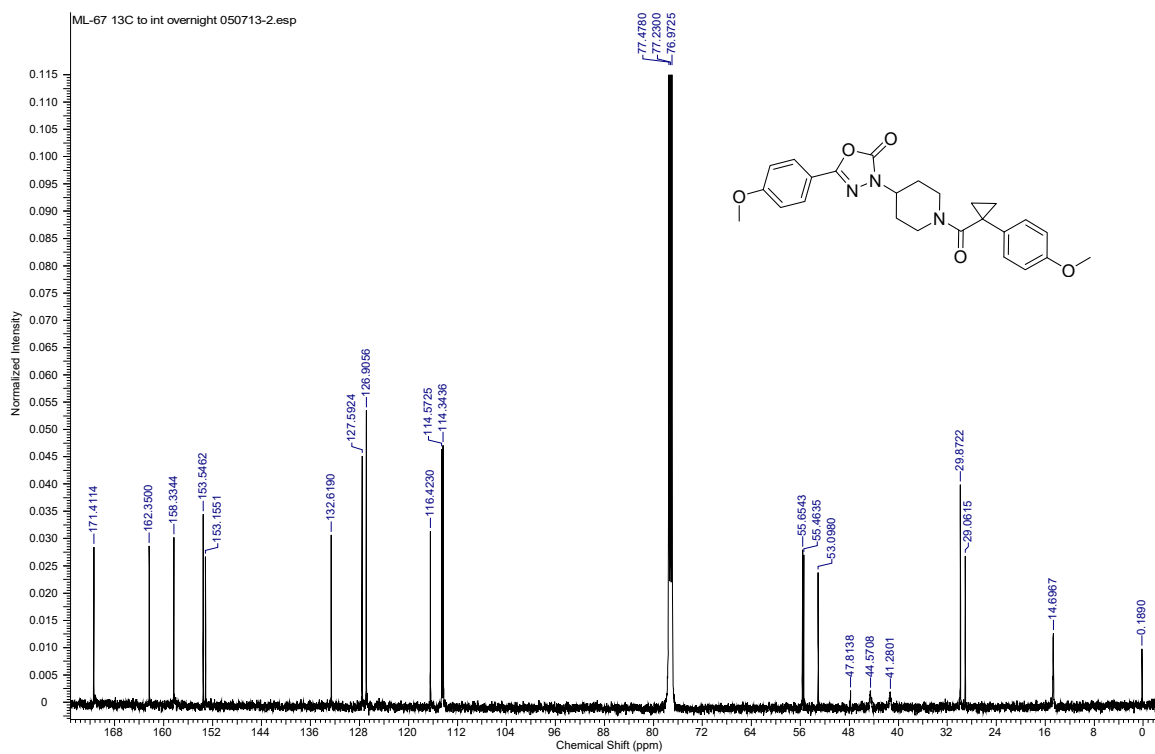


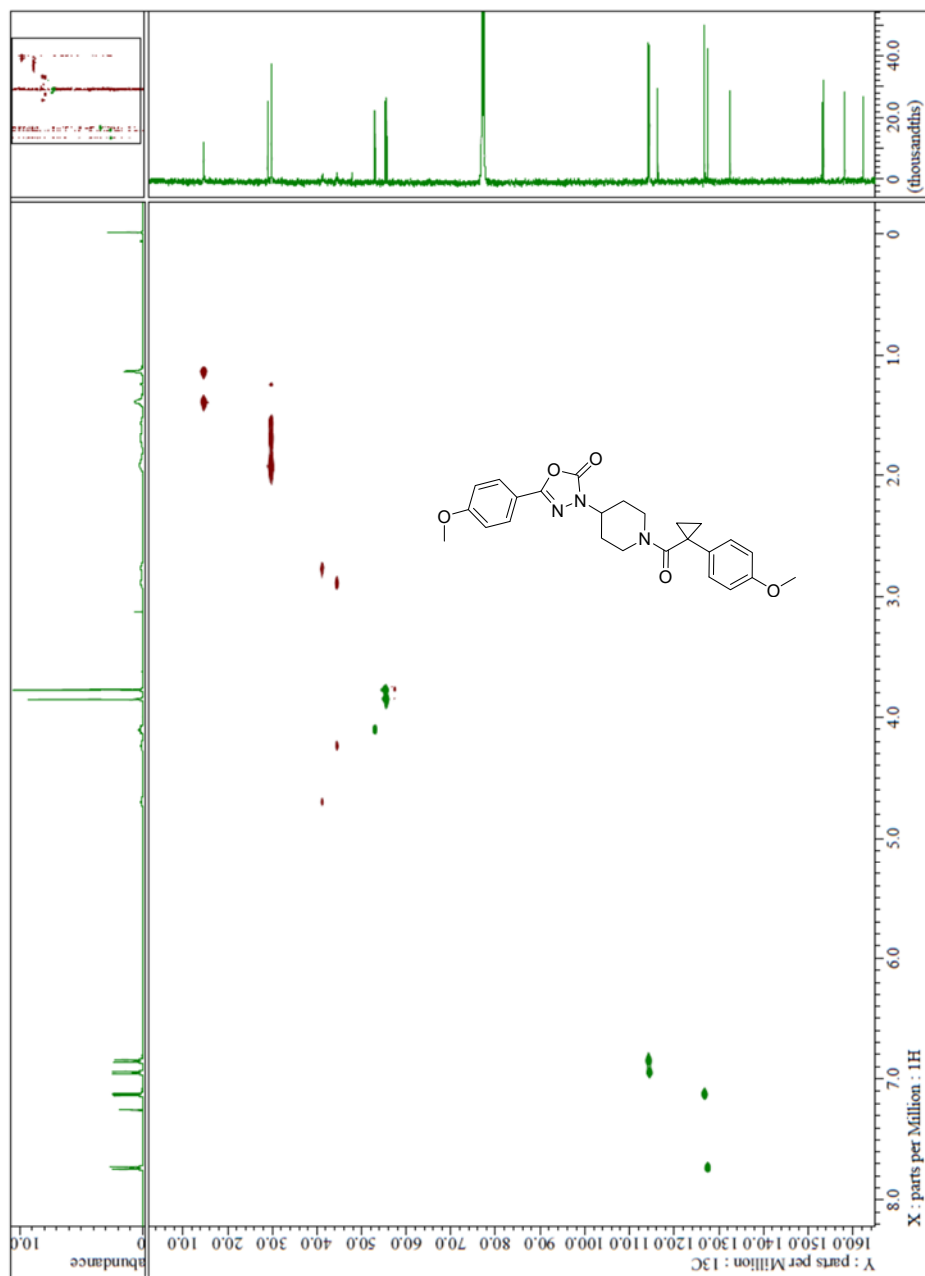


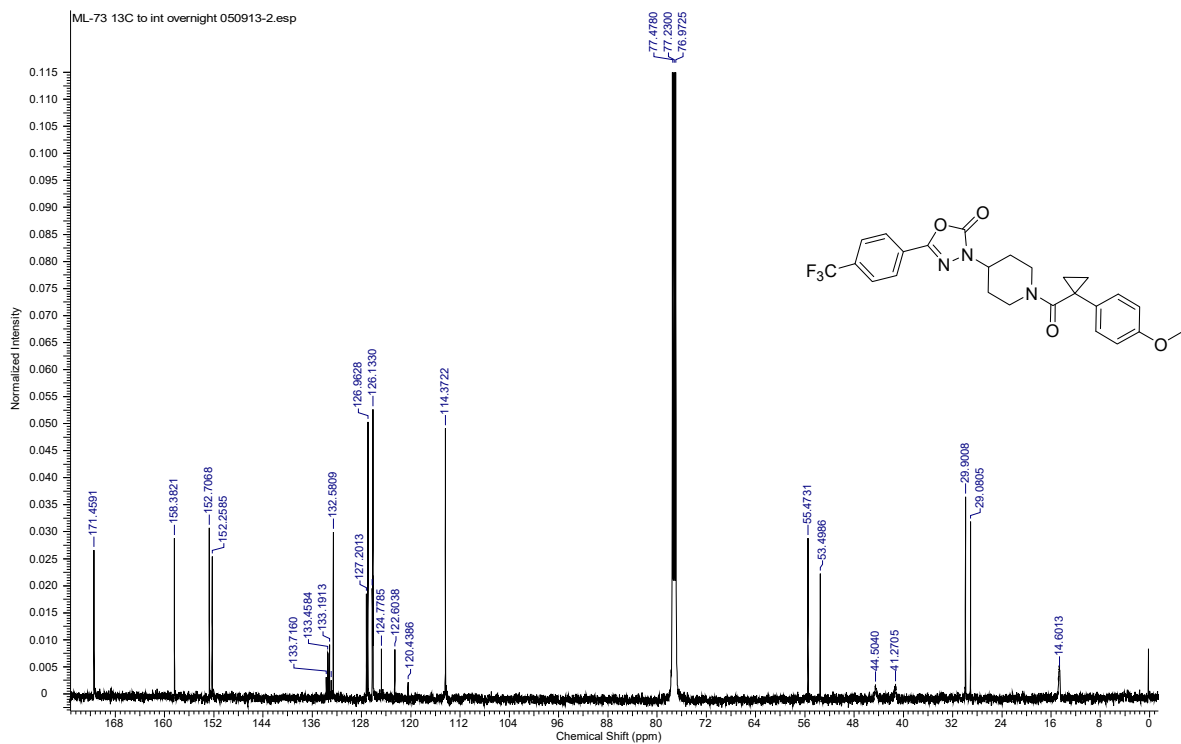
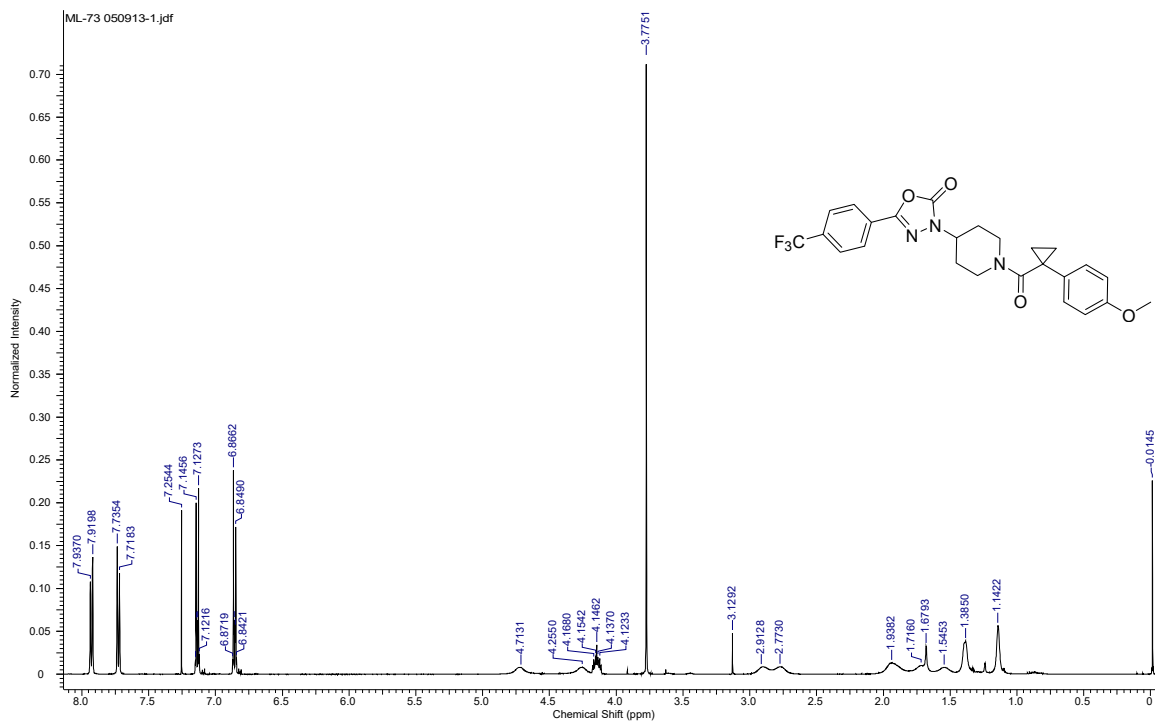


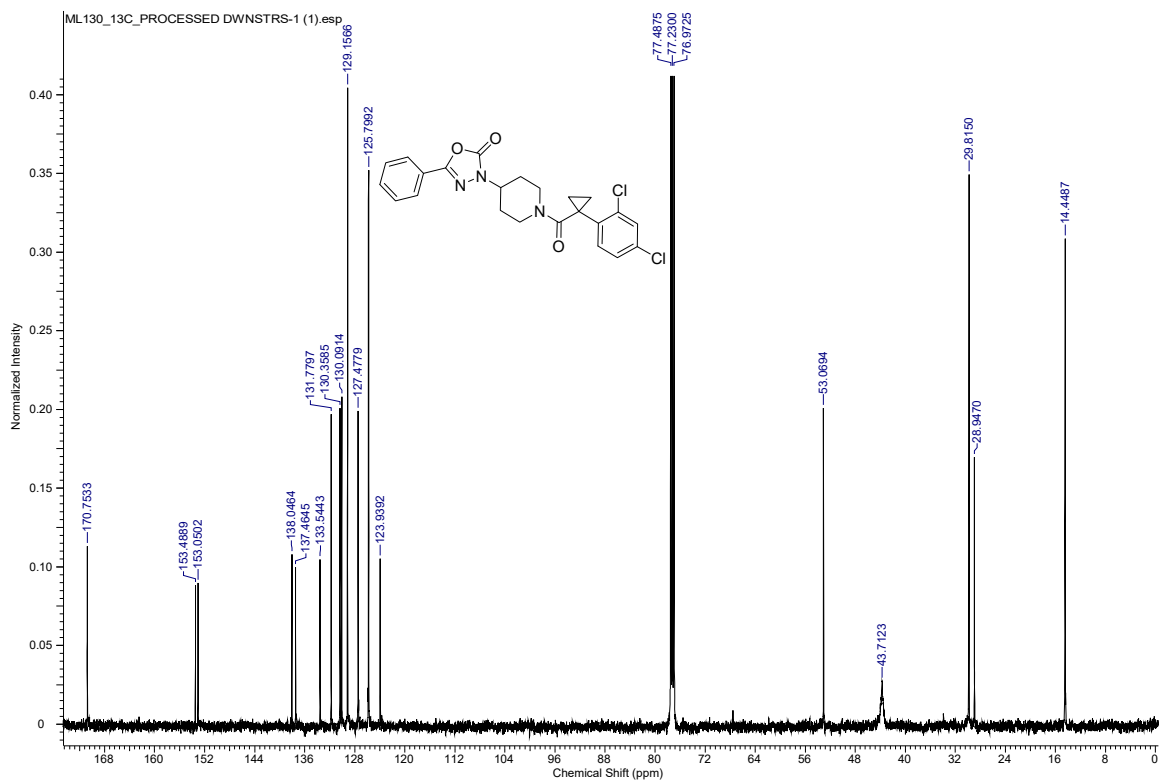
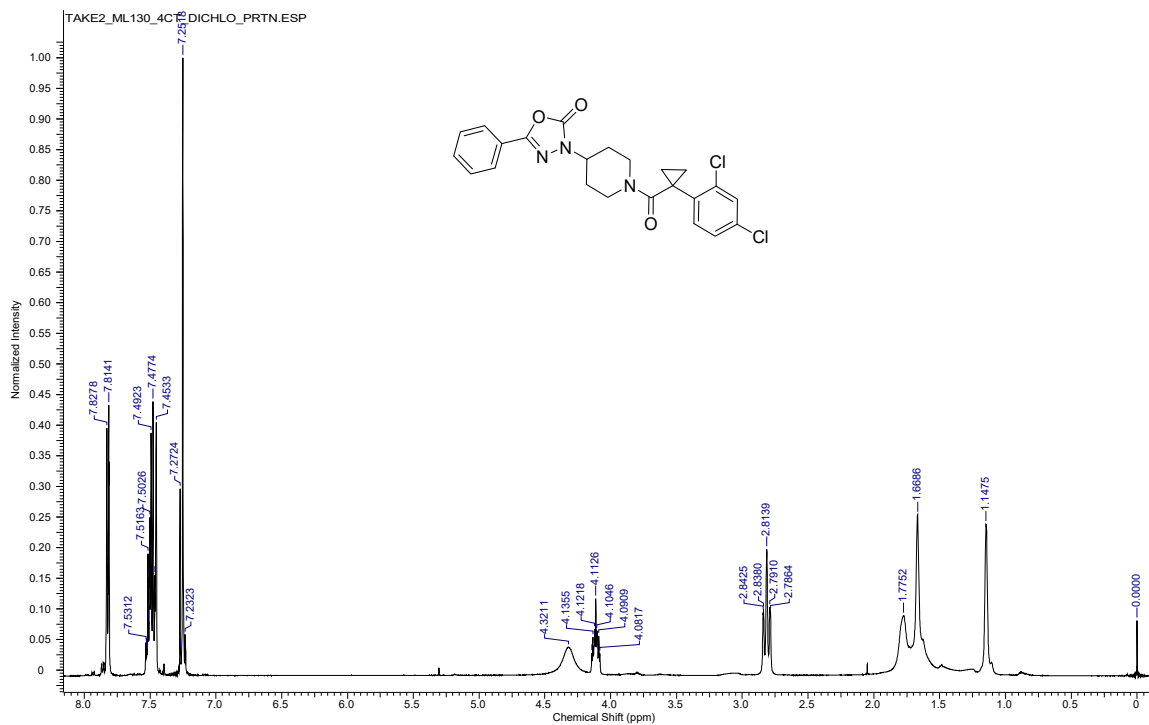


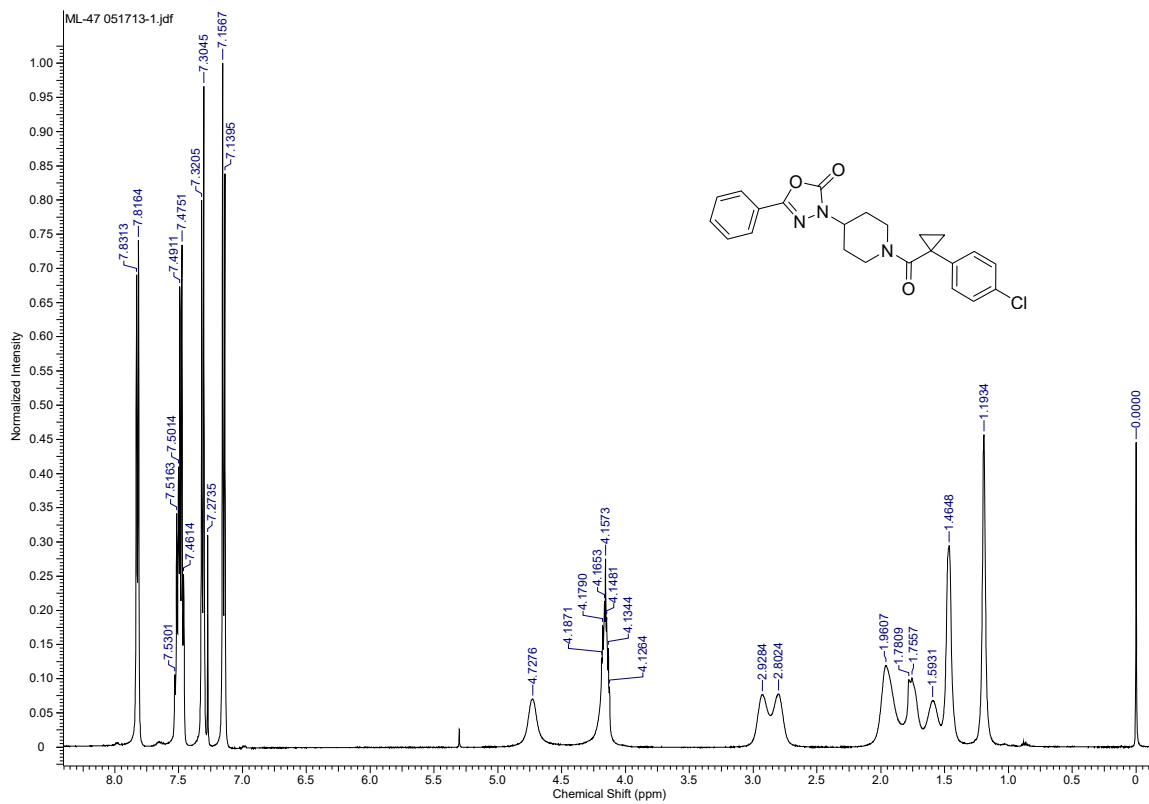


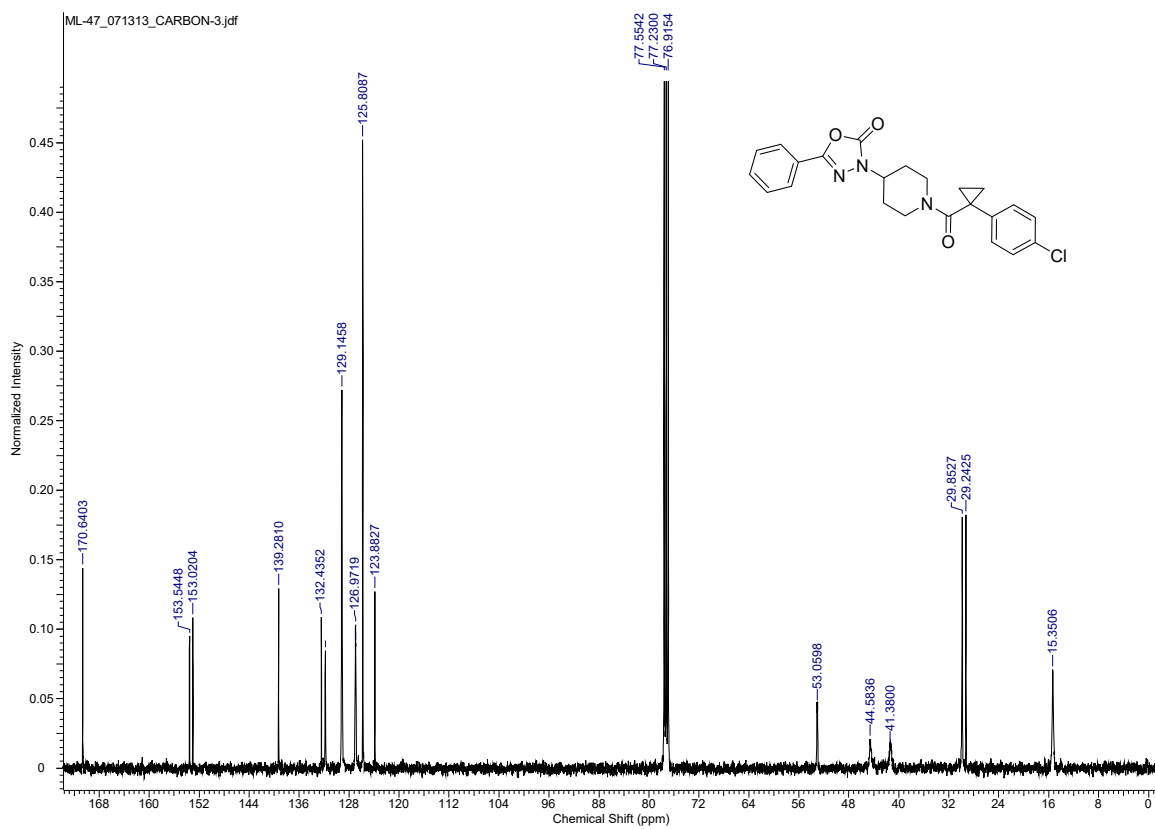


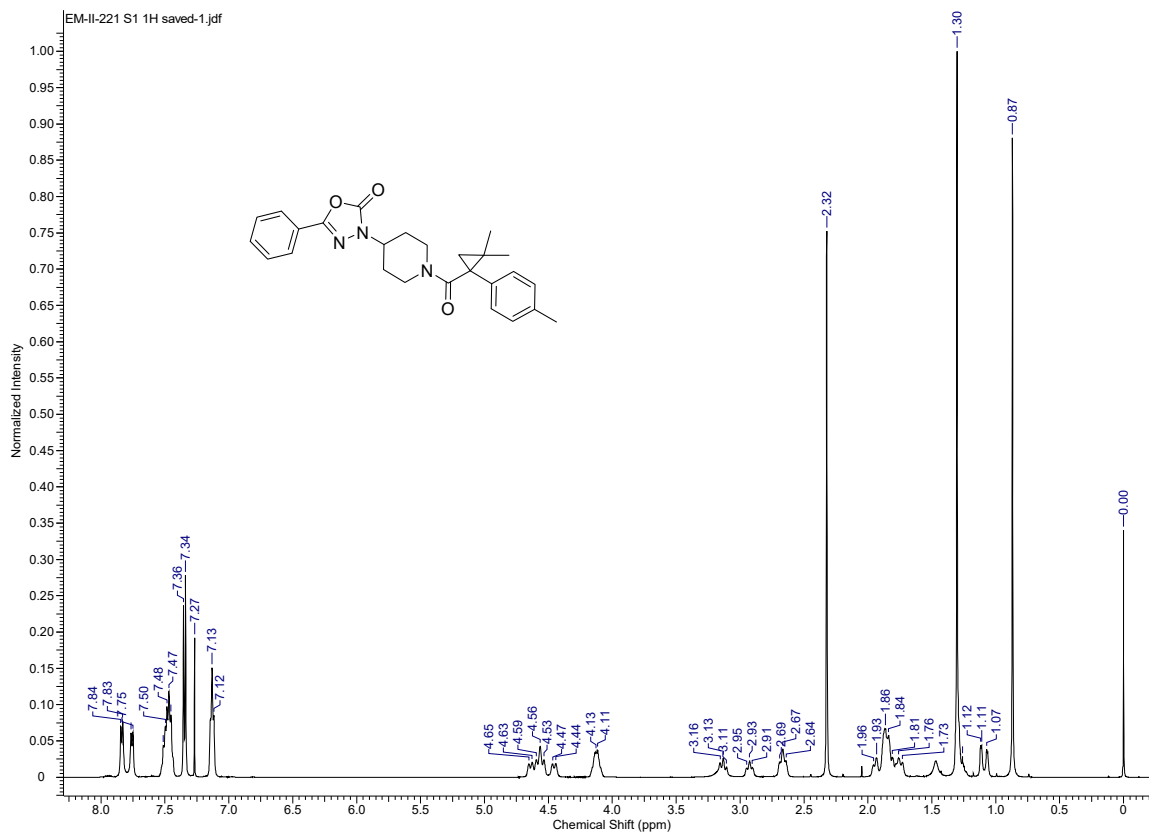


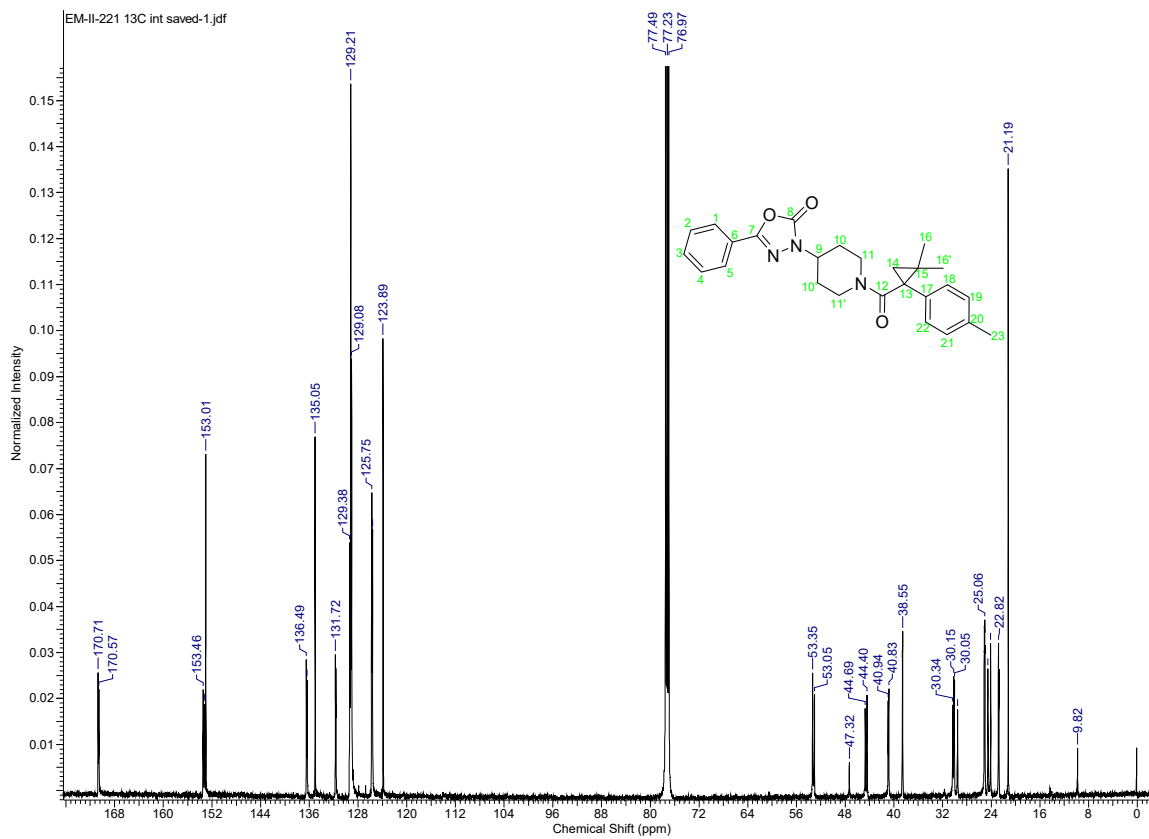


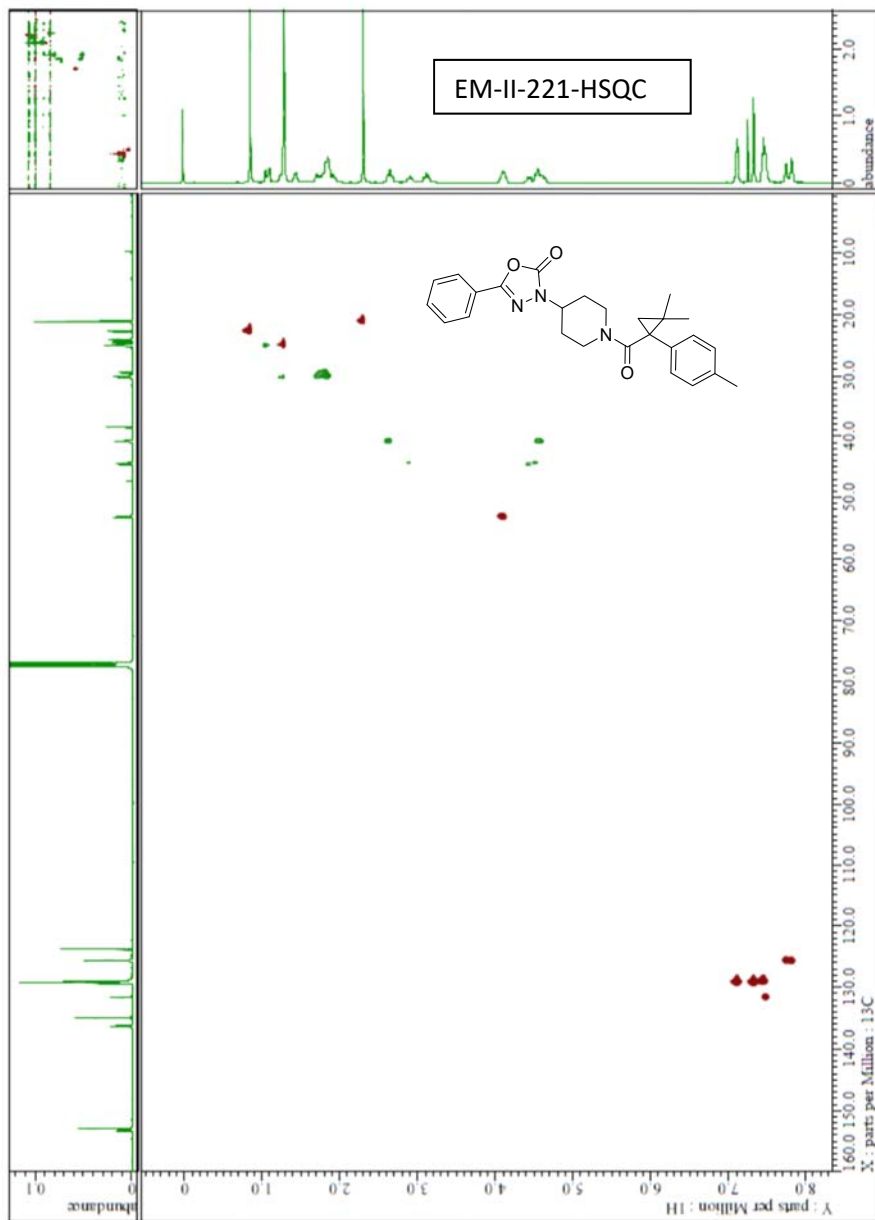


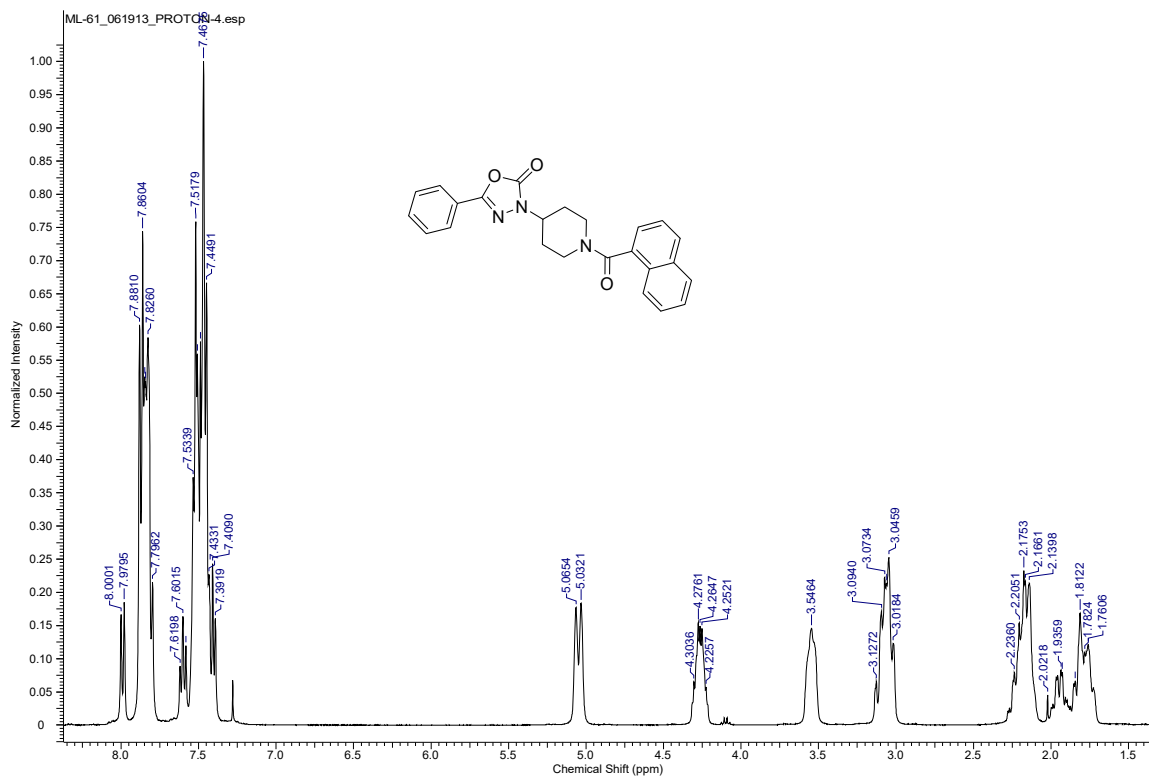


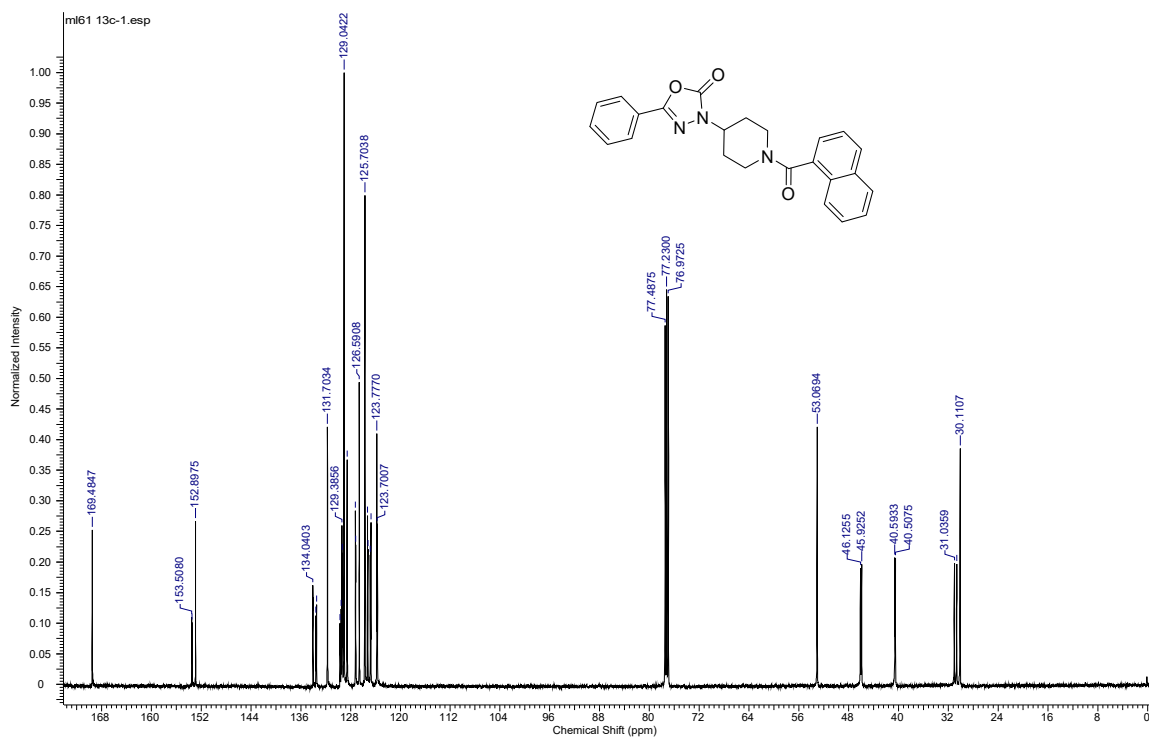


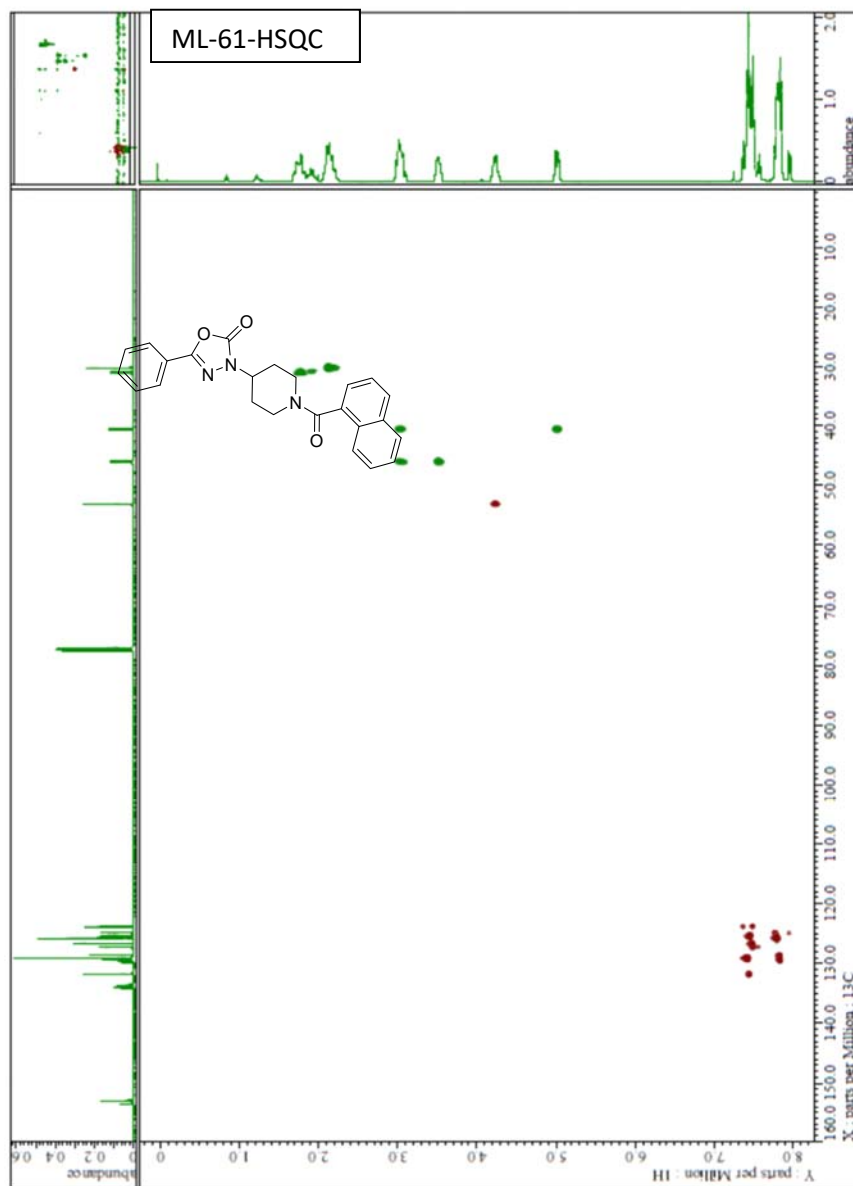












Biological Assay

Antagonist activity was evaluated based on the inhibition of LPI-induced β -arrestin activity through the use of two differential means of β -arrestin quantitation, and in two different cellular backgrounds. Compounds were initially screened in an image based cell assay to identify their antagonist activity on their ability to inhibit LPI-induced β -arrestin recruitment. In this assay, U2OS cells over-expressing GPR55 (modified at the C-terminus, GPR55E) and GFP tagged β -arr2, are grown on glass coverslips and pre-incubated (30 minutes) with candidate antagonists prior to LPI exposure (6 μ M; 40 minutes). Images of cells were taken using a fluorescent microscope and analyzed with Image J (<http://rsbweb.nih.gov/ij/>) using a custom written plug-in. The modified GPR55E receptor, concentration of agonist (EC_{80}), and details of the β -arrestin recruitment assay have been previously described.^{11,12} Compounds with an IC_{50} below 15 μ M were also evaluated employing DiscoverX PathHunter® Complementation technology. CHO-K1 cells stably expressing GPR55 (fused to a β -galactosidase enzyme fragment), and β -arrestin (fused to an N-terminal deletion β -galactosidase mutant), were grown in selection media and were passaged up to 10 times according to manufacturer protocols. In the presence of agonist (LPI, 90 minutes), and PathHunter® detection reagents containing β -galactosidase substrate, a chemiluminescent signal is generated due to the forced complementation of the GPR55 fused β -galactosidase fragment and the β -arrestin fused N-terminal deletion mutant fragment of β -galactosidase. A concentration response curve was generated, and antagonist activity was evaluated based on the inhibition of the LPI-

induced chemiluminescence signal. Prior to exposure with LPI (37 °C, 90 minutes) cells were preincubated with putative antagonists for 30 minutes (37 °C).

The chemiluminescence signal was measured using a Perkin Elmer Envision plate reader for 1 second. Experiments were run in triplicate and repeated at a minimum of 3 times. Ligand readings, expressed as relative luminescence units, were subtracted from corresponding vehicle readings and analyzed in GraphPad Prism version 5.0 (GraphPad, San Diego, CA). IC₅₀ values of antagonists were similar in both β -arrestin methodologies, and in both cellular backgrounds.

Modeling Methodsⁱⁱ

Conformational Analysis of ML191 ((CID23612552), 5-phenyl-3-(1-(1-(p-tolyl)cyclopropane-carbonyl)piperidin-4-yl)-1,3,4-oxa-diazol-2(3H)-one). A complete conformational analysis of ML191 was performed using *ab initio* Hartree-Fock calculations at the 6-31G* level as encoded in Spartan '08 (Wavefunction, Inc., 18401 Von Karman Ave., Suite 370, Irvine, CA 92612). In each conformer search, local energy minima were identified by rotation of a subject torsion angle through 360° in 60° increments (6-fold search), followed by HF 6-31G* energy minimization of each rotamer generated. To calculate the energy difference between the global minimum energy conformer of ML191 and its final docked conformation, rotatable bonds in the global minimum energy conformer were driven to their corresponding value in the final docked conformation and the single point energy of the resultant structure was calculated at the HF 6-31G* level.

Electrostatic Potential Map Calculation - The electrostatic potential density surface for ML191 was calculated using Spartan '08 (Wavefunction, Inc., 18401 Von Karman Ave., Suite 370, Irvine, CA 92612). The electrostatic potential energy was calculated using the *ab initio* Hartree-Fock method at 6-31G* level of theory and was mapped on the 0.002 isodensity surface of each molecule. The surface was color coded according to the potential, with electron rich regions colored red and electron poor regions colored blue.

Receptor Model Development - The construction of our initial GPR55 receptor homology model was described previously in Kotsikorou *et al.*ⁱⁱⁱ This homology model used the crystal structure of β_2 -AR^{iv} as the template. This initial model has been modified to reflect several structural elements found in the x-ray crystal structure of CXCR4 in its inactive state, a receptor with which the GPR55 receptor has high homology.^v 1) TMH2 and TMH4 of GPR55 were modeled using the corresponding helices in the CXCR4 structure. GPR55 and CXCR4 have prolines in the positions 2.58 and 4.59 that would lead to very different conformations of TMHs 2 and 4 compared to the β_2 -AR template which has prolines at 2.59 and 4.60. In addition, preceding the prolines at positions 2.56 and 4.57, CXCR4 has threonines in a g- conformation that influence the overall bend of each helix. Analogously, GPR55 has serines at 2.56(76) and 4.57(153) that can assume a g- conformation. Therefore, the use of the CXCR4 TMH2 and TMH4 as templates is well-justified. 2) The high sequence homology between GPR55 and CXCR4 in the extracellular ends of TMHs 6 and 7, dictated the introduction of extracellular (EC) helical extensions to the EC3 loop of GPR55 to match that of

CXCR4. 3) The EC2 loop in CXCR4 contains a beta sheet. Due to high sequence similarity in this region, as well, the beta sheet motif was built into the EC-2 loop in GPR55. 4) In addition to the disulfide bridge between the EC-2 loop and C3.25, CXCR4 has another disulfide bridge between a Cys in the N-terminus Cys(28) and Cys(274) in the EC-3 loop. The same residues (Cys(10) and Cys(260)) are found in the GPR55 sequence, so this second disulfide bridge was added to the GPR55 model. Recent C(10)A and C(260)A mutation studies suggest that the C(10)/C(260) disulfide bridge exists in GPR55 (M. Lingerfelt et al., 2016, manuscript submitted). The GPR55 inactive state model is also characterized by an intracellular hydrogen bond between R3.50(119) and Q6.30(221) that closes off the intracellular domain of the receptor, preventing G-protein interaction. The resultant homology model was energy minimized to relieve any steric overlaps.

Docking of Ligands - The lowest energy conformation of ML191 was used as input for receptor docking studies. The Schrödinger workflow, Induced Fit, (Schrödinger Inc. Portland, OR) was used to explore possible binding conformations and receptor site interactions in the GPR55 R model. The Induced Fit Docking workflow was used to dock subject ligands in the binding site of the GPR55 R receptor model. The binding site of the receptor was defined by the area enclosed in a box with dimensions 26Å x 26Å x26Å (the default value). Because the endogenous ligand, LPI, is negatively charged, it is very likely that a positively charged amino is the primary interaction site for GPR55 ligands. The only positively charged amino acid in the binding pocket is K2.60(80). Recent K2.60A mutation studies suggest that this residue is essential for ligand activation at

GPR55 (M. Lingerfelt et al., manuscript in preparation). For this reason, K2.60(80) was set as the center of the box and a hydrogen bond with K2.60(80) was defined as a constraint. The two constraints (enclosing box and hydrogen bond) were used for both docking steps that Induced Fit Docking performs. The initial receptor minimization that Induced Fit Docking performs in preparation for docking the ligand was omitted since the receptor model was already energy minimized. For the first Glide calculation, the receptor and ligand Van der Waals radii were set to the default value of 0.50 and the number of maximum poses to be produced was also set to 40. During the Prime stage of the calculation, amino acids within 5.0Å of the ligand were refined to better accommodate the ligand. Since the GPR55 receptor is a transmembrane protein, an implicit membrane was used during the Prime refinement step. Then, during the second Glide step, the top 30 poses produced by the first calculation were redocked to the receptor. Docked poses that were within 40.0 kcal/mol from the lowest one were kept.

Ligand/Receptor Minimization - To optimize the ligand/receptor interaction in the receptor/ligand complexes, each was minimized using Macromodel 9.1 (Schrödinger Inc.; Portland, OR). Since the receptor model was minimized before the docking of the ligands, a brief minimization was adequate to resolve any steric clashes after docking. To this end, 500 steps of Polak-Ribier conjugate gradient minimization using force field defined dielectric were performed. A harmonic constraint was placed on all the TMH backbone torsions (ϕ , ψ , and ω) to preserve the general shape of the helices during minimization. The sidechains of the TMH region, the loops and termini were allowed to relax. The Generalized Born/Surface Area (GB/SA) continuum solvation model for water

as is implemented in Macromodel 9.1 was used for minimizing the loop regions. An 8.0Å nonbonded cutoff (updated every 10 steps), a 20.0Å electrostatic cutoff, and a 4.0Å hydrogen bond cutoff were used in each stage of the calculation. The transmembrane region and the docked ligand were frozen while the loops were minimized.

Results

ML191 Global Minimum Energy Conformer. Overall, the GPR55 probe molecules have three regions. The first two regions include a broad head connected to a central portion of the ligand that is vertical. Together, this gives ML191 the shape of the number “7”. The third section at the end of the vertical segment is a pendant aromatic or heterocyclic ring that is nearly perpendicular to the vertical segment. In the global minimum energy conformer of ML191, the *para*-methylphenyl ring is at an angle with the carbonyl group that joins the cyclopropyl and the piperidine rings ($C1-C2-C3-C4 = 53.5^\circ$ and $C2-C3-C4-N6 = 72.5^\circ$). The piperidine, which is in a chair conformation, and the attached 1,3,4-oxadiazole-2-one ring form the vertical segment of the “7”. The 1,3,4-oxadiazole-2-one ring is perpendicular to the plane of the piperidine ring ($H-C9-N10-C11 = -179.9^\circ$) and the pendant phenyl ring is in plane with the 1,3,4-oxadiazole-2-one ring ($O12-C13-C14-C15 = -0.4^\circ$). The global minimum energy conformer of ML191 is illustrated in Figure 15B (bottom).

ML191 Molecular Electrostatic Potential Map - Figure 15B (top) illustrates the molecular electrostatic potential map (ranges in kJ/mol given next to ligand) of the docked conformation of ML191 at GPR55 R. Below this map, the ML191 conformer used to calculate the map is shown in tube display (Figure 15B (bottom)). ML191

possesses a broad head region connected to a central portion of the ligand that has a thin profile. The most electronegative region of ML191 is located close to the end of this central section and this portion is followed by a pendant ring that juts out nearly perpendicular to the central portion of the molecule. The carbonyl oxygen of the 1,3,4-oxadiazole-2-one ring of ML191 is the most electronegative region of the ligand and forms the part of ML191 that interacts with K2.60(80) (see docking results below).

Compound Docking in GPR55 Inactive State (R) Model – Docking studies identified the putative binding site for ML191 to be the TMH 2-3-5-6-7 region of the GPR55 R model. K2.60(80), the only positively charged TMH residue in the putative binding site, was used as the primary interaction site for all the ligands docked. Figure 15A illustrates the final ML191/GPR55 R complex obtained using Induced Fit. The ML191 1,3,4-oxadiazole-2-one carbonyl oxygen forms a hydrogen bond with K2.60(80). The hydrogen bond (N-O) distance and (N-H—O) angle are 2.81 Å and 154° respectively. ML191 forms a number of aromatic stacking interactions. The methylphenyl ring next to the cyclopropyl group forms a stack with the EC2 loop residue F169 (ring centroid to centroid distance is 5.08 Å and the angle between ring planes is 55°). The pendant phenyl group adjacent to the 1,3,4-oxadiazole-2-one ring stacks with F6.55 (246). The ring centroid to centroid distance is 5.41 Å and the angle between ring planes is 50°. The total pairwise interaction energy for ML191 with GPR55 is -33.16 kcal/mol. The major interaction energy contributions for this compound are the hydrogen bonding interaction with K2.60(80) and Van der Waals interactions with M7.39 (274). Aromatic stacking interactions with F169 and Van der Waals interactions with Y3.32

(101) also contribute to the interaction energy. The remainder of the aromatic stacking interactions identified contribute less to the overall interaction energy. The pendant phenyl group prevents a change in the χ_1 of the toggle switch residue, M3.36 (104) and therefore keeps GPR55 in the inactive state.

Literature Cited

ⁱ Harish, K. P.; Mohana, K. N.; Mallesha, L.; Prasanna Kumar, B. N. *Eur. J. Med Chem.* **2013**, *65*, 276-283.

ⁱⁱ Kotsikorou, E.; Sharir, H.; Shore, D. M.; Hurst, D. P.; Lynch, D. L.; Madrigal, K. E.; Heynen-Genel, S.; Milan, L. B.; Chung, T. D.; Seltzman, H. H.; Bai, Y.; Caron, M. G.; Barak, L. S.; Croatt, M. P.; Abood, M. E.; Reggio, P. H. *Biochemistry* **2013**, *52*, 9456.

ⁱⁱⁱ Kotsikorou, E.; Madrigal, K. E.; Hurst, D. P.; Sharir, H.; Lynch, D. L.; Heynen-Genel, S.; Milan, L. B.; Chung, T. D.; Seltzman, H. H.; Bai, Y.; Caron, M. G.; Barak, L.; Abood, M. E.; Reggio, P. H. *Biochemistry* **2011**, *50*, 5633.

^{iv} Cherezov, V.; Rosenbaum, D. M.; Hanson, M. A.; Rasmussen, S. G.; Thian, F. S.; Kobilka, T. S.; Choi, H. J.; Kuhn, P.; Weis, W. I.; Kobilka, B. K.; Stevens, R. C. *Science* **2007**, *318*, 1258.

^v Wu, B.; Chien, E. Y.; Mol, C. D.; Fenalti, G.; Liu, W.; Katritch, V.; Abagyan, R.; Brooun, A.; Wells, P.; Bi, F. C.; Hamel, D. J.; Kuhn, P.; Handel, T. M.; Cherezov, V.; Stevens, R. C. *Science* **2010**, *330*, 1066.

APPENDIX B**SUPPLEMENTAL INFORMATION FOR CHAPTER IV****Supporting Information For****Identification of Crucial Amino Acid Residues Involved in Agonist****Signaling at the GPR55 Receptor***

* This material is available free of charge via the Internet at <http://pubs.acs.org>.

Corresponding Author

*Address correspondence to either Mary E. Abood at the Center for Substance Abuse Research, Lewis Katz School of Medicine at Temple University, Philadelphia, Pennsylvania 19140, United States (mabood@temple.edu; 215-707-2638)

or

Patricia H. Reggio at the Department of Chemistry and Biochemistry, UNC-Greensboro, Greensboro, North Carolina 27402 United States (phreggio@uncg.edu, 336-334-5333).

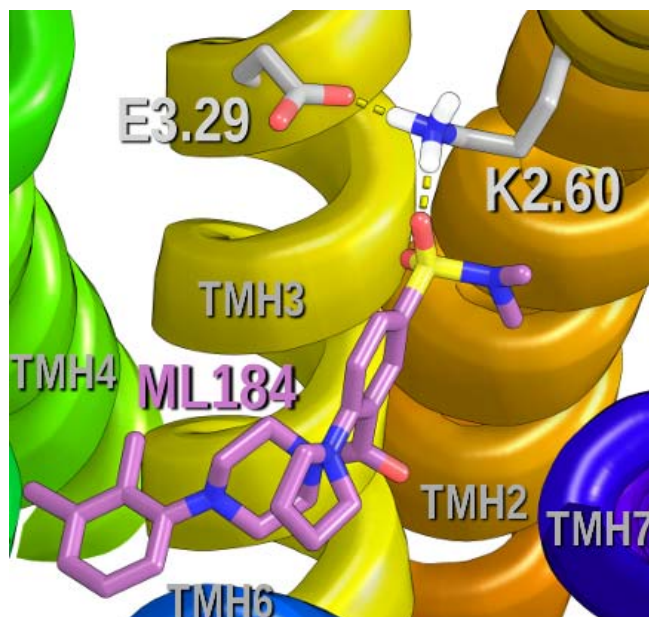
Author Contributions

MEA and PHR designed the study and wrote the paper and contributed equally to this work. MAL and PZ also contributed to writing the manuscript and contributed equally to this work. MAL and DPH constructed the molecular model in consultation with PHR. PZ designed and constructed vectors for expression of mutant proteins and Mary A. Lingerfelt, Pingwei Zhao, Haleli P. Sharir, Dow P. Hurst, Patricia H. Reggio and Mary E. Abood analyzed the mutant phenotypes in vitro. HPS designed and constructed vectors for expression of mutant proteins. All authors reviewed the results and approved the final version of the manuscript.

Table of Contents

Figure S1177

Table S1. ML184/GPR55 R* Complex Interaction Energy178



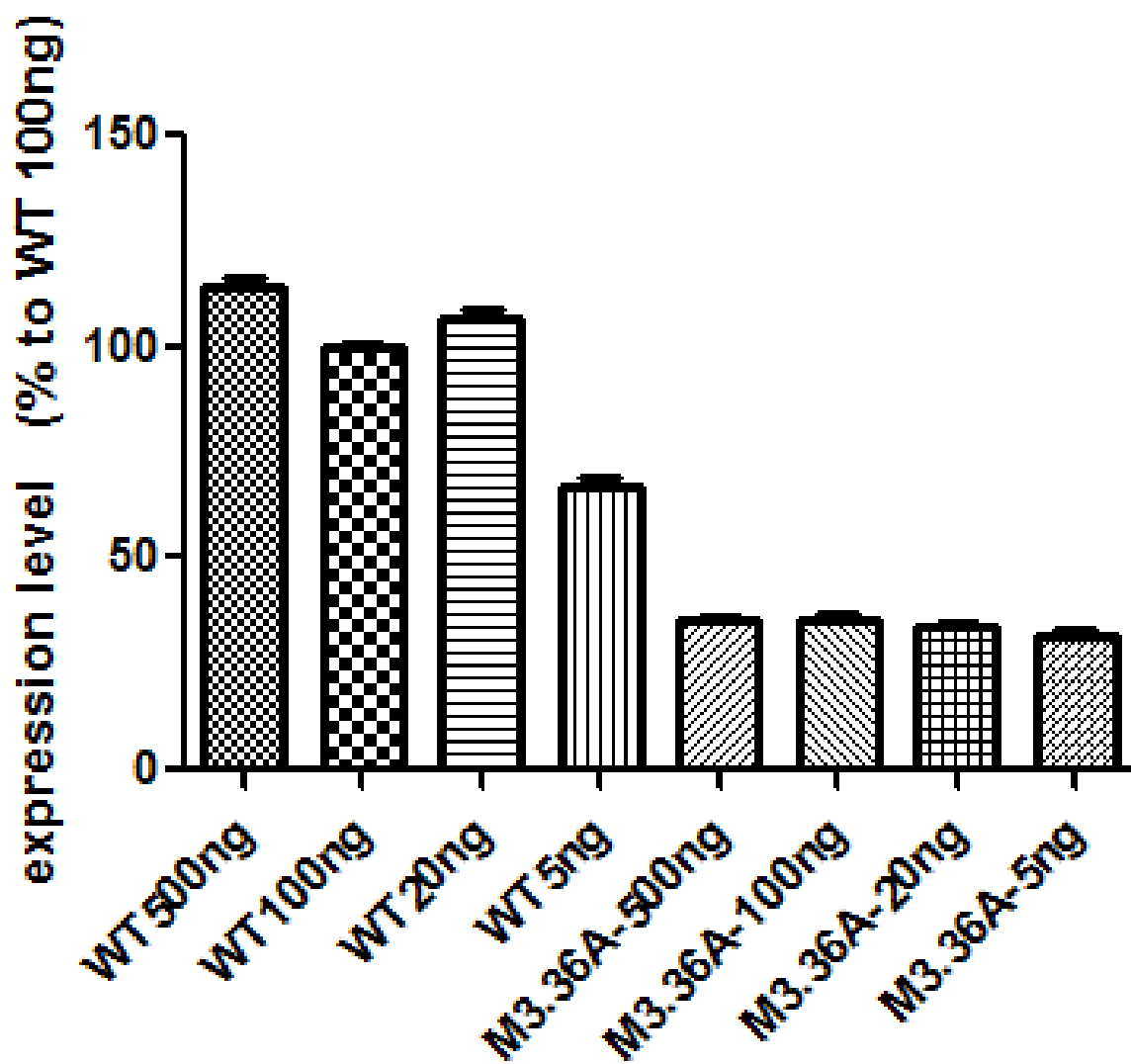


Figure S1.

Table S1

ML184/GPR55 R* Complex Interaction Energy

GPR55 B&W	Electrostatic (kcal)	Vdw (kcal)	Total Interaction Energy (kcal)
K2.60(80)	-8.0	-1.4	-9.4
Y3.32(101)	-3.1	-5.1	-8.2
F6.55(246)	-0.1	-5.0	-5.1
V6.51(242)	-0.1	-4.5	-4.6
F5.47(190)	-0.1	-4.0	-4.0
M7.39(274)	-0.1	-3.7	-3.8
F3.33(102)	-0.1	-3.7	-3.8
H(170)	-2.7	-0.8	-3.5
F5.39(182)	-0.1	-3.1	-3.2
E5.43(186)	-0.4	-1.9	-2.2
L5.42(185)	0.3	-2.2	-2.0
M3.36(105)	0.1	-1.9	-1.8
Y3.37(106)	0.4	-1.4	-1.0
M(172)	0.2	-1.2	-1.0
N7.43(278)	0.2	-0.8	-0.6
L7.35(270)	0.0	-0.6	-0.6
H1.39(27)	0.0	-0.3	-0.3
H6.52(243)	0.0	-0.2	-0.2
P6.50(241)	-0.1	-0.2	-0.2
G5.46(189)	0.1	-0.2	-0.2
S7.42(277)	0.1	-0.3	-0.2
M2.61(81)	0.0	-0.2	-0.2
Q1.35(23)	0.1	-0.3	-0.1
L2.57(77)	0.0	-0.2	-0.1
I4.60(156)	0.0	-0.1	-0.1
Q6.58(249)	0.1	-0.2	-0.1
L2.53(73)	0.0	-0.1	-0.1
E3.29(98)	<u>2.2</u>	<u>-0.7</u>	<u>1.5</u>
	-10.6	-45.3	-55.9
-55.9	Interaction E (kcal/mol)		
1.91	Ligand Conformational Cost (kcal/mol)		
-54.0	Total Interaction Energy (kcal/mol)		